

Enhancing Fuel Cell Lifetime Performance  
through Effective Health Management

by

Benjamin Davies

A Doctoral Thesis

Submitted in partial fulfilment of the requirements for the award of  
Doctor of Philosophy of Loughborough University

April 2018

© by Benjamin Davies 2018

# Abstract

Hydrogen fuel cells, and notably the polymer electrolyte fuel cell (PEFC), present an important opportunity to reduce greenhouse gas emissions within a range of sectors of society, particularly for transportation and portable products. Despite several decades of research and development, there exist three main hurdles to full commercialisation; namely infrastructure, costs, and durability. This thesis considers the latter of these.

The lifetime target for an automotive fuel cell power plant is to survive 5000 hours of usage before significant performance loss; current demonstration projects have only accomplished half of this target, often due to PEFC stack component degradation. Health management techniques have been identified as an opportunity to overcome the durability limitations. By monitoring the PEFC for faulty operation, it is hoped that control actions can be made to restore or maintain performance, and achieve the desired lifetime durability.

This thesis presents fault detection and diagnosis approaches with the goal of isolating a range of component degradation modes from within the PEFC construction. Fault detection is achieved through residual analysis against an electrochemical model of healthy stack condition. An expert knowledge-based diagnostic approach is developed for fault isolation. This analysis is enabled through fuzzy logic calculations, which allows for computational reasoning against linguistic terminology and expert understanding of degradation phenomena.

An experimental test bench has been utilised to test the health management processes, and demonstrate functionality. Through different steady-state and dynamic loading conditions, including a simulation of automotive application, diagnosis results can be observed for PEFC degradation cases.

This research contributes to the areas of reliability analysis and health management of PEFC fuel cells. Established PEFC models have been updated to represent more accurately an application PEFC. The fuzzy logic knowledge-based diagnostic is the greatest novel contribution, with no examples of this application in the literature.

## Acknowledgements

Firstly, I would like to thank my supervisors Prof Lisa Jackson and Dr Sarah Dunnett. Through your the support, guidance, and patience this work has come to fruition. I am grateful for the opportunity to undertake this research.

Secondly, I would like to thank Andrey Vasilyev, for your friendship through the past four years. Thank you for making the past four years enjoyable, and your company at all the conferences, seminars, and writing sessions in the café.

Thanks go to Dr Ben Todd and the engineering staff at Arcola Energy, for welcoming me during my secondment and allowing me to contribute to your organisation.

To my parents and my siblings, thank you for the support and inspiration to always be my best. I hope I have made you proud.

Last but not least, I would like to thank Dr Anne Canning. I am so grateful to have met you, and had you by my side through this time. Thank you for your love, tireless support, and endless proofreading. I look forward to our next adventure.

## Publications

The following peer reviewed publications are associated with this body of work:

Ben Davies, L. Jackson, and S. Dunnett. Fuzzy Modelling for Fuel Cell Control and Fault Diagnosis. *Advances in Risk and Reliability Technology Symposium 2015*, 2015.

Ben Davies, L. Jackson, and S. Dunnett. Fault Diagnostic Modelling for Polymer Electrolyte Fuel Cells. *5<sup>th</sup> European PEFC and H<sub>2</sub> Forum*, 2015.

Ben Davies, L. Jackson, and S. Dunnett. Development of a fuzzy logic diagnostic model for polymer electrolyte fuel cells. *Safety and Reliability of Complex Engineered Systems: ESREL 2015* pp. 2373–2378, 2015.

Ben Davies, L. Jackson, and S. Dunnett. Test and evaluation of a fuzzy diagnostic model for PEFC. *Risk, Reliability and Safety: Innovating Theory and Practice: Proceedings of ESREL 2016* pp. 1937–1941, 2016.

Ben Davies, L. Jackson, and S. Dunnett. Expert diagnosis of polymer electrolyte fuel cells. *International Journal of Hydrogen Energy* 42(16):11724-11734, 2017.

# Contents

<b>List of Figures</b>	<b>xi</b>
<b>List of Tables</b>	<b>xii</b>
<b>1 Introduction</b>	<b>1</b>
1.1 Motivation . . . . .	1
1.1.1 Transitioning to the hydrogen economy . . . . .	1
1.1.2 Hydrogen Fuel Cells . . . . .	2
1.2 Polymer Electrolyte Fuel Cells . . . . .	5
1.2.1 PEFC Construction . . . . .	5
1.2.2 PEFC Applications . . . . .	9
1.2.3 Hurdles to PEFC usage . . . . .	10
1.3 Prognostics and Health Management . . . . .	11
1.3.1 History of maintenance strategies . . . . .	11
1.4 PHM for PEFC Systems . . . . .	14
1.4.1 Data acquisition . . . . .	14
1.4.2 Data processing . . . . .	17
1.4.3 Condition assessment . . . . .	17
1.4.4 Diagnosis . . . . .	18
1.4.5 Prognosis . . . . .	19
1.4.6 Decision support . . . . .	19
1.4.7 Human-machine interface . . . . .	19
1.5 Summary . . . . .	20
1.6 Research Objectives . . . . .	20
1.7 Thesis Layout . . . . .	21

<b>2</b>	<b>Durability and Health Management – Literature Review</b>	<b>22</b>
2.1	PEFC Fault Mechanisms . . . . .	22
2.1.1	Polymer membrane . . . . .	23
2.1.2	Platinum catalyst . . . . .	24
2.1.3	Gas diffusion electrode . . . . .	25
2.1.4	Bipolar plates . . . . .	26
2.1.5	Sealing gaskets . . . . .	27
2.1.6	Water management . . . . .	27
2.2	PEFC Condition Assessment Techniques . . . . .	28
2.2.1	Empirical threshold fault detection . . . . .	28
2.2.2	Model-based fault detection . . . . .	30
2.3	PEFC Diagnostic Techniques . . . . .	31
2.3.1	Model based fault diagnosis . . . . .	31
2.3.2	Data driven fault diagnosis . . . . .	32
2.3.3	Rule based fault diagnosis . . . . .	33
2.4	Summary . . . . .	34
<b>3</b>	<b>Detection System</b>	<b>36</b>
3.1	Fuel Cell Modelling . . . . .	37
3.1.1	Nernst voltage calculation . . . . .	37
3.1.2	Activation loss . . . . .	39
3.1.3	Ohmic loss . . . . .	39
3.1.4	Mass transport loss . . . . .	41
3.1.5	Side reaction losses . . . . .	42
3.1.6	Complete model equation . . . . .	42
3.2	Condition Assessment . . . . .	43
3.3	Summary . . . . .	44
<b>4</b>	<b>Diagnostic System</b>	<b>46</b>
4.1	Fuzzy Logic . . . . .	47
4.1.1	Fuzzy sets . . . . .	47
4.1.2	Operations on fuzzy sets . . . . .	50
4.1.3	Structure of the fuzzy system . . . . .	50
4.1.4	Comparison to probability . . . . .	52
4.2	Knowledge Engineering . . . . .	53

4.3	Fuel Cell Diagnostic System . . . . .	54
4.3.1	Process selection . . . . .	55
4.3.2	Creating the fuzzy logic system . . . . .	56
4.3.3	Knowledge acquisition . . . . .	57
4.3.4	Final rules base . . . . .	72
4.3.5	Membership functions . . . . .	74
4.3.6	Integration and Validation of the Expert Diagnostic System . . . . .	80
4.4	Summary . . . . .	81
<b>5</b>	<b>Experimental Methodology</b>	<b>82</b>
5.1	Test Bench . . . . .	82
5.1.1	Fuel Cell . . . . .	83
5.1.2	Ancillary subsystems . . . . .	85
5.2	Fuel Cell Control and Monitoring Software . . . . .	88
5.2.1	Integration of the fault detection and diagnosis . . . . .	92
5.3	Experimental Methodology . . . . .	93
5.3.1	Testing procedures . . . . .	94
5.3.2	Characterisation . . . . .	99
5.4	Full Testing Sequence . . . . .	99
5.5	Summary . . . . .	101
<b>6</b>	<b>Validation Testing Results</b>	<b>102</b>
6.1	FC100-1 Steady-State Normal Loading . . . . .	102
6.2	FC100-1 Steady-State High Current Loading . . . . .	107
6.3	FC100-1 Steady-State Low Current Loading . . . . .	110
6.4	FC100-1 Steady-State Open Circuit Voltage . . . . .	114
6.5	FC100-1 High Current Cyclic Loading . . . . .	118
6.6	FC100-1 Low Current Cyclic Loading . . . . .	121
6.7	FC100-1 Open Circuit Cyclic Loading . . . . .	124
6.8	FC100-1 Drive Cycle Loading . . . . .	127
6.9	Summary . . . . .	131
<b>7</b>	<b>Conclusions and Future Work</b>	<b>134</b>
7.1	Conclusions . . . . .	134
7.2	Contributions . . . . .	135
7.3	Future Work . . . . .	136

<b>Bibliography</b>	<b>137</b>
<b>A FCCM LabVIEW Code</b>	<b>157</b>

# List of Figures

1.1	US annual total electricity production 1949 – 2015 . . . . .	1
1.2	PEFC stack components, here as a single cell unit . . . . .	5
1.3	A generic polarisation curve for PEFC . . . . .	16
2.1	Cyclic voltammogram result . . . . .	25
2.2	EIS results for water management problems . . . . .	27
2.3	Fault detection based on pressure change . . . . .	28
2.4	Generalised electrical equivalent model . . . . .	30
3.1	System architecture for fault detection modelling . . . . .	37
3.2	Theoretical fuel cell performance from the Nernst voltage calculation . . . . .	38
3.3	Effect of activation losses on fuel cell performance . . . . .	39
3.4	Effect of ohmic losses on fuel cell performance . . . . .	40
3.5	Effect of mass transport losses on fuel cell performance . . . . .	41
3.6	Theoretical fuel cell performance from the Nernst voltage calculation . . . . .	42
3.7	Examples of PEFC performance from the voltage model calculation . . . . .	43
4.1	A membership function for general classical set $C$ . . . . .	48
4.2	A membership function for general fuzzy set $A$ . . . . .	49
4.3	Other potential membership function shapes . . . . .	49
4.4	Example fuzzy sets to characterise room temperature . . . . .	50
4.5	Fuzzy logic system structure . . . . .	51
4.6	The fuzzy logic knowledge engineering process . . . . .	53
4.7	Creating the fuzzy logic system . . . . .	54
4.8	Change in cathode electrocatalyst surface area during cycling experiments comparing different scan rates . . . . .	66
4.9	Fuzzy input sets for stack voltage . . . . .	75
4.10	Fuzzy input sets for stack voltage cycle number . . . . .	75

4.11	Fuzzy input sets for anode stoichiometry . . . . .	76
4.12	Fuzzy input sets for cathode humidity . . . . .	77
4.13	Fuzzy input sets for humidity change . . . . .	78
4.14	Fuzzy input sets for stack temperature . . . . .	79
4.15	Fuzzy output sets for degradation mode certainty . . . . .	80
4.16	System architecture for fault diagnosis . . . . .	80
5.1	General arrangement of the fuel cell test bench . . . . .	83
5.2	Image of the MEA for reference and scale . . . . .	84
5.3	The faces of the monopolar plates in the <i>FC100</i> ; flow fields left, coolant channels right . . . . .	85
5.4	Electical subsystems of the PEFC test bench . . . . .	88
5.5	FCCM state machine design . . . . .	89
5.6	FCCM initialisation interface . . . . .	89
5.7	FCCM main interface . . . . .	90
5.8	FCCM system view interface . . . . .	91
5.9	System architecture for fault detection and diagnosis integrated with the test system	93
5.10	Example stepped dynamic loading profile, normal–low . . . . .	96
5.11	NEDC drive cycle, and the resultant fuel cell loading cycle . . . . .	98
5.12	Outline of full testing procedure . . . . .	100
6.1	Voltage output during FC100-1 normal loading test . . . . .	103
6.2	Condition assessment output during FC100-1 normal loading test . . . . .	104
6.3	Example of the diagnostic output in the FCCM . . . . .	104
6.4	Diagnostic output during FC100-1 normal loading test . . . . .	105
6.5	Polarisation characterisation after FC100-1 normal loading test . . . . .	107
6.6	Voltage output during FC100-1 high loading test . . . . .	108
6.7	Condition assessment output during FC100-1 high loading test . . . . .	108
6.8	Diagnostic output during FC100-1 high loading test . . . . .	109
6.9	Polarisation characterisation after FC100-1 high loading test . . . . .	110
6.10	Voltage output during FC100-1 low loading test . . . . .	111
6.11	Condition assessment output during FC100-1 low loading test . . . . .	111
6.12	Diagnostic output during FC100-1 low loading test . . . . .	112
6.13	Polarisation characterisation after FC100-1 low loading test . . . . .	113
6.14	Voltage output during FC100-1 OCV loading test . . . . .	114

6.15	Condition assessment output during FC100-1 OCV loading test . . . . .	115
6.16	Diagnostic output during FC100-1 OCV loading test . . . . .	116
6.17	Polarisation characterisation after FC100-1 OCV loading test . . . . .	117
6.18	Detail of voltage output during FC100-1 cyclic high loading test . . . . .	118
6.19	Voltage output during FC100-1 cyclic high loading test . . . . .	119
6.20	Condition assessment output during FC100-1 cyclic high loading test . . . . .	119
6.21	Diagnostic output during FC100-1 cyclic high loading test . . . . .	120
6.22	Polarisation characterisation after FC100-1 cyclic high loading test . . . . .	121
6.23	Voltage output during FC100-1 cyclic low loading test . . . . .	122
6.24	Condition assessment output during FC100-1 cyclic low loading test . . . . .	122
6.25	Diagnostic output during FC100-1 cyclic low loading test . . . . .	123
6.26	Polarisation characterisation after FC100-1 cyclic low loading test . . . . .	124
6.27	Voltage output during FC100-1 cyclic OCV loading test . . . . .	125
6.28	Condition assessment output during FC100-1 cyclic OCV loading test . . . . .	125
6.29	Diagnostic output during FC100-1 cyclic OCV loading test . . . . .	126
6.30	Polarisation characterisation after FC100-1 cyclic OCV loading test . . . . .	127
6.31	Voltage output during FC100-1 drive cycle loading test . . . . .	128
6.32	Condition assessment output during FC100-1 drive cycle loading test . . . . .	128
6.33	Diagnostic output during FC100-1 drive cycle loading test . . . . .	129
6.34	Polarisation characterisation after FC100-1 drive cycle loading test . . . . .	130
A.1	FCCM main interface code structure during initialisation . . . . .	157
A.2	FCCM main interface code structure during monitoring . . . . .	158
A.3	FCCM main interface code structure during shut down . . . . .	158
A.4	FCCM initialisation interface code structure during data entry . . . . .	159
A.5	FCCM initialisation interface code structure during start up . . . . .	159
A.6	FCCM view panel code structure . . . . .	160
A.7	FCCM control interface code structure during monitoring . . . . .	160
A.8	FCCM control interface code structure during polarisation . . . . .	161
A.9	FCCM diagnostic interface code structure . . . . .	161
A.10	Fuzzy logic diagnostic code structure for inputs . . . . .	162
A.11	Fuzzy logic diagnostic code structure for inputs (cont.) . . . . .	163
A.12	Fuzzy logic diagnostic code structure for outputs . . . . .	164
A.13	Fuzzy logic diagnostic code structure for rules . . . . .	165
A.14	Fuzzy logic diagnostic code structure for rules (cont.) . . . . .	166

A.15 Fuzzy logic diagnostic code structure for rules (cont.) . . . . .	167
A.16 Fuzzy logic diagnostic code structure . . . . .	168

# List of Tables

1.1	Fuel cell classifications . . . . .	4
1.2	Characterisation techniques available for PEFC systems. . . . .	15
3.1	Semi-empirical model variables used in figure 3.7 . . . . .	43
3.2	System measurements required for the model . . . . .	44
4.1	Set operation in classical set theory . . . . .	50
4.2	Membrane degradation knowledge base . . . . .	59
4.3	Reduced membrane rule base . . . . .	62
4.4	Catalyst degradation knowledge base . . . . .	65
4.5	Reduced catalyst rule base . . . . .	67
4.6	Gas diffusion electrode degradation knowledge base . . . . .	68
4.7	Reduced GDE rule base . . . . .	69
4.8	Water management problems knowledge base . . . . .	71
4.9	Reduced water management problems rule base . . . . .	72
4.10	Final reduced rule base . . . . .	73
4.11	Water content coefficient value . . . . .	78
5.1	Flow conditions for the test schedule . . . . .	94
5.2	List of testing procedures . . . . .	101
6.1	Model parameters . . . . .	107

# Chapter 1

## Introduction

### 1.1 Motivation

#### 1.1.1 Transitioning to the hydrogen economy

Global policy makers are committed to working toward a low-carbon, energy-secure economy, relinquishing dependence on fossil fuels [1]. To date, much of the world’s energy is still derived from carbon-based fossil fuels; coal, oil, and natural gas. The dominance of fossil fuels in energy supply is a historic trend that holds for the majority of regions around the world [2].

In the US for example, coal-fired power plants accounted for 33% of the national electricity generation in 2015, and consequently 70% of the sector’s carbon dioxide (CO<sub>2</sub>) emissions – over 25% of the national emission [3]. Figure 1.1 shows historic data of electrical generation from different major sources. The dominance of fossil fuels in the energy mix can be seen, as well as limited uptake of renewable sources. Coal is seen to be the primary energy source throughout the observed time period, peaking around 2005 with 50% of total electricity generation.

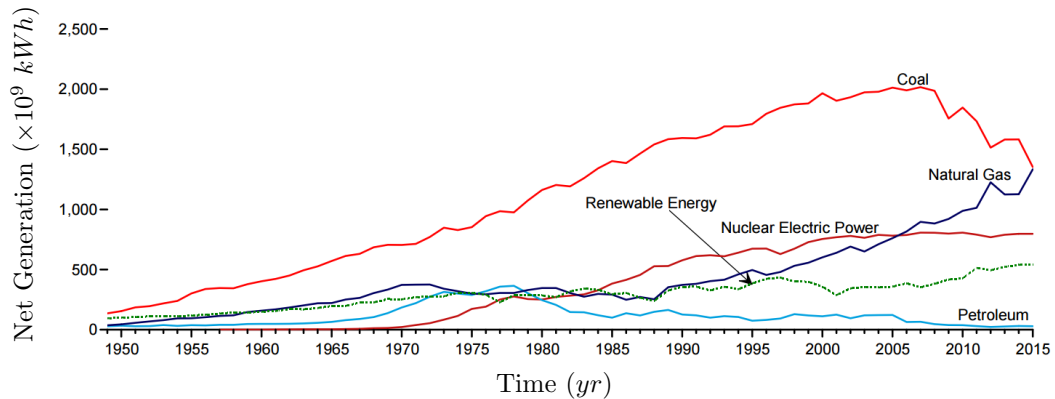


Figure 1.1: US annual total electricity production 1949 – 2015, from [3]

One pressing consideration is for the development of low-carbon technologies. The impact of carbon dioxide as a greenhouse gas is well documented and scientifically studied, as well as the influence of human activity in increasing the concentration in the atmosphere. Anthropogenic carbon dioxide emissions are sourced from fossil fuels used in a range of industrial and domestic activities, some of the largest sectors include electricity production, transportation, and space heating [3]. Many proposed strategies to reduce combustion emissions focus on increased electrification. This approach has already decarbonised various materials industries by using electricity for processes such as electro-thermal heating, and lead to an increased availability of battery electric vehicles (BEVs) and recharging infrastructure for consumers [4, 5].

The second economic issue is to achieve energy security. Energy has become essential to modern, industrial economies, and so security of this resource is to mitigate the risks in its availability and have control over features like pricing. With the current dependence on fossil fuels comes certain contradictions to this goal, as they are of course a depletable resource, non-renewable with a finite amount available on the planet, as well as certain regional access. This results in a dependence on international trade of fossil fuels, as well as the threat of exhausting supply. Security of energy supply includes policy strategies to transition away from fossil fuels to alternative technologies which include the expansion of renewable electricity generation, nuclear power, and energy storage.

Hydrogen energy, and the hydrogen fuel cell, is proposed as one solution to these issues. Hydrogen fuel ( $H_2$ ) contains no carbon, so mitigates carbon dioxide emissions (at point of use). Fuel cells can be used in a range of consumer and industrial applications, from small scale portable electronics, to vehicular power plants, to distributed electrical supply infrastructure. Hydrogen fuel can also be manufactured with renewable electrical generators, coupling the technologies as an energy storage medium, increasing overall availability and security within these intermittent but “green” energy sources.

### 1.1.2 Hydrogen Fuel Cells

Hydrogen fuel cells are electrochemical energy conversion devices. They extract the chemical energy stored in a hydrogen fuel source and output electrical energy to an external circuit. This is achieved without a combustion reaction, instead using chemical reactions similar to the internals of a battery. Generally, the fuel cell combines hydrogen with oxygen (often from the air) to create water as an exhaust product, as in reaction 1.1:



Several architectures of fuel cell exist; they all commonly consist of an anode and cathode – the electrodes where reactions take place, through which electrons are conducted – and an electrolyte – the ionic conducting solution which connects the two electrodes. The different fuel cell types are distinguished by the electrolyte material. The phosphoric acid fuel cell (PAFC) was the first of the technology commercialised, in the mid-1960s. These fuel cells operate at relatively high temperatures in the region of 150 – 200 °C, which favours use as a stationary generator. Alkaline fuel cells (AFC) are another older form of the technology, developed in the 1960s for usage on the NASA Space Shuttle Orbiter [6]. Molten carbonate fuel cells (MCFC) also have high operating temperatures, and are capable of using methane ( $\text{CH}_4$ ) directly as a fuel source. The high temperature chemistry (650 °C) allows for a form of internal reformation reaction, however carbon emissions are inherent in this usage.

Solid oxide fuel cells (SOFC) are a newer generation of the technology, another high temperature version (600 – 1000 °C) with fuel flexibility – these are capable of using hydrogen, methane, or carbon monoxide (CO) as a fuel source. The polymer electrolyte fuel cell (PEFC) is the current generation of lower temperature fuel cell technology (c. 70 °C), and receives a large proportion of research and commercial attention in recent years [7]. PEFCs also have the flexibility to use methanol ( $\text{CH}_3\text{OH}$ ) as a liquid fuel source, in a reaction which generates carbon dioxide in the exhaust. The lower operating temperature means these systems are strong contenders for use in transport and portable applications. Table 1.1 summarises the differences between these various fuel cell designations.

All fuel cell types are based on the same electrochemical principles, though using different materials, at different temperatures, and different performance characteristics. The fuel cell reaction generates electrons, which travel through the external circuit, and ions, which pass through the internal electrolyte medium.

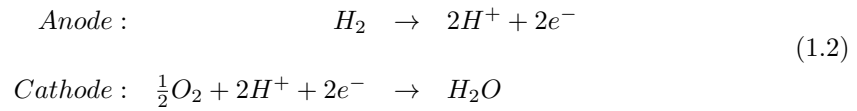
As mentioned, polymer electrolyte fuel cells have been a development focus in the past three decades, both for design and manufacture, application, and economic viability. In addition to research efforts, industrial forerunners such as Arcola Energy [8], Toyota [9], Horizon Fuel Cells [10], and Johnson Matthey [11] have brought PEFC technology to the consumer market. PEFCs will thus be the focus within this research, with further discussion of the technology and applications in the following section.

	PEFC	PAFC	AFC	MCFC	SOFC
Electrolyte	Polymer membrane	Liquid $H_3PO_4$	Liquid $KOH$	Molten carbonate	Ceramic
Charge carrier	$H^+$	$H^+$	$OH^-$	$CO_3^{2-}$	$O^{2-}$
Operating temperature	50 – 100 °C	200 °C	60–220 °C	650 °C	600–1000 °C
Catalyst	Platinum	Platinum	Platinum	Nickel	Perovskites
Main cell materials	Carbon based	Carbon based	Carbon based	Stainless based	Ceramic based
Fuel compatibility	$H_2$ , $CH_3OH$	$H_2$	$H_2$	$H_2$ , $CH_4$	$H_2$ , $CH_4$ , $CO$

Table 1.1: Fuel cell classifications, adapted from [12, 13]

## 1.2 Polymer Electrolyte Fuel Cells

The polymer electrolyte fuel cell (PEFC) is a hydrogen-oxygen fuel cell; it operates with purified hydrogen as a fuel source, and completes the reaction using oxygen. PEFC operation is centred around the polymer electrolyte membrane. This material conducts ionic hydrogen (protons) through its thickness from the anode to the cathode. The anode is therefore responsible for the hydrogen oxidation reaction (HOR) whilst at the cathode is the oxygen reduction reaction (ORR). Equation 1.2 gives these two half reactions responsible for voltage generation in the fuel cell [12].



### 1.2.1 PEFC Construction

The PEFC is constructed of a series of components, assembled as a cell unit, and arranged in a stack. These control the many transfer mechanisms through the fuel cell, and the reactions noted in equation 1.2. For the purposes of working with the PEFC, a good knowledge of the components and their functions is established herein. Each component is discussed; the membrane, catalyst, gas diffusion electrode (GDE, these three components making the membrane electrode assembly MEA), the bipolar plates, and the sealing gaskets. A representation of the stack construction is seen in figure 1.2.

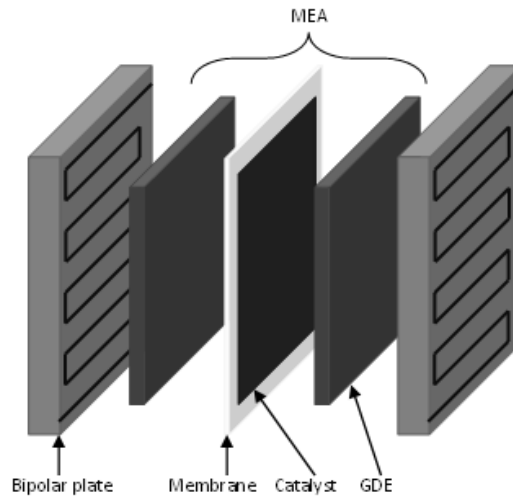


Figure 1.2: PEFC stack components, here as a single cell unit

## Polymer Membrane

The membrane is the polymer electrolyte material for which the PEFC is named. Each individual cell unit in the stack is centred about the membrane. A key requirement for this material is to be chemically stable in the PEFC environments; acidic in the anode compartment, as well as oxidising at the cathode. The modern standard chemical formulation is perfluorosulphonic acid (PFSA) with the most common brand being Nafion<sup>®</sup>, developed by DuPont. Membranes of this chemistry include sulphonic acid groups (SO<sub>3</sub>H), which enable the transport of protons.

To facilitate the ionic transport, the membrane also requires a water content. A dry membrane has much higher impedance due to reduced conductivity, compared to one fully soaked in water [14].

The inherent impedance of the membrane is related to how easily the ions may cross this interface; slower transit reduces reaction mechanics and incurs resistive losses within the fuel cell. The distance the ions must pass has been seen to be the major contributor, so thinner membranes are preferred. Nafion<sup>®</sup> is produced commercially from 200  $\mu\text{m}$  down to 20  $\mu\text{m}$ .

In addition to ionic transfer, the membrane separates the two electrode compartments, and the respective reactant gases. This function requires the membrane to be impermeable to both hydrogen and oxygen. To allow direct mixing would constitute a fuel inefficiency (not involved in the desired reactions) as well as a possible safety hazard due to hydrogen combustion. The two electrodes are also electrically charged, meaning the membrane must insulate current from short circuiting directly between the electrodes and not powering the external circuit.

These separation requirements are somewhat at odds with the ionic impedance consideration; a thicker membrane would be better at separating gases and insulating the electrodes, though would increase resistive losses. Thus some design consideration has been made for membrane thickness, to show good functionality in both regards [15].

## Platinum Catalyst

On the face of both sides of the membrane is deposited a catalyst material. Platinum (Pt) is known to be the best catalyst material for both the HOR and ORR reactions. It is however an expensive metal, so as a compromise between reactive surface area and material cost, nanoparticles are used.

These platinum nanoparticles are supported on carbon structures to ensure good distribution and connectivity. The platinum is also responsible for electronic conductivity to the external circuit, so it must be directly connected to the surrounding charge carriers. Reactions take place at the triple-point between the membrane, catalyst, and reactant gases.

## **Gas Diffusion Electrode**

The membrane is held between two gas diffusion electrodes (GDE). These provide multiple functions within the PEFC. As is suggested by name, these materials must diffuse the reactant gases to the catalyst reaction sites, as well as transport product water away at the cathode, to ensure continued gas access. Thus, the GDEs are porous materials, with hydrophobic properties to aid rapid water transport. As electrodes, the GDEs also provide the electrical conductivity from the platinum catalyst particles to the external circuit. There must therefore be a continuous electrical path through the GDE material thickness.

The GDEs also provide mechanical support to the fragile membrane. The PEFC stack is clamped together to ensure good fit and connectivity between components; the GDE ensures the membrane stays flat and somewhat protected from puncture by other components. Variations in gas supply pressure to each electrode compartment can impinge a force on one side of the membrane, which the GDE would also support to prevent excessive deformation and possible tearing. As with other components, the materials selection for the GDE must be one that can survive in the chemical environments of each electrode compartment.

Thus the GDE materials must meet several requirements for porosity, electrical conductivity, mechanical strength, and chemical stability. Carbon papers and cloths are traditionally used, providing this desirable combination of traits. This is true for both anode and cathode sides of the PEFC.

The combination of these components listed so far – membrane, catalyst particles on both sides, and two GDEs – is considered the membrane-electrode assembly (MEA). This is frequently treated as a single component-of-components in research, and as sold by manufacturers.

## **Bipolar Plates**

The major structural components of the PEFC come in the form of the bipolar plates (BP). These sit external to the MEA, one for each electrode compartment. As before, the BP material must show good chemical stability in the fuel cell internal conditions. Indeed, these components feature a network of channels which define the gas compartments.

The channels are termed flow fields, and are responsible for the large-scale transport of reactant gases around the MEA face. The goal is to have good distribution of concentration and pressure of the reactant gases, as well as removing liquid water efficiently.

Like the GDEs, the BPs continue the electrical conductivity through the fuel cell to the external circuit. The BP material must therefore have high conductivity to avoid a resistive loss.

As the main structure of the PEFC, the BPs are thicker and more robust than the MEA components. However, this can add significant weight to the fuel cell (which is an important consideration in some weight-critical applications). Current technologies use either coated-metals or graphite composite materials for the BPs, showing a good match for all the requirements. These can be from a foil-thickness to several millimetres thick, and contribute less to overall stack weight than bulk materials.

### **Gasket Seals**

With the numerous components in the stack construction there are many interfaces which could cause gas leaks. This is particularly prevalent for hydrogen, being a small molecule, and could introduce a combustion hazard in certain conditions. The leakage of any gas will reduce efficiency because of the loss of reactants.

Seals are included throughout the stack, bounding any gas-chamber, and traditional silicone materials may be used. This soft material will conform to any irregularities in the sealing surfaces, as well as reducing the chance of penetrating the fragile membrane. Silicone also ensures electrical insulation between components, avoiding short circuits. Sealing gaskets are found between each BP and MEA in the fuel cell stack construction.

### **Ancillary subsystems**

To function, the PEFC stack also requires several ancillary subsystems to support its operation. These handle the supply of reactants to the fuel cell stack, the removal of exhaust flows, management of stack temperature, and the delivery of electricity to the application system. Control systems may also be applied, either with an active or passive strategy, to manage operation safely and monitor performance.

The reactant feed system has control component requirements. Pressure and mass flow rates are regulated in most experimental and practical applications, so as to control performance and fuel usage.

The oxygen for the cathode feed can either be from a pure source (bottled or filtered) or from atmospheric air. In this latter case an air compressor will run to ensure pressurisation matches between the two electrode compartments. Using atmospheric air will introduce other gases and compounds however. Nitrogen and carbon dioxide do not affect PEFC performance beyond diluting the oxygen and decreasing stoichiometric (air-fuel) ratio. Certain compounds are known as contaminants for the PEFC component functions; this shall be discussed with degradation topics in chapter 2.

For efficient operation, the electrolyte membrane requires water content to transport ions. Most applications introduce this water through the reactant feeds, by humidifying the gases. Relative humidity is typically controlled to near 100%, based on stack temperature, to ensure full hydration.

Temperature regulation is also important for the PEFC. As has been mentioned, the membrane requires liquid water content to operate, so the stack must be kept within suitable temperature limits. Most PEFCs are rated to operate at 80 °C. The hydrogen-oxygen reaction is exothermic, so larger stacks require designed cooling to maintain temperature. Common solutions include air forced-convection, evaporative, or integrated water-coolant circuits.

The final ancillary system is the power-conditioning unit (PCU) for managing the fuel cell's electrical output. These devices condition the output voltage so that it is suitable for the application. This may be any combination of DC/DC, DC/AC, and AC/AC conversion stages [16].

PCU subsystems will very much depend on the powered system requirements. As such, power electronics are considered lumped with the electronic loading, i.e. the fuel cell electrical contacts are the boundary of the two subsystems. Experimental methods frequently employ simple resistive loads to represent all electrical loading.

### 1.2.2 PEFC Applications

The PEFC is a scalable power source, meaning the same technology may be used for a variety of different applications. The smallest applications are for hand held electronics, where the fuel cell would replace battery power. A PEFC of this scale would output 1 – 100 W. This has the benefit of using refuelling rather than recharging to recondition the power supply, which is significantly quicker, so overall system availability is increased. Examples include hand-held mobile phone chargers.

Larger scale PEFCs can be used for automotive power plants. Similar to the previous, these would replace the batteries in battery electric vehicle (BEVs) powertrain architectures, which in turn is a carbon-free replacement for the traditional internal combustion engine. Automotive applications require sufficient power for drive as well as sub-systems specific to the vehicle architecture, in the order of 10 – 50 kW. Automotive fuel cell electric vehicles (FCEVs) enjoy the benefits of both an electric powertrain and a fuel supplied system to mitigate recharging delays.

Larger still PEFC applications are used in stationary power supply. These systems would output 50 – 200 kW, capable of generating electrical power for a home, or back-up power for essential services such as hospitals or telecommunications. Stationary PEFCs can also be designed

to make functional use of the heat generated in the reaction, which is normally wasted to the environment for movable systems. Such a combined heat and power (CHP) system can achieve 80% efficient useful output based on fuel energy input. In stationary configurations, the PEFC is suggested to replace the standard energy supply or internal-combustion generators (including grid-outage and remote power solutions).

### 1.2.3 Hurdles to PEFC usage

The quoted power scales are examples of standard applications expected for fuel cells. Commercially, the PEFC is yet to see widespread usage. Three hurdles are widely acknowledged to be limiting commercial success; infrastructure availability, system costs, and system durability [17].

Infrastructure includes all motivation around fuel manufacture and distribution. This often amounts to a chicken-and-egg problem, wherein fuel manufacturers are reluctant to invest without a large enough user-base, and consumers reluctant to use fuel cells without the fuel infrastructure. Fuel cell electric vehicles (FCEV) are a key example of this, where only a few geographic locations currently have refuelling stations available. At time of writing, there are 13 hydrogen fuelling stations active in the UK, most found attached to major universities and specific research projects [18].

Cost is a problem rooted in materials and manufacturing. As the PEFC has limited applications at this time, manufacture remains low-volume, and comparably high cost. Economies of scale are expected to come into effect when volume increases, reducing costs. Material costs are also a factor in PEFC manufacture – the platinum catalyst for one is expensive, although research continues to reduce the amount required in each MEA, as well as seeking lower cost alternatives.

Durability is an issue arising from the broad and varied application envelope expected for PEFC systems. Fuel cells typically prefer consistent operation within narrow control boundaries. The nature of micro-portable and transport scaled applications is for transient loading cycles, and performance is expected across a range of global climates.

Focussing on automotive applications – durability criteria are well defined in this regime – FCEVs must perform comparably to battery electric vehicles (BEV) and (perhaps more importantly) conventional internal combustion vehicles (ICV), to gain popular acceptance and increased use. The US Department of Energy have laid out guidelines; 5000 hours total usage, without 10% loss in voltage performance [19]. To date, demonstrator projects exhibit only half of the desired time – the US National FCEV Learning Demonstration has exhibited 2,000 hours of reliable operation [20].

In the pursuit of extending useful functional lifetime a number of approaches may be taken; including improving the fuel cell design, improving the component and material durability, or by applying control strategies to manage performance. This is the topic of this piece of work; investigating control and monitoring strategies to manage system health, and avoid component degradation.

## 1.3 Prognostics and Health Management

### 1.3.1 History of maintenance strategies

In the modern industrial world, there is ever growing demand for performance systems to exhibit a combination of high reliability, resilience, and safety. Reliability is the ability of the system to perform as designed, for a duration at least as long as required; resilience in this context is a tolerance to disruption, for example off-design conditions or (one or more) component faults, while the system can continue to operate satisfactorily; system safety is the condition of managing risk to an acceptable level, avoiding hazards to both user and system. Together, these factors indicate the “health” of a system. Whilst correct system design and usage can contribute to these parameters, developers are increasingly looking to supporting processes and control systems for even greater levels of system health, and its active management.

Maintenance is a well established process to recondition components to performance standard. This is an efficient means of saving against the cost of high-reliability components, whilst gaining benefits of extending lifetime and availability. Maintenance strategies have evolved over time; the most basic approach being corrective repair (after failure). This could be the most expensive approach, as failed equipment might cause damage to other parts of the system and hence more failures. An example would be in typical road repair routines, where surfaces are maintained only once cracks and holes have appeared, despite these potentially causing damage to vehicles in the intervening time.

A more advanced approach is in preventive maintenance. By maintaining equipment before failure, this strategy aims to increase availability and safety. Preventive maintenance tends to follow an inspection schedule to monitor the development of equipment wear at discrete time-points, and perform repairs to avoid failures. Though this approach is more intensive for the monitoring effort, costs can be saved in avoiding system down-time as well as safety violations. Another example is provided; preventive maintenance is largely followed in the civil sector, as failures of buildings or infrastructure would have very significant consequences [21].

Condition-based maintenance (CBM) is the latest strategy development, as an extension of

the preventive maintenance goals. In short, it is an approach to perform maintenance exactly as and when required. The distinction with preventive maintenance is that CBM utilises monitoring and real-time data to detect deterioration of components or performance, and take maintenance actions when it is decided to be optimal, i.e. with minimal impact to availability (downtime), safety, and costs. Thus, an intelligent CBM approach for a fuel cell vehicle power plant may indicate to the user when is best to pursue a service, before a catastrophic failure occurs, or to compliment known usage patterns.

### **Architecture of CBM**

The development of CBM as a unified strategy was developed by an industrial team in the early 2000s. The standard is distributed by the Machinery Information Management Open Systems Alliance (MIMOSA) initiative, as the Open System Architecture for Condition Based Maintenance (OSA-CBM). This standardises maintenance strategies for a wide range of industrial, commercial, and military applications, in defining the information processing and exchange for a CBM software architecture. As proposed by OSA-CBM, the architecture of CBM processes is composed of 7 functional levels:

**Data acquisition** – This first module covers all sensors, transducers, and techniques for capturing information about the observed system. It may also be feasible for the operator to enter basic reference data (date, duration, observation about fault causes of effects). This module outputs raw data to be utilised by the CBM system.

**Data processing** – Live signals from observed systems are often disrupted with noise and interference, which is cleaned through this module. Also, certain higher modules may require specific filtering for data signatures or features, which are processed here.

**Condition detection** – At this stage of CBM, the state of health (SoH) of the system is determined. Different approaches may be used depending on the application, though this is frequently defined by comparing real-time measurement data to expected performance values. The result from this module should trigger alerts based on known safety thresholds.

**Diagnostic** – With faulty condition detected, the next module will suggest which failure mode is occurring. This stage of the CBM process isolates the cause of the performance loss, in terms of a particular component or phenomena which has degraded or failed.

**Prognostic** – This module makes an estimation of the future remaining useful life (RUL) duration, based on the current amount of degradation and the projected future usage of the monitored system.

**Decision support** – This module draws together information from the lower stages. Based on knowledge of operating conditions, SoH, degradation, RUL, and future usage, maintenance actions can be suggested and scheduled. An effective schedule will allow the system to complete its mission, possibly with acceptable levels of degradation if function can be continued.

**Human-machine interface** – The final module of the CBM process is to report to operators or maintainers on current performance and maintenance actions. The human-machine interface (HMI) accepts information from all previous modules.

This OSA-CBM architecture is defined specifically for intelligent maintenance procedures. However, in generalised forms, the definitions laid out can be applied for management of any failure mechanism. Thus, the CBM architecture listed here is proposed to describe processes for prognostics and health management (PHM). PHM is considered more generalised, and can be utilised for monitoring and health management of any system or activity.

In adaptation for PHM use, certain changes are suggested to the CBM processes. The lower five modules are sufficiently defined; sensor suites, feature extraction, models and calculations will all be specific to the monitored system. At process 6, *decision support*, not only are maintenance activities considered, but also control strategies that will adapt operation. Such control actions could restore, mitigate, or otherwise account for degradation to performance. Changes to control strategy could be performed automatically, or presented to the user through the *HMI*, process 7.

### **Data within the PHM application**

The PHM hierarchy standardises how data and information is passed between modules. This means modules can be developed and operated separately, so long as understanding of the overall process interaction is retained.

The power of the PHM application is dependant on the quality of each individual module. For example, the data acquisition stage is where information is introduced to the software. It may be assumed that the sensor suite is able to accurately represent the observed system behaviour. Good quality data will allow for more accurate and useful health indicators, whereas bad information limits how applicable the entire PHM process can be. Similarly, more powerful models in the diagnostic and prognostic calculations will provide the user with more detailed information about the state of the operating system. All of these considerations – quality and accuracy of sensors, models, and processors – must be balanced against system cost, run-time, and functionality to provide a useful PHM solution.

## 1.4 PHM for PEFC Systems

Whilst the research effort toward the development of PEFCs has been significant in recent years, prognostics and health management has seen limited uptake for the challenges of fuel cell control and performance. Of the research works regarding PEFC reliability, few have followed the PHM approach explicitly in their methodology. Publications by the *FC-LAB* research group of Belfort, France have been the main drivers of this discipline, including review publications [22–24] and a focus on prognostic methods [25]. However, some publications from other research studies are seen to contribute to PHM practices, either wholly or in part, and these have been sought as a foundation existing within the topic. The following preliminary review considers each PHM processing layer in turn, as studies frequently exist only within a single area.

It is important to note the definitions and scope of the specific health management processes, as there is often a confusion in literature. For example, the term “diagnosis” is found within some publications which only cover condition assessment practices; this is a misuse of the term diagnosis from the point of view of PHM practices [26]. Elsewhere, literature denoting “estimated lifespan” may describe long term component testing, but falls short of the remaining useful life prediction evoked under prognostics processing. Thus, literature will be grouped correct to the PHM architecture.

### 1.4.1 Data acquisition

The PEFC is a complex energy transfer device. Interactions exist on a full range from molecular scale reaction kinetics at the catalyst to metre scale transfers through the entire stack. Equally, these interactions combine chemical, electrical, thermal, and mechanical domains. Data acquisition covers the wide range of monitoring sensors and characterisation techniques for these various phenomena.

Sensor selections found in experimental literature are often customised to meet the specifications of the research project, the fuel cell scale, and application. A minimal sensor requirement for a small portable PEFC presented by Tüber et al. only utilised power conditioning and hydrogen fuel pressure to control performance, in order to reduce complexity of the overall system [27].

In the maximal case, the Fuel Cells and Hydrogen Joint Undertaking (FCH JU) have established a standard sensor suite for fuel cell test benches, as discussed by Harms, Köhrmann, and Dyck in [28], by Araya et al. in [29], and by Piela and Mitzel in [30]. The recommendation is for the following sensors; temperature, flow rate, pressure, humidity, and purity on cathode and anode, both inlet and outlet; temperature, pressure, flow rate, and purity of coolant flow,

Test	Phenomena	Sources
Current-voltage measurement (polarisation)	Electrical performance	[31]
Electrochemical impedance spectroscopy (EIS)	Electrical losses	[32]
High frequency resistance (HFR)	Internal resistance	[33]
Cyclic voltammetry (CV)	Catalytic area	[34]
Linear sweep voltammetry (LSV)	Hydrogen crossover rate	[35, 36]
Current interrupt (CI)	Internal resistance	[33]
Chronoamperometry	Oxygen crossover rate	[37]
Optical cell	Water management	[38]
Microscopy	Various physical structures	[39]
Neutron imaging	Water management	[40]
NMR spectroscopy	Water diffusion	[41]
X-ray diffraction (XRD)	Catalyst particle size	[42]
X-ray photoelectron spectroscopy	Membrane molecular structure	[43]
Infrared spectroscopy	Membrane molecular structure	[44]

Table 1.2: Characterisation techniques available for PEFC systems.

both inlet and outlet; electrical current and voltage of the entire stack, as well as individual cell voltage. This approach would capture all pertinent variables for detail, though an application system would expect to use a reduced set, to compromise against the volume of measurement data, and costs of transducers and computing.

Further to the sensors for direct variable measurement, there exist an array of techniques and instruments which may be employed to characterise specific features and interactions within the PEFC. Several of these characterisation techniques originate in materials science or electrochemical practice, and feature prominently in the development and validation of new PEFC materials and designs. Examples of the most widely used characterisation tests are listed in table 1.2.

The current-voltage measurement is among the most ubiquitous electrochemical testing techniques, providing an overall evaluation of electrical performance. As electricity is usually the desired output for the fuel cell, it is important to robustly demonstrate capabilities, especially for new innovations. Typically the measurements are made galvanostatically; a current load is applied to the PEFC stack, and the voltage is allowed to settle for the measurement.

Current-voltage measurements are typically made across a range of current demands, to define a full performance envelope, and plotted to define the polarisation curve [12, 13, 45]. A typical polarisation curve can be seen in figure 1.3. An in depth explanation of the current-voltage performance and the form of the polarisation curve can be found in chapter 3.

A great variety of characterisation techniques are available for PEFC test and development, however they have significant limitations in practical applications; generally one or more of cost,

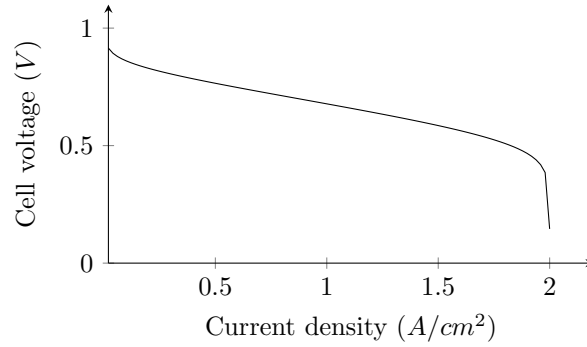


Figure 1.3: A generic polarisation curve for PEFC

transportability, reliability of measurement, and interrupting fuel cell use.

Costs are usually associated with the extra equipment necessary to undertake the characterisation procedures. Many of the spectroscopy tests require signal generators and analysers, which are large pieces of equipment for full-scale PEFC stacks.

The additional equipment is also a consideration toward the transportability of the characterisation technique. Obviously these are limiting for the non-stationary PEFC applications, including hand-held and automotive, where the size and weight of the system is at a premium.

Reliability of the measurement is an important consideration for the accuracy of the health management analysis; as mentioned previously, good quality data will lead to good quality health assessment. Unreliability can be introduced by new design complexities, such as transparent materials in optical cells. Measurement accuracy can also be balanced against complexity; techniques such as CI, HFR, EIS and current-voltage all provide similar information with different levels of investment.

Many of the tests are also identified as obstructive to the normal operation of the fuel cell. This may be to apply a specified electronic load profile, change the gas supply to the electrode chambers, or even deconstruct the stack. Such procedures would negatively impact the availability of the PEFC, and whilst the tests would provide detailed degradation information, they may be considered unacceptable for the mission profile or the user's expectations.

It is the view of the author that these detrimental consequences of characterisation tests should be avoided as much as is reasonable, to increase the applicability of the proposed PHM system. Commercial success will be easier to achieve if the system cost is not compounded by monitoring sensors and equipment, and the overall system availability is increased, not impaired by performing test procedures. Characterisation tests will continue to be useful in development and validation however.

### 1.4.2 Data processing

The data acquisition techniques identified will provide a stream of data from the target PEFC system. In order to achieve useful analysis, this data should be processed to extract the relevant information. The choice of techniques for data processing will be closely related to the processing performed in higher layers of the PHM structure. Generally, the data processing will fall under one of four categories; signal processing, feature extraction, model fitting, or statistical treatment. These techniques typically bear the limitations of the data acquisition approaches they are associated with.

Signal processing covers a collection of techniques that extract frequency-domain information from the data, which is otherwise difficult to discover within the raw time-domain. Within PEFC literature, two signal processing techniques are identified; fast Fourier transform (FFT) [46] and wavelet transform (WT) [47]. Signal processing techniques can be limited however by poor applicability to non-stationary signals.

Feature extraction techniques exhibit the greatest variety and dependence on characterisation tests, and the requirements of higher processing. One example is the current-voltage measurements established previously. Plotting these measurements as a series of polarisation curves through the lifetime of the system, the evolution of system health can be observed in the changing curves [48, 49]. Feature extraction also includes image processing methods for the optical and microscopy tests. The limitations of this technique will follow those of the image capturing technique, such as only applicable to visible faults [50, 51], or by being destructive to the component material [52].

Where models are to be used for detection and diagnostic processes, the measured data can be fit to the empirical model parameters. This can be followed for current-voltage relationships [53, 54] and EIS testing [55].

Statistical treatments are used when there seems to be a correlation between the measured variables. A simple statistical correlation is used by Zeller et al. in [56] to fit randomised model parameters to measurement data. Principle component analysis (PCA) is another correlation technique, which seeks trends between multiple data variables and the performance indicator. PCA is employed in [57] to discover which system variables most influence PEFC voltage performance.

### 1.4.3 Condition assessment

Condition assessment, also known as fault detection, is the processing layer for recognising that a problem has occurred in the target system. This is typically accomplished when a particu-

lar variable has departed from an expected value or range. This is summarised as two main approaches; empirical thresholds, or model-based behaviour prediction.

Empirical thresholds are defined when the allowable range for a given variable is known, and thus a measurement or feature which has deviated will indicate a fault. Examples include a voltage loss threshold defined by Lebreton et al. which triggers an alarm for performance loss [58]. Also, Bosco and Fronk detail a detection method for water management issues, by comparing pressure values to acceptable thresholds [59]. This will trigger an alert and lead to corrective actions by the control system. Both are simple, single parameter strategies, which rely on predefined values for the thresholds of unacceptability for the particular system.

Models of PEFC system behaviour can also be used for fault detection. The model predicts performance under healthy conditions, the comparison between the prediction and measurements generates a residual, which defines system health state, this approach is followed in [54, 60, 61]. These models only need to represent normal healthy behaviour, and the scale of the residual indicates the severity of performance loss.

In most instances, voltage is considered the primary performance measure [62]. All examples of PEFC applications are primarily electrical generators, with additional useful heat being of secondary concern.

#### 1.4.4 Diagnosis

Closely linked to the process of condition assessment, fault diagnosis is used to isolate the cause for the observed performance loss. In the case of PEFC, this will be one or more of the internal components degrading and failing to provide their normal functions. In general there are two classes of diagnostic techniques in PEFC literature; model-based, or data-driven.

Model-based diagnosis, similar to the fault detection method, acts by generating residuals between the measured performance and modelled behaviour. As an extension of the previous process, further analysis is performed to correlate the residuals to a specific fault. This may be achieved through a multi-variable approach, where residuals for many measurements define a unique signature for each considered fault condition [63].

An alternative approach is to model the abnormal behaviour of the system, and use model fitting to identify which parameters are responsible for the observed degradation. Hernandez et al. combined flow dynamics with electrical modelling to generate a complicated model for diagnosing two states of water management problems [64]. This illustrates the difficulties of fault modelling for the PEFC processes; the more fault states considered, the greater complexity of the model. Any model-based diagnostic approach is potentially limited in effectiveness by the

number of fault phenomena which may be robustly diagnosed within the scope of the model.

Data-driven approaches are empirically defined based on historic observations of fault occurrences. These methods use artificial intelligence (AI) to pair the recently observed system performance with a matching dataset which represents a known fault condition [24]. Neural network (NN) [65], fuzzy logic (FL) [61], and Bayesian network (BN) [66] are techniques which can classify data into similar groups, through learning the prior data. Similar to the limitations of model approaches, data-driven diagnosis is somewhat limited by the volume of historic training data about faults. Whilst an unmatched fault observation would define a new dataset, the responsible fault would need to be defined a posteriori.

#### **1.4.5 Prognosis**

Prognostic techniques, for predicting future performance and remaining useful lifetime (RUL), are mainly absent in PEFC literature. These techniques operate similar to the AI data-driven diagnostic approaches in learning from the previous performance trends, and extend this by projecting forward to approximate RUL. An adaptive neuro-fuzzy inference system (ANFIS) is found in works by Vural et al. [67], Becker and Karri [68], and Silva et al. [69]. The ANFIS approach combines the techniques of neural networks and fuzzy logic to learn information about a dataset. In these publications, the input dataset is a combination of system functional parameters (temperatures, pressures, current, etc.) and the ANFIS outputs a voltage prediction.

In [70], Jouin et al. presents a framework for prognostics of PEFCs using particle filtering (PF). This is a signal processing approach to estimate the state of health of the system, as well as quantifying the confidence of the RUL prediction.

#### **1.4.6 Decision support**

Decision support is not well represented in PEFC literature. Bosco and Fronk [59] present the most complete strategy for corrective actions following a water flooding fault detection approach. Once the alert for unacceptable pressure-differential is observed, the control system makes an automated corrective action to dehumidify the reactant gas feeds, and allow the PEFC to recover performance.

#### **1.4.7 Human-machine interface**

No research specifically detailing PHM interfaces are found in PEFC literature, for the general users of application systems. Institutions are inclined to design customised HMIs for in-house test benches, and their own specific requirements; such examples which are presented are by Hua

et al. [71] and Ziogou et al. [72]. These would be significantly different to those expected for application systems. A researcher expects measurement data, performance histories, and high levels of manual control, but this would not be suitable for the “ordinary” user.

## 1.5 Summary

Fuel cells are a range of technologies which can support the transition to a low-carbon, hydrogen energy economy. PEFCs have application opportunities across a range of functions, with portable and transportation systems expected to have the greatest viability for commercial success. These application areas are also expected to have a broad variability in operating conditions and therefore the greatest need for health management processes.

PHM architecture provides a standardised approach to deliver this health management, and enhance lifetime performance. Within existing publications, the lower processing layers are most well represented, with data acquisition, processing, and fault detection processes commonly used in PEFC system demonstrations and component development. Diagnosis and higher processes are less well represented, often with methods focused on singular fault conditions. Also, there is to date a reliance on specific testing events to characterise problems.

Thus there is scope to develop a control system which can provide online and real-time diagnosis for multiple PEFC component degradations, foregoing the need for characterisation tests.

## 1.6 Research Objectives

The main aims of this thesis will be to develop health management techniques for PEFCs, specifically fault detection and diagnosis. This will be accomplished through the following objectives:

1. Gain an understanding of PEFC durability issues, namely component degradation under different operational conditions.
2. Establish the state of the art of fault detection and diagnosis for PEFC systems existing in the literature.
3. Based on the literature;
  - (a) develop a fault detection process to characterise the state of health of the target PEFC system.

- (b) develop a diagnosis process to isolate the fault responsible for any observed performance loss.
- 4. Validate these health management processes with experimental testing of a representative PEFC system.

## 1.7 Thesis Layout

The remaining content of this thesis is as follows:

### **Chapter 2** – Durability and Health Management – Literature Review

Knowledge and understanding of the durability and component degradation issues for PEFC stacks is outlined. Following this, a review of the current literature regarding methods for fault detection and diagnosis of PEFCs is presented. This establishes the techniques used in the following chapters.

### **Chapter 3** – Detection System

An electrochemical model of PEFC current-voltage behaviour is developed. This will enable fault detection and condition assessment of the observed system.

### **Chapter 4** – Diagnostic System

An expert knowledge fault diagnostic approach is developed. This collates the expert knowledge available regarding PEFC component degradation and failure.

### **Chapter 5** – Experimental Methodology

A description of experimental work that is to be followed to validate and assess the functionality of the detection and diagnostic systems is presented.

### **Chapter 6** – Validation Test Results

Results of the validation testing are presented and the outcome of the health management processes are discussed.

### **Chapter 7** – Conclusions and Future Work

This chapter reviews the contributions of the work, and the options for further developments in future research.

## Chapter 2

# Durability and Health

## Management – Literature Review

Voltage has been established as the main performance criteria for PEFCs, both in terms of useful output for the application system, and for the performance targets defined by the US Department of Energy in [19]. For vehicular fuel cell systems, lifetime durability is aimed for 5000 hours before a 10% loss in voltage. PEFCs are as of yet unable to present the lifetime performance required, due to degradation of the system components under design and off-design operating conditions. The first section of this chapter presents the range of degradation and failure mechanics known in the literature. Understanding the degradation phenomena and the conditions which cause them is an important first step toward developing the health management processes.

In the following section, approaches to fault detection and diagnosis within fuel cell literature are reviewed. This builds upon the preliminary review presented in section 1.4. The review will follow the classification framework devised by Venkatasubramanian et al. [73–75]. Namely, this shall divide model and non-model based techniques, and further classify different approaches beyond this. The review will lead to the opportunities for this thesis to contribute to the field.

### 2.1 PEFC Fault Mechanisms

Chapter 1 introduced the components which make up the PEFC; the membrane, catalyst particles, gas diffusion electrodes (GDEs), bipolar plates (BPs), and sealing gaskets. Each of these components have their own functional contribution to the fuel cell voltage generation reaction. They also therefore suffer their own fault modes which limit their functionality, leading to a loss

in performance. All degradation to the functionality of a component will reduce its contribution to voltage generation in the PEFC reaction. The normal operating conditions for a PEFC system will be defined to minimise component degradation; off-design conditions which cause accelerated degradation effects will be identified in this review.

### 2.1.1 Polymer membrane

Degradation and failure of the polymer membrane can be categorised primarily as either mechanical, chemical, or thermal. Whilst the Nafion<sup>®</sup> membrane can be very thin (as little as 20  $\mu\text{m}$ ), the tensile strength and puncture resistance is found to be satisfactory for contemporary PEFC usage [76]. A mechanical fault considers any loss of the structural integrity of the membrane, and a failure to separate the anode and cathode gas compartments.

Mechanical issues are most often introduced during the fabrication of the membrane electrode assembly (MEA), where folds, pinholes, tears, or cracks can cause early-life failure [76]. Mechanical stresses can also be introduced in the PEFC stack construction, where the contact pressure of the BP flow fields and sealing gaskets may be non-uniform across the MEA. Improperly installed membranes can suffer pinching or shearing forces between the other components in the stack [77].

Temperature and humidification during the PEFC lifetime are also contributors to the membrane mechanical stresses. With greater or lesser water absorbed into the membrane, it will swell and shrink, and can significantly change in dimension [78]. As these parameters cycle through use (for example, daily usage patterns of a fuel cell vehicle), fatigue stresses can propagate to full membrane failure.

Chemical degradation of the membrane is associated with a chemical attack of the molecular structure by free radical species [79]. Hydroxyl ( $\cdot\text{OH}$ ) and hydroperoxyl ( $\cdot\text{OOH}$ ) radicals are the main perpetrators in the PEFC chemistry; they are produced through partial completion of the hydrogen-oxygen reaction [80]. The radicals react with the polymer chains and cause them to “unzip” or depolymerise. The membrane will thin, leading to perforation and ultimately failure.

The radical formation is generally understood to occur at open circuit loading conditions, when hydrogen more readily permeates the membrane when the fuel cell generation reaction is inactive [81]. The hydrogen that crosses over the membrane is in direct presence of the cathode oxygen and the radical species may form. Therein, the radicals readily react with the Nafion<sup>®</sup> membrane.

Thermal decomposition is the third means of the polymer membrane breaking down. This only occurs at temperatures in excess of 400 °C.

Chemical and thermal degradation of the PEFC membrane can be monitored through fluoride release in the exhaust gas flow. Degradation of the polymer chain causes this loss of fluorine. The rate of release involves periodically collecting the effluent water from the PEFC, and testing for fluoride ion concentration using ion chromatography [82]. This chromatography method separates the chemical constituents based on their ionic charge, isolating the amount of fluorine in the water sample. This measurement is largely a lab-based approach however, and not necessarily suitable for in-situ monitoring on board a vehicle.

The main indication of total membrane failure – whether mechanical damage, or as a final result of chemical or thermal degradation – is free gas crossover between the two electrode compartments [83]. This is directly opposed to the membrane’s function to separate the fuel and oxidant gases. Crossover may be detected where pressures are different in either electrode compartment, or from concentrations of heat where the oxygen and hydrogen are reacting directly. These hotspots can accelerate localised membrane degradation, increasing the size of holes in a self-propagating manner [84].

### 2.1.2 Platinum catalyst

For efficient use of the expensive platinum catalyst material, nanoparticles are used to leverage as much electrochemically active surface area as possible. Degradation of the platinum catalyst may be through particle ripening (growing in size), migration, loss, or poisoning. The result is a loss in overall active area [85].

Nanoparticles have a relatively high surface energy; this is the energy of atoms at the surface of the material, and it is thermodynamically unfavourable (bulk materials are more stable). Because of this high surface energy, the nanoparticles will form larger particles [77]. Mechanisms for this include; particle migration, whole particles moving closer together; or Ostwald ripening, in which platinum atoms diffuse from one nanoparticle to another [52].

The catalyst nanoparticles can also be rendered ineffective by detaching from the MEA structures. The particles may remain locally within the MEA, but with no electrical pathway to the external circuit, or be lost entirely from the stack in the PEFC exhaust. This fault can be detected as powdered remains of the catalyst MEA layer after dismantling the fuel cell stack [86].

The platinum catalyst can also suffer chemical poisoning. Carbon monoxide (CO) bonds strongly with platinum, blocking the surface from the electrochemical reactions [87]. The CO may be introduced to both the anode and cathode gas streams. Hydrogen which has been manufactured through hydrocarbon reformation can carry some of this remnant of the carbon fuel precursor, whilst atmospheric air can be contaminated with CO, particularly in urban

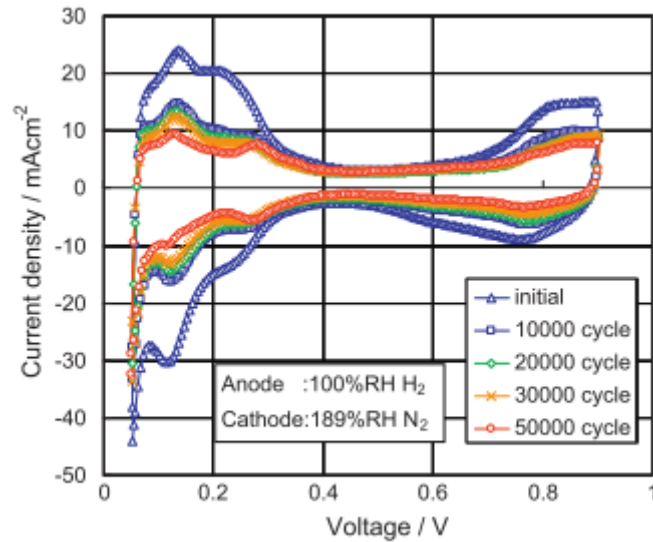


Figure 2.1: Cyclic voltammogram result, from [90]

environments, where CO is an emission from existing fossil-fuel vehicles.

Platinum catalyst nanoparticles can be visualised in lab-based scanning electron microscopy (SEM) [88] and transmission electron microscopy (TEM) [89]. Both these methods use electron beams as a source of illumination, as opposed to light photons, to achieve greater resolution in the imagery. Catalyst particles can therefore be directly observed for size and distribution, and comparing images across the life of the PEFC, the particle migration and ripening can be monitored.

Electrochemical active surface area can be characterised through cyclic voltammetry (CV) [90]. In this technique, a voltage source is applied to the PEFC, whilst the anode and cathode are fed with hydrogen and nitrogen respectively. The voltage is then swept back and forth across a range, and the current response is monitored. The resultant plot is a representation of the relative catalytic activity. Further tests can be compared throughout the PEFC lifetime to reveal any catalyst degradation, as in figure 2.1 where the graph bounded area decreases. This method monitors the effects of catalyst degradation, but cannot distinguish between the different mechanisms.

### 2.1.3 Gas diffusion electrode

The gas diffusion electrode (GDE) is the porous support layer for the catalyst and membrane layers of the MEA, typically made of a carbon paper or fabric material. As a carbon material this can suffer corrosion through oxidation, forming carbon dioxide ( $\text{CO}_2$ ) or carbon monoxide (CO). Carbon corrosion is seen to occur under fuel starvation conditions, where the carbon is consumed to maintain the PEFC reaction [91]. Corrosion will lead to a loss of material in the

GDE, possible problems with electrical conductivity as well as mass transport of gasses and water. Carbon monoxide can also affect the platinum, as mentioned previously.

Carbon corrosion is detected through the gaseous emissions in the exhaust of the PEFC [92]. Gas chromatography separates the constituent compounds by mass, to reveal the amounts of CO, CO<sub>2</sub>, and water [93]. Alternatively, the simpler nondispersive infrared spectroscopy (NDIR) can be used to indicate the relative proportions of these exhaust gases [94].

#### 2.1.4 Bipolar plates

Bipolar plates (BPs) are exposed to both the highly reducing and highly oxidising environments within the PEFC, so chemical stability under both conditions is a key requirement, and corrosion is a key degradation consideration. BPs are generally more than capable of handling the mechanical loads in the PEFC, so the structural requirements are of less concern than the electrochemical requirements. Corrosion mechanisms depend strongly on the material of choice for the BPs; either carbon composite materials, or metallic BPs are seen in PEFCs.

Carbon-based plates are seen to have good stability in the chemical environments of the PEFC. However, as for the GDE materials, fuel starvation can promote carbon-corrosion. It is however highly likely that the GDE materials will corrode before the BPs [95].

Metallic BPs are desirable for the cheapness of the materials and ease of manufacture; metals such as titanium, aluminium, and stainless steel. However, in the cathode environment, these metals will oxidise, forming a layer with high electrical resistance. This would greatly reduce the electrical performance of the stack [96]. In the acidic anode environment, corrosion of steel materials can lead to contaminant depositions across the MEA [97]. These contaminants can lead to several types of loss mechanism, including decreased reaction kinetics, increased resistance, and problems with fluid transport [98]. Iron cations also greatly encourage radical formation and Nafion<sup>®</sup> chemical breakdown.

Degradation in the bipolar plates can be observed visually when the stack is dismantled; surface pitting and discolouration being signs of corrosion or oxidation respectively [99]. Increased electrical resistance can be detected through electrochemical impedance spectroscopy (EIS) [100]. When performing EIS, a small voltage perturbation is applied to the PEFC, and the resultant current response is characterised to discover different aspects of the fuel cell's internal resistivity. EIS is quite detailed and can be used to measure a great number of fuel cell performance characteristics [64].

### 2.1.5 Sealing gaskets

Seals within the PEFC construction ensure the reactant gases remain in their respective electrode compartments. Silicone is a popular choice [101]. This material is generally stable in the electrode chemical environments, however long-term contact with the acidic Nafion<sup>®</sup> polymer material can lead to silicone decomposition. This breakdown has been observed at both electrodes of the PEFC, with the silicone accumulating in the GDE and catalyst layers [102]. This resulted in a propensity for water building up within the GDE (water flooding is discussed in the following section). Degradation of the silicone in this way is observed largely through visual inspection.

### 2.1.6 Water management

Water management is an important factor of PEFC performance, which is related strongly to operating conditions more than to a specific component. Nafion<sup>®</sup> requires a water content absorbed into the material to enable the ionic transfer; a dehydrated membrane will exhibit significantly lower proton conductivity. Excess water in the PEFC in contrast can flood the GDE pores and block the gas diffusion to the reaction sites, resulting in localised gas starvation. Some PEFC systems use humidification to maintain proper hydration of the membrane [103], though the water which is generated internally by the hydrogen-oxygen reaction can also contribute [104]. Both of these water management issues are tied to the system temperature, humidity in the gas streams, and the reaction product itself.

Poor water management can be characterised using the current-voltage and EIS techniques mentioned previously. Flooding will limit the maximal current which can be sustained [98]. Dehydration will instead increase the resistivity of the membrane [105]. Figure 2.2 shows the EIS results for both of these effects; dehydration giving a step-increase in the resistance measurement, flooding greatly limiting the range of the plot [54].

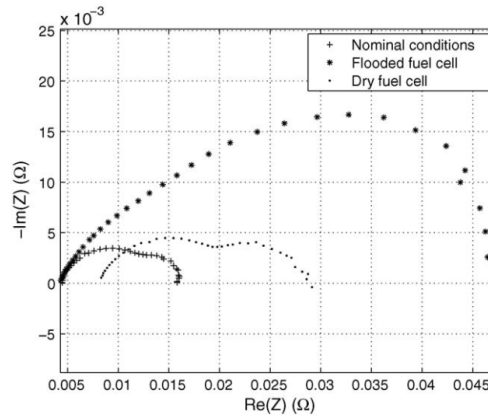


Figure 2.2: EIS results for water management problems, from [54]

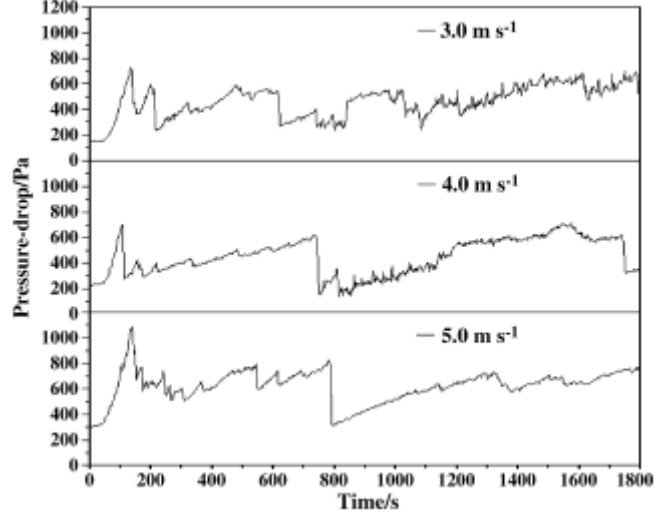


Figure 2.3: Fault detection based on pressure change, from [107]

## 2.2 PEFC Condition Assessment Techniques

As introduced in chapter 1, condition assessment is the process by which the state of health of the observed system may be determined. This is typically accomplished when a particular variable has departed from an expected value or range, either through an empirical threshold, or a model-based approach.

### 2.2.1 Empirical threshold fault detection

Threshold based fault detection is among the more simple techniques. Single variables can be compared to known values of allowable performance, and high, low, or deviation limits. As the useful PEFC output, perhaps the most important threshold definition is for stack voltage. A lifetime target for transport PEFC systems has been set by the US Department of Energy for 5000 hours of operation with less than 10% loss of voltage performance compared to start-of-life [19]. This value is accepted as a working target for most vehicular PEFC demonstrations.

Pressure differential across the cathode is a common fault detection parameter. He et al. [106], Bosco and Fronk [59], and Ma et al. [107] use this variable as an indication of water build up within the fuel cell. In all cases the pressure differential  $\Delta P$  is a calculated value, by subtracting the outlet pressure from the inlet pressure, and a threshold for the sudden decrease which is the indication of the fault event. This pressure change can be clearly seen in figure 2.3, for 5  $\text{ms}^{-1}$  flow rate at 800 seconds. Ma et al. complimented the  $\Delta P$  measurement with a transparent cell to visually confirm the presence of liquid water.

One safety critical fault for the PEFC system as a whole is for hydrogen leakage. Hydrogen

can form an explosive atmosphere if mixed with air in the correct quantities (4 – 75% concentration) and so ventilation and leak detection is an important design requirement. Ingimundarson et al. [108] present thresholds for hydrogen sensor outputs, adaptable depending upon the ventilation availability. Detection of hydrogen leakage should be tied to a user alarm and potentially automatic shutdown control actions.

Empirical thresholds can also be applied to the results of characterisation tests. In [36], Cooper presents a linear sweep voltammetry test for membrane hydrogen permeability within the PEFC. A threshold for current density is proposed to define increased crossover rate and membrane end-of-life. This approach uses additional equipment to perform the test; an external source of power, and an alternative inert gas supply to the cathode. These extra pieces of equipment would not ordinarily be carried with the target system, so the author suggests testing after initial cell assembly, and periodically through the system lifetime. This approach may be suitable for steady-loading or stationary PEFC systems, where characterisation testing can be easily scheduled and results tracked, however more variable transport systems will not benefit as effectively.

Electrochemical impedance spectroscopy (EIS) testing is identified as a popular characterisation test in PEFCs, and shall be seen for both detection and diagnosis processes. For example, Hissel et al. drew measurements out of EIS testing to describe the limits of the spectra [109]. Fuzzy logic was then applied as a clustering tool to group similar residual values as either a healthy or faulty condition. The technique was effective at characterising steady-state conditions, however some values were unassigned as the stack transitioned between states. This method is also reliant on the EIS technique, including the time duration for testing and the equipment required (an external power source and signal generator/analyser).

Mench et al. describe a novel technique for detecting water distribution in the PEFC [110]. Using gas chromatography as a characterisation test, the composition of the anode and cathode gas streams could be analysed. Where excess water content was found – above a threshold set for the gas stream capacity – flooding events were found to be more likely. This technique was found to be effective for online application (whilst in operation), whilst the fuel cell was in use, however it does require a gas chromatograph as well as alternative gas supplies for calibration.

In [50], Tüber et al. apply a threshold to the current output of the PEFC as a condition assessor, again for flooding. The excess water would block the flow channel and cause a sudden decrease in the current which could be supported by the fuel cell. This method however has limited applicability directly to full scale systems; a very simple PEFC design with only 2 flow channels is tested. Here, the water flooding has a large effect on performance. Larger scale

application systems typically feature many gas flow channels to mitigate the fuel starvation effects seen in this publication.

## 2.2.2 Model-based fault detection

Fuel cell models exist in the literature for a range of parameter approaches and applications: simple electrochemical models for design [111, 112], empirical models which are fit to existing performance [49, 113], flow dynamic approaches within the gas diffusion media [114, 115], full system-scale simulations [116]. For fault detection purposes, the model can be used to fit measurement data and extract parameters, or provide a representation of healthy performance against which measurements can be compared.

In [54], Fouquet et al. fit EIS test data to an electrical equivalent model, as in figure 2.4. These models are useful representations of the electrical domain of the PEFC in isolation. The components in the model represent the different impedance effects found in the EIS;  $R_m$  is the ohmic resistance of the membrane,  $R_{ct}$  is the polarisation resistance of the cathode reaction,  $C_{dl}$  is the double layer capacitance of the electrode/electrolyte interfaces, and  $Z_W$  is a Warburg element, which represents mass transport and diffusion. Relative change of the values assigned to each of these parameters indicates faults with the electrical function of the PEFC. Of course, this method is again less desirable because of the requirement for EIS equipment and test events; over 150 spectra were recorded for this publication.

Hernandez et al. present a novel take on the electrical equivalence model in [64], which includes model parameters representing gas fluid dynamics in addition to the electrical performance of the stack. The model has been validated experimentally to show a good representation of the system dynamics. The residuals generated from the model for gas pressure and stack voltage are used to detect faults in the gas flows associated with flooding. The detail in this model enables its use for diagnostics, though this has not yet been completed.

Hissel et al. present a model of the current-voltage behaviour of the PEFC enabled using

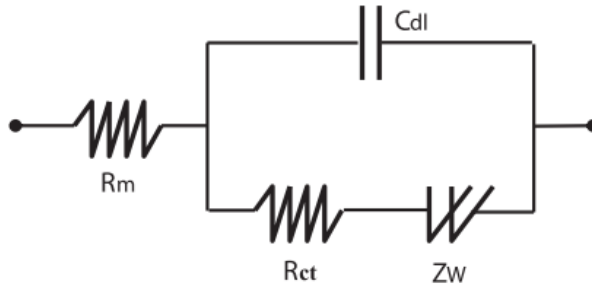


Figure 2.4: Generalised electrical equivalent model, from [24]

fuzzy logic [61]. This method uses inexact set boundaries to define how close the observed performance is to the expected values. The calculated residual, or “satisfaction rate”, has a narrow threshold to define the healthy condition. This approach is effective in usability of the condition assessment output, with one threshold true across the full current-voltage envelope.

## 2.3 PEFC Diagnostic Techniques

Closely related to the condition assessment and fault detection process, fault diagnosis is used to isolate the cause of the performance loss observed in the system. PEFC performance loss will be due to degradation of components within the stack construction, and the nature of the damage will be influenced by the operational conditions. Reviews exist in the literature, with diagnostic approaches being generally classed as either model-based [23] or data-driven [24]. Rule-based diagnosis is another classification defined by Venkatasubramanian et al. [75], though with much fewer applications in PEFC diagnosis, as shall be seen.

### 2.3.1 Model based fault diagnosis

The model-based diagnostic approaches are very similar to the initial fault detection process; residuals are calculated between the observed system and a model of healthy conditions. In the more detailed approach of diagnosis, a *fault signature* must be discovered, as a unique set of residuals for each fault phenomenon. These may be present as different value ranges, or residuals associated with entirely different sensors.

The diagnostic approach presented by Zeller et al. is one of parameter fitting and identification [56]. An electrochemical model equation is used to represent the current-voltage relationship, and the model parameters are fit to data from current-sweep tests. During the lifetime of the PEFC, as components degrade, the values of the associated parameters will degrade accordingly.

The EIS fit electrical equivalence models as seen previously can also be used in a parameter identification approach. Similarly faults may be diagnosed based on the relative change of the model parameters through the lifetime operation. Works by Fouquet et al. [54], Asghari et al. [117], Narjiss et al. [118], and Legros et al. [119] use electrical equivalence models for diagnosis. Typically these are used for water management problems – flooding or dehydration – however, Asghari et al. also investigated the effects of clamping force in stack assembly. In [118], Narjiss et al. are developing the integration of the signal generator equipment with the DC/DC power converter; as such, no additional equipment would be required for EIS tests, and this would greatly increase the availability of this approach.

In [120], Vasilyev et al. propose a bond graph approach to PEFC diagnosis. This modelling technique is useful for simulations of different physical domains in a single model; electrical, chemical, thermal – as found in PEFC systems. This generates residual signatures, termed “analytical redundancy relations”, against combinations of sensors from the target system. This method is promising for the comprehensive simulation of PEFC operation.

A diagnostic technique based on state space modelling is present by Aitouche et al. in [121]. This approach uses a simplified version of the electrochemical equations of PEFC performance. Residuals are generated by comparing the measured quantities with their mathematical representation in the model. Residual signatures are defined for four system faults in the ancillary subsystems. Parameter thresholds are adaptive to increase robustness of the diagnostic for acceptable variations in the PEFC system.

### 2.3.2 Data driven fault diagnosis

Fault diagnosis by a data-driven approach is mostly concerned with pattern-matching against historic observations of faulty operation. The intention is to describe various system states by unique data sets or features. These methods are frequently dependent on the volume of data or knowledge which is available for the target system; only previously experienced faults can be diagnosed with no theoretical basis.

One family of techniques to achieve pattern recognition is the use of neural networks (NNs). These artificial learning systems must be supplied with good quality data to train their description of the PEFC process. Shao et al. utilised NNs to diagnose four different system faults, including failure of the polymer membrane for hydrogen crossover [122]. This method could successfully diagnose the different events with over 90% accuracy, using only sensor measurements directly available from the PEFC system.

Fuzzy logic is another computational tool which mimics nature and human understanding. Fuzzy logic has been used for pattern-matching through a clustering approach [123]. Zheng et al. utilised their expert knowledge to define which EIS measurement features would provide the diagnosis, and could output the result as linguistic terms “young”, “middle aged”, “old” for ease of understanding. The fuzzy logic approach was found to be advantageous for combining a complex system with human knowledge, and easy interpretation of results.

An alternative diagnostic approach is to follow statistical analysis. Bayesian networks (BNs) provide a probabilistic tool for dealing with the diagnostic problem; uncertainty, decision and reasoning. In [66], Riascos et al. use BNs to diagnose fault conditions across the PEFC system, using readily available sensor measurements such as voltage and temperature. Wasterlain et

al. also used BNs in [124], to diagnose faults based on EIS measurements. Both of these investigations required significant amounts of prior data to populate the trending databases for the networks.

### 2.3.3 Rule based fault diagnosis

An alternative use of historic observations in fault diagnosis is through expert knowledge of fault states. This is typically a qualitative approach, as befits the nature of the human-expert interpretation of different variables [125]. Indeed this diagnostic technique is similar to approaches in the medical field. Such examples are the treatment of “high blood pressure” as a linguistic variable in [126], a diagnosis tool for speech impairment in [127], and the rules approach to classifying patients’ disorders in [128].

Extended to the health management techniques in engineering and technical fields we find a framework defined by Isermann in [129], and such examples as a rule based approach to fault diagnosis in an internal combustion engine in [130], or a power transformer in [131]. These approaches share a commonality in using fuzzy logic to codify the linguistic terms and reasoning provided by the expert diagnosticians. This provides an advantage for easy interpretation by developers and users to understand the diagnosis system function and outputs. It also means diagnostic information can be quickly compiled from experienced individuals (or historic test records [131]) even when vagueness is inherent in the knowledge.

Only one example of a rule based diagnostic approach is found in the PEFC literature. The method presented by Zheng et al. in [132] uses fuzzy logic in the diagnosis of water management problems in a PEFC; flooding and dehydration. This example uses fuzzy logic in two applications. Firstly as a clustering algorithm applied to historic test data to identify the features of the EIS analysis which relate to the different fault states, as has been discussed previously in relation to [123]. Secondly, fuzzy logic and a rules base of expert knowledge is used to perform the diagnosis classifications.

This method is found to be advantageous for the complex PEFC system where limited human knowledge is available, for effective handling of the inexact nature of the PEFC fault conditions, and for providing the high level of interpretability for the researchers. However, the diagnosis remains limited to only the two water management problems, and is reliant on the EIS testing to provide the input features.

## 2.4 Summary

This chapter has reviewed existing literature detailing durability issues for PEFC components, as well as condition assessment and fault diagnosis techniques used in their detection and isolation. Degradation of the fuel cell components ultimately leads to the loss in output performance that is seen in durability studies and application system case studies. Whilst set operating conditions have been defined to maximise component durability and system performance, off-design conditions are observed to accelerate the degradation phenomena and reduce lifetime.

The polymer electrolyte membrane may be damaged through mechanical stresses, chemical attack from radical species, or thermal breakdown of the Nafion material at extreme temperatures. Under these modes the membrane will lose ionic conductivity, increasing resistance and decreasing PEFC performance, and ultimately fail when integrity is lost and the reactant gases can mix directly. The platinum catalyst nanoparticles are observed to dissolve and migrate due to voltage effects, decreasing the availability of reaction sites within the MEA. The carbon materials used in the GDE layers can be corroded by the harsh conditions within the electrode gas chambers, and lose material.

Bipolar plates can also be corroded, through different mechanisms depending on whether metallic or composite materials are used, though the net effect is to increase the PEFC internal resistance. Sealing gaskets are generally stable, compared to the other PEFC components, though they too can become corroded from contact with the membrane material. The final degradation modes observed in the PEFC are related to the management of water content both in the MEA and the reactant gas streams; too little and the membrane becomes dehydrated and loses ionic conductivity, too much and the gas pathways can become flooded and induce localised reactant starvation.

Understanding these modes, their influencing conditions, and their effects to the PEFC performance is important to be able to design the health management processes for this thesis. Component degradation will lead to a lower output voltage, which can be used as a measurement in fault detection. Analysing the problem conditions can lead to the fault diagnosis processes which will isolate the degradation phenomena. The two processes are closely linked, and some similar techniques are seen.

Detection processes are well represented in the literature. Measurement thresholds define a simple assessment of the state of health of the observed system. Acceptable parameter values and ranges are often defined by the material limits of the components, and by stack manufacturers. Voltage is however seen as the most important performance indicator for the PEFC; electrical work is the primary output of the fuel cell, and voltage degradation defines the functional targets

for commercial systems [19].

Relatively simple electrochemical models are used effectively for system design, and can contribute to condition assessment practices also. The approach in [61] is effective; a model of healthy current-voltage behaviour, with thresholds of acceptability assigned to the measurement-model residuals. For condition assessment processes in this thesis, an electrochemical model should be developed to represent healthy conditions, against which faulty operation can be detected, and voltage targets can be most visible.

Diagnosis is the more complex process to be achieved. Existing examples, whether model-based or data-driven, concern themselves with diagnosis of only between two and four faulty states. Indeed, in the majority of research, water management problems – flooding and dehydration – are most often the target of the diagnosis. This presents an opportunity for a diagnostic approach that has the capability to isolate multiple faults within a single technique.

Methods for diagnosis show great variety. Model-based techniques are typically more complex to develop, as sufficient model parameters are required to represent each fault mode. An example is to compare the electrical equivalence models of Fouquet et al. [54] and Hernandez et al. [64], where the latter has significantly more parameters once flow conditions are taken into consideration.

The non-model, data-driven diagnostics are perhaps more straight forward to compose, however these are reliant on large volumes of historic data for trending and learning procedures. This is not currently available within the research project, effectively eliminating these methods from consideration.

One area of diagnosis which is not well represented in fuel cell literature is qualitative rule based diagnostics. These approaches capture expert knowledge to represent the target system, and mimic human reasoning processes [75]. These hold advantages for ease of development, and greater transparency in reasoning, as linguistic terms are frequently used. The fuzzy logic approach by Zheng et al. is the only example in this field, defining rules based on the features of EIS measurements.

Thus a fuzzy logic rule based diagnostic approach shall be developed, drawing on linguistic knowledge from expert systems. This shall match the observed operating conditions to the known fault phenomena, with continuous monitoring and without the requirement for discrete characterisation test events.

## Chapter 3

# Detection System

Detecting that the fuel cell is degrading or operating in some faulty state has been defined in chapter 1 as an act of comparing the measured performance output – including potential losses – to a value of expected behaviour for a healthy system. Through the review of fault detection methodologies in chapter 2, model based condition assessment has been seen to have wider reach than using purely empirical performance thresholds. The latter often only hold true within a small window of test conditions, such as temperatures and pressures, whilst these conditions can be included as model parameters and enable the broader applicability of modelling approaches.

Electrochemical models have been used in design and system simulation practices, and are well validated against different application systems, such as the generalised steady-state electrochemical model presented in [111, 133]. This gives good endorsement to use this style of model for fault detection, as the representation of healthy PEFC performance.

Thus an electrochemical modelling approach has been selected for fault detection and condition assessment purposes. This will provide the voltage prediction – as the useful output of a PEFC system – assuming a healthy stack condition. All model parameters will be defined to healthy, start-of-life values. The model will function in parallel to the stack. It should accept the same system inputs as the PEFC, drawn from the appropriate flow measurements and current loading. This structure can be seen in figure 3.1.

The residual is to be taken between the modelled voltage prediction and the measured PEFC output, and will confer the state of health of the PEFC stack. The voltage output is of course considered the primary functional output of PEFC systems [45], as well as being the parameter defined in lifetime targets [134]. Voltage losses will define the severity of any degradation or fault. The following diagnostic process will isolate which component or reaction phenomenon is responsible for the given loss.

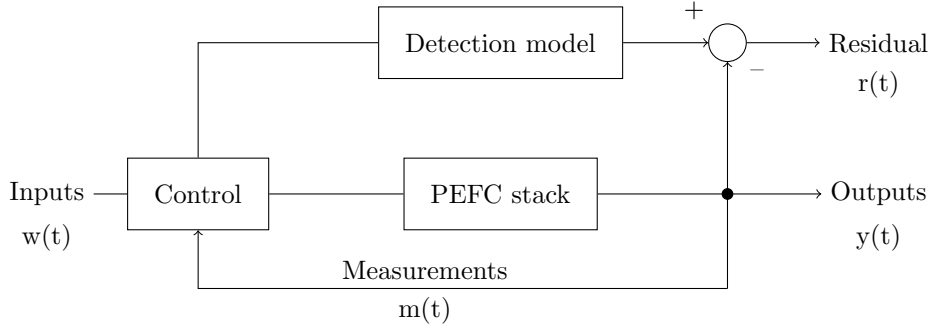


Figure 3.1: System architecture for fault detection modelling

This chapter proceeds to define the modelling equations and their implications for PEFC stack performance, and a further description of the fault detection in implementation.

## 3.1 Fuel Cell Modelling

As established in chapter 2, simple electrochemical models have been shown in the literature to be useful for PEFC stack design as well as implemented for condition assessment processes. These models are useful for calculating the current-voltage behaviour under given flow conditions. The model approach is routed in calculations by O’Hayre et al. [12] and Mann et al. [111]; both of these calculations are validated in the literature. This shall consider the theoretical Nernst voltage generation, and the different loss mechanisms across the operational envelope; namely activation, ohmic, and mass transport losses.

### 3.1.1 Nernst voltage calculation

In electrochemistry, the Nernst equation is used to calculate the reduction potential for a given reaction. Reduction potential measures the amount of energy which becomes available as the system chemistry changes. Each chemical species  $i$  involved will contribute a certain potential, based on its activity  $\alpha$  in the chemical reaction. In general, the Nernst equation is defined as:

$$E_{Nernst} = \frac{-\Delta\hat{g}_{rxn}^0}{nF} - \frac{RT}{nF} \ln \left( \frac{\prod a_{products}^{v_i}}{\prod a_{reactants}^{v_i}} \right) \quad (3.1)$$

where  $\Delta\hat{g}_{rxn}$  is the change in Gibbs free energy, the theoretical energy available from the reaction when in equilibrium under standard conditions (J/mol);  $n$  is the number of electrons leveraged in the reaction;  $F$  is the Faraday constant (96 487 C);  $R$  is the universal gas constant (8.314 J/K mol);  $T$  is the reaction temperature (K);  $a_{products}$  and  $a_{reactants}$  are respectively the chemical activities for the product and reactant species, each raised by its corresponding

stoichiometric coefficient  $v_i$ .

The Nernst equation is applied to the fuel cell hydrogen-oxygen reaction:



Thus the PEFC specific Nernst equation 3.1 is now written as:

$$E_{Nernst} = \frac{-\Delta\hat{g}_{rxn}^0}{nF} - \frac{RT}{nF} \ln \left( \frac{a_{H_2O}}{a_{H_2}a_{O_2}^{1/2}} \right) \quad (3.3)$$

Note the oxygen activity is raised to its stoichiometric coefficient of 1/2, as from equation 3.2. Other coefficients in this equation are the change in Gibbs free energy  $\Delta\hat{g}_{rxn} = -237\,140$  J/mol – the energy available from the formation of liquid water – and  $n = 2$  – the number of electrons liberated from one mole of hydrogen and donated to the oxygen in the reaction.

The activity for the different chemical species depends on their chemical nature and concentration. As liquid water is the only product (equation 3.2), the activity of this is taken as 1 [12]. The activity of the reactant species, gaseous hydrogen and oxygen, are taken as their respective partial pressures. For hydrogen, this is directly the inlet pressure at the anode; for oxygen, this is 21% of the cathode inlet pressure if air is supplied. This yields the final version of the Nernst voltage calculation:

$$E_{Nernst} = \frac{-\Delta\hat{g}_{rxn}^0}{nF} - \frac{RT}{nF} \ln \left( \frac{1}{p_{H_2}p_{O_2}^{1/2}} \right) \quad (3.4)$$

where  $p_{H_2}$  and  $p_{O_2}$  are respectively the partial pressures of hydrogen and oxygen.

This voltage would theoretically be generated by the PEFC, taking consideration of stack temperature and reactant pressures, and regardless of current demand. Thus the current-voltage response would be as illustrated in figure 3.2. This performance is not representative of the true PEFC, which is limited by the voltage loss mechanisms discussed herein.

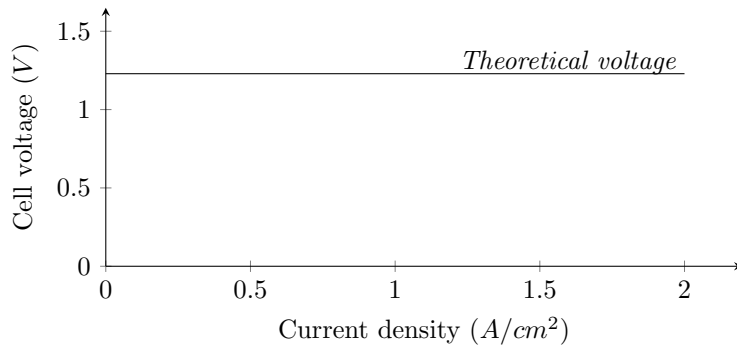


Figure 3.2: Theoretical fuel cell performance from the Nernst voltage calculation

### 3.1.2 Activation loss

The activation loss is the voltage drop due to the kinetics of the chemical reactants at the anode and cathode interfaces. Full investigation of the nature of the electrochemical kinetics is beyond the scope of this simple model; the distinguishing feature is an energy barrier which must be overcome in the conversion of reactants to products, which dictates the rate of reaction. The activation loss is calculated by:

$$V_{act} = \frac{RT}{\alpha nF} \ln \left( \frac{j}{j_0} \right) \quad (3.5)$$

where  $R$ ,  $T$ ,  $n$ , and  $F$  are as defined previously;  $\alpha$  is the dimensionless transfer coefficient between 0 and 1, which expresses how the electrical potential affects the rate of reaction;  $j$  is the current density loading applied to the fuel cell ( $A/cm^2$ );  $j_0$  is the exchange current density associated with equilibrium of the electrochemical reaction ( $A/cm^2$ ). The parameter  $j_0$  represents the energy barrier in product conversion.

The transfer coefficient  $\alpha$  is 0.5 for PEFC fuel cell reactions [12]. The exchange current density  $j_0$  will be defined empirically, by fitting the voltage model to the fuel cell performance at the start of life; typically this is in the order  $10^{-4}$  to  $10^{-9}$ , depending particularly on the catalyst layer design. Current density  $j$  is drawn directly from the current measurement of the fuel cell, divided by the membrane active area (in  $cm^2$ ).

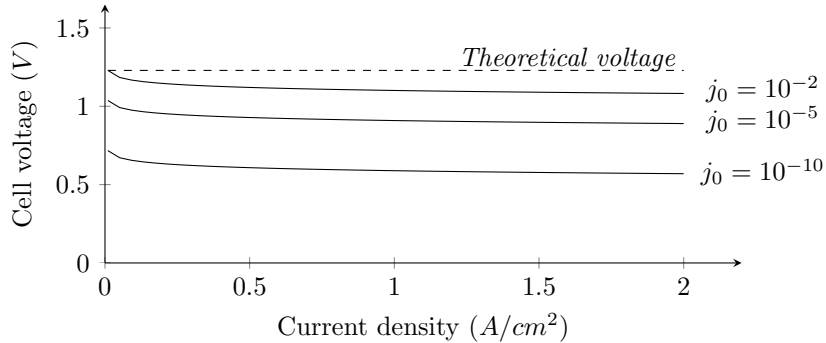


Figure 3.3: Effect of activation losses on fuel cell performance

The current-voltage relationships shown in figure 3.3 describe the activation loss under different values of exchange current density  $j_0$ . It can be seen that this loss most affects the behaviour at small current loads.

### 3.1.3 Ohmic loss

Ohmic losses are inherent in any charge transport process; a resistance to the current conductivity through electrode materials and an equivalent resistance to the ionic transport within the membrane. Because the current produced in the fuel cell must pass in series through all of the

layers in the construction, the resistances are additive. In practice, it is extremely difficult to measure the individual component contributions because of the fuel cell construction, as well as the way operating conditions (compression, hydration, temperature) may affect features such as contact resistance between components. The different contributions can however be grouped together in to a single term, which is similar to Ohm's law ( $V = iR$ ):

$$V_{ohm} = iR_{stack} \quad (3.6)$$

where  $V_{ohm}$  is the ohmic voltage loss (V);  $i$  is the current load on the PEFC stack (A);  $R_{stack}$  is the total electrical resistance ( $\Omega$ ). The ohmic loss is one of the simpler mechanisms within this model, it acts as a gradient loss across the full current envelope. This equation can alternatively be defined by converting total resistance to an area specific resistance  $ASR$  ( $\Omega \text{ cm}^2$ ), by multiplying by the fuel cell active area  $A_{active}$ :

$$ASR_{stack} = R_{stack} \cdot A_{active} \quad (3.7)$$

The result is defined for the current density loading  $j$  as in the other loss equations:

$$V_{ohm} = jASR_{stack} \quad (3.8)$$

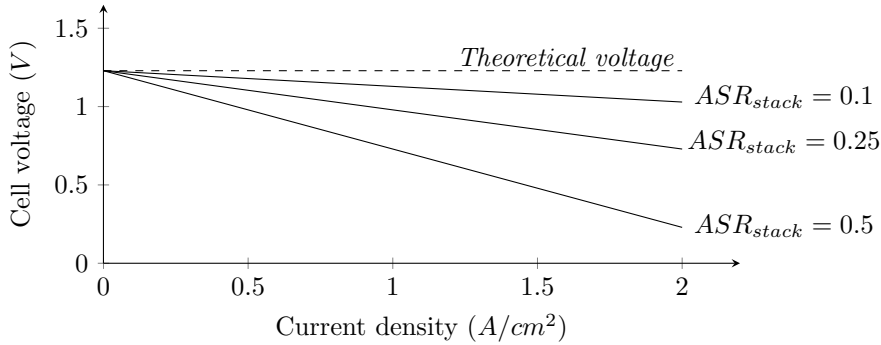


Figure 3.4: Effect of ohmic losses on fuel cell performance

Ohmic voltage losses are linear with respect to current load, as in figure 3.4. The influence is found across the entire current envelope; larger values of resistance  $ASR_{stack}$  will lead to very great losses at higher loading conditions.

### 3.1.4 Mass transport loss

This loss mechanism arises from the concentration of reactants at the reaction interface. Fuel and oxidant must be continuously supplied to the PEFC to produce electricity. At the same time, the product water must be transported away from the reaction interface to avoid build up blocking the reaction sites.

The complexities of mass transport in the fuel cell depend on the design of the electrodes and flow fields. The flow fields in the bipolar plates are responsible for large scale transport across the fuel cell active area, whilst the gas diffusion electrodes are responsible for the small scale transport of chemical species to and from the reaction sites. Flow rates lower than those required to support the electrical generation will result in reactant depletion. This appears as a limit in current production, dependent on fuel cell designs.

The mass transport loss is calculated by:

$$V_{conc} = \frac{RT}{nF} \left( 1 + \frac{1}{\alpha} \right) \ln \frac{j_L}{j_L - j} \quad (3.9)$$

where  $R$ ,  $T$ ,  $n$ ,  $F$ ,  $\alpha$ , and  $j$  are as defined previously;  $j_L$  is the limiting current density ( $A/cm^2$ ). The parameter  $j_L$  is constrained by various features of the gas diffusion electrode design, and is often defined empirically [111]. Thus the ratio  $j_L/(j_L - j)$  reflects approaching the limit of current production.

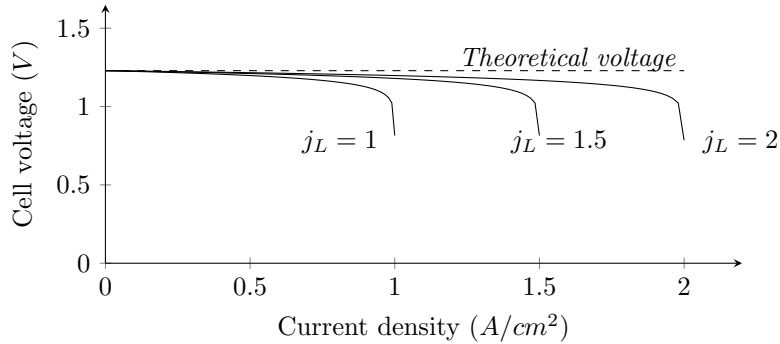


Figure 3.5: Effect of mass transport losses on fuel cell performance

Figure 3.5 gives the form of the mass transport loss under different values of limiting current density  $j_L$ . This loss is seen to affect voltage at the upper ranges of current loading, preventing electrical generation beyond the defined limit.

### 3.1.5 Side reaction losses

When working with real-life practical systems, they often do not perform as theorised, because of certain realities in the PEFC that are not considered in the loss mechanisms presented thus far. The practical PEFC may experience parasitic side reactions, not accounted for theoretically, and which cause further voltage losses. The general model outlined by Mann et al. [111] and used in the previous sections can be improved upon by including a novel term to account for side reaction losses.

These side reactions are assigned to hydrogen crossover (the membrane is not perfectly impermeable) and to the oxidation of platinum at the catalyst. Hydrogen crossover refers to molecular hydrogen passing through the membrane without contributing to the anode HOR reaction; also, the catalyst particles can oxidise in the cathode, forming platinum oxide (PtO), instead of contributing to the cathode ORR reaction. These reactions are exposed in experiments by Zhang et al. [135] and accounted for as a correction to the Nernst voltage. The term  $E_{corrected}$  (V) will be defined empirically, and subtracted from the theoretical voltage:

$$V_{side} = E_{corrected} \quad (3.10)$$

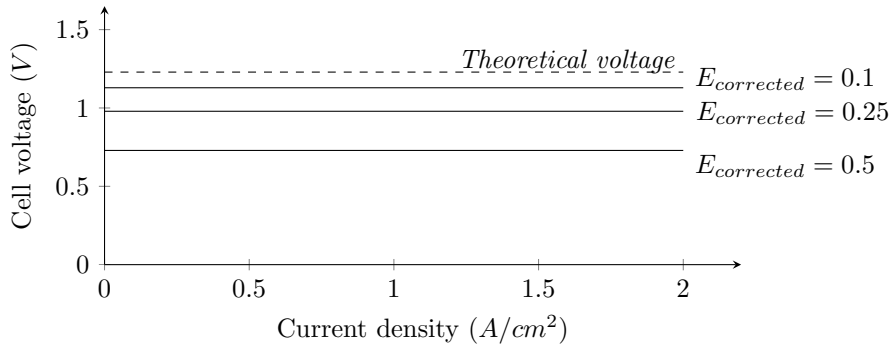


Figure 3.6: Theoretical fuel cell performance from the Nernst voltage calculation

The side reactions will cause a step-wise decrease in the voltage output across the operational envelope, as in figure 3.6. The voltage correction  $E_{corrected}$  will be most noticeable as a decrease in the open circuit voltage (OCV) measurement [135].

### 3.1.6 Complete model equation

The voltage prediction model is defined by the combination of the previously defined equations; starting with the thermodynamically predicted voltage and subtracting the various losses:

$$V_{model} = E_{Nernst} - V_{act} - V_{ohm} - V_{conc} - V_{side} \quad (3.11)$$

Alternatively, giving voltage as a function of current density loading  $j$ :

$$V_{model}(j) = \frac{-\Delta\hat{g}_{rxn}^0}{nF} - \frac{RT}{nF} \ln\left(\frac{1}{p_{H_2}p_{O_2}^{1/2}}\right) - \frac{RT}{\alpha nF} \ln\left(\frac{j}{j_0}\right) - jASR_{stack} - \frac{RT}{nF} \left(1 + \frac{1}{\alpha}\right) \ln\frac{j_L}{j_L - j} - E_{corrected} \quad (3.12)$$

Employing this equation across the range of current density for the PEFC gives the full polarisation performance for the fuel cell. The example curves in figure 3.7 use the different semi-empirical variable values listed in table 3.1. Of these examples, model A represents very good fuel cell performance; much better in comparison to model C, which would not output significant electrical power.

Model	$j_0$ (A/cm <sup>2</sup> )	$ASR_{stack}$ ( $\Omega$ cm <sup>2</sup> )	$j_L$ (A/cm <sup>2</sup> )	$E_{corrected}$ (V)
A	10 <sup>-2</sup>	0.1	2	0
B	10 <sup>-3</sup>	0.25	1.5	0.1
C	10 <sup>-5</sup>	0.5	1	0.2

Table 3.1: Semi-empirical model variables used in figure 3.7

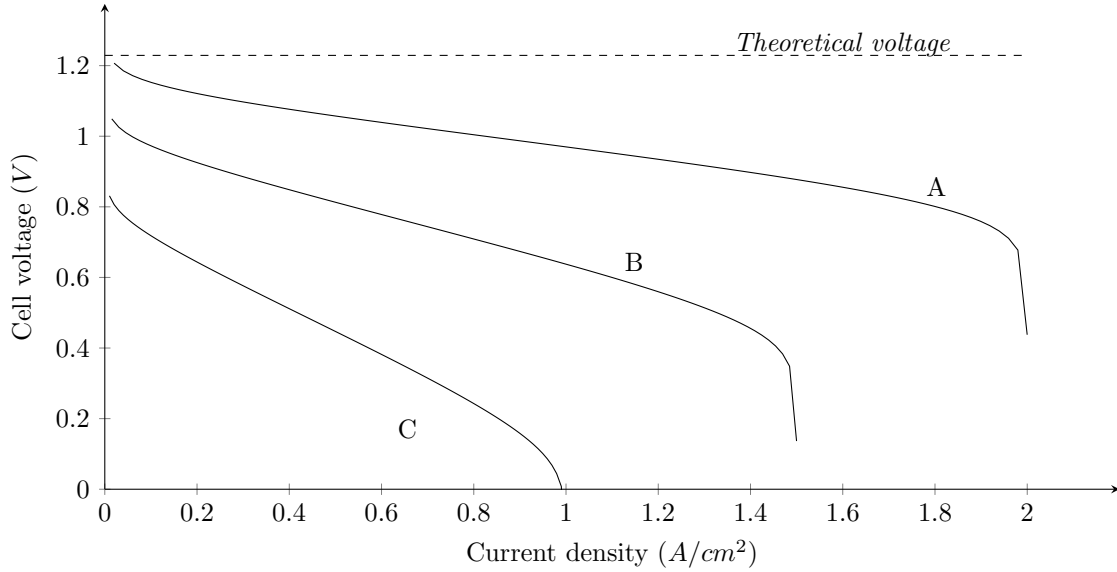


Figure 3.7: Examples of PEFC performance from the voltage model calculation

## 3.2 Condition Assessment

This voltage prediction model is implemented alongside the PEFC stack, as in figure 3.1. As has been presented, the model will accept measurements from the test system as parameters to make the calculation; these parameters are listed in table 3.2. Additionally, the values of exchange

Measurement	Model parameter
Stack current density loading (A/cm <sup>2</sup> )	$j$
Stack temperature (K)	$T$
Anode inlet pressure (Pa)	$p_{H_2}$
Cathode inlet pressure* (Pa)	$p_{O_2}$

\*As air is supplied, 21% of the cathode pressure measurement is used

Table 3.2: System measurements required for the model

current density  $j_0$ , area specific resistance  $ASR_{stack}$ , limit current density  $j_L$ , and OCV voltage correction  $E_{corrected}$  will be defined empirically at the start of the fuel cell's lifetime, such that the model will represent the PEFC in a healthy condition. This maintains a representation of the ideal fuel cell performance, against which faults and degradation can be assessed.

The condition assessment process is based on the voltage residual between the model and measured stack output. This is to be expressed relative to the predicted value such that the voltage loss is calculated by:

$$\Delta V = \frac{V_{model}(j, T, p_{H_2}, p_{O_2}) - V_{measured}}{V_{model}} \quad (3.13)$$

This approach is in alignment with the format of the targets set out by the US Department of Energy (useful life ends at 10% permanent voltage loss) [19]. For example; at 6 A, model B from figure 3.7 predicts 0.62 V. If 0.60 V were measured from the fuel cell, then a voltage residual of 0.02 V would be reported, a relative voltage loss  $\Delta V$  of 0.0323 or 3.23%.

The condition assessment value will feed forward to the diagnostic process and the user interface. Small  $\Delta V$  will define a healthy state, or negligible degradation condition. As the relative residual increases, this is read as an indication of the severity of the degradation, and the loss of system health. The value will be presented alongside the diagnostic output.

### 3.3 Summary

This chapter has detailed the electrochemical model which is used to provide condition assessment for the PEFC system. The model calculations follow those in the literature from O'Hayre et al. [12] and Mann et al. [111], with an additional contribution of an empirical corrective term which takes into account the side reaction losses. The model functions in parallel to the practical stack, providing a prediction of voltage performance in real-time. Measurements of temperature, pressure, and current loading from the live system allow the model to simulate under the same operating conditions. Parameters inherent to the design of the PEFC stack will be fit against

the model at the start of life. The resultant voltage residual is the condition assessment result, and will be presented to the user alongside the diagnostic outcome which shall be introduced in the following chapter.

## Chapter 4

# Diagnostic System

In chapter 2 the different diagnostic approaches were reviewed; these were broadly classified as either model-based, data-driven, or expert rule-based. A full model-based diagnostic approach is seen as difficult to achieve because of the complex, multi-domain nature of the PEFC degradation characteristics. A detailed data-driven approach is also not possible within the research group, as the necessary historic database of different degradation modes does not exist. These approaches seen in the literature utilise thousands of hours of data to characterise a single fault condition [136].

Expert rule-based approaches do not feature in the existing fuel cell literature, so this presents an opportunity for a novel contribution to the diagnostics field. A linguistic approach can capitalise on the volume of PEFC literature and the broad understanding within their findings. That is to say, the observations presented in degradation studies represents the expert knowledge in this field, with statements such as *higher temperature causes the membrane to dry out* [137] or *flow-field channels' obstruction by liquid water can induce local fuel starvation* [85]. A fuzzy logic approach can utilise these linguistic observations for fast diagnosis of a range of degradation conditions. The outcome can be representative of all PEFC technology, whilst independent of specific system designs, scales, and applications.

The first section of the chapter introduces fuzzy set theory and the logical operators that can be performed upon these sets. After this, the development of the diagnostic rules is discussed, illustrating the acquisition of expert knowledge and its collation for the final rule base.

## 4.1 Fuzzy Logic

Fuzzy logic is a form of logic calculation that handles the concept of partial truth. That is, a fuzzy variable has a degree of membership with a particular set *between* 0 and 1. This contrasts with Boolean logic methods, where truth values of variables may only be crisp values *either* 0 or 1.

Fuzzy logic was introduced by Zadeh in 1965 in his development of fuzzy set theory [138]. This served to better represent the “real world” cases where objects are defined in imprecise sets, such as “taller”, “more beautiful”, “colder”, etc. Such sets are frequently used in human understanding and communication, and fuzzy logic allows their application in computing also.

Fuzzy logic therefore provides a framework to use linguistic terms and knowledge in the proposed diagnostic process. This means literature sources and experience can be used directly to populate the knowledge base, calling upon human understanding without some translation to an analytical equation. Used in this way, the process will accept measurement information about operational conditions and failure symptoms to infer degradation modes based on expert knowledge.

The following section describes general fuzzy set theory in contrast to the classical, the implications for logic calculations, and the methods for fuzzy system creation.

### 4.1.1 Fuzzy sets

For a defined universe of discourse  $X$ , elements are denoted as  $x$ , such that  $x \in X$ . Thus,  $X$  is a collection of objects sharing the same characteristics. Examples of elements in various universes may be rotational speeds of a motor, operating temperature of a CPU, or a person’s answers to an opinion poll. For the diagnostic system, the universes will be populated by measurement quantities and observations.

Classical set theory is well known in mathematics and computation, and its features are established to contrast with those of the fuzzy set. The membership function  $\mu_C(x)$  of variable  $x$  in a classical set  $C$  is defined by:

$$\mu_C(x) = \begin{cases} 1 & \text{iff } x \in C \\ 0 & \text{iff } x \notin C \end{cases} \quad (4.1)$$

For example, if the set boundary is defined by an arbitrary value  $r$ , the membership is as depicted in figure 4.1.

This means that variable  $x$  either is a member of set  $C$ , where  $\mu_C(x) = 1$ , or it is not,

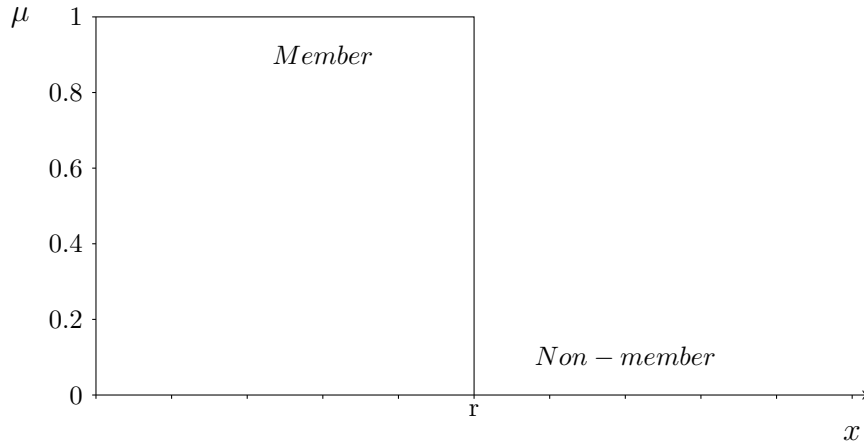


Figure 4.1: A membership function for general classical set  $C$

where  $\mu_C(x) = 0$ . In this way classical set theory is defined by crisp values for membership or non-membership. This is useful for computation under Boolean logic methods, as an example.

In many “real world” cases however, the crisp in-or-out classification can not represent imprecise sets; such examples as a person which is “taller”, artwork that is “more beautiful”, or a fuel cell that is “colder”. Such sets are however frequently used in human understanding and communication, using a vague interval within learnt boundaries. For these cases, fuzzy logic would enable their application in computing, using fuzzy set theory as an extension of the classical.

Fuzzy sets were introduced by Zadeh in 1965, with membership existing within an interval;  $\mu_A(x) \in [0, 1]$ . Thus, for the universe of discourse  $X = \{x_1, x_2, x_3, \dots\}$ , a fuzzy set is defined as the aggregation of all individual element memberships:

$$A = \sum_i \frac{\mu_A(x_i)}{x_i} \quad (4.2)$$

where  $\mu_A(x)$  is the membership function for variable  $x_i$ . The classical definitions are applied at the boundaries; if  $\mu_A(x) = 0$  then  $x$  is not included in the fuzzy set, and if  $\mu_A(x) = 1$  then  $x$  is fully included. Between these,  $x$  is known as a fuzzy member, such that membership is graduated  $0 < \mu_A(x) < 1$ . The complete set  $A$  is represented in two distinct sections; the *core* of the set is  $\{x \in A | \mu_A(x) = 1\}$ , and the *support* is  $\{x \in A | \mu_A(x) > 0\}$ , as defined by:

$$\mu_A(x) = \begin{cases} 1 & \text{if } x \leq a \\ \frac{x-a}{b-a} & \text{if } a < x < b \\ 0 & \text{if } x \geq b \end{cases} \quad (4.3)$$

where values  $a$  and  $b$  define the set boundary, as seen in figure 4.2.

The straight linear membership function as seen in figure 4.2 is often used as a first approxi-

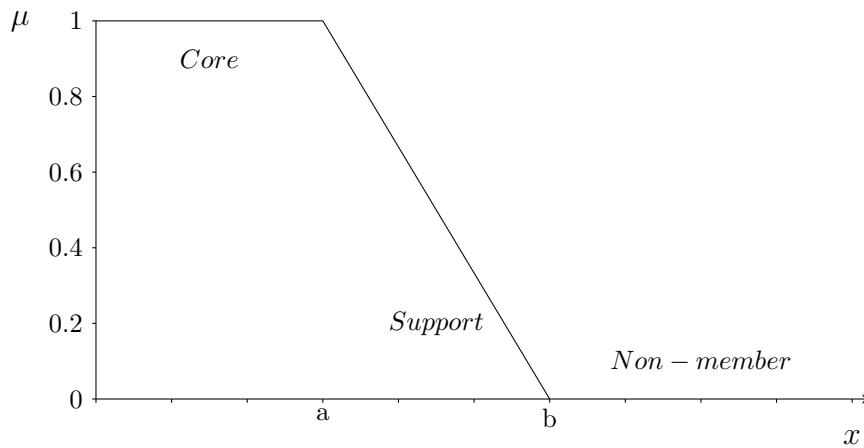


Figure 4.2: A membership function for general fuzzy set  $A$

mation of the set boundary. However, fuzzy sets do not always need to be bounded as triangles, or with symmetry. Membership may show any function that best represents the variable within the numeric range. Figure 4.3 shows some variations; notably asymmetric (left), interval-linear (centre), and Gaussian distributions (right).

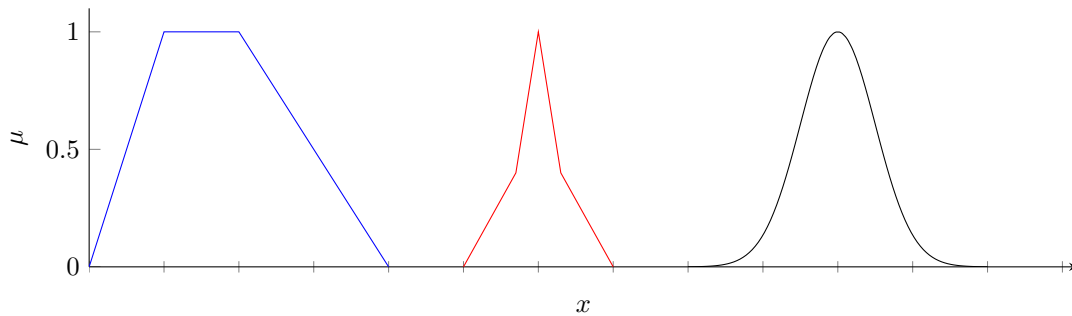


Figure 4.3: Other potential membership function shapes

Fuzzy membership functions are used to map the input variables to the output sets by “degrees of truth”. An example fuzzy system used to characterise room temperature is seen in figure 4.4 as described here. Within this example, the range of measurable temperatures serve as the input universe of discourse  $X$ . These are mapped onto linguistic fuzzy sets which may be defined and understood by a person describing the room temperature; it is truly “cold” below  $0\text{ }^{\circ}\text{C}$ , “cool” at temperatures around  $10\text{ }^{\circ}\text{C}$ , a comfortable “warm” temperature ranging from  $15$  to  $20\text{ }^{\circ}\text{C}$ , and “hot” above  $25\text{ }^{\circ}\text{C}$ . These definitions give the core representation of each fuzzy set, where the output is a fully represented value of 1. Between, the supports for each set overlap to define partial truth and representation of both values. For example, a room temperature of  $13\text{ }^{\circ}\text{C}$  equates to 0.6 truth of the “warm” set and 0.4 of “cool”. This information is used in the fuzzy logic system for inferring knowledge and making control decisions.

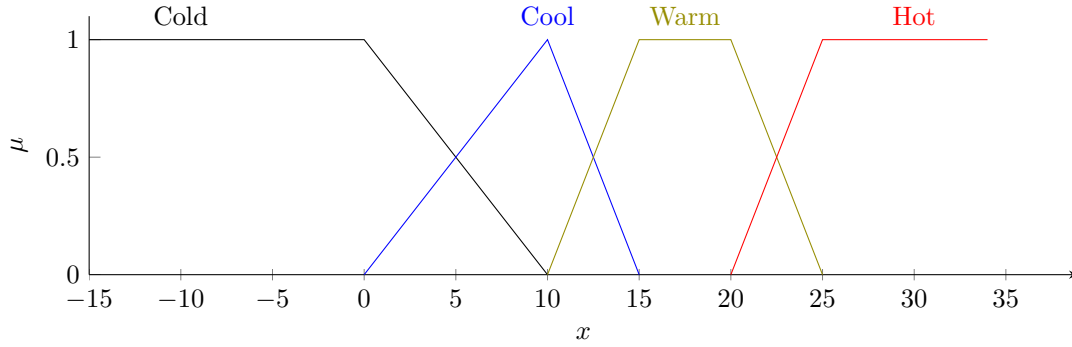


Figure 4.4: Example fuzzy sets to characterise room temperature

### 4.1.2 Operations on fuzzy sets

Fuzzy sets use a similar range of operations as in classical set theory. Intersection (OR logic), union (AND logic) and compliment (NOT logic) of sets is well known for classical sets, as defined in table 4.1.

Sets		Intersection	Union	Compliment
$A$	$B$	$A \wedge B$	$A \vee B$	$\neg A$
0	0	0	0	1
0	1	0	1	1
1	0	0	1	0
1	1	1	1	0

Table 4.1: Set operation in classical set theory

These same operators are used in fuzzy set theory. However, as set membership is no longer restricted to crisp values  $\{0,1\}$ , the operations cannot be uniquely defined as in figure 4.1. Zadeh [138] defined the common operators in his original work, as extensions of those for classical sets:

$$\begin{aligned}
 \mu_{A \cap B} &= \min(\mu_A(x), \mu_B(x)) && \text{Intersection} \\
 \mu_{A \cup B} &= \max(\mu_A(x), \mu_B(x)) && \text{Union} \\
 \mu_{A'}(x) &= 1 - \mu_A(x) && \text{Compliment}
 \end{aligned}$$

These functions are used in the inference calculations under the fuzzy logic method as discussed in the following sections.

### 4.1.3 Structure of the fuzzy system

The concepts established previously – fuzzy sets and logical operations – are combined in the full fuzzy system, the high level structure of which is defined by Abonyi in [139] and shown in figure 4.5. As depicted, the fuzzy system is a process of mapping inputs (such as measurements

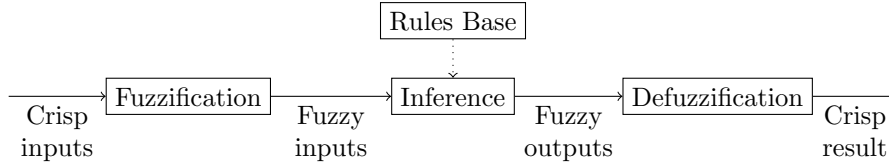


Figure 4.5: Fuzzy logic system structure, adapted [139]

and observations) to outputs (such as a diagnostic statement) based on a comparison to a knowledge base using the fuzzy mappings. Each process therein is described.

### Fuzzification

Fuzzification maps the crisp numerical inputs onto fuzzy sets. These sets are frequently defined linguistically, as understood by the expert operator, and carried forward within the system. In the room temperature example from figure 4.4, the linguistic ranges have been divided into the fuzzy sets “cold”, “cool”, “warm”, “hot”. Any number of set divisions may be used, as best represent the particular universe of discourse. The membership function equations are defined by the expert knowledge to represent the target variable, and give the truth-level assigned to each set.

### Rule base

The rules database is the central knowledge-store for the fuzzy logic system. The assumption is that the functional process of the measured system has uncertainty – is unobservable, unmeasurable, or internally inaccessible – but useful information is accessible based on external measurements. The rules are parsed as “IF...THEN...” statements, relating measurement inputs to system outputs. Each rule defines a causal link between the antecedent “IF” clause and the consequent “THEN” clause. These follow the format:

$$R_n : \text{“IF } x_1 \text{ is } A_{1,n} \text{ and ... and } x_i \text{ is } A_{i,n} \text{ THEN } y \text{ is } B_n\text{”, } n = 1, 2, \dots, N$$

where  $R_n$  is the  $n$ th rule, relating the universe of input measurements  $X$  to an output  $y$ . Fuzzy sets  $A_{i,n}$  and  $B_n$  are respective of both the input element  $x_i$  and rule  $R_n$ , and are described by membership functions  $\mu_{A_n}(x) \in [0, 1]$  and  $\mu_B(y) \in [0, 1]$ .

Following the room temperature example, different rules would exist to represent the knowledge for each input set; “cold”, “warm”, “hot”, etc. These rules would represent the knowledge the operator holds about the observed heating system, for example “IF the temperature is cold THEN the heater is malfunctioning”. The fuzzy logic system is able to make a diagnostic

judgement based on the inferred causality “known” by the rules.

### Inference

The inference engine is the computational method for calculating the *firing strength* for each rule, based on the fuzzified inputs. The antecedent membership function defines the degree of truth represented by the input  $x$  in the fuzzy set  $A_n$ . This corresponds to the firing strength  $\beta$  of the given  $n$ th rule.

Most rule-based systems will however involve more than one rule which may overlap in the consequent definitions. In this case the rules must be aggregated; the AND logic is utilised. This provides the firing strength  $\beta$  as:

$$\beta_n = \prod_{i=1}^I A_{i,n} \quad (4.4)$$

where  $A_{i,n}$  is the membership function of input  $x_i$  for rule  $n$ .

### Defuzzification

The defuzzifier compiles the outputs of each of the rules proportional to firing strength, to give a unified result. This means combining the fuzzy set truths to give a single crisp result. The commonly used approach for this calculation is the centroid method. This finds the “centre-of-gravity”,  $y$ , of the fuzzy truth area:

$$y = \frac{\sum_n \beta_n B_n}{\sum_n \beta_n} \quad (4.5)$$

where, for each of  $N$  rules,  $\beta_n$  is the firing strength and  $B_n$  is the output membership.

The result of the centroid defuzzification method is a weighted-average of the consequences of the rules. This provides a truth value for each consequent (degradation mode under diagnosis) as described by the input universe

#### 4.1.4 Comparison to probability

Fuzzy logic and probability both address uncertainty in a system, though from different approaches [140]. Probability theory conceptually details how probable is it that a variable exists within a set; this is under the classical in-or-out definition of set membership, with a degree of uncertainty. Conversely, fuzzy set theory deals with a truth of set membership; how well a variable is included in a set, but not necessarily with uncertainty as to the degree. The distinction is that probability is related to chance, whilst fuzzy logic handles vagueness.

Toward diagnosis, fuzzy logic holds value in the way it calculates this truth-measure. Degradation will occur during the fuel cell’s lifetime – there will be off-design operational conditions

and observable symptoms of the degradation, leading to a loss of power-performance – and the diagnostic task is to define the degree that each degradation mode may be responsible. This will be achieved by mapping the measurable system parameters to the degradation phenomena through an expert knowledge base.

## 4.2 Knowledge Engineering

The broad field of knowledge engineering covers all technical aspects of knowledge-based systems including, of course, fuzzy logic. In this context, this section deals with the procedure followed in the development of the expert diagnostic system. Figure 4.6 shows the main steps followed in this process. This methodology has been drawn from Harris' introduction to fuzzy logic (FL) methods in application [141], though it appears as a common method in other knowledge engineering approaches.

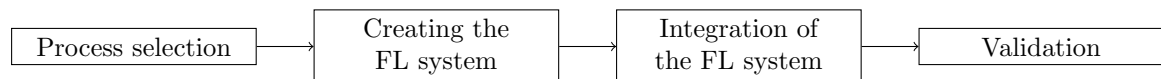


Figure 4.6: The fuzzy logic knowledge engineering process [141]

### Process selection

The first step in creating the fuzzy logic diagnostic system is to adequately define the application process. The functional boundaries should be identifiable, as well as the inputs and outputs which will be monitored. The degradation phenomena which will affect the process inputs and outputs should have some uncertainty to warrant the use of fuzzy logic, though the uncertainty should not be of a random or stochastic characteristic. Defining the scope and boundaries of the process under consideration is important to focus development and to validate a successful system design.

### Creating the fuzzy logic system

This stage in the development can be further divided into the steps shown in figure 4.7. First is to characterise the parameters related to the problem process. In the case of diagnosis, this means understanding the degradation modes expected in the monitored system, the monitoring capabilities, and prioritising these where possible.

Knowledge acquisition is to gather all existing information and understanding related to the selected problems. This knowledge will come from expert sources, including existing publications and experience using PEFC systems. This information is then organised into the fuzzy logic

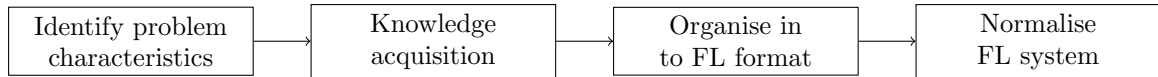


Figure 4.7: Creating the fuzzy logic system [141]

format; that is creating appropriate propositions from the raw knowledge, framing the input-output functionality.

The final step is to normalise this raw fuzzy logic system. This means defining the boundaries of inputs and outputs in the fuzzy sets, phrasing the rules suitably to reflect the problem characteristics, and defining the operators used in the fuzzification and inference processes. This can be an iterative process with its own smaller validation tests to ensure consistency in the diagnostic output.

### Integration of the fuzzy logic system

Once established, the fuzzy logic system must be integrated into the observed process. The integration will be within the control software and in parallel to the normally operating processes, similar to the detection system discussed in chapter 3. In the knowledge acquisition and fuzzy logic system creation, recommendations may be made toward certain measurement requirements or data processing, which should be accommodated. The diagnostic should not however adversely impact the operation of the main process.

### Validation

Since the fuzzy logic system is established using expert knowledge and understanding, it must be validated to confirm functionality and quality of the rules included. This is the final step in development. The diagnostic system is to be tested experimentally to ensure satisfactory results. Where possible, this can be compared to existing systems to add weight to the validation conclusion.

## 4.3 Fuel Cell Diagnostic System

This section will cover the development of the fuzzy logic diagnostic system. The fuzzy logic calculations are supported natively within the National Instruments LabVIEW software platform as presented in chapter 5, and so the development focuses on the knowledge engineering methodology. This will follow the format laid out in figure 4.6, as well as identifying design challenges.

### 4.3.1 Process selection

The selected process that the fuzzy logic is acting upon is degradation to the PEFC stack components and a loss in overall electrical performance. The membrane electrode assembly (MEA) is chosen as the focus of the diagnostic system; this vital element of the PEFC has the most bearing on the reaction kinetics which influence electrical generation. Discussed in chapter 1, the MEA is a component-of-components, including the polymer membrane, the platinum catalyst, and the gas diffusion electrode; each of these constituents shall be considered for their functions and the degradation thereof. The catalytic activity, ionic transfer, and small-scale mass transport are all loss mechanisms dependent on the MEA materials.

The MEA also fulfils the uncertainty criteria. As this component is internal to the PEFC, both desired performance and degradation phenomena are not normally directly observable during operations. Tests which do exist to characterise between different degradation phenomena often require dismantling the fuel cell (in the case of microscopy techniques) or otherwise interrupting normal operation (testing current-voltage interactions). The fuzzy logic diagnostic shall be based upon a pattern matching between known influencing factors and the degradation modes.

The MEA is selected in isolation to other system components because its constituent materials are standardised to a great degree for different PEFC scales and applications [142]; Nafion<sup>®</sup> membrane, platinum catalyst, and carbon GDE material. As suggested in chapter 2, the materials and design of the bipolar plates and seals are less standardised, with different metallic or composite materials for the former [143], and a variety of integral and compressive strategies for the latter [101]. The diagnostic for these stack components would in necessity be tailored accordingly, and would make the initial scope of this development too large. Degradation of the MEA materials will be similar across PEFC technologies, and the diagnostic process will be applicable across the range. Thus the diagnostic scope shall exclude the bipolar plates and sealing gaskets.

The balance of plant (BoP) and support ancillary subsystems are also excluded from the diagnosis. The selection of components such as pipes, valves, storage vessels, and electrical circuitry will vary based on application. Also, the degradation and failure of components such as these are more commonly understood in terms of existing reliability analysis and lifetimes, and thus not within the scope of this new development.

The degradation process boundary will be defined by the imposed operating conditions and the measurable current-voltage relationship. Variables such as temperature, pressure, and electrical loading are the inputs to the diagnostic system. The outputs shall be a judgement for

which degradation phenomena are acting upon the PEFC, and their relative severity based on the voltage loss observed.

### 4.3.2 Creating the fuzzy logic system

The diagnostic problem is one of relating the monitored system variables to the degradation processes internal to the PEFC. This is largely a parameter matching approach, wherein the operating conditions which are known to cause and accelerate damage to the MEA must be recognised and linked to their respective degradation modes. The “normal” operating conditions are defined to maximise the PEFC lifetime, and minimise component degradation. It is off-design conditions which must be identified in the knowledge acquisition, and monitored for during operation, in order to isolate the degradation that is imposed on the PEFC stack.

The knowledge acquisition detailed in the next section looks to existing publications and observations from case studies and degradation testing. Inputs are selected from monitored and measurable properties including temperatures, pressures, flow rates, relative humidities, current loading, and voltage response. The linguistic set terms (“high”, “fast”, “lower”, “cold”, etc.) will be drawn directly from the literature source. From the durability review in chapter 2, the degradation modes considered are for membrane breakdown, platinum catalyst dissolution, carbon corrosion in the GDE materials, and water management issues being dehydration of the membrane, and liquid water flooding of the gas diffusion media.

One design challenge that is constant in this process is in the definition of the linguistic set terms. In the establishment of the rules, the expert knowledge may not define the ranges implied by these words, or they may be used in connection to a single testing condition. It is the task of the author, through the organisation and normalisation into fuzzy logic sets, to decode these ranges and combine them as seems appropriate to PEFC operation. For example, if a number of sources describe “normal” stack temperature for a range of 50 °C [144] to 70 °C [145] or even greater [146], then the truth is some combination or compromise that fits the general case.

Another challenge lies in the symptomatology of the degradation modes. It is a common outcome that all degradation leads to decreasing voltage performance. Whilst the different degradation modes affect different loss mechanisms across the PEFC operational envelope, no distinction can necessarily be made on a moment-by-moment basis using current-voltage performance alone. The diagnostic must consider the sum of contributing factors in order to isolate the fault.

The output of the diagnostic analysis is the certainty of any one degradation mode occurring. Greater correlation between the influencing conditions results in higher certainty that a particular

degradation mode is responsible for any performance loss. Conversely, operating away from the degrading conditions infers that the degradation mode is not occurring in the PEFC. Where the expert sources report greater correlation between operating conditions and higher degradation rates, the diagnosis level is “certain”; at normal operating conditions diagnosis outcomes give a certainty level of “none”. Between these two levels, when operating conditions only partially correlate with the degradation state, then the diagnosis level is “evidenced” – the degradation mode might be occurring, but the expert knowledge is not fully certain. The diagnosis output for each degradation mode is dynamic throughout operation, as certainty levels increase and decrease as monitored conditions change.

Following the rules base knowledge acquisition, the fuzzy set membership functions are also defined, relative to the boundaries established in the rules sources. Through the normalisation of the rules base, the goal is to establish the minimal, necessary, and unique set of parameter observations required to support the degradation diagnostic rules.

### **4.3.3 Knowledge acquisition**

As the rules base is the knowledge store for the fuzzy system, this is the most detailed part of the development. The knowledge is compiled from existing publications for PEFC development and demonstration projects; those using state-of-the-art materials and methods for testing chosen to represent the technology as used in commercial practice.

In the first instance, a large amount of knowledge is collated. The intention is to capture all operational conditions and degradation observations available in the literature, to ensure completeness of the knowledge acquisition. However the resultant rules base, as shall be seen, can become unruly in size and too detailed for the input data requirements. The excessively detailed system would not use the fuzzy logic process to its best capability because of duplication and difficult management for a human operator.

Thus this section shall also provide the rule reduction that was followed to create a balance between detail in the rules and efficiency in generation, management, and operation of the fuzzy logic system. The reduction of the rules is performed by extracting and combining those which describe the same key operating conditions. The rules are also extended beyond just the off-design conditions which are identified in durability studies; normal conditions are defined as non-degrading states also. This process represents the normalisation of the rules to a more general case that correctly utilises the fuzzy logic processing.

## Membrane degradation

Polymer electrolyte membranes ultimately fail as a result of pinholes forming, allowing reactant gases to mix directly. As such, the reactants would not contribute to the overall power production for the PEFC, and reduce performance and efficiency. Microscopic pinholes form as a result of the membrane material breaking down during usage. In practice, this degradation can be caused through three main mechanisms; chemical, thermal, or mechanical.

Chemical degradation is caused by radical species attacking the polymer chain, causing it to un-link and decompose. The radicals are often generated as by-products of the main PEFC reaction. Thermal decomposition takes place when the membrane is heated to at least 400 °C. Such high temperatures allow the polymer chain to spontaneously breakdown and separate. Mechanical degradation on the membrane comes about through fatigue stresses. Because the membrane is mechanically constrained in the fuel cell construction, humidity and temperature cycles can cause dimensional changes, inducing these stresses.

Table 4.2 lists the findings of the knowledge search into membrane degradation. This includes major degradation studies with sufficient detail into the materials and methods used in experimental work. A discussion of the rules is also included below.

The first rule deals with increased operating temperature and its effect on chemical reaction mechanics. This increases reaction mechanics, and in turn increases the rate of degradation chemistry, as described in rule one. Hydrogen peroxide decomposes into hydroxyl radicals ( $\cdot\text{OH}$ ), which is responsible for chemical attacks at polymer endgroups. This degradation mode is known to release fluoride from the polymer chain, as such its release rate is proportional to the chemical breakdown rate. Experimental work by Curtin et al [81] gives further detail, that high temperature and low relative humidity increases how aggressive this degradation can be.

Rules two and three give particular conditions for peroxide generation in the fuel cell. Operating at open circuit voltage (OCV) allows hydrogen to permeate the membrane without needing to contribute to the voltage generation reaction. This can be further accelerated by poor manufacturing. Having overlap between the anode and cathode GDEs, and the mismatched potential distribution; peroxide generation is more severe for cathode overlap. The electrode positioning consideration in these rules is more relevant to MEA design however, and can be eliminated in manufacture [147].

The hydroxyl radicals are produced from off-design reactions between the PEFC reactants. Such reactions still require platinum as a catalyst, for hydrogen oxidation, and so with increased platinum catalyst there are more reaction sites for potential radical production, as per rule four [148].

Rule	IF	THEN	Source
1	Stack temperature is high AND Humidity is low AND Peroxide is present	Membrane chemical breakdown is fast AND Fluoride release rate is high	[81]
2	Anode overlaps cathode AND Voltage is OCV	Membrane chemical breakdown is fast	[147]
3	Cathode overlaps anode AND Voltage is OCV	Membrane chemical breakdown is very fast	[147]
4	Platinum loading is high	Radical production is higher AND Chemical breakdown is faster	[148]
5	Humidity is high AND Voltage is OCV	Gas crossover rate is high	[149]
6	Humidity is low AND Voltage is OCV	Proton conductivity is low AND Gas crossover rate is low	[147]
7	Humidity is high AND Voltage is OCV	Proton conductivity is high AND Gas crossover rate is high	[147]
8	Hydrogen pressure is high AND Oxygen pressure is normal	Gas crossover rate is high	[147, 149, 150]
9	Membrane is thinner	Gas crossover rate is higher	[43, 81, 151]
10	Membrane is thicker	Gas crossover rate is lower	[43, 151, 152]
11	Membrane is very thin	Membrane chemical breakdown is slower	[43, 151, 152]
12	Membrane is thinner AND Current density is high	Voltage degradation rate is lower	[81]
13	Current density is high	Hydrogen utilisation is high AND Gas crossover is low	[148]
14	Gas crossover rate is high AND Voltage is OCV	Membrane chemical breakdown is high	[150]
15	Compression is high	Membrane resistance increases	[81, 144]
16	Membrane hydration increases	Membrane swells AND Mechanical stress increases	[144, 153]
17	Temperature increases AND Water content is high	Mechanical strength decreases	[154]
18	Membrane hydration increases from medium to high AND Temperature is low	Membrane strength decreases	[153, 154]
19	Membrane hydration is none or low AND Temperature increases	Membrane modulus decreases significantly	[154]
20	Membrane hydration is high AND Temperature increases	Mechanical modulus decreases slightly	[154]
21	Hydration decreases (from full to none)	Mechanical stress very high	[155]
22	Humidity cycling	Mechanical toughness decreases	[153]
23	Humidity cycling	Membrane mechanical cracking	[156]
24	Membrane mechanical breach	Rapid total failure	[157]
25	Membrane chemical damage is medium or high	Membrane mechanical degradation rate increases	[83]
26	Hydrogen gas crossover	Membrane thermal degradation	[149]
27	Membrane temperature is extremely high	Glass transition	[158]

Table 4.2: Membrane degradation knowledge base

In rules five, six, and seven, the membrane water content is seen to increase hydrogen permeability. The water bonded to the polymer membrane increases its flexibility, allowing the hydrogen molecules to pass more easily [149]. This gas crossover rate is responsible for small losses throughout the fuel cell polarisation performance, however it is still orders of magnitude lower than the crossover through a pinhole.

A similar effect can be found for pressure imbalance between the anode and cathode supply pressures in the eighth rule. Pressure difference between the anode and cathode gas compartments will encourage hydrogen to pass through the membrane, under influence of forced diffusion.

Rules six and seven also identify the relationship between membrane water content and proton conductivity. This again is related to performance, where low proton conductivity equates to increased membrane resistance and ohmic losses.

The thickness of the membrane is also a factor in hydrogen permeability. A thicker membrane offers greater distance for hydrogen gas crossover; gas permeability coefficients remain constant and independent of thickness [159]. This is represented in rules nine through twelve.

Of course, the capability for hydrogen gas to crossover is dependent on a concentration gradient between the gas chambers at each electrode. When the hydrogen is consumed in the fuel cell reaction, the concentration of free hydrogen at the membrane surface drops considerably. Thus, as described by rule 13, when the fuel cell is generating current, the hydrogen fuel is used and not readily available to permeate the membrane.

Gas crossover through the membrane is of importance here because of the direct hydrogen-oxygen reaction. This, as reflected in rule 14, leads to the hydroxyl radical production and increased chemical breakdown rate. This rule relates back to the others describing gas crossover, which ultimately contributes to membrane chemical breakdown.

Rule 15 is another that considers fuel cell construction. As the membrane is clamped between the bipolar plates, the compression force is relevant to the fuel cell performance. With increased compression load the polymer matrix can be crushed, reducing the available volume for water capacity. As is indicated in rules six and seven membrane water content influences proton conductivity, and by extension, resistivity of the cell.

The complement to rule 15 is to consider how membrane water capacity changes the compressive loading in rule 16. As the polymer takes up water it swells, though it is constrained between the bipolar plates. The result is to increase the compressive forces acting on the membrane, and hence increase the mechanical stress.

Rules 17 through 20 consider various combinations of hygrothermal stress; changing conditions of humidity and temperature influencing the membrane mechanical strength. High water

content at lower temperatures acts as a plasticiser, decreasing stiffness and strength. However, at higher temperatures, the water acts to stabilise the membrane, whilst dryer membranes lose the majority of their strength. The preference is therefore to maintain consistent hydration and temperature for predictable mechanical strength.

Rules 21 through 23 originate in experimental work detailing significantly changing the membrane hydration. Removing a significant amount of water from the membrane (all water content in rule 23) will cause it to shrink significantly. Because of the constraints within the fuel cell construction, tension loads can exceed the material limits. Cycling the PEFC through large humidity variations will cause cracks and pinholes to form in the membrane, and decrease the strength of the remaining material.

Mechanical damage to the membrane is a total failure mode for the PEFC. Allowing the reactant gases to mix and react directly means they are no longer contributing to power generation in the fuel cell, so local performance is hugely decreased. In addition, the direct combustion reaction between hydrogen and oxygen is exothermic, and the high temperature will cause further damage to the membrane and other PEFC components, in a self-propagating failure cascade. This is noted in rules 24 and 26.

Chemical and mechanical damage to the membrane are not mutually exclusive, with rule 25 noting their connectivity. Chemical degradation to the polymer material can thin the membrane, decreasing the local mechanical strength. The result is a structurally weaker membrane which is more vulnerable to mechanical stressing discussed previously.

Polymer materials are susceptible to extremely high temperatures, causing them to crystallise and glass transition. This eliminates the ionic conductivity capabilities of the membrane and severely decreases performance, as well as being non-recoverable damage. This occurs at temperatures above 200 °C, the “extreme temperature” quoted in rule 27 [158].

### **Membrane degradation reduced rule set**

The scale and diversity of table 4.2 illustrates the need for the organisation and reduction of the rules base into a usable version for the diagnostic system. Firstly, consulting a larger number of rules would make the overall system function slower. Secondly, the inputs and outputs are not unified, with respect to which variables are to be measured and which degradation mode is isolated (such as rules eight through ten refer to gas crossover without extending this to a degradation effect). Diagnostic outputs are defined for the chemical and mechanical modes, with the “certain”, “evidenced” or “none” levels as described previously. Manufacture specific rules should also be removed as materials and membrane thickness are not controllable parameters.

Rule	IF	THEN
A	Stack voltage is very high	Membrane chemical breakdown is certain
B	Stack voltage is high	Membrane chemical breakdown is evidenced
C	Stack voltage is normal OR Stack voltage is low	Membrane chemical breakdown is none
I	Anode humidity change is large AND Cathode humidity change is large	Membrane mechanical stress is certain
J	Anode humidity change is large OR Cathode humidity change is large	Membrane mechanical stress is evidenced
K	Anode humidity change is small AND Cathode humidity change is small	Membrane mechanical stress is evidenced
L	Anode humidity change is none OR Cathode humidity change is none	Membrane mechanical stress is none

Table 4.3: Reduced membrane rule base

Thus the rules listed in table 4.2 have been reduced to the set given in table 4.3 (the discontinuous lettering is relevant to the compiled rules table 4.10, presented in full at the end of this section). The final rules base captures the essential off-design operational conditions that are common among the different studies. These rules also have consideration for the monitoring capabilities of the test rig, as shall be discussed.

The first three rules of table 4.3 diagnose degradation of the membrane under chemical radical attacks. In the larger rules study, open circuit voltage (OCV) is the main condition responsible for generating the hydroxyl radical agents, noted in table 4.2 rules 2, 3, 5-7, and 14. In the PEFC operating envelope, OCV is considered “very high” voltage, so chemical degradation is certainly evident in final rule A, and will continue to be a factor at “high” voltages near to this limit, rule B.

The consideration to OCV also reflects the availability for hydrogen to permeate the membrane. As was discussed with previous rule 13, higher current loading consumes the hydrogen before it is available to crossover. Therefore, at “normal” or “low” voltage operation, membrane chemical breakdown will no longer considered to be occurring. This is stated in table 4.3 rule C.

Rules regarding membrane, GDL, and catalyst manufacture are discounted. It is assumed all MEA manufacturing will be correct and optimal, and decided in the design process. The rules two and three which are related to electrode overlap, rule five related to platinum loading, and nine through twelve dealing with membrane thickness are not required. These conditions will not change during PEFC operation, and the physical characteristics of the materials are not related to flow conditions. These rules are not carried forward at this time.

For membrane mechanical degradation, again it is assumed manufacture is correct; the mem-

brane is pristine when installed, and is not mechanically pinched between the flow field plates (rule 15 is not used). With these assumptions, mechanical stress to the membrane will arise primarily from dimensional changes caused by water uptake. Hydration is the topic of rules 16 to 20 in table 4.2, indicating that increasing the water content in the membrane causes it to swell, increasing compressive loads within the stack constraints. Conversely, dehydrating the membrane, in rule 21, will cause it to shrink and experience tension loads, again due to the mechanical constraint within the stack construction. Cycling between these two hydration states will also accelerate their impact, as in rules 24 and 25.

Membrane hydration conditions are evaluated in the final rules I, J, K, and L, table 4.3. These rules consider hydration of the reactant feeds changing by various degrees. The reactant feeds are the main source of membrane hydration in the experimental PEFC stack. The more severe the change in humidity, the more severe the mechanical stress acting on the membrane. Therefore the diagnosis is “certain” for very large changes in the humidity of both reactant feeds, and lesser for smaller changes to water content.

Thermal degradation of the membrane is not considered at this time. Glass transition only occurs at extremely high temperatures, and the PEFC system would be prevented from reaching these levels by other safety systems. Equally, the thermal stress imposed by perforated membranes and direct hydrogen combustion would not be significant, as the PEFC would be unusable if performance dropped so significantly in a rapid total membrane failure. Rules 26 and 27 are not carried forward.

### **Catalyst degradation**

Degradation of the platinum catalyst layer manifests as decreasing surface area. Reducing the catalytic area reduces the overall fuel cell efficiency, as there are fewer reaction sites available. The platinum nanoparticles can lose surface area through particle growth and agglomeration, detachment and material loss, or through surface contamination.

Agglomeration and particle growth is the dominant degradation mode observed in PEFCs. Nanoparticles are known to possess high surface energy, and therefore have a tendency to agglomerate into larger particles. Longer operational times shows the evolution of this mode, as well as accelerating operational conditions, such as power cycling.

Physical loss of the platinum metal itself will reduce active area as there is simply less catalyst material available. The platinum can dissolve into the electrolyte or liquid water in the gas channels and become lost. This is similar to the agglomeration action, but with loss of material rather than resettling, occurring at voltage levels about 0.9 V [160]. Also, the particles

can themselves detach from carbon supports and the membrane surface, meaning they are no longer conducting to the power output.

In the third loss mechanism, the platinum surface can become poisoned by various chemical agents in the reactant gas streams. Carbon monoxide (CO), sulphur oxides (SO<sub>2</sub>, SO<sub>3</sub>), hydrogen sulphide (H<sub>2</sub>S), and nitrous oxides (NO<sub>x</sub>) can all be introduced to the fuel cell through either impure hydrogen fuel or from chemically-dirty atmospheric air. These compounds bond strongly with the platinum, thus prohibiting access to the reaction surface. The initial knowledge acquisition for catalyst degradation mechanisms is given in table 4.4.

Potential is found to be the most significant factor for platinum catalyst degradation. Dissolution and agglomeration occur when metal atoms are able to dissolve from the nanoparticles and into either liquid water present in the cell, or the ionomer material of the membrane. This is evident in table 4.4, through rules one, three, and twelve; experimental results show that the rate of platinum dissolution increases when a voltage greater than 0.8V is imposed on the cell [161]. At very high voltages – above 1.15V – platinum dissolution rate decreases as the particles form a protective oxide coating; this is referenced in rule 13.

Rule two states that voltage degrades faster when under load, compared to OCV. This is based on experimental work by Ferreira et al. [161], under steady state conditions. The suggestion that degradation is less at OCV compared to under normal power loading is perhaps a misrepresentation; catalyst active area is lost at a greater rate at the higher cell voltage, however this is less limiting to the measurable output at OCV, when reaction activity is not a factor. That is to say, more platinum area is lost at OCV, but this degradation will be felt once operational loads are applied.

Voltage cycling is one of the most frequently applied accelerated stress conditions in experimental testing. Rules four, five, six, seven, eight, nine, and ten all stipulate that cyclic voltage conditions give much increased catalyst degradation compared to steady state loading. Once voltage cycling is established, parameters such as increased range (rule five), increased temperature (rule seven), and increased humidity (rule eight) can all make the degradation rate worse.

Results by Borup et al. [162] also indicate that the number of cycle traversals is more important than the time exposed to a certain voltage condition; this is called in rule six, and represented in figure 4.8. This figure shows that the same amount of degradation (loss in surface area) can be seen after approximately the same number of cycles, independent of the rate of cycling, or duration at the higher voltage levels. It is the voltage transition that is the dominating factor.

Rule	IF	THEN	Source
1	Voltage is increased to very high (0.9 – 1.1 V)	Catalyst dissolution rate increases	[160,161]
2	Stack is under load	Voltage degradation rate increased, compared to OCV	[161]
3	Voltage is OCV	Catalyst area loss rate is increased	[161]
4	Voltage is cycled (0.6 – 1.0 V)	Catalyst are loss is considerable	[161]
5	Voltage is cycling AND Voltage range is greater	Catalyst area loss is greater	[162]
6	Voltage cycle number is greater	Catalyst area loss in greater	[90,162]
7	Temperature is greater AND Voltage is cycling	Catalyst particle growth rate is greater	[162]
8	Humidity is greater AND Voltage is cycling	Catalyst particle growth rate is greater	[162]
9	Voltage is cycling AND Voltage range is greater	Catalyst support (carbon) corrosion is greater	[162]
10	Humidity is lower AND Voltage is cycling	Catalyst support (carbon) corrosion is greater	[162]
11	Voltage is not very high (below 0.9V)	Catalyst support (carbon) corrosion is lower	[142]
12	Voltage is very high	Catalyst dissolution rate increases	[163]
13	Voltage is extremely high (over 1.1V)	Catalyst dissolution rate decreases	[164]
14	Anode feed is contaminated	Catalyst poisoning exists	[142]
15	Air feed is contaminated	Catalyst poisoning exists	[142]
16	Voltage is OCV OR Voltage is high AND Duration is short	Catalyst dissolution rate is high	[52]
17	Voltage is OCV OR Voltage is high AND Duration is medium	Catalyst dissolution rate is low OR none	[52]
18	Voltage is OCV OR Voltage is high AND Duration is long	Catalyst dissolution rate is high	[52]
19	Stack temperature is very high	Catalyst contamination is low	[165]

Table 4.4: Catalyst degradation knowledge base

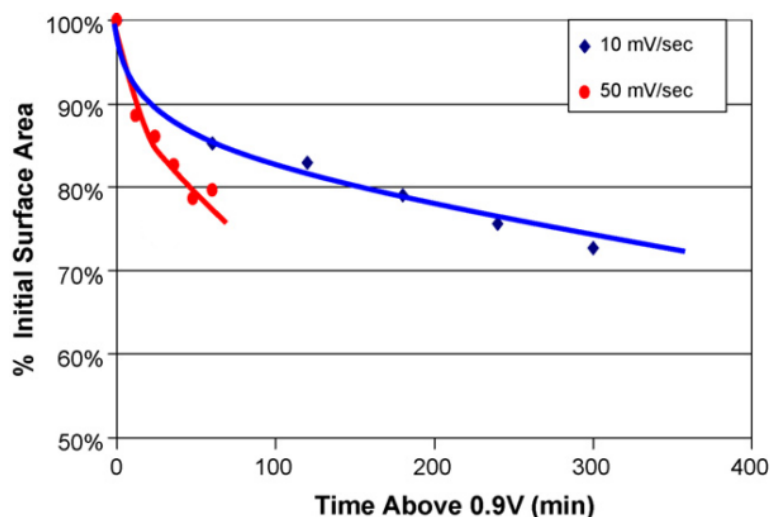


Figure 4.8: Change in cathode electrocatalyst surface area during cycling experiments comparing different scan rates, from [162]

Rules 14 and 15 consider platinum poisoning, when exposed to a variety of chemical agents. On the anode side, poisons may arise from the hydrogen production method, including hydrocarbons (such as  $\text{CH}_4$ ), carbon monoxide ( $\text{CO}$ ), sulphur compounds (such as  $\text{H}_2\text{S}$ ), and ammonia ( $\text{NH}_3$ ). In the air supply, contaminants include nitrogen oxides ( $\text{NO}$ ,  $\text{NO}_2$ ), sulphur oxides ( $\text{SO}_2$ ,  $\text{SO}_3$ ) and carbon monoxide ( $\text{CO}$ ). At both electrode catalyst layers, these compounds are understood to block active sites and decrease kinetic activity. The effects are typically cumulative, so even when low rates of contamination as present, effects can build up significantly over long duration operation.

### Catalyst degradation reduced rule set

The final rules base for catalyst degradation focuses on increased platinum solubility under defined voltage regimes. This mechanism accounts for both particle growth and agglomeration, and elemental loss through exhaust water. Detachment is attributed to loss of the catalyst supports, through carbon degradation which is considered in the gas diffusion electrode rules. Table 4.4 reveals that cell voltage is the dominant factor in platinum dissolution, both in steady and cyclic conditions.

Experimentally, controlled contamination is not possible in the experimental setup for two reasons. Whilst there is the possibility for poisoning compounds to be introduced from the filtered atmospheric air, this is assumed to be of negligible amounts, especially compared to imposed accelerated degradation conditions. Similarly, high purity hydrogen gas is used as the fuel feed, negating contaminant effects in the anode. Therefore, rules 14 and 15 which consider contaminant poisoning are not carried forward.

Rule	IF	THEN
A/B	Stack voltage is high OR Stack voltage is very high	Catalyst dissolution is evidenced
C	Stack voltage is normal OR Stack voltage is low	Catalyst dissolution is none
D	Stack voltage cycle number is high	Catalyst dissolution is certain
E	Stack cycle number is low	Catalyst dissolution is evidenced
F	Stack voltage cycle number is none	Catalyst dissolution is none

Table 4.5: Reduced catalyst rule base

Table 4.5 gives the reduced set of catalyst degradation rules. Rules A, and B represent the requirement for higher voltage levels to stimulate platinum dissolution (above 0.9V). This represents rules 1, 3, 12, 13, 16, 17, and 18 from table 4.4. When steady state and normal range loading conditions are experienced, extremely low catalyst degradation is expected, and voltage loss can be associated with other component modes. This completes the voltage envelope, and references rule 11.

Rules D, E, and F give consideration to the significance of voltage cycling on platinum degradation; as seen in previous rules four, five, six, seven, eight, nine, and ten. Cycles will be counted, and losses will be assigned as the number increases. Boundaries for a low number of cycles will be after 10's initially, and transition to high after 1000s are experienced, as reflected in figure 4.8 and rule six previously.

The rules lettering in table 4.5 follows the convention laid out previously for the membrane degradation rules set from table 4.3, and for the final rules base in table 4.10. Stack voltage measurements, in rules A, B, and C, relate to both membrane chemical degradation diagnosis and platinum catalyst degradation diagnosis. This illustrates the uncertainty in isolating individual degradation modes in the PEFC; it is not incorrect to have two degradation phenomena occur under the same operating conditions, as identified in the expert knowledge. For the final rules base, the rules for stack voltage will be collated as a single input, with multiple diagnostic outputs.

### Gas diffusion electrode degradation

The gas diffusion materials see the most limited degradation testing in research literature. This is in part because the established materials (carbon paper and cloths) are not specially developed for fuel cell applications – unlike the membranes and catalyst formulations – and partly because the degradation is difficult to separate from the water flooding losses. In this area of the knowledge acquisition only carbon materials will be considered, whilst water management

Rule	IF	THEN	Source
1	Voltage is at 0.55V	CO <sub>2</sub> release is moderate	[167]
2	Voltage is very high	CO <sub>2</sub> release is high	[167]
3	Air starvation (120% demand)	Cell reversal occurs	[168]
4	Fuel starvation (100% demand)	Cell reversal is severe	[85,169]
5	Cell reversal	GDE carbon corrosion serious	[142]
6	No fuel supply during shut-down sequence	Local cathode carbon corrosion	[142]
7	Air in anode during start-up sequence	Local carbon corrosion	[170,171]

Table 4.6: Gas diffusion electrode degradation knowledge base

problems are discussed separately in the following section.

The primary mode by which these carbon materials may fail is in material loss through consumption by side reactions in the fuel cell. Although carbon is chosen for its chemical stability, under certain conditions the PEFC may oxidise the GDE and platinum support material. This occurs when insufficient hydrogen is supplied and water electrolysis reactions oxidise the carbon to provide the required charge [166]. The corrosion may be seen on a cell wide scale, during low hydrogen feed, or locally during incorrect start-up/shut-down procedures [142].

The result of the carbon corrosion is catalyst particle detachment, reducing active area, decreased electrical connectivity to certain parts of the cell, also reducing the chemically active area, and potential collapse of the gas diffusion media. Table 4.6 details the knowledge based on this degradation scope.

Rules one and two are drawn from ex-situ experimental work by Roen et al. – electrochemical cycling on a fuel cell supplied with helium (cathode) and dilute hydrogen (4%, anode). The carbon dioxide release at 0.55 V is associated with the oxidation potential of carbon monoxide from the surface of the platinum catalyst; this is not itself a sign of carbon material oxidation, but should be noted in the knowledge study for reference and may possibly contribute to mitigation strategies. Carbon dioxide release at voltages above 1 V is associated with GDE corrosion, as this is the voltage required to consume the carbon material in a water electrolysis reaction [167].

Rules three and four state that cell reversal conditions may occur when insufficient reactant feed is supplied to the PEFC. Cell reversal is the effect of relative electrode voltage levels being exchanged; normally cathode voltage is higher than at the anode. This is a sign that water electrolysis reactions are occurring in order to maintain the high power demand – relative to reactant availability. In rule four, hydrogen starvation is seen to be much more severe than oxygen/air starvation. It should be noted, both of the experiments by Taniguchi et al. could not distinguish between carbon corrosion and catalyst agglomeration, which may occur together

under these voltage conditions [168, 169]. Rule five reveals, from a durability review by Zhang et al. [142], that when cell reversal occurs, the GDE damage is a serious concern for the PEFC health, and causes irreversible damage in the fuel cell.

Whilst high electrical demand loads can mean widespread reactant starvation, non-uniform distribution of hydrogen can also cause local-regions of fuel starvation. During start-up and shut-down sequences, different combinations of load and fuel supply may arise, meaning a boundary of fuel and air may occur within a single electrode compartment. The resultant cell reversal voltage will again induce carbon corrosion, most severe when hydrogen is the limited reactant, as stated in rule five, six, and seven. The GDE thinning can even be visually seen at the cathode, as in [171].

### GDE degradation reduced rule set

The diagnosis of GDE carbon corrosion focuses on the conditions which cause widespread carbon corrosion, rather than small-scale localised degradation. Broader corrosion is seen to be more severe for the PEFC health than the localised corrosion conditions; equally, it is not possible to validate very localised corrosion in the experimental test bench, as presented in chapter 5. This means the rules six and seven are not carried forward, and start-up/shut-down protocols should be followed to avoid localised degradation (both in testing and as advised for application systems) [171]. The final rules will also use the certainty rating terminology used in the other diagnostic outputs. Thus the reduced rule set is as in table 4.7.

Although only a small number of rules have been identified in table 4.6, the organisation and reduction process should still be followed to bring the terminology in line with the other diagnostic outputs. Reactant starvation (rules three and four) has been identified as the key operational condition which leads to GDE carbon corrosion. *Starvation* however is not a measurable parameter from the PEFC sensors; this is a linguistic term referring to having insufficient reactant to support the power generation reaction. Stoichiometry is the feature which characterises the ratio between the reactant supply and reaction demand. Its calculation is described thoroughly in the following section, when establishing the fuzzy input sets.

Low anode supply is seen in rule four to be a much more severe condition than low cathode

Rule	IF	THEN
G	Anode stoichiometry is normal OR Anode stoichiometry is excess	GDE corrosion is none
H	Anode stoichiometry is low	GDE corrosion is evidenced

Table 4.7: Reduced GDE rule base

stoichiometry [85]. Thus the anode flow condition is taken as the variable which defines GDE corrosion, table 4.7. If excess fuel is provided (“normal” or “excess” stoichiometry) then corrosion is avoided, is in rule G. If, however, insufficient fuel is provided to the PEFC, then carbon corrosion becomes more likely, rule H.

GDE corrosion diagnosis does not reach “certain” levels, as the carbon materials are seen to be sufficiently stable to mitigate degradation. In most cases of fuel starvation, the PEFC output will decrease in line with the reaction kinetics as modelled in chapter 3, rather than reach cell reversal conditions. The experimental work referenced in the knowledge acquisition process was produced ex-situ, with an external power supply to ensure the mode was experienced [167]. Therefore, the knowledge of GDE carbon corrosion cannot support a diagnosis beyond “evidenced” levels.

### **Water management problems**

Maintaining correct water levels within the PEFC is important for efficient functionality in several of the components. The membrane must be sufficiently hydrated for proton conductivity, and have consistent water content to avoid mechanical stressing as discussed in the rules of table 4.3. The GDEs can be blocked due to liquid water settling in the porous structure. Thus poor water management can influence ohmic losses, mass transport losses, as well as major physical damage to the MEA.

The knowledge acquisition performed for table 4.8 reveal that water management problems arise from a combination of water introduced to the cell through reactant humidification, water produced by the PEFC reaction, and the amount of water transported out of the cell exhaust. Temperature can also play an important role; water vapour is easier to transport, though it may condense on colder stack surfaces.

In table 4.8, rules one through five, eight, and nine characterise the effects of proper hydration in the membrane; “moderate” levels of hydration are preferred, too “low” and drying out occurs, increasing resistance, too “high” and liquid water condenses outside of the membrane in the GDE. Good hydration of the membrane equates to higher power efficiency. As a secondary effect, low content of water can also reduce thermal conductivity in the MEA components, meaning the stack as a whole is not as thermally homogeneous as it could be.

Stack temperature is a factor when considering water management; as mentioned previously, evaporation and condensation are intertwined with transport effects. Rules six and seven are from experimental work at elevated temperatures (above 100 °C) [165]. The hotter fuel cell reduced the rate of flooding in the gas channels, as well as allowing more water content in the exhaust gas.

Rule	IF	THEN	Source
1	Membrane hydration is moderate	Performance is best AND conductivity is high AND ohmic resistance is small AND efficiency is high	[79]
2	Membrane hydration is low	Proton conductivity decreases AND ohmic resistance increases AND power efficiency decreases	[79]
3	Membrane hydration is high	Liquid water condenses AND gas concentration decreases AND GDE gas channels become blocked AND power efficiency decreases	[79,104]
4	Membrane hydration is low	Ohmic resistance increases	[104]
5	GDE humidity is high	Ohmic resistance increases	[104]
6	Stack temperature increases	Exhaust humidity increases AND membrane hydrophobia increases	[79]
7	Stack temperature is high	Flooding rate is low	[165]
8	Membrane is dehydrated	Conductivity decreases AND ohmic resistance increases AND voltage decreases	[104,172]
9	Membrane is dehydrated	Thermal management “difficult” AND voltage decreases AND ohmic resistance increases AND temperature increases	[110]
10	Anode humidity is very low	Performance is very bad AND voltage decreases rapidly AND back diffusion rate is high	[173]
11	Anode humidity is low AND cathode humidity is increased	Performance improves AND voltage increases	[78]
12	Anode humidity is high AND cathode humidity is increased	Performance decreases AND flooding rate increases	[78]
13	Anode humidity is high AND cathode humidity is decreased	Performance increases AND flooding rate decreases	[78,79]
14	Cathode humidity is very low	Membrane dehydration at inlet AND uneven current distribution AND membrane ageing	[104]
15	Cathode humidity is high AND anode humidity is increased	Performance decreases AND flooding rate increases	[78]
16	Cathode humidity is high AND anode humidity is decreased	Performance increases AND back diffusion rate is high AND flooding rate decreases	[78]

Table 4.8: Water management problems knowledge base

Rules 10 through 16 all consider the level of humidification in the reactant feeds. Some operational strategies call for external humidification to ensure the membrane maintains water content, and this is another variable to be managed. Low input humidity, in either feed, is seen to result in low membrane humidification, and the associated performance detriment. Increasing humidification will improve electrical performance, as in rule eleven, though going beyond membrane saturation will increase the flooding rate.

### Water management problems reduced rule set

The knowledge acquisition has revealed that the stack temperature and reactant feed humidity are the most dominant conditions in causing water management problems. This leads onto the reduced rules set in table 4.9. Because it is also the location of water production the PEFC, the cathode is the most likely location for flooding events to initiate, and cathode feed humidification is acknowledged in rules M, N, and O. These three rules may alternatively be triggered by stack temperature; colder leading to flooding, hotter leading to evaporation and dehydration.

Rules P and Q consider the water produced within the stack by the PEFC reaction. Because of the inverse relationship between voltage and current in the PEFC polarisation, lower voltage equates to higher current, greater water production, and increased flooding potential – rule P. Within a normal power loading, water production should be accounted for in the stack design. These rules P and Q consider stack voltage for the same ranges as defined in rules A, B, and C (table 4.2) though in different combinations so are listed separately to the previous.

Rule	IF	THEN
M	Stack temperature is cold OR Cathode humidity is high	Flooding is certain AND Dehydration is none
N	Stack temperature is normal OR Cathode humidity is normal	Flooding is evidenced AND Dehydration is none
O	Stack temperature is hot OR Cathode humidity is low	Flooding is none AND Dehydration is certain
P	Stack voltage is low	Flooding is evidenced
Q	Stack voltage is normal OR Stack voltage is high	Flooding is none

Table 4.9: Reduced water management problems rule base

### 4.3.4 Final rules base

Thus the final rules sets are compiled in table 4.10. This brings together the knowledge acquisition and organisation for the fuzzy diagnostic system, from all the reduced rules presented in tables 4.3, 4.5, 4.7, and 4.9, for each considered component and degradation mode. The rules

Rule	IF	THEN
A	Stack voltage is very high	Membrane chemical breakdown is certain AND Catalyst dissolution is evidenced
B	Stack voltage is high	Membrane chemical breakdown is evidenced AND Catalyst dissolution is evidenced
C	Stack voltage is normal OR Stack voltage is low	Membrane chemical breakdown is none AND Catalyst dissolution is none
D	Stack voltage cycle number is high	Catalyst dissolution is certain
E	Stack voltage cycle number is low	Catalyst dissolution is evidenced
F	Stack voltage cycle number is none	Catalyst dissolution is none
G	Anode stoichiometry is normal OR Anode stoichiometry is excess	GDE corrosion is none
H	Anode stoichiometry is low	GDE corrosion is certain
I	Anode humidity change is large AND Cathode humidity change is large	Membrane mechanical stress is certain
J	Anode humidity change is large OR Cathode humidity change is large	Membrane mechanical stress is evidenced
K	Anode humidity change is small AND Cathode humidity change is small	Membrane mechanical stress is evidenced
L	Anode humidity change is none OR Cathode humidity change is none	Membrane mechanical stress is none
M	Stack temperature is cold OR Cathode humidity is high	Flooding is certain AND Dehydration is none
N	Stack temperature is normal OR Cathode humidity is normal	Flooding is evidenced AND Dehydration is none
O	Stack temperature is hot OR Cathode humidity is low	Flooding is none AND Dehydration is certain
P	Stack voltage is low	Flooding is evidenced
Q	Stack voltage is normal OR Stack voltage is high OR Stack voltage is very high	Flooding is none

Table 4.10: Final reduced rule base

function by considering the operating conditions observed for the PEFC, and outputting the certainty of any single degradation mode affecting voltage performance. This list of rules is a novel representation of the on- and off-design operating conditions which influence component degradation in the PEFC.

The linguistic sets which are provided in table 4.10 have been drawn directly from the outcomes and conclusions of the fuel cell and component durability knowledge in literature. These relate to fuzzy sets, which define the boundaries for each range. These are similarly defined using the expert knowledge and experience which populate the rules, in the following section.

### 4.3.5 Membership functions

With the rules base identifying the necessary variables that must be monitored, the following process is to define the fuzzy set boundaries for each linguistic term. That is to say, define what is meant by “hot” temperature, or “normal” stack voltage, etc. As with the rules definitions, this relies on expert knowledge for the operating boundaries of the PEFC. As this is the first time these sets have been defined, the trapezoidal membership functions have been used as the initial approximation, as was described previously in figure 4.2. The following sets are used in fuzzification and defuzzification as appropriate.

#### Stack voltage

The stack voltage operating envelope is well defined for PEFC systems, as seen in the modelling approach in chapter 3. Because all PEFCs utilise the same hydrogen-oxygen electrochemical reaction, similar performance is seen for hydrogen-based fuel cells. Model equations [12] and polarisation testing [174] has defined the different voltage regions well, which relate to the fuzzy boundaries in figure 4.9.

At the upper range of the performance envelope, “very high” stack voltage represents the open-circuit voltage level which was identified in membrane and catalyst degradation mechanisms. This is defined with full representation above 0.95 V by Ferreira et al. [161], Inaba et al. [149], and Sompalli et al. [147].

The “normal” stack voltage range is defined for the voltage range which PEFC systems are recommended to be used; 0.6 V is typically defined by manufacturers, as well as literature sources by Ramos-Paja et al. [175], and Chung et al. [52]. Other reports of “normal” voltage range up to 0.7 V from Ramaswamy et al. [148] and Borup et al. [176], or down to 0.5 V from Khan et al. [115]. Thus the core of the “normal” voltage set will span from 0.5 to 0.7 V; 0.6 V is the “normal” target, though some variation is permissible based on the evidence.

“Low” voltage is defined below the normal range, when the PEFC would be at higher loading conditions, and likely to be operating in the region dominated by mass transport losses. Ramaswamy et al. [148] and Chung et al. [52] both evoke “low” voltage conditions below 0.4 V.

The “high” voltage range fits between the “normal” and “very high” ranges. Testing results are common for voltage ranges both normal, close to 0.6 V, and OCV. However, conditions with only small loads applied, close to the OCV level are less common. This voltage range is strongly tied to catalyst testing protocols, which report on voltages above 0.8 V [52], 0.85 V [148], or above 0.88 V [85]. The core for the “high” voltage set is defined between 0.8 and 0.9 V. Part of the validation testing is to check on the behaviour characteristics within this range.

Between these core voltage ranges, the linear set boundaries are defined, which smoothly transition from one set to the next. These ranges and features can be seen in figure 4.9.

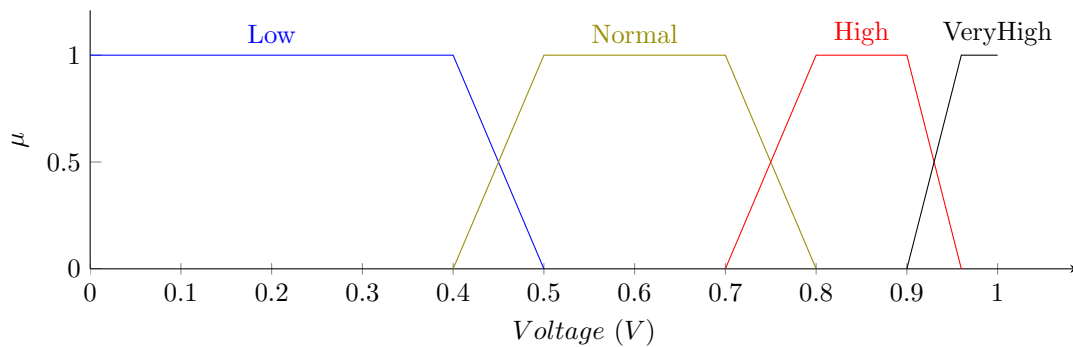


Figure 4.9: Fuzzy input sets for stack voltage

### Stack voltage cycle number

The voltage cycle counting is a feature which has been identified for catalyst degradation. It is the experimental results from Borup et al. that demonstrate this connection, presented in figure 4.8. Extracting the number of cycles from these results shows that after 250 repetitions the platinum area loss can be clearly detected. A different degradation rate is then observed for further cycling. After approximately 1000 cycles, at least 25% of the original electrochemically active surface area had been lost and performance was affected [91]. The testing concluded at approximately 2000 cycles, deemed a sufficiently “high number”.

These thresholds define the fuzzy sets for voltage cycle number; “none” is obviously defined for 0 cycles, a “low” number for cycles is between 250 and 1000; and above 2000 cycles is a “high” number, with minimal distinction in further losses. The study by Borup et al. also defines the threshold for the catalyst degradation effects and counting the cycles above 0.9 V [176]. This value shall be used in data processing to detect cycling loads, counting one for every transition through 0.9 V.

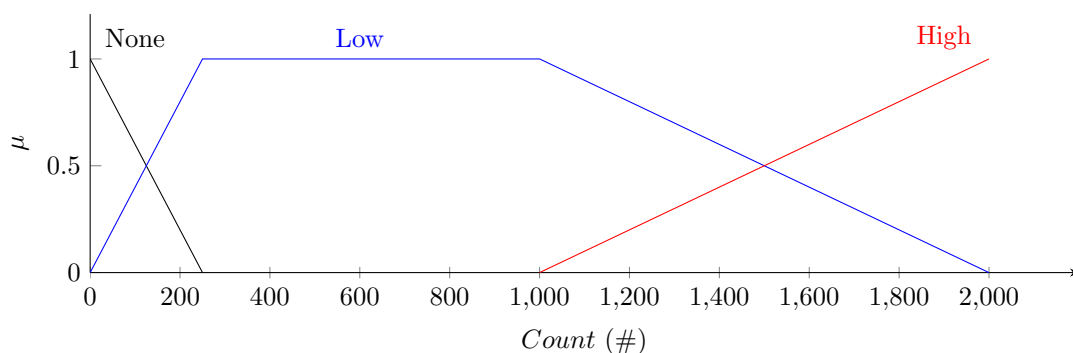


Figure 4.10: Fuzzy input sets for stack voltage cycle number

## Anode stoichiometry

Stoichiometric ratio is not a direct measurement from the observed system; it must be calculated based on the current loading and the flow rate of hydrogen supplied to the anode. This is a simple relationship between how much hydrogen is required to support the current being demanded, and what is actually being supplied. This follows the following calculation;

$$\lambda = \dot{n}_{H_2} \cdot \frac{2F}{I \cdot N} \quad (4.6)$$

where  $\lambda$  is the dimensionless stoichiometric ratio;  $\dot{n}_{H_2}$  is the flow rate of hydrogen into the PEFC stack, expressed in terms of molar rate (mol/sec);  $I$  is the applied current load (A);  $N$  is the number of cells in the PEFC stack; and  $F$  is the Faraday constant (96 487 C).

A stoichiometric value of 1 would represent perfect balance between supply and demand, greater values is an excess in supply, and lower values represents fuel starvation. Typically, the PEFC should be operated close to the balanced 1 stoichiometric ratio, or with some excess to account for load changes in the short term. Literature by Yousfi-Steiner et al. [85] and Kim et al. [65] indicates that between 1.5 and 1 stoichiometry, the PEFC performance is stable. Indeed, the larger scale PEFC stack developed by Scholta et al. was operated at a constant 1.25 stoichiometric ratio [103]. The “normal” stoichiometric core range is defined between 1 and 1.5.

The core of the “low” stoichiometry range is defined 0, where no fuel is supplied to the PEFC stack; the fuzzy boundary between 1 and 0 represents the transition through increasing severity of fuel starvation. “High” stoichiometry is defined for any excess ratio, where fuel supply rates are not a limiting concern. Theoretical analysis by Kulikovsky suggests that a “high” stoichiometric ratio of 5 is functionally the same as an infinite supply and this defines the core of the upper fuzzy set [177].

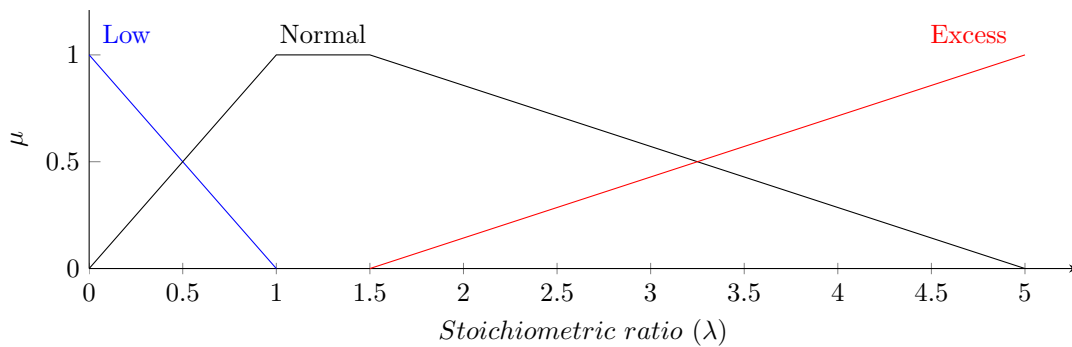


Figure 4.11: Fuzzy input sets for anode stoichiometry

## Cathode humidity

Humidity levels in the stack are measured from the gas supply inlet dew point. Expert sources are unified in defining “low” humidity condition as fully dry gas supply, at a 0 °C dew point; Bauer et al. [154], Endoh et al. [178], and Borup et al. [42] all use dry gases for severe durability testing. The “normal” range of humidity levels is somewhat broader than those for other input measurements, as the membrane can accept water from both reactant gas streams, the reaction product water, as well as maintaining an absorbed water content [50]. Recommended humidity dew points are found as low as 30 °C in [154] and by Debenjak et al. in [179], though usually greater humidity is used; 75 °C by Chen et al. in [180], 70 °C by Panha et al. in [181], or 80 °C by Zhang et al. in [135]. The core of the “normal” humidity set is defined between 30 °C and 80 °C to represent this range.

The “high” humidity range is associated with excess water content in the cathode gas stream, which becomes more prone to condensing and causing water flooding in the GDE and flow field. Literature reports dealing with humidity in this range indeed often only present the level as “excess” or “oversaturated”, as liquid water flooding makes true humidity measurement difficult [50]. Ex-situ stress testing by Huang et al. utilised humidities in excess of 100 °C; this shall define the core of the “high” humidity range.

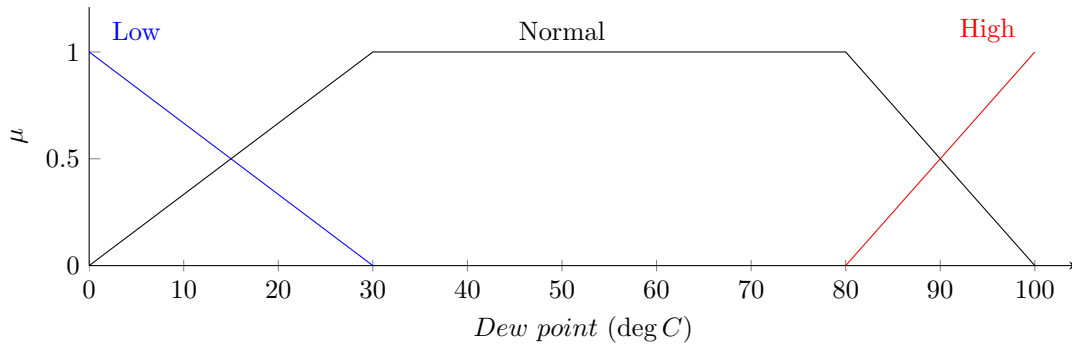


Figure 4.12: Fuzzy input sets for cathode humidity

## Cathode and Anode humidity change

The changes in humidity levels have been defined as affecting membrane mechanical stress and strength. Defining the change in membrane water content is a dimensionless coefficient ( $\lambda$ ) representing the ratio of water molecules to ionic groups in the polymer membrane, as proposed by Zawodzinski et. al [41]. This coefficient was further investigated by Huang et al. in [153] to define the change in reactant gas feed humidity. Defined empirically, the value ranges as in table 4.11:

Humidity	$\lambda$
0	1
40	4
60	8
70	22

Table 4.11: Water content coefficient values, from [153]

For the purpose of the fuzzy system input, measured humidity values are linearly extrapolated from between these empirical values. The ex-situ experiments by Huang et al. also describe the linguistic ranges of the coefficient change that is utilised in this diagnosis [153]. Very small changes in water content coefficient could be accounted for by the material without degradation, a “small” change was noted for a relative difference close to 4, and a “large” change for  $\sim 7$  or 8 and greater.

The fuzzy sets are defined as a fuzzification of these values; “around” 4 being a core of 3 to 5, “around” 7 being a core of 6 and greater values, and “none” being a core between 0 and 2, as in figure 4.13. These sets have the least expert evidence, so the boundaries may be adjusted in future iterations of the diagnostic.

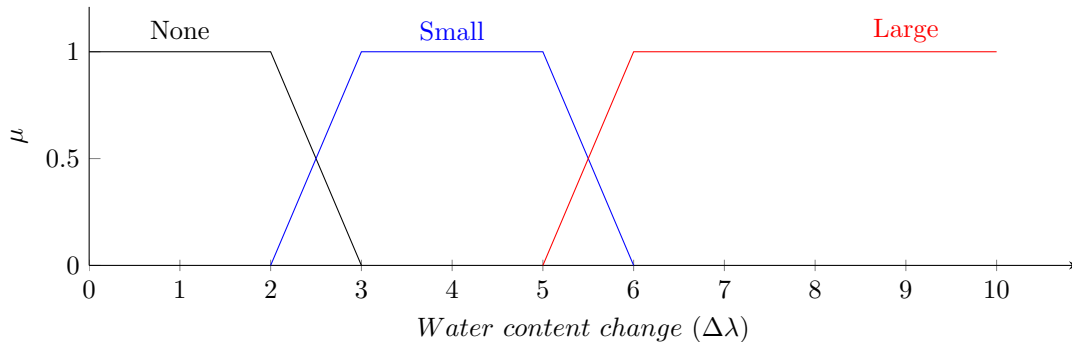


Figure 4.13: Fuzzy input sets for humidity change

### Stack temperature

Stack temperature is a direct measurement from the fuel cell, using temperature probes in the outlet coolant flow, or inserted directly into the stack structure. Of course, temperature will not be equal throughout the PEFC stack; the centre will retain more heat than the edge regions, and exothermic reaction output may vary across the face of the MEA, or between different cells. However, as a generalisation, the coolant outlet temperature will be assumed as the homogeneous stack temperature. This is seen as a good approximation, and is used in other experimental approaches, such as in [29, 93, 182].

The fuzzy boundaries for stack temperature are defined by the operational parameters for the equipment in consideration. Typically, PEFCs are operated at approximately 60°C, within a small window. This is in an effort to maintain predictable performance and water management, as well as stable conditions for the internal materials. Thus the “normal” stack temperature range is between 55 and 65°C.

Below the normal temperature, the “cold” range is represented at 0°C. This is an undesirable temperature range because of the increased water management difficulty; at very low temperatures ice may form. Elevated temperatures above the normal range should also be avoided, because of undue stress on the membrane. The “hot” stack temperature range is above 100°C, which is approaching the glass-transition temperature of common Nafion membrane material.

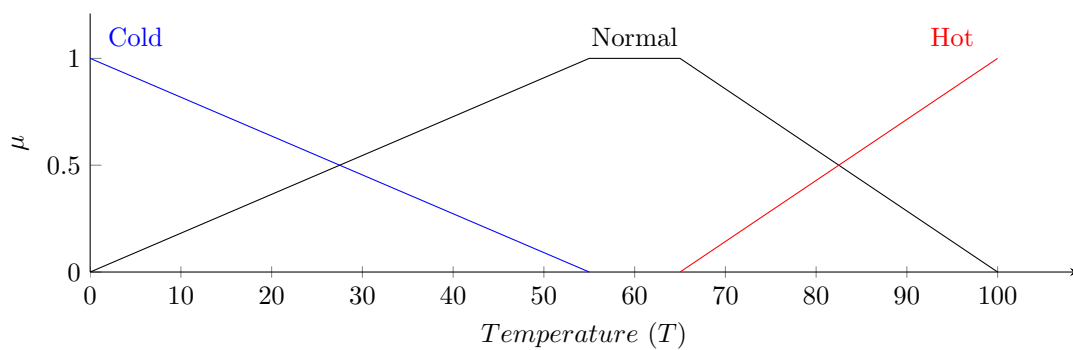


Figure 4.14: Fuzzy input sets for stack temperature

### Degradation modes

All of the defuzzification sets for the diagnostic outputs use the same group of fuzzy sets. These follow the format of “none”, “evidenced”, and “certain”, as seen in figure 4.15. These levels define how well the observed conditions are correlated with each degradation mode, and so the certainty of the expert assessment that any one fault is occurring. The outputs are used for all modes; membrane chemical breakdown, membrane mechanical damage, platinum catalyst dissolution, carbon material corrosion, liquid water flooding, and membrane dehydration.

An example is given here following rules E and F in table 4.10, and the correlation between voltage cycling and catalyst dissolution. Initially, when 0 or fully “none” cycles are counted, then the logic follows rule F for only a “none” diagnosis of platinum degradation. The membership value (Voltage cycles none  $\mu = 1$ ) is input at the antecedent of rule F, and carried to the output as the membership of the diagnostic consequent (Platinum degradation none  $\mu = 1$ ). The area of the “none” output set is averaged for a crisp numerical result of 0.05.

Progressing, as the number of cycles increases, and the “low” cycle count becomes true, so rule E outputs that the certainty of the diagnosis raises to “evidenced” levels. An example count

value of 200 voltage cycles gives input memberships for both “low” (Voltage cycle low  $\mu = 0.8$ ) and “none” (Voltage cycle none  $\mu = 0.2$ ). These are respectively handled by rules E and F to the two diagnostic consequent outputs (Platinum degradation evidenced  $\mu = 0.8$  and platinum degradation none  $\mu = 0.2$ ). The centroid of these combined areas outputs the crisp numerical result of 0.387.

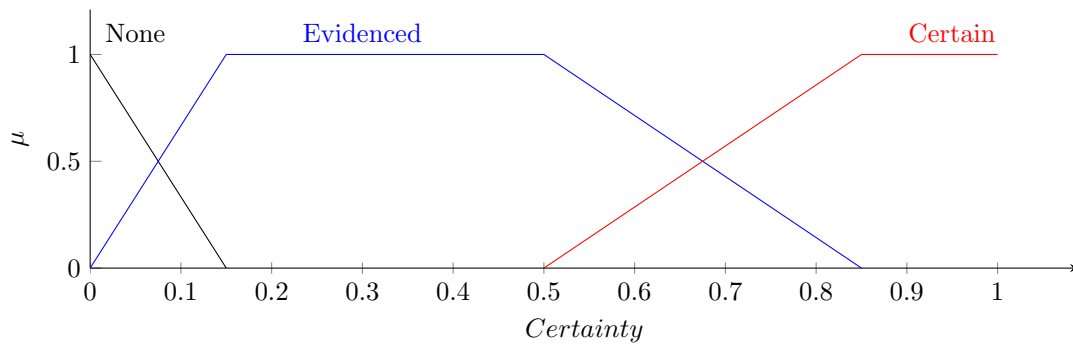


Figure 4.15: Fuzzy output sets for degradation mode certainty

### 4.3.6 Integration and Validation of the Expert Diagnostic System

The expert diagnostic system is to be integrated with the practical experimental test bench and tested to demonstrate operability. Control and monitoring is achieved through a National Instruments LabVIEW based software package, this shall be further discussed in chapter 5. The diagnostic system draws measurements directly from the PEFC, as in figure 4.16, and performs the necessary preprocessing to extract features such as cycle count before the diagnostic assessment. The output result is also integrated into the software interface for the operator’s information, and to guide control decisions.

Validation testing will amount to operating the PEFC in various on- and off-design modes and confirming diagnosis against the known degradation phenomena. Fuzzy sets have been

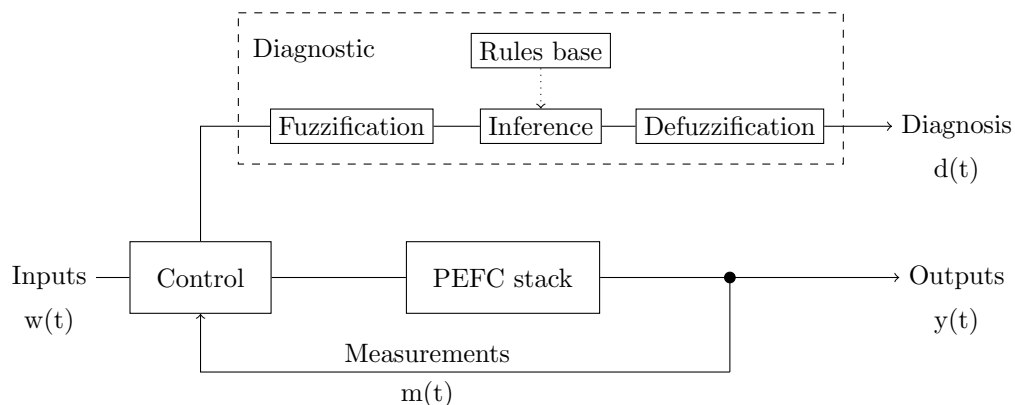


Figure 4.16: System architecture for fault diagnosis

defined based on knowledge and literature observations. Whilst the rules system is designed to account for degradation on all scales of system, tuning may be needed for the boundaries of the fuzzy sets. This can also be achieved during the validation process.

## 4.4 Summary

This chapter has detailed the development of the expert diagnostic system, and the fuzzy logic concepts which have enabled the direct use of linguistic and literature knowledge. The diagnostic processing will accept measurement signals from the functioning PEFC system, and use logic reasoning to diagnose which faults may be occurring in the fuel cell stack. Overall, this is a novel approach to the diagnostic problem for PEFCs that is not seen in the literature.

This chapter has established a rules database using expert literature sources from a range of durability testing and PEFC application case studies. This is the first such compilation of diagnostic knowledge for PEFC systems. Through the knowledge acquisition and organisation, the fundamental conditions influencing the different degradation modes have been distilled.

This thesis has also defined the fuzzy sets which will be used for the inputs and outputs of the reasoning process. This is an original approach to unifying the outcomes of PEFC publications, where authors frequently describe conditions using the same linguistic terms (“high”, “faster”, “cold”, etc.) though for different discrete values. The fuzzy set definitions capture the ranges which show similar behaviours.

The diagnostic process functions in real time, in parallel to the PEFC system. The inputs to the diagnostic are the measurement and control signals from the fuel cell test bench controller; voltage, stack temperature, and reactant humidities are directly measured, and data processing provides voltage cycle counting, and stoichiometry values. These inputs are fuzzified and compared to the rules base for degradation modes. Where greater correlation exists, so the diagnostic output reports a higher certainty that a particular mode is causing performance loss in the PEFC. The degradation modes considered are for membrane chemical and mechanical breakdown, platinum catalyst dissolution, GDE carbon corrosion, and water management problems being flooding and drying out. The result is presented to the operator to provide durability information and influence further control decisions.

## Chapter 5

# Experimental Methodology

This chapter describes the experimental equipment used in testing and validation for the diagnostic system. A high-specification PEFC has been acquired for these procedures. Testing methodologies are devised to investigate degradation phenomena under various operational conditions; a range of electronic loading and temperature conditions are applied to examine the diagnostic rules.

The first section of this chapter introduces the test bench, fuel cells and hardware elements. Following is a discussion of the design of the bespoke Fuel Cell Control and Monitoring (FCCM) software. The chapter closes in describing the testing methods and the goals therein.

### 5.1 Test Bench

The experimental equipment is constructed around the fuel cell stack, based on the operating requirements. Figure 5.1 shows the general arrangement of the fuel cell testing system. The components in the system include; fuel cell itself; the gas supply lines originating in pressure vessels and the air compressor, the high pressure regulators *HPR* and low pressure regulators *LPR*, valves *V* and mass flow controllers *MFC* which control the reactant flows; the humidifiers *H*; the back pressure valves *BPV* and water condenser *Trap* at the exhaust of the system; the temperature control circuit featuring a water pump, heat exchanger *Heat Ex*, and header tank; the positions of various temperature *T*, pressure *P*, and flow *F* sensors; and the electronic load bank. In the following sections, firstly the fuel cell is described to establish its construction and requirements, leading to a description of the supporting ancillary systems.

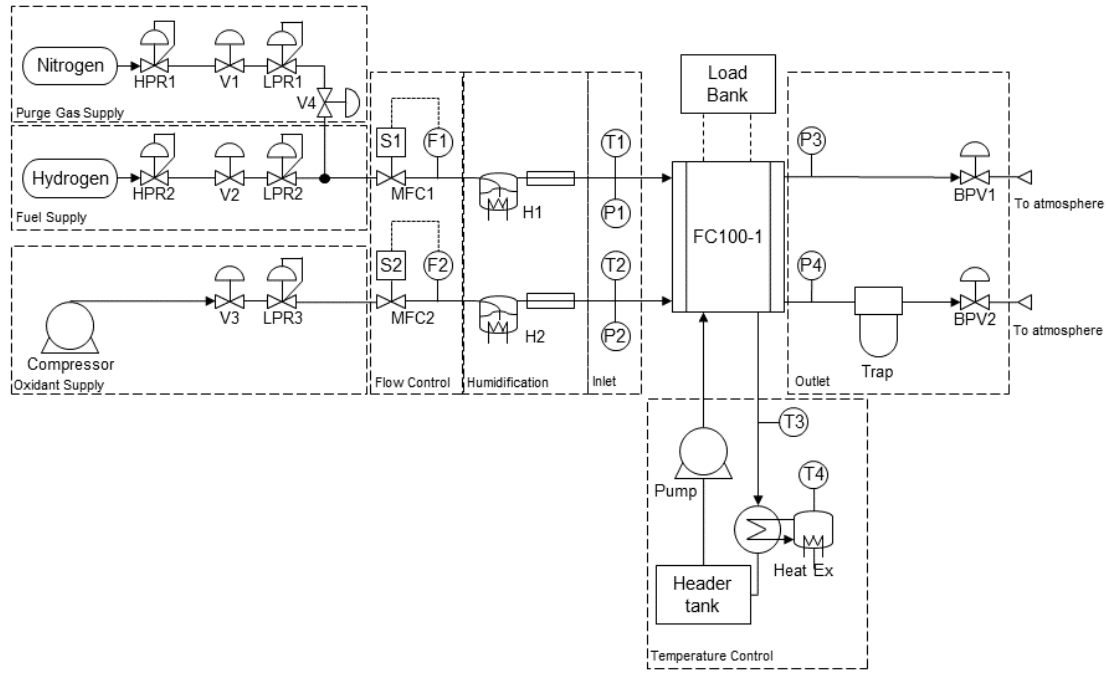


Figure 5.1: General arrangement of the fuel cell test bench

### 5.1.1 Fuel Cell

The PEFC which has been sourced for the experimental testing is produced by Pragma Industries. It is designed for research and development activities, as well as easy integration into application systems. This uses the materials and technologies available and commonly used for commercial solutions. Thus this PEFC is representative of the state-of-the-art in both academic and industrial practices.

The *FC100-1* is a single cell PEFC construction, with  $100 \text{ cm}^2$  cell active area (this is identified in the stack designation coding). The membrane is a  $25 \mu\text{m}$  thick Nafion-XL polymer. On either face is the catalyst layer; platinum catalyst, supported on carbon-black particles, to a loading of  $0.2 \text{ mg}/\text{cm}^2$ . The GDE layers are Sigracet 10 BC, a carbon paper material with a hydrophobic PTFE coating to promote water shedding. These components constitute the MEA, and are supplied pre-assembled as a single component as seen in figure 5.2.

The MEA is supported between two monopolar plates (only one face is in contact with an MEA) which include gas diffusion channels on one face and water cooling channels on the reverse. The gas diffusion pattern is a seven-fold serpentine through-flow arrangement for both electrodes. The cooling pattern has three serpentine channels on each half of the plate area. Figure 5.3 shows these two faces, and the arrangement of the flow channels. Other notable features are the reactant and coolant manifolds which distribute the fluids through a multiple cell stack construction.

The monopolar plates are produced in Graphtek LLC GR-940 composite graphite material. This material is utilised for its chemical stability in the fuel cell electrode compartment conditions, low hydrogen permeability, and adequate thermal and electrical conductivity throughout the PEFC. The gas and water flow channels are machined onto the faces of the plate. The monopolar plates are sealed to both sides with silicone gaskets. These contain and separate the various fluid flows within the fuel cell.

At either end of the FC100-1 construction are gold-plated current collectors. These conduct all electricity generated within the fuel cell to the external circuit. A surface coating of gold is used here to minimise electrical losses due to contact-resistance. The current collectors are backed in a thick silicone insulator to prevent current flowing to the end-plates, which would pose a safety hazard as well as a performance loss.

The end-plates are thick anodised aluminium structural elements which are designed to evenly distribute compression loading across the face of the MEA. This is important for good sealing performance, and electrical contact between MEA and monopolar plates for even current loading. The entire construction is held together with screw-threaded compression bolts; twelve around the perimeter. By adjusting the torque on the bolts, the amount of compression force can be controlled, which has been seen to affect performance. Compression force however is not a tested variable during this project, hence it will be constant for all testing procedures at 8 Nm torque per bolt (as recommended by the manufacturer). The compression bolts are also insulated from the monopolar plates with plastic sleeves, to prevent short-circuiting. Fittings on the outer face of the end-plates are for the various flow pipes to be connected; the inlets and outlets for the anode, cathode, and coolant flows.

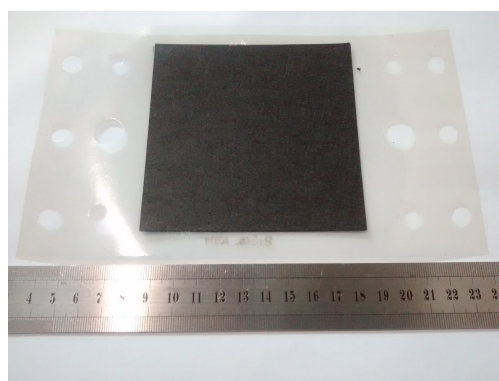


Figure 5.2: Image of the MEA for reference and scale

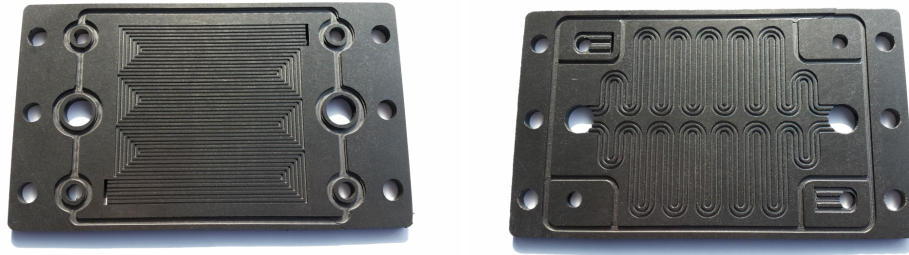


Figure 5.3: The faces of the monopolar plates in the *FC100*; flow fields left, coolant channels right

### 5.1.2 Ancillary subsystems

A number of ancillary subsystems are included in the test bench, as seen in figure 5.1, which support the function of the fuel cell. These supply reactants, remove exhaust, control temperature, and apply electronic loading. The computer systems are also included in this set, which monitor and control the overall system.

#### Fuel supply

The hydrogen fuel is sourced from a compressed gas vessel. This ensures continuity of supply and high fuel purity, and is equivalent to the storage vessels present in portable and vehicular fuel cell application systems. Fuel flow is controlled at the vessel outlet through a high pressure regulator *HPR2*, protecting the fuel supply subsystem pipes from excess pressure. Adjacent to the test bench the isolation valve *V2* and low pressure regulator *LPR2* provide manual control for the supply directly to the anode inlet. All control equipment for this subsystem is manually configured and remains constant throughout operation.

#### Oxidant supply

Oxidant used at the FC100-1 cathode is air; sufficient volume of oxygen should be available from atmosphere, and this is also equivalent to the systems used in application. An air compressor pressurises and dries the supplied oxidant flow, providing a continuous pressurised flow. Similar to the fuel supply subsystem, a regulator *LPR3* and isolation valve *L3* are installed directly adjacent to the test bench to control flow to the cathode supply pipes.

#### Purge gas supply

This third gas supply available to the test bench is nitrogen gas, used to purge the fuel cell anode gas chamber of air before test procedures. This is particularly relevant for the anode chamber and direct air-fuel mixing. As with hydrogen fuel supply, nitrogen purge gas is sourced from a

compressed gas vessel, with an integral high pressure regulator *HPR1* and isolation valve *V1*, as well as a low pressure regulator *LPR1*. The valve *V4* allows to select between the fuel flow or the purge flow as required.

### **Flow control**

Downstream of the supply subsystems, mass flow controllers provide the system control for how much gas is supplied to either electrode chamber. The control and measurement signals for the mass flow controllers are communicated through the low voltage electrical subsystem. Flow controllers are used on both anode (*MFC1*) and cathode (*MFC2*) supply lines.

### **Humidification**

Downstream of the mass flow controllers, the reactants pass through gas humidifiers *H1* and *H2* – both anode and cathode lines are humidified. These are bottle-type humidifiers, where the gas flows bubble through the heated water volume, increasing moisture content. Upon exiting the humidifier, the gas stream continues through a heated hose. This ensures the gas flow maintains temperature and water content, and does not condense immediately.

The humidifiers are controlled using individual heater power supplies. The requested temperatures are set manually and controlled externally to the fuel cell control software.

### **Inlet sensors**

Directly before the FC100-1 inlet, temperature and pressure sensors measure the supplied gas feed parameters at both the anode and cathode. In figure 5.1, *T1* and *P1* measure the anode inlet, and *T2* and *P2* measure the cathode inlet. The temperature measurement is from a K-type probe; sufficient for -200 – +1350 °C, and more than adequate for the PEFC temperature range. The housing for these probes are stainless-steel, and well suited for both gas feed environments with low chance of damage or contamination. Pressure measurements are made using a powered transducer. These instruments have a detection range of 0 – 10 Bar, as is again well suited for the gas feed environments. The low voltage subsystem supplies the power to, and receives measurement signals from these sensors.

### **Outlet lines**

At the outlet of the FC100-1, further pipe lines carry the excess fuel flow and exhaust air away from the fuel cell. Pressure transducers *P3* and *P4* monitor the outlet gas pressures, as well as the cathode outlet line including a water condenser *Trap*. As the reaction product water is

expelled at the cathode, this exhaust will see increased humidity and any condensation could block the outlet line downstream; the water trap aims to avoid any complications arising.

Both anode and cathode outlet lines terminate in manual back pressure valves *BPV1* and *BPV2*, as a final flow restriction to create pressurisation across the system. Pipes continue downstream of the BPV to safely vent to atmosphere.

### **Temperature control circuit**

As the *FC100-1* includes integral water coolant channels, a separate circuit for deionised (DI) water flow and temperature control is included in the test bench. The electric water pump pushes the DI coolant through the fuel cell. The DI water flow passes through a water-water heat exchanger *Heat Ex*, with integral electric water heater. This can heat up the water within the heat exchanger and in turn the “coolant” water flow – it should be noted, because of the smaller scale of this fuel cell, it may not maintain temperature based only on the fuel cell reaction. The water heater can be used to increase the coolant temperature. Upon the return flow the DI water passes through a header tank to remove air bubbles. At the fuel cell outlet, temperature probe *T3* measures the coolant flow temperature, which is assumed to be equivalent to the stack internal temperature at steady state conditions. Probe *T4* monitors the heat exchanged temperature.

In practice, the pump must remain on throughout usage to maintain pressure balance against the gas flows. If the gas chamber pressure exceeds the water coolant pressure, there could be internal gas leakage, which would be detrimental to performance and potentially hazardous in the case of hydrogen leakage.

### **High voltage electrical**

The purpose of the high voltage electrical subsystem is to simulate the application power demand on the fuel cell. This is achieved with a resistive electronic *load bank*. High voltage cables connect to the fuel cell, and measurement of voltage, current, and electrical power are communicated to the computer and control software. This is visualised in the top portion of figure 5.4, with the *FC100-1*, the *Load Bank*, and *PC* in their relative positions.

### **Low voltage electrical**

The low voltage electrical subsystem supports all other instrumentation. Power is supplied for the mass flow controllers and pressure transducers, as well as the coolant pump motor, and the water heater in the coolant subsystem. The signal outputs from the instruments are

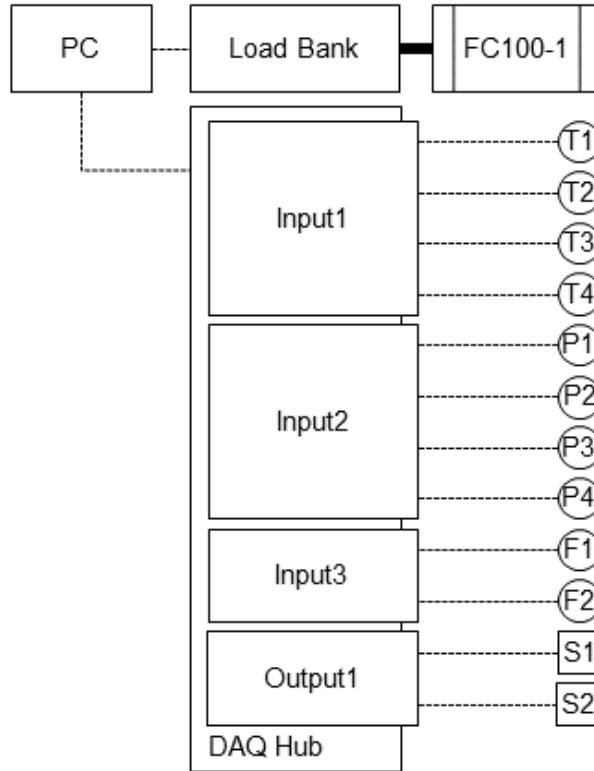


Figure 5.4: Electrical subsystems of the PEFC test bench

communicated to a National Instruments data acquisition USB hub *DAQ Hub*, as indicated in figure 5.4. The three different input modules are connected each for temperature, pressure, and flow measurements. The output module sends the flow rate demands to each of the solenoid valves in the mass flow controllers; *S1* for the anode flow and *S2* for the cathode flow. The data acquisition hub provides easy connectivity between the various instruments and the computer control software.

## 5.2 Fuel Cell Control and Monitoring Software

The final subsystem is the control software, running on the test bench computer, named the Fuel Cell Control and Monitoring software (FCCM). The FCCM has been developed by the author, programmed within the National Instruments LabVIEW environment. This is a visual programming language that easily interfaces with instruments and the data acquisition hub, the high voltage load bank, as well as offering the capability to run protocols for testing and monitoring. The full LabVIEW code can be found in appendix A.

The control software is designed as a state machine, following the processing flow as depicted in figure 5.5. After starting the FCCM software, the initialisation accepts process metadata regarding the fuel cell stack and testing objectives from operator inputs. The initialisation

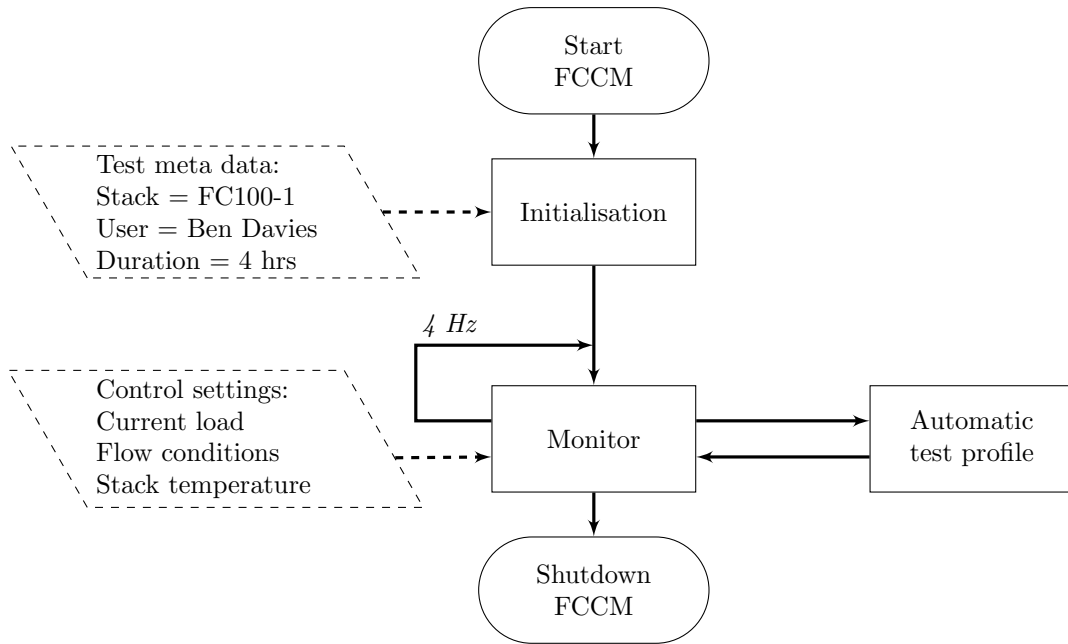


Figure 5.5: FCCM state machine design

interface can be seen in figure 5.6. This information forms the header to the datalog file, which is created before the fuel cell is activated and monitoring begins. Other parameter inputs will define limits to be observed by instrumentation and software during the testing, for example current and voltage limits for the load bank.

Transitioning to the main monitoring process will activate the various powered hardware elements – instruments such as the mass flow controllers and pressure sensors, and engaging the electronic load. The monitoring action loops every 250 ms (4 Hz). Each iteration will read measurements from the instruments and issue the user controls – the required current loading to the high voltage subsystem and reactant mass flow rates – as well as making rudimentary control decisions for stack temperature. Figure 5.7 shows the main FCCM interface. Measurement signals may be traced in the chart at the top of the panel, as well as the main electrical outputs

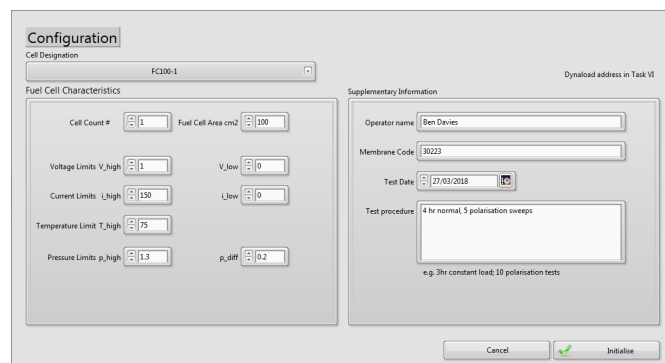


Figure 5.6: FCCM initialisation interface

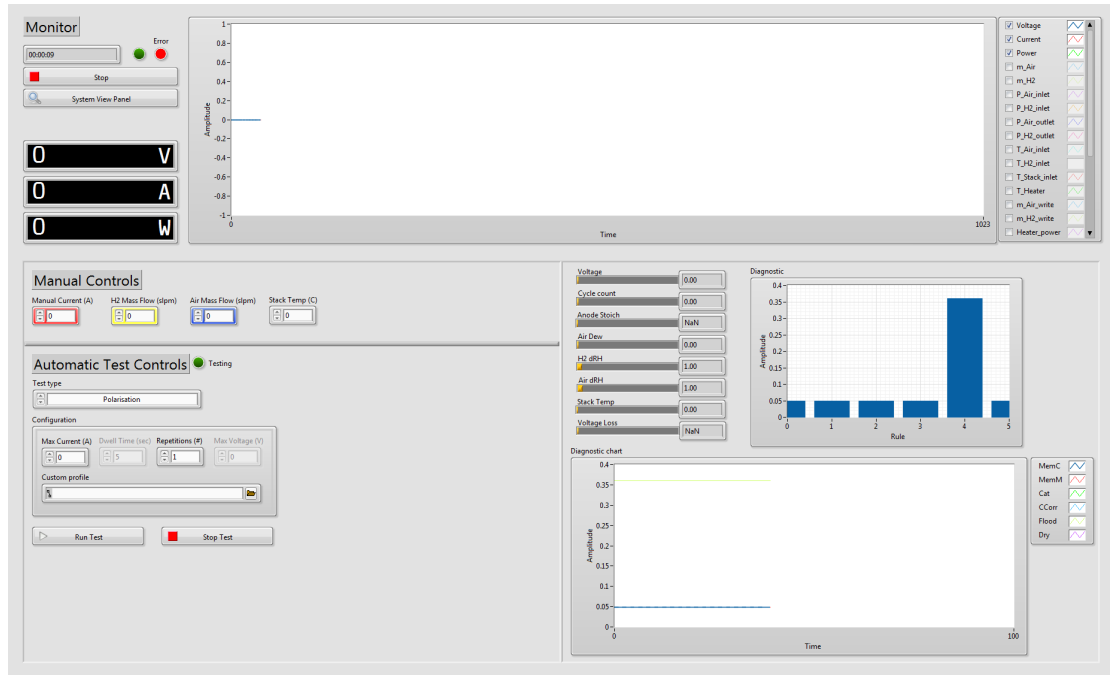


Figure 5.7: FCCM main interface

being presented numerically at all times. Below this, to the left, is the test control panel, where the operator may adjust the test bench variables manually, or initiate an automatic test procedure; current profiles are managed within the software to ensure accuracy and repeatability.

To the lower right of the interface in figure 5.7 is the diagnostic panel. This presents the outputs of the fault detection model and expert diagnostic process. Within this panel, to the left are the diagnostic inputs which allows the operator to track any changes to performance in comparison to knowledge and experience. The bar chart to the right shows the diagnostic outputs for the 6 degradation modes; these are the defuzzified certainty values ranging from 0 to 1 for lower to higher respectively. This allows the operator to compare the relative levels of the diagnoses, to determine which mode is dominating the performance loss. At the bottom of the diagnostic panel, a chart traces the 6 outputs with time to provide the operator with more detail as to the progression over time. The diagnostic operates as a subroutine alongside the main FCCM process; no automatic control decisions are fed back to the main program.

The third interface of the FCCM is a simple system view panel, which presents the measurements values from the test bench, relative to their position around the PEFC. This can be seen in figure 5.8. The anode gas flow is to the left, the cathode to the right, the electrical loading measurements are above the PEFC image, and the temperature circuit measurements below. This provides the operator the up to date operating conditions at a glance.

Measurement values are recorded to the datalog file, as well as the manual commands in order

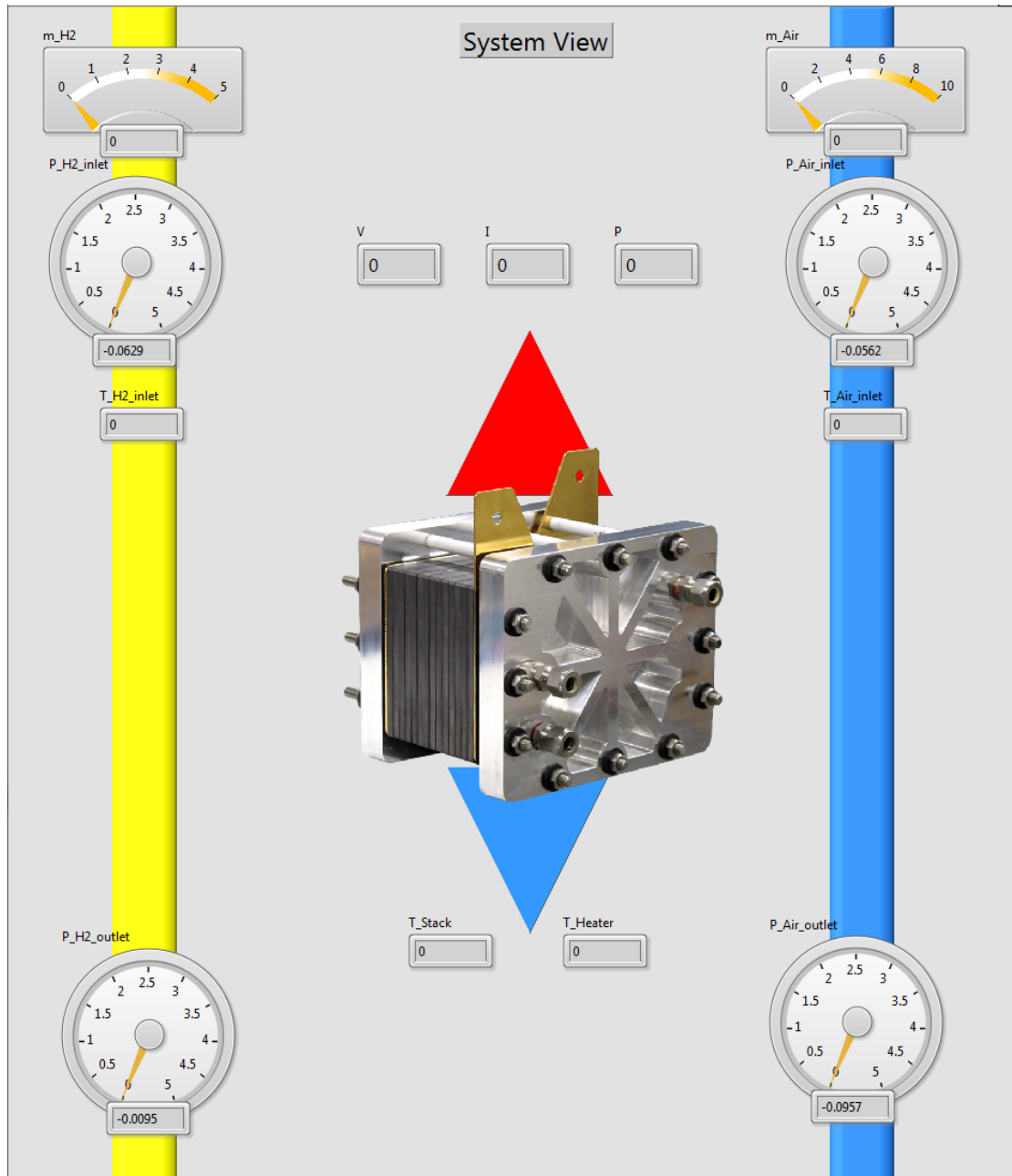


Figure 5.8: FCCM system view interface

to keep an account of the operator inputs and make comparisons to measured performance when required. It should be noted, not all parameters can be controlled within the FCCM software. Reactant pressure delivered by the fuel supply subsystem is managed by manual regulators; the humidifier temperature controllers are self-contained units with no software interaction; exhaust back-pressure valves are manually adjusted to give the desired pressurisation through the system. However, these particular parameters are usually maintained constant throughout operation and so it is unnecessary to include them in the monitoring software.

Automated voltage procedures can be delivered by the FCCM, with the testing process step. In a sub-panel of the main interface window, the operator may select from predefined testing procedures or input a custom current loading-profile. Whilst operating in the testing state the FCCM restricts the manual controls from the user, in preference of delivering the carefully timed procedure. The program continues to iterate at 4 Hz, recording measurements and commands to the datalog file.

The exit from the monitoring process of the FCCM is via a power down state. This is not the shut down procedure followed for the fuel cell – that is usually completed within the main programming iteration – rather, power down sends final commands to ensure instruments are de-powered, the electronic loading is removed, mass flow controllers are closed, etc. The result is to end the fuel cell operation, and put the test bench into a dormant state.

The FCCM software has been developed by the author to meet the specific requirements of this experimental test bench. The high level of manual control and live data-presentation allows the test operator to impose the desired conditions on the PEFC with good precision, and feedback of the progression of the test. The modular display interface also provides visual indications of different measurement progressions through time.

Automating the testing procedures is seen as a vital function towards ensuring tests are highly controlled and repeatable. Under the present design, only current loading is managed during automated testing; this is the main investigation variable as seen in the following section. As the FCCM software has been designed by the author and bespoke for the test bench, the automated testing capabilities may be expanded in the future.

### **5.2.1 Integration of the fault detection and diagnosis**

As has been indicated in previous chapters 3 and 4, the designed fault detection and diagnosis processes function in parallel to the PEFC system and on-line within the FCCM software platform. Figure 5.9 represents the combined system architecture. The user inputs a set of control demands  $w(t)$  to the FCCM interface; current demand, reactant gas supply, and stack temper-

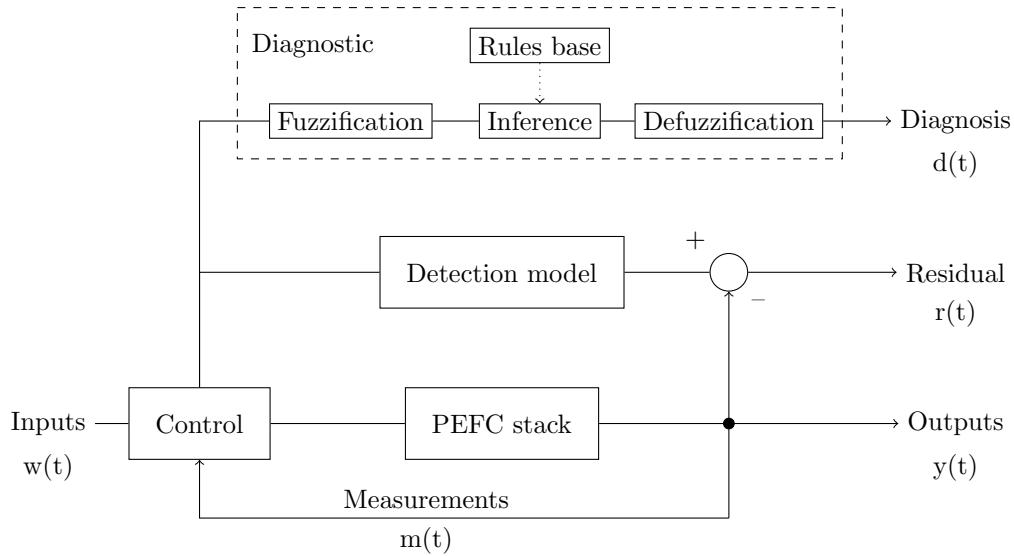


Figure 5.9: System architecture for fault detection and diagnosis integrated with the test system

ature set point. This actuates the controllable instruments across the test bench to operate the PEFC. Measurement signals for temperature, pressure, flow rate, current and voltage are returned from the sensors.

The detection model calculates the voltage prediction based on the operating conditions at that time, accepting measurements of current, stack temperature, and gas pressure at each inlet. The relative voltage differential  $r(t)$  is provided as the state of health indicator, for how great the difference is between the measured performance and the value expected from the model. At the same time, the expert diagnostic system makes an assessment of which degradation modes may be acting within the FC100-1, if any. The fuzzification processing accepts measurements of voltage, stack temperature, gas feed dew point temperature, and the calculated features of voltage cycle count, fuel stoichiometric ratio, and humidity change. The diagnostic outputs certainty ratings for each of the six degradation modes; these results are presented as bar charts so the operator can assess the progression of the test.

### 5.3 Experimental Methodology

The experimental test bench has been constructed to provide a high level of control and monitoring features. To this end, many different experimental procedures are available to the operator. This section shall detail the testing procedures carried out as a part of this study. The goal of these tests are to firstly establish normal performance for the FC100-1, before imposing degrading conditions.

The testing procedures are defined by the current loading conditions applied to the PEFC.

Parameter	Value
Stack temperature	50 °C
Air flow rate	1.2 slpm
Fuel flow rate	4 slpm
Air humidity	100%
Fuel humidity	55%
Inlet pressures	1 barg

Table 5.1: Flow conditions for the test schedule

Flow conditions are not tested at this time, and the parameters are controlled based on the manufacturers recommendations. The values listed in table 5.1 are used for all tests.

### 5.3.1 Testing procedures

Much of the testing is defined based on a series of individual procedures performed in sequence to achieve the desired overall operation. Start up and shut down procedures are naturally performed at the beginning and end of the test schedule, with certain specific electronic loading conditions applied in between. The following describes the individual procedures.

#### Start up

This start up process is followed to ensure the PEFC is in the best possible state before every testing process. Start up includes a nitrogen purge-gas supply to the anode inlet, heating up the fuel cell, humidifiers, and other equipment as required, and establishing nominal performance before testing.

After the fuel cell is constructed or stored, air may have been allowed to enter the anode chamber. If hydrogen were to be supplied immediately, a hydrogen-oxygen direct mixing would be present, known to result in degradation phenomena. By purging the anode chamber with nitrogen, any air (and associated oxygen) can be removed, replaced by the inert gas. During the anode purge, the cathode is supplied with normal air flow, and the coolant flow pump is activated; this ensures all mechanical forces normally acting within the stack are present, and the membrane does not suffer undue stress from partial-pressurisation.

The start up process also allows the PEFC and supporting ancillary subsystems to reach their desired operating temperatures. Inadequate temperature can significantly detriment the output performance not only of the fuel cell, but of the humidification and temperature control subsystems also. Pre-heating before beginning testing will mean designed performance can be established quicker than for a cold-start.

The pre-heat and purge period lasts for approximately 20 minutes. Once all temperatures are approaching set-points and gas flows have been checked for flow and pressurisation, the hydrogen fuel reactant feed can begin. The nitrogen supply to the anode is shut off and hydrogen flow started; after a short delay the stack output will rapidly reach OCV levels, as electronic loading remains disabled at this time. Observing OCV is one performance indicator available pre-test, and as a check that reactant flows are present and the PEFC is ready for use.

Open circuit voltage however should not be a long-term loading condition (unless this is the nature of the testing procedure) as this has been shown to induce component degradation. Soon after OCV is established, the electronic load is to be activated and brought to a “normal” current-voltage level. Load is applied stepwise until 0.6 V is achieved, as was defined in chapter 4 for voltage ranges. This “normal” current-voltage performance is a second indicator that the PEFC is in good working order, ready for the desired testing to begin. This concludes the pre-testing start up procedure.

### **Steady state loading**

Steady state loading is the most simple electronic loading condition available, and achieved by programming the desired current demand to the high voltage load bank. Typically, loading is applied stepwise to reach the desired set point – this allows the operator to observe the loading response and validate the current-voltage relationship without over-shooting. The current loading is then held constant for the test duration. Within the limitations of this test bench the longest operational time possible is approximately 4 hours.

Voltage ranges will match the fuzzy linguistic ranges defined in chapter 4, section 4.3.5; “very high” (approximately 0.95 V, open circuit voltage), “high” (0.85 V), “normal” (0.6 V) or “low” (0.35 V). The associated current loading values are; 0 A for “very high” voltage, 2 A for “high” voltage, 15 A for the “normal” voltage level, and 40 A to give “low” voltage. These values have been defined through empirical experience working with the test bench and the FC100-1. During steady state loading tests, temperature, pressure, flow rate, and humidity settings will all remain constant. Only voltage will be adjusted as the tested variable.

The different voltage levels are expected to exhibit different degradation modes and diagnostic responses. Long term operation at a “normal” level should not induce significant degradation, and there should be no diagnostic output, as in rule C in the rules base, table 4.10. Operating instead at a “low” voltage follows rule P, where this is expected to increase water production and induce water management problems. The higher current loading may also instigate some carbon corrosion, should hydrogen stoichiometry be sufficiently low, which would activate rule

H from the rules base.

Allowing the fuel cell to operate at steady open circuit voltage is expected to cause irreversible chemical degradation to the membrane. Some platinum agglomeration may also occur, however because of the steady state operation the membrane will be most significantly affected. This is to test the diagnostic outputs of rule A. It is not wholly clear from the literature evidence in chapter 4 what the expected result of long term low load operation is, at a “high” voltage output. This level may avoid both the platinum and membrane degradation voltage range, and will test the function of rule B from table 4.10. The results of this test have the potential to contribute to knowledge of degradation modes at this previously untested current range.

### Dynamic loading

Steady state power draw is not typically expected in true PEFC application. Whether the fuel cell is used for small scale portable electronics or larger transport applications, output power requirements will vary dynamically throughout a given usage cycle. This even holds true for the larger stationary power generators, where the fuel cell may experience changing loads throughout a long term usage period, as well as the potential for start-stop cycles.

Voltage ranges follow the values defined for the steady state loads, with dynamic transitions between. The first loading pattern is tested for rapid, stepped transitions between the two current levels. Figure 5.10 gives an example of the dynamic loading procedure. A dwell time of 10 seconds is allowed such that current-voltage response will stabilise, and the MEA may experience the full effect of the loading change. This testing regime is similar to some seen in the literature, such as in [161, 183–185]. Because the FC100-1 is of a smaller active area than those used in some of these studies a shorter duration is allowed for stabilisation, and 10 seconds has proven sufficient in experience working with the test bench.

The second loading pattern is tested for a simulation of an automotive drive cycle. This draws

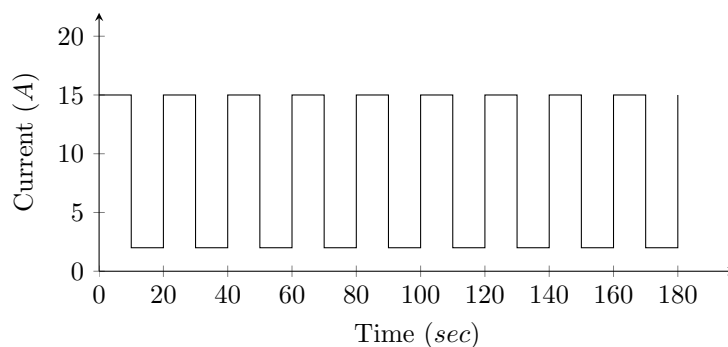


Figure 5.10: Example stepped dynamic loading profile, normal–low

on the New European Driving Cycle (NEDC) as a pattern for vehicle operation within Europe. Whilst this drive cycle has received some criticism as a poor representation of true driving patterns [186], it is however broadly utilised for testing fuel cell electric vehicles in automotive applications, as in [176, 187–189].

In this testing regime, the fuel cell is assumed to be used for direct drive power, with no energy storage or auxiliary loads. This means the fuel cell must account for the full range of motor loads, including hard acceleration and OCV idle; this is the most extreme loading condition for a PEFC in automotive applications. The vehicle speeds are converted to current loading using approximations for vehicle design and use, as below:

$$P_{drive}(t) = \frac{F_{acc}(t) + F_{drag}(t) + F_{roll}(t) \times v(t)}{\eta} \quad (5.1)$$

where  $P_{Drive}$  is the drive power required,  $F_{acc}$ ,  $F_{drag}$ ,  $F_{roll}$  are the forces acting on the vehicle for acceleration, aerodynamic drag, and rolling resistance, respectively,  $v$  is the vehicle speed,  $\eta$  is the transmission efficiency. The force variables are defined in the following calculations:

$$F_{acc}(t) = M_{veh} \times a(t) \quad (5.2)$$

$$F_{drag}(t) = \frac{1}{2} \times \rho \times v(t)^2 \times A_{veh} \times C_d \quad (5.3)$$

$$F_{roll}(t) = M_{veh} \times C_{rr} \quad (5.4)$$

where  $M_{veh}$  is the mass of the vehicle, taken as 1500 kg,  $a$  is the instantaneous vehicle acceleration,  $\rho$  is air density under standard conditions,  $A_{veh}$  is the vehicle cross-sectional area, approximated at  $1.8 \times 1.5$  m,  $C_d$  is the dimensionless coefficient of drag, approximated at 0.24,  $C_{rr}$  is the rolling resistance coefficient, 0.02 for modern tyres on tarmac. These values are modelled after the Toyota Mirai, as the primary example of commercial fuel cell electric vehicles [190].

Equation 5.1 offers an approximate power train output required to produce the designed drive cycle. The result is then scaled such that maximal power required during acceleration is equal to the maximal power attainable by the FC100-1.

Figure 5.11 demonstrates the highly variable nature of this drive cycle simulation. The larger spikes in loading relate to the additional power required to accelerate the vehicle; flat, steady-state loading is applied during periods of constant driving speeds. The fuel cell will be operating at OCV when the vehicle is decelerating or stationary. The total NEDC cycle lasts for approximately 20 minutes, and so this shall be repeated multiple times to account for 4 hours of test operation.

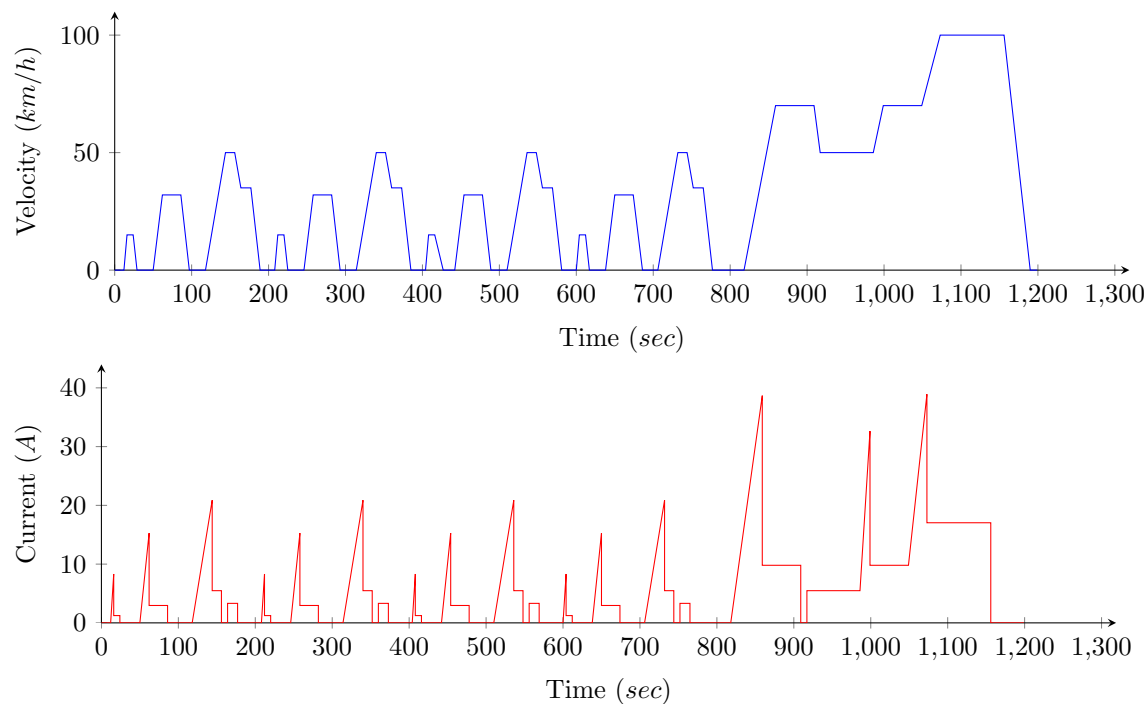


Figure 5.11: NEDC drive cycle, and the resultant fuel cell loading cycle

This drive cycle offers several different power loading conditions for the tested fuel cells. Both rapid ramped loads and steady-state loads are applied, with several periods of idle non-operation. This represents the most complex current loading conditions for the test procedure. It is expected that multiple degradation modes will be imposed on the PEFC, and the diagnosis response will give different outputs during the time series.

### Shut down

The shut down process is the reverse of start up; reducing the applied load and removing reactant feed to stop voltage production. This allows the fuel cell to be stored in a dormant state without hydrogen present in the anode compartment, reducing the likelihood of degrading reactions in the intervening time. The process is followed at the end of every testing procedure, as described below.

Firstly, loading is returned to a normal value of 0.6 V. This is the final performance indicator of the test procedure; if any degradation has occurred during the test then the current load associated with this “normal” voltage level will have decreased.

The fuel supply should be stopped and replaced with the nitrogen purge flow. This will begin to replace whatever hydrogen remains in the anode chamber with the non-reactive nitrogen. Because the electronic load is still applied during this period, any hydrogen which remains adsorbed on the MEA active sites will be consumed. Cell voltage output will decrease, and so

the load should be steadily decreased to maintain in the “normal” range as far as possible, to avoid a fuel starvation condition.

Ultimately, no voltage output is observed and all ancillaries can be switched off, including temperature control and gas feeds. This leaves the PEFC in a dormant state, suitable for storage without internal currents causing degradation outside of testing procedures.

### 5.3.2 Characterisation

Establishing performance is a key criterion, as degradation phenomena will result in changes to the fuel cell reaction performance. Characterisation testing is performed to quantify the performance and any losses that have resulted from the test conditions.

Polarisation, or current-voltage measurement, is the main characterisation technique for comparing these PEFC systems. From the existing current loading value – which may be “normal” or some other level – current is then increased step wise to find the maximum power condition. Current loading then automatically follows the progression laid out by the Fuel Cells and Hydrogen Joint Undertaking (FCH JU) in [29], with 10 % steps from maximum power to OCV and back to maximum power. By running the polarisation sweep both ascending and descending (in terms of current progression) any performance hysteresis between the two directions can be observed in the current-voltage results. A fixed dwell time of 5 seconds is used for each step of the sweep to allow the output to stabilise and the final measurement value is used to represent that load step. This dwell time has been defined through empirical experience with the test bench.

## 5.4 Full Testing Sequence

Testing procedures will follow a systematic approach in increasing complexity and scope. Initially, nominal performance must be established – typically both the steady state “normal” performance output, and a polarisation test for “healthy” operation. Testing will then impose various off-design operating conditions in order to induce degradation, and verify the diagnostic output. Polarisation characterisation will be employed to validate the degraded system health.

As mentioned previously, procedures will draw on the individual generalised tests in combination to achieve the desired operation. Figure 5.12 describes the testing sequence; the “Test Loading” phase is dependent on the applied test, as listed in table 5.2.

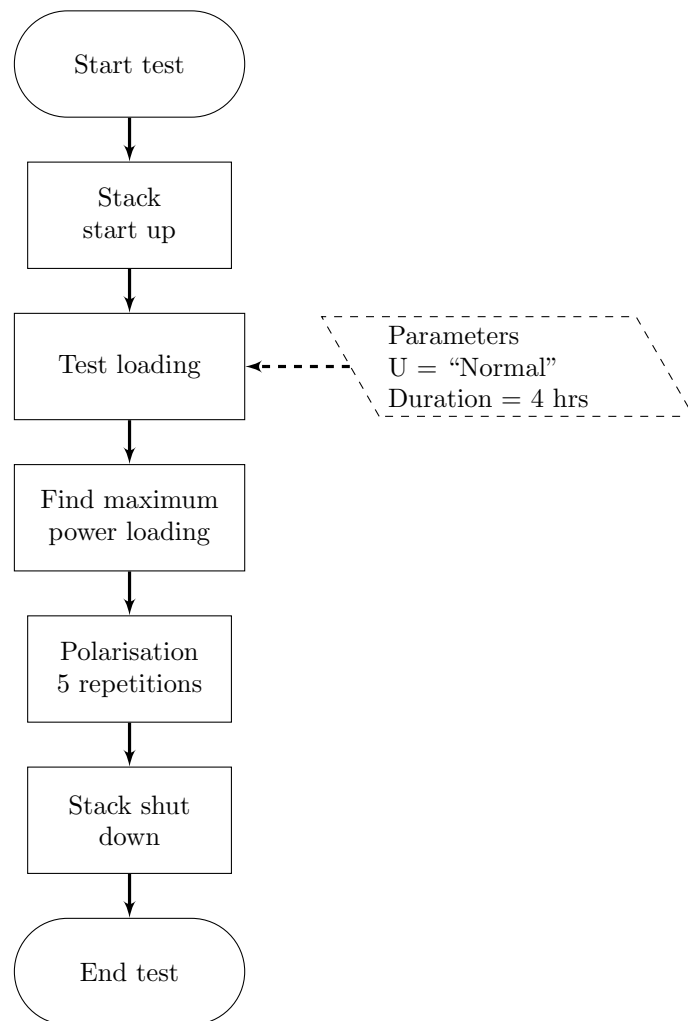


Figure 5.12: Outline of full testing procedure

Test condition	
1	Steady state “normal” voltage
2	Steady state “low” voltage
3	Steady state “high” voltage
4	Steady state “open circuit” voltage
5	Dynamic “normal” to “low” voltage
6	Dynamic “normal” to “high” voltage
7	Dynamic “normal” to “open circuit” voltage
8	Dynamic drive cycle loading

Table 5.2: List of testing procedures

## 5.5 Summary

This chapter has introduced the experimental test bench which is used to validate the health management processes – fault detection and diagnosis – as well as the FCCM software which manages the operations. The PEFC which has been sourced from Pragma Industries represents the current state of the art for materials and technologies which would be used in an application fuel cell stack. This provides credence that the function and degradation of this system will be equivalent to that of the PEFC systems put to use in the target portable and transportation applications.

The FCCM software has been designed by the author to control and monitor the entire test bench (barring the instruments which do not allow this functionality), and provide continuous feedback for performance and test progression. As is common with the test bench interfaces in other research projects this meets the specific requirements of this work, but would be too detailed for a general user. The validation test results are saved for full analysis in the following chapter 6.

The testing schedule has been designed to validate the functionality of the detection and diagnostic processes which have been developed in this thesis. The schedule begins with “normal” operation – as defined by the literature knowledge and manufacturer’s recommendations – and builds in complexity and severity to demonstrate the health management approaches. Each test is expected to elucidate different combinations of diagnostic rules. The tests are expected to expose different degradation behaviours in the PEFC to confirm the loss mechanisms that have been established in the literature.

## Chapter 6

# Validation Testing Results

The results presented in this chapter follow the chronology of the fuel cell testing schedule completed for this study. The testing has been performed to demonstrate the functionality of the health management processes, and to attempt to induce degradation modes in the test PEFC. The first test is for “normal” steady-state operation; this follows the ideal operating conditions for the FC100-1 (as defined by the manufacturer and durability knowledge) and so should not lead to any faulty behaviour or notable voltage loss. The performance here shall also be used to define the parameters of the detection model, representing the stack in a healthy state at the beginning of its lifetime. The proceeding tests each increase the severity and complexity of the operating condition, to validate the functionality of the diagnostic rules base.

Each test discussion presents the measured voltage observations and modelled prediction through the test duration, as this is the primary useful output of the fuel cell and key performance indicator. The condition assessment of the PEFC, the relative residual  $\Delta V$ , is also presented. The accompanying diagnostic responses are then included to demonstrate the evolution of the output through the test duration. The diagnostic plots show the defuzzified numerical certainty levels for each degradation mode, and the relevant linguistic terms will also be alluded to in the discussion. Each test does also present the concluding polarisation sweeps as a characterisation of any degradation experienced within the PEFC. The analysis is used to determine the effectiveness of the fault detection and diagnostic approaches for the health management of the PEFC system.

### 6.1 FC100-1 Steady-State Normal Loading

The first test performed on the FC100-1 test bench is for steady-state loading under “normal” design conditions. This is performed at the start of life, whilst the stack is assumed to be at full

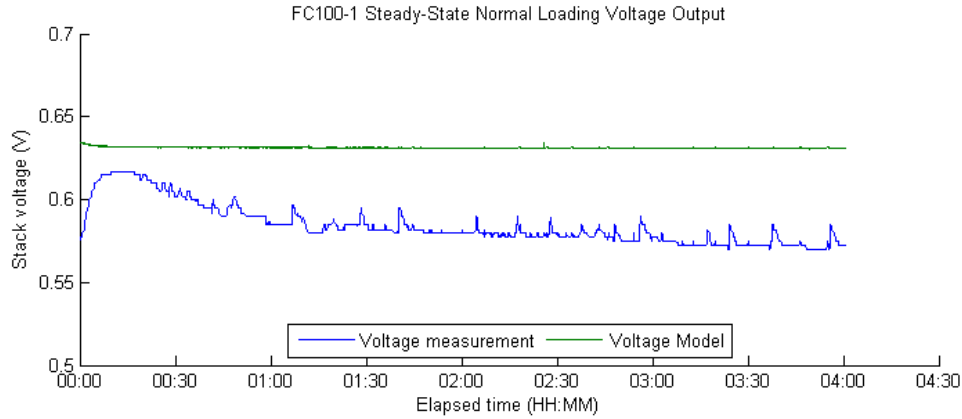


Figure 6.1: Voltage output during FC100-1 normal loading test; H<sub>2</sub>/Air, 45 °C, 15 A steady-state

health and should give the best output performance. Figure 6.1 shows the voltage performance throughout the test duration. Both the measured voltage output and the voltage model prediction are presented. The model parameters are defined from the polarisation after this test, however the prediction is added in post-processing for completeness of the results.

There is a notable long-duration voltage fluctuation during the initial 30 minutes of the test, amounting to a 0.03 V range. It is believed this behaviour is due to some platinum-Nafion interaction within the catalyst layer, lingering after the break-in of the new MEA, as discussed by Yuang et al. in [191]. Break-in is a procedure for conditioning a brand new MEA in order to establish performance at the start of life; during this time the PEFC performance is unstable and may fluctuate as observed here. This is not considered as a degradation phenomena in the diagnostic, as the effects of manufacture were eliminated during the knowledge acquisition process in chapter 4.

Otherwise, and as should be expected, the voltage level holds relatively constant at 0.57 V throughout the remainder of the test period. Smaller fluctuations can be seen in figure 6.1, but these are short-duration and less than 0.01 V in magnitude; this is most likely deemed to be some measurement noise. The on-design operating conditions afford the best functional lifetime, without accelerated component degradation, and no gross drop off in voltage over the observed time period.

Accompanying the voltage observation is the condition assessment from the  $\Delta V$  calculation performance in figure 6.2. This is the difference between the measured output and the predicted performance as calculated by the detection model in chapter 3. Whilst only small voltage degradation (decline over time) is observed in the measurements, the output is however a fixed value below the prediction, after the initial voltage fluctuation.

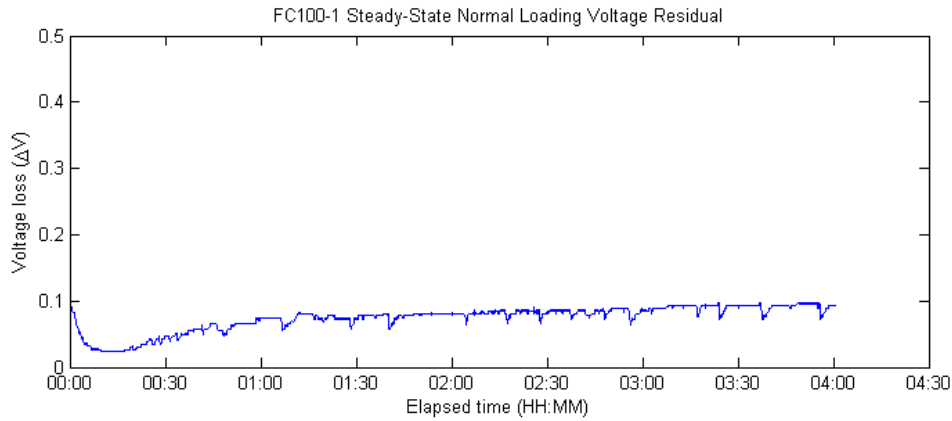


Figure 6.2: Condition assessment output during FC100-1 normal loading test; H<sub>2</sub>/Air, 45 °C, 15 A steady-state

The  $\Delta V$  value is approximately 0.085, meaning the measured 0.57 V is 8.5% lower than the predicted 0.63 V. This is already approaching the 10% limit for full lifetime loss, so is of concern to the operator and health management assessment. As the conditions of this test are the on-design “normal” values, it is not clear the reason for this difference, however the diagnostic can be consulted for further information.

Figure 6.3 shows an example of the fuzzy logic diagnostic output within the FCCM interface. The diagnostic inputs are seen to the upper left and provide the operator with a sense of the operational state; which levels are high or low within their expected range. To the upper right are the diagnostic outputs at that time point. This shows all degradation modes are very low in the “none” state, except for output 4 which relates to flooding, which is at the “evidenced” level. The chart at the bottom of figure 6.3 allows the test operator to track the recent diagnostic changes. Instead of this representation, the numerical values for the diagnostic will be graphed.

The expert diagnostic outputs throughout the test are presented in figure 6.4. This graphs the defuzzified output result for each degradation mode considered by the system, as discussed

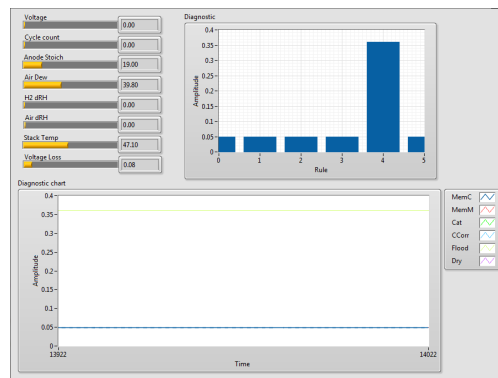


Figure 6.3: Example of the diagnostic output in the FCCM

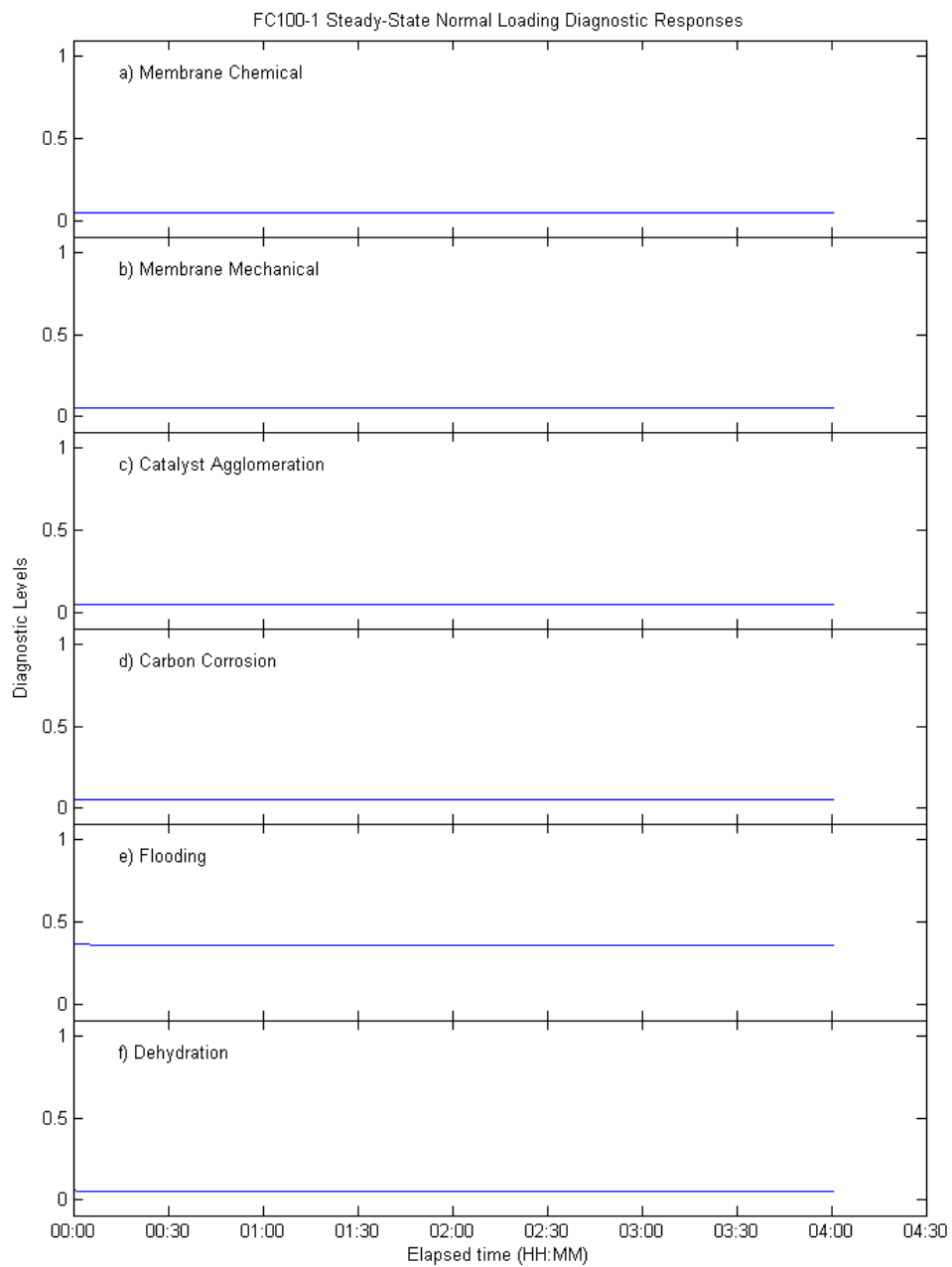


Figure 6.4: Diagnostic output during FC100-1 normal loading test; H<sub>2</sub>/Air, 45 °C, 15 A steady-state

in chapter 4. Each sub-figure relates to the progression of each diagnosis throughout the test duration. As the operating conditions are at optimal levels, most of the diagnostic measures remain close to 0 (membrane chemical fig. 6.4.a, membrane mechanical fig. 6.4.b, catalyst agglomeration fig. 6.4.c, carbon corrosion fig. 6.4.d, and dehydration fig. 6.4.f). This diagnostic is for the “none” level, and is as expected, confirming that no false diagnostic alerts have been generated.

The flooding diagnostic in fig. 6.4.e reports a medium certainty output throughout the test; 0.35 for an “evidenced” level. This is related to rule N from table 4.10 which cites cooler stack temperatures as the cause of water condensation and flooding events. Because of limitations with the fuel cell test rig, the FC100-1 temperature cannot reach the desired 60 °C, instead reaching 46 °C during this test.

The diagnosis of flooding accounts for the residual in the voltage measurement given in figure 6.2. Excess water in the GDE and flow fields is likely causing mass transport difficulties and small-scale reactant starvation. The combination of the flooding diagnosis and the 8.5% voltage loss informs the operator to take reparative action, such as reducing the amount of humidification in the gas streams.

The polarisation characterisation at the end of this normal loading test is considered to be full-health for all constituent components. This is despite the flooding diagnostic result in figure 6.4. Flooding is known to be a temporary and reversible degradation state, which can be eliminated without the PEFC being permanently damaged [192]. Sweeping the current loading through the polarisation range can avoid further flooding because of the relationship between current and product water; lower current leads to lower flooding rates. This is referenced in rule Q of the rules base table 4.10, and is seen in the literature [193]. Indeed, the polarisation measurement reports greater voltage at the same current loading as was used in the steady-state test, adding credence to this assessment.

The performance characterisation in figure 6.5 is considered the baseline health condition, and is used to define the parameters for the condition assessment model. Table 6.1 lists these parameters as used in equation 6.1, reproduced here from chapter 3. These values are fitted against the measurement data with 99.93% accuracy based on mean squared error analysis.

$$V_{model}(j) = \frac{-\Delta\hat{g}_{rxn}^0}{nF} - \frac{RT}{nF} \ln \left( \frac{1}{p_{H_2} p_{O_2}^{1/2}} \right) - \frac{RT}{\alpha nF} \ln \left( \frac{j}{j_0} \right) - jASR_{stack} - \frac{RT}{nF} \left( 1 + \frac{1}{\alpha} \right) \ln \frac{j_L}{j_L - j} - E_{corrected} \quad (6.1)$$

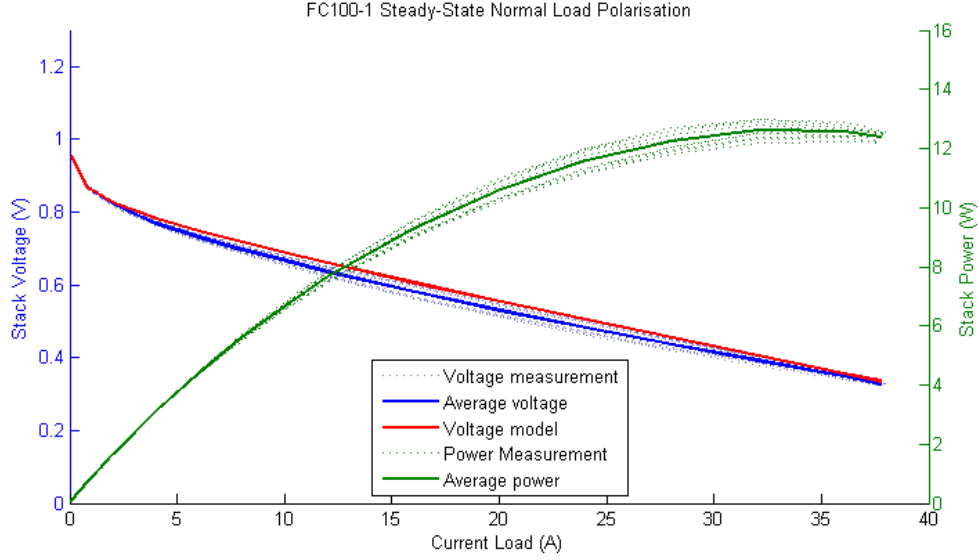


Figure 6.5: Polarisation characterisation after FC100-1 normal loading test,  $\text{H}_2/\text{Air}$ ,  $45^\circ\text{C}$

Parameter	Value
$j_0$	$0.0251 \text{ A/cm}^2$
$ASR_{stack}$	$1.058 \Omega$
$j_L$	$1 \text{ A/cm}^2$
$E_{corrected}$	$0.375 \text{ V}$

Table 6.1: Model parameters

As seen in figure 6.5, the current-voltage relationship exhibits the expected form. Open circuit voltage, at 0 A loading, is at 0.96 V. At low current loads, from 0–3 A, the activation losses dominate, with the logarithmic form. Across the remaining loading range, the roughly linear ohmic loss region is observed. A maximum power of 13.2 W is measured at 34 A loading. The mass transport losses are not distinct within this current range.

Other interesting observations in the polarisation include the clear hysteresis between the descending and ascending current sweeps, at 0.05 V at its greatest magnitude. This hysteresis is expected behaviour, associated with the water production variations as noted previously. Polarisation measurements are typically averaged from the multiple current sweeps in the literature [192, 194]. This method shall also be followed here, with average values seen in figure 6.5 and further test results.

## 6.2 FC100-1 Steady-State High Current Loading

The first off-design procedure performed was steady-state at a high current loading, with a low voltage output based on the current-voltage relationship. The current loading was 40 A to give a

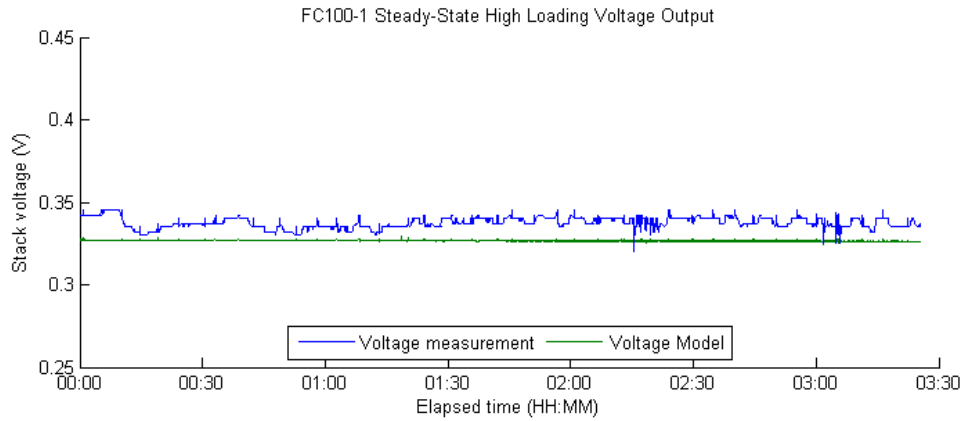


Figure 6.6: Voltage output during FC100-1 high loading test;  $\text{H}_2/\text{Air}$ , 50 °C, 40 A steady-state target voltage output of 0.35 V. Figure 6.6 shows the observed voltage response, which remained relatively steady throughout the test. No voltage degradation is observed for this test; indeed, measured performance is observed to be greater than the detection model prediction of 0.33 V.

Figure 6.7 presents the relative difference between the measurement and model. For this test the value of  $\Delta V$  ranges between 0 and -0.05, as the real performance is greater. It is unexpected for the model to under-estimate the voltage behaviour, as typically there will be further parasitic losses and of course degradation that is not modelled. For the current health management system, no performance problems would be identified as long as the FC100-1 is out-performing the expectations. However, the model could be adjusted to account for this observed performance in further iterations. Whilst the model calculations are validated for the core performance (close to the normal range) in the literature, there is scope for future work to improve the accuracy at these extremes of the current-voltage envelope.

The diagnosis in figure 6.8 shows “evidenced” chance of flooding occurring in the fuel cell,

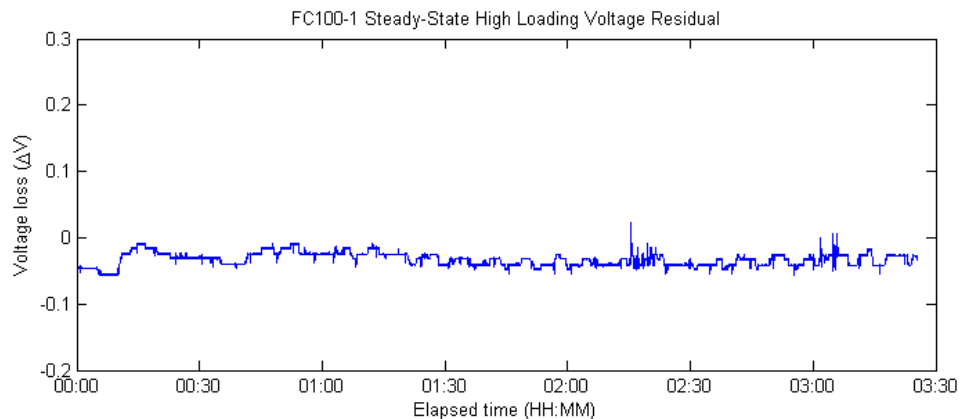


Figure 6.7: Condition assessment output during FC100-1 high loading test;  $\text{H}_2/\text{Air}$ , 50 °C, 40 A steady-state

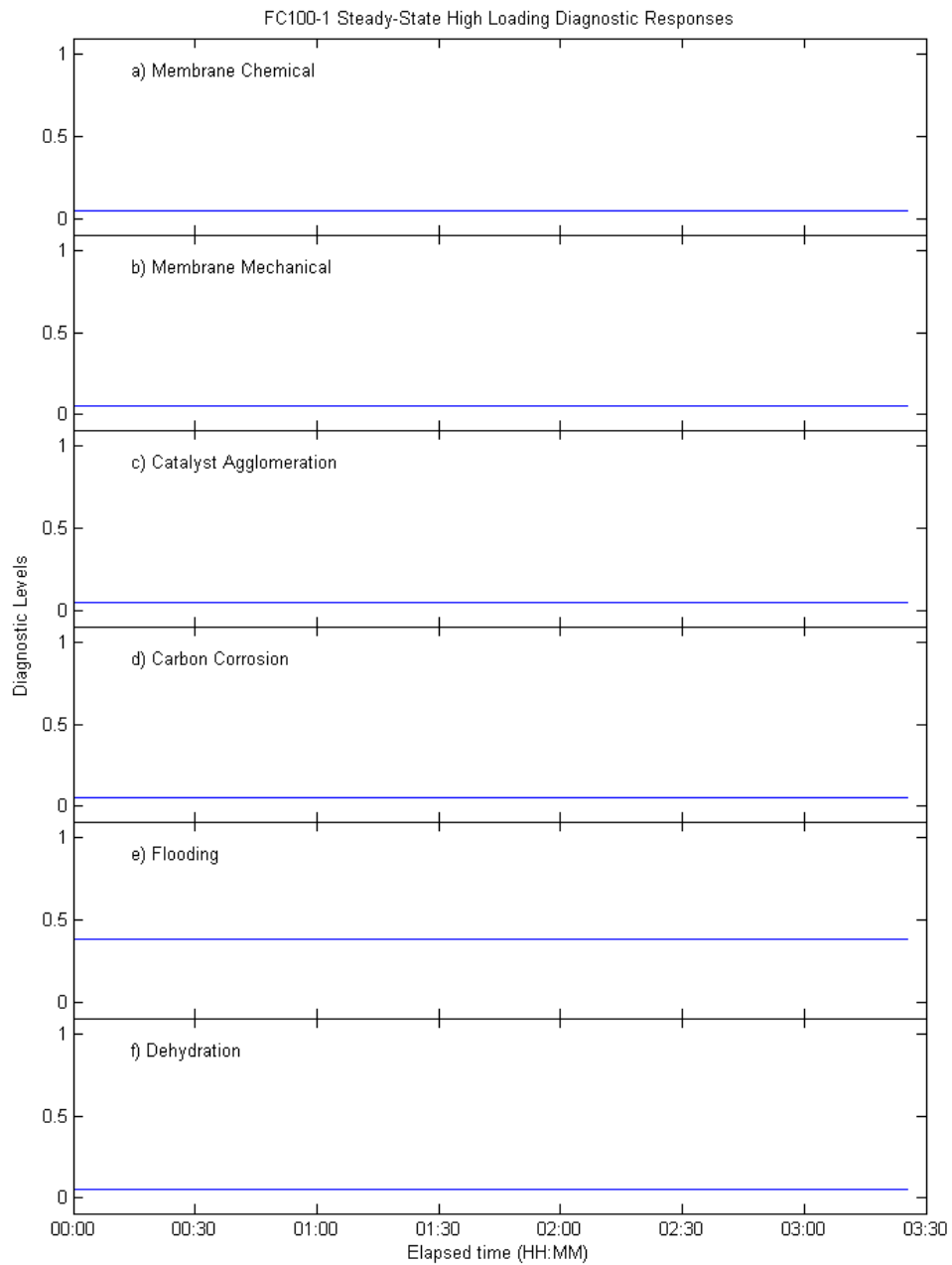


Figure 6.8: Diagnostic output during FC100-1 high loading test; H<sub>2</sub>/Air, 50 °C, 40 A steady-state

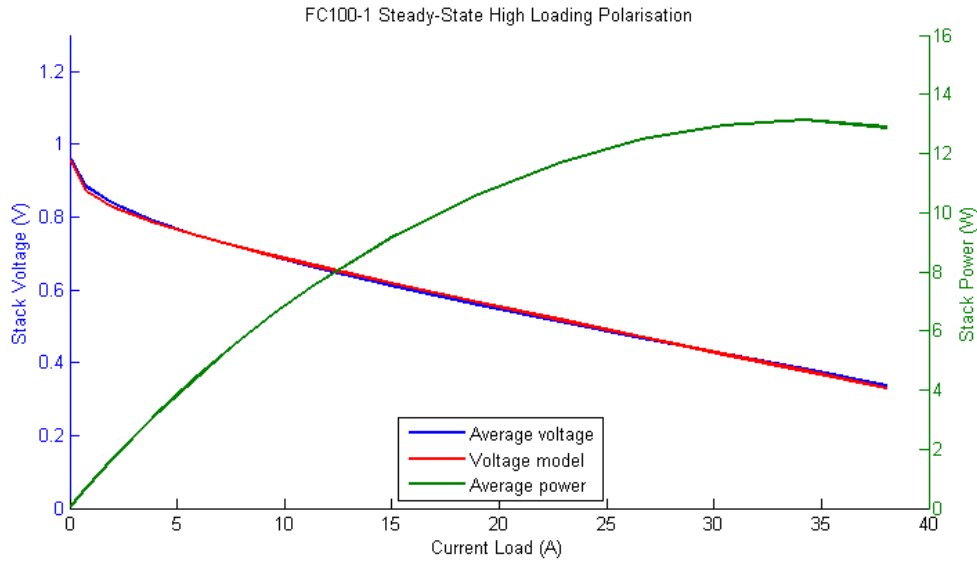


Figure 6.9: Polarisation characterisation after FC100-1 high loading test,  $\text{H}_2/\text{Air}$ ,  $50^\circ\text{C}$

associated with increased water generation at a higher current level in rule P from table 4.10. Though no voltage loss is observed, the diagnosis relates to an increased chance that flooding could occur under these conditions. Indeed, water management may be the culprit for the small voltage fluctuations observed in figure 6.6. Flooding is the only output from the diagnostic. Hydrogen supply rates are sufficiently high to mitigate the chance of fuel starvation, and therefore the carbon corrosion diagnosis in figure 6.8 remains “none”.

The polarisation characterisation in figure 6.9 trends very closely with the modelled behaviour, showing a very similar result as the steady-state normal loading test in figure 6.5. The model and measured polarisation match within 0.01% across the swept range. Maximal power is output at 13.4 W, also at 34 A current. The increase in high-current performance is also observable, as the measured values exceed the model above 35 A. Overall no performance loss is seen for this test procedure, and indeed some improvement is observed, potentially associated with better membrane hydration.

### 6.3 FC100-1 Steady-State Low Current Loading

The low current load test was performed to investigate if any degradation may occur when *close to* the open circuit voltage (OCV) level. It is unclear in the literature and knowledge base whether this loading condition would belong more to the “normal” behaviour or the detrimental OCV condition. The results here will either validate the current fuzzy set boundaries for “high” and “very high” voltage, or guide further development of the rules base, and contribute to PEFC

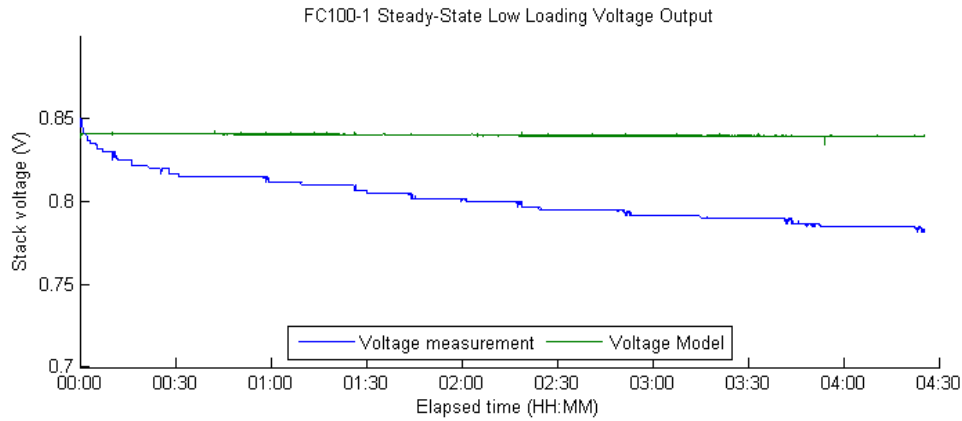


Figure 6.10: Voltage output during FC100-1 low loading test; H<sub>2</sub>/Air, 45 °C, 2 A steady-state degradation knowledge.

The current load was held constant at 2 A to give an expected output of 0.85 V. This voltage measurement was observed initially, however did decline as in figure 6.10. Within the first few minutes of operation a high voltage decay rate is experienced, with 0.03 V being lost within the first 30 minutes of operation. As the test progresses, the degradation is less severe with a diminishing rate of 0.0075 V/h across the remaining 4 hours. The end-of-test result is a 0.06 V difference between the predicted and measured voltage values.

Whilst the degradation rate is quite noticeable in figure 6.10, because of the “high” voltage level the relative loss is not so great as was seen in the previous “normal” loading condition. In figure 6.11 the value of  $\Delta V$  climbs to 0.066, or 6.6% by the end of the test duration. This is in contrast to the “normal” condition assessment result in figure 6.2, which was a step-difference, but stable. This result should be compared to the following OCV test also. Whilst the operator may need to be aware of the trend for the voltage degradation rate, this level is not yet critical

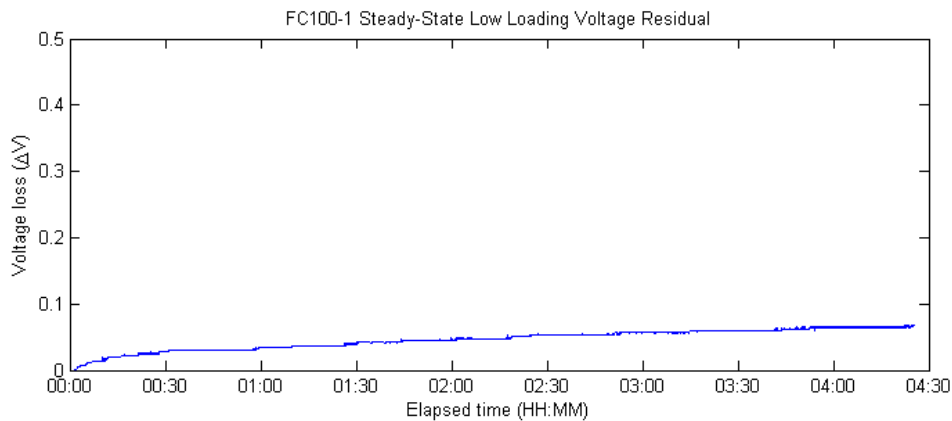


Figure 6.11: Condition assessment output during FC100-1 low loading test; H<sub>2</sub>/Air, 45 °C, 2 A steady-state

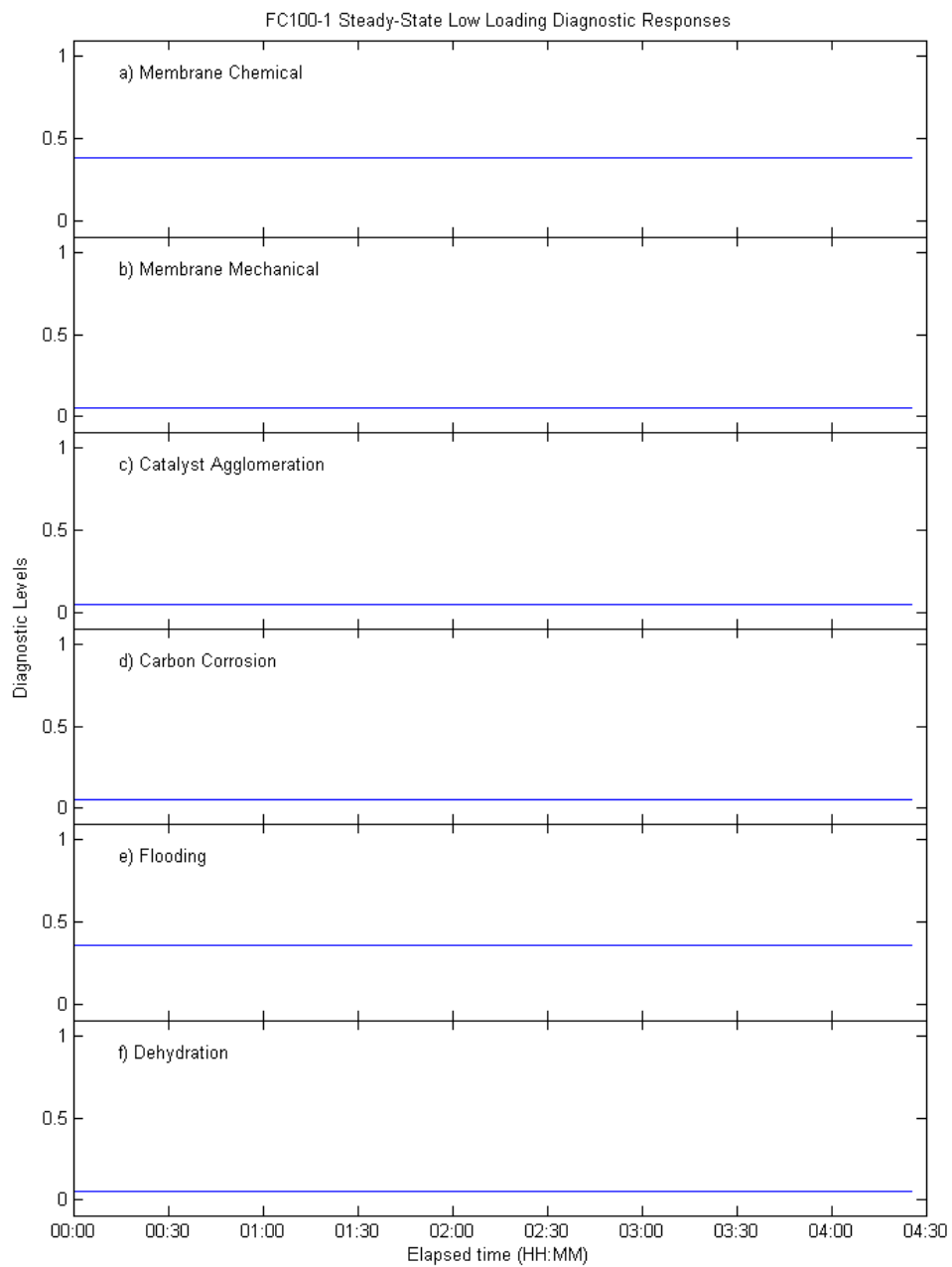


Figure 6.12: Diagnostic output during FC100-1 low loading test;  $H_2$ /Air, 45 °C, 2 A steady-state

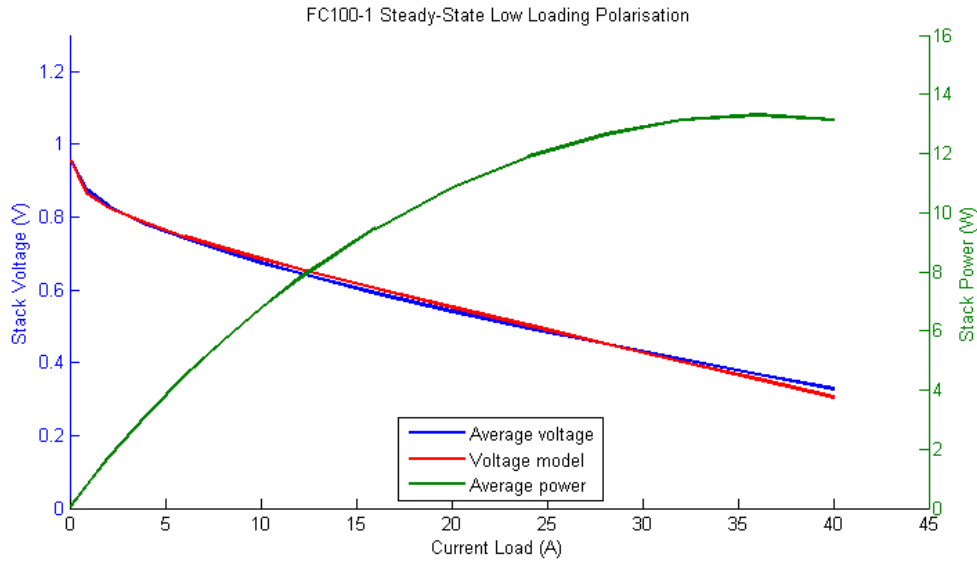


Figure 6.13: Polarisation characterisation after FC100-1 low loading test, H<sub>2</sub>/Air, 45 °C

to the PEFC health.

At this voltage level a diagnostic response is seen for membrane chemical degradation in figure 6.12.a. This output is at the “evidenced” level; the result of rule B in table 4.10. No catalyst degradation is predicted in fig. 6.12.b, as this test is outside the voltage range for the platinum dissolution mechanism [52]. Membrane mechanical, carbon corrosion, and dehydration diagnoses also present the “none” diagnosis. Flooding remains an evidenced problem because of the lower fuel cell operating temperature.

The polarisation characterisation from the end of the steady-state low current operation test, figure 6.13, provides a very similar result as the previous polarisation for the high current load test; generally good agreement with the modelled behaviour within 1%. This would imply that there has been no permanent degradation of the fuel cell after the low loading condition, and performance was recovered by performing the current sweeps during the polarisation characterisation. One interesting feature is seen in the performance at the high power portion of the polarisation, where the 40 V measurement is again greater than the model.

Whilst the permanent effects of the diagnosed degradation mechanisms are not fully realised in the polarisation characterisation, the trend for voltage decline in figure 6.10 over time is unlike the observation for “normal” current loading in figure 6.1. This would confer that the distinctions between the “normal” and “high” voltage in the fuzzy input sets are correct.

## 6.4 FC100-1 Steady-State Open Circuit Voltage

Continuous operation at open circuit voltage is typically considered the worst condition for the fuel cell in terms of health and functional lifetime, with the potential for permanent degradation of both the membrane and catalyst materials [195]. The voltage observation in figure 6.14 shows initially good correlation with the voltage model, at 0.95 V compared to 0.955 V predicted. This reading does rapidly decline during the initial hour of the test to 0.92 V, and continues at a lower rate to 0.9 V after 4 hours. It is expected that the diagnostic result will reveal both the membrane and catalyst degradation modes are acting.

The voltage residual in figure 6.15 rises to 0.05 by the test conclusion; as previously, because of the higher voltage condition the relative loss is not so great as the original “normal” result. This loss trend is very similar to the voltage observation in the previous test, steady-state low loading in figure 6.11, implying that these conditions could be similar. The diagnostic should be consulted to reveal whether this is due to the same degradation mechanisms.

The diagnostic response for the OCV loading provides several different outputs, as in figure 6.16. Membrane chemical degradation is initially diagnosed 0.7 “certain” in fig. 6.16.a, decreasing to a 0.5 rating for the “evidenced” range after 30 minutes. From rule A in table 4.10, this mode is mostly strongly influenced by voltage. Because the voltage output decreases through the test so too does the diagnostic. The wording for this rule was intended to capture the 0 A loading condition, however the diagnosis incorrectly diminishes because of the voltage degradation itself. This is considered an error, as the diagnostic rules should reference a 0 A condition for hydrogen crossover and membrane breakdown, and the OCV voltage range reserved for the platinum agglomeration reaction [196].

Catalyst degradation is also diagnosed as a result of the voltage level in fig. 6.16.c. This

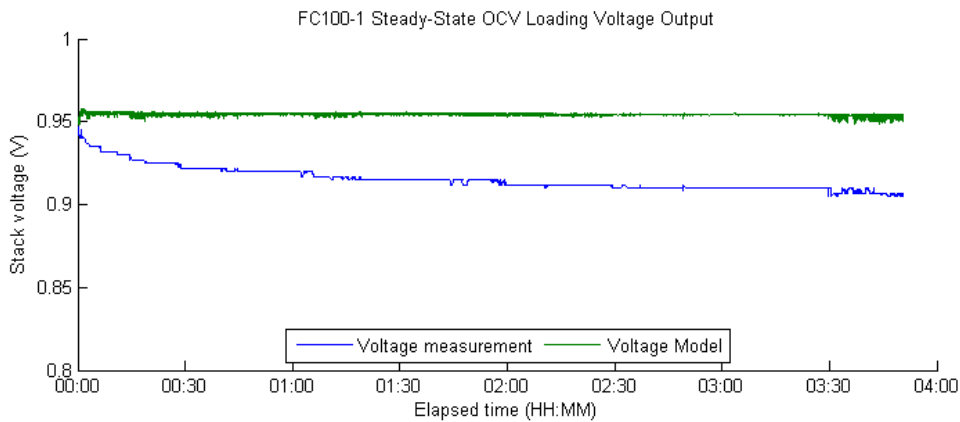


Figure 6.14: Voltage output during FC100-1 OCV loading test; H<sub>2</sub>/Air, 45 °C, 0 A steady-state

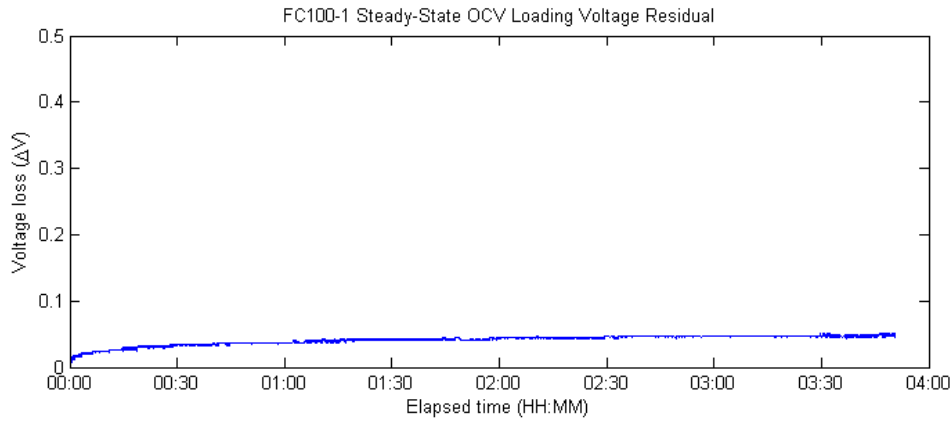


Figure 6.15: Condition assessment output during FC100-1 OCV loading test; H<sub>2</sub>/Air, 45 °C, 0 A steady-state

mode is less influenced by the observed change in stack voltage, and so the response remains in the “evidenced” region at a 0.4 defuzzified value throughout. This diagnostic does show some detail of the voltage perturbations experienced in the final minutes of the test – their scale is heightened because they are at the transition of the “high” and “normal” sets. This diagnostic result is correct, as the catalyst degradation reaction is governed by voltage level [161].

This result would confer that membrane chemical degradation is the dominant degradation factor in this test, and that catalyst degradation a secondary factor. Flooding is again diagnosed as a result of stack temperature in fig. 6.16.e. However, because the fuel cell is unloaded, water management would have less effect on the OCV voltage output. Thus flooding should be a lower diagnostic result than the membrane degradation mode, with the rules change proposed. All other diagnosis outputs are within the “none” rating, and are not a factor to the observed voltage loss in figure 6.15.

The polarisation behaviour in figure 6.17 continues to show generally good agreement with the modelled prediction, and little evidence of permanent degradation. There is some loss in the mid-range of current loads; between 2 and 20 A the measured voltages are 2.5% below prediction at the greatest magnitude. The high correlation between the model and measured performance would confer that most of the voltage loss observed in this test was non-permanent, and the PEFC recovered performance during polarisation sweeping. Knowledge would state that both membrane chemical breakdown and catalyst dissolution are permanent degradation effects, and so this polarisation result would disagree with the diagnosis.

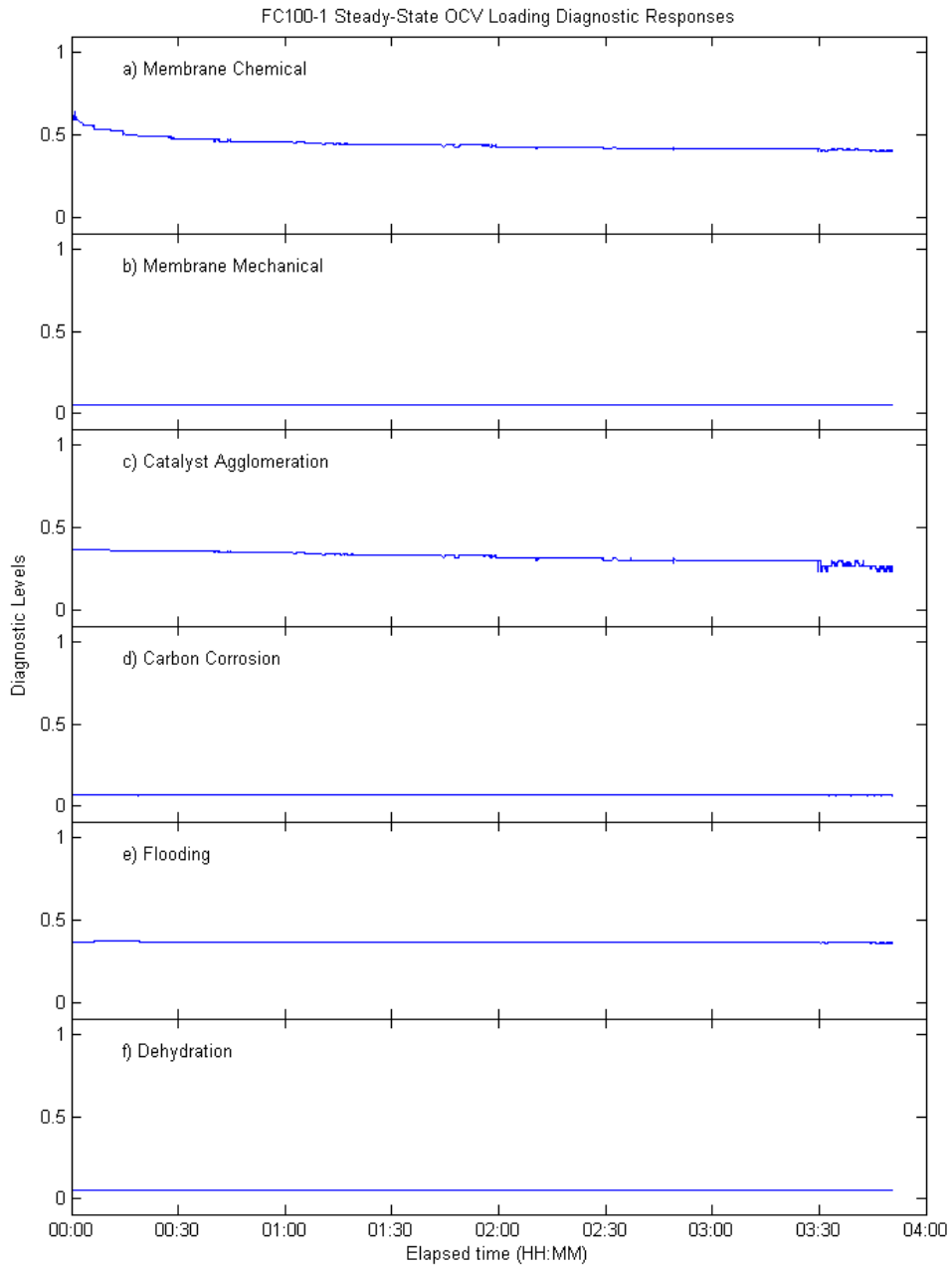


Figure 6.16: Diagnostic output during FC100-1 OCV loading test; H<sub>2</sub>/Air, 45 °C, 0 A steady-state

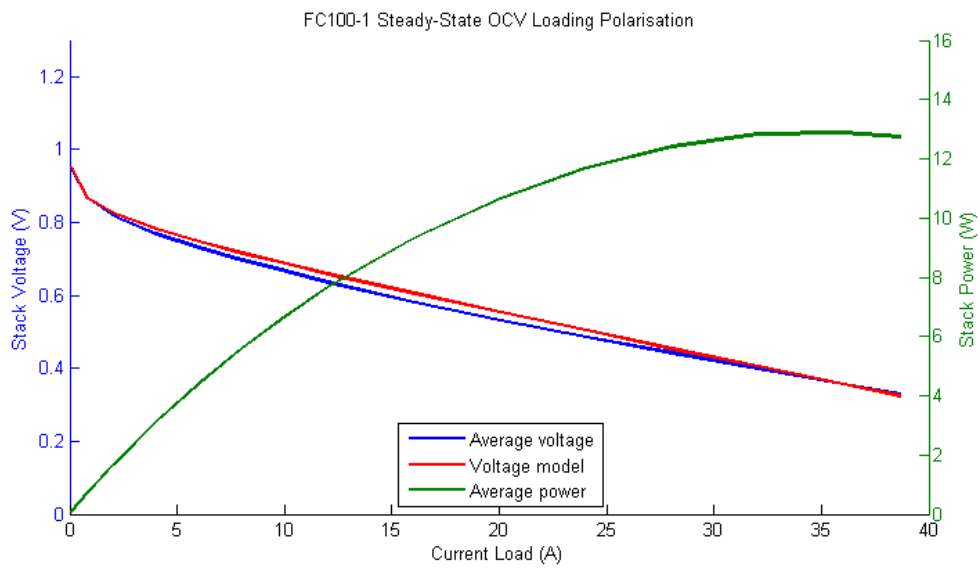


Figure 6.17: Polarisation characterisation after FC100-1 OCV loading test, H<sub>2</sub>/Air, 45 °C

## 6.5 FC100-1 High Current Cyclic Loading

The first dynamic load applied to the PEFC stack is for a loading switch between the normal and high current levels. Due to the high rate of load cycling across a comparatively long time-duration, the full test profile cannot be easily presented. Figure 6.18 shows the detail of the test results on a minute-scale; this shows the rate of loading transitions, as well as the short duration it takes for the PEFC output to stabilise at the new condition. Figure 6.19 instead shows the trends for the upper and lower ranges of the cycle separately, captured at the final measurement for each 10 second time step. This latter presentation format is used for the other two rapid cyclic loads in the subsequent sections.

These cyclic loading tests are applied to investigate the degradation which may be induced in contrast to the steady-state conditions. Rapidly changing loads are representative of the usage patterns for the portable and transport scale fuel cells which have been identified as a key application format [197]. An example may be start-stop usage expected when driving in urban traffic, an approach which is further investigated in the NEDC drive cycle test.

The trends for both of the voltage outputs remain constant throughout the test, similar to the results of the steady-state conditions for each current load; compare to normal current test in figure 6.1 and high current test in figure 6.6. Neither load was seen to induce a degradation individually and the same holds true in cyclic behaviour. The rapid switching of loads does not induce a degradation problem for the fuel cell in-and-of itself.

The voltage residuals  $\Delta V$  during this test are 0.04 at the normal loading condition and -0.06 at the high current condition. These values are also similar to the previous results, with the negative result meaning the model is again under-predicting the performance at the higher demand. Figure 6.20 also shows some outliers which have arisen from a lag between the fuel cell

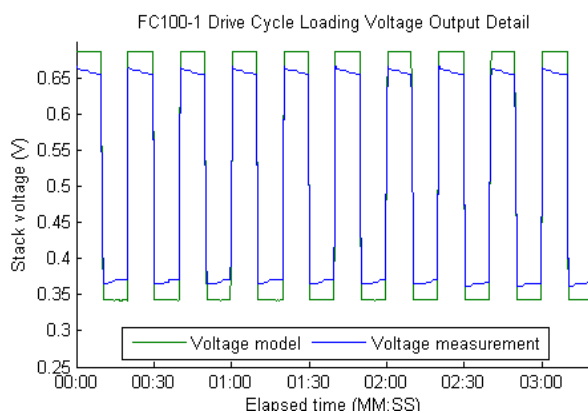


Figure 6.18: Detail of voltage output during FC100-1 cyclic high loading test;  $H_2$ /Air, 50 °C, 15–40 A transitions

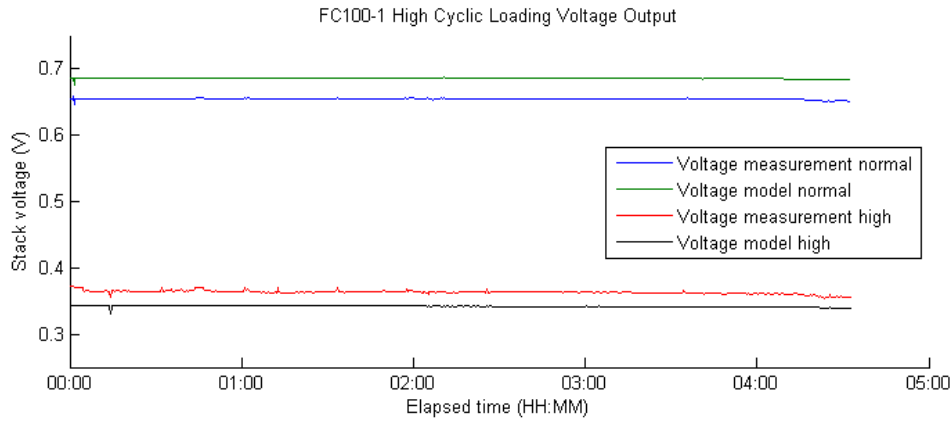


Figure 6.19: Voltage output during FC100-1 cyclic high loading test; H<sub>2</sub>/Air, 50 °C, 15–40 A transitions

relaxing to the new current level, and the model which responds instantaneously. These represent singular time-points (250ms) when the residual value exceeds the magnitude of the bulk values. Because of the simpler and steady-state nature of the model calculation, the prediction updates quicker than the real FC100-1. These errors do not have a great impact on the condition assessment however, because of the irregularity by which they appear. Further discussion is provided in the following OCV cycle in section 6.7.

These voltage observations indicate that no degradation is occurring in the PEFC, and this is confirmed in the diagnostic responses, figure 6.21. All diagnoses are at the minimal “none” level, except for the change of flooding, which remains moderately “evidenced” as a result of stack temperature. The range in the flooding diagnosis is a sign of the stack temperature generated by the higher loading condition.

The observed voltage output continues to be greater than the modelled behaviour in the polarisation characterisation, for the high load region. In figure 6.22 the final voltage-current

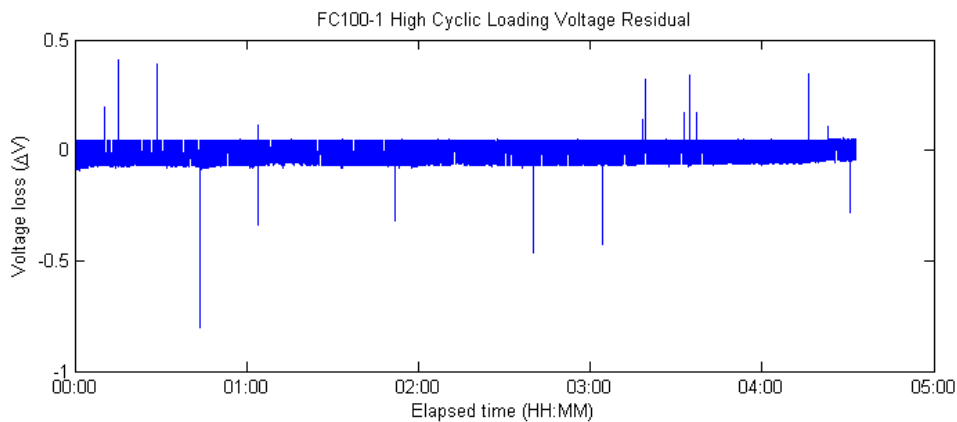


Figure 6.20: Condition assessment output during FC100-1 cyclic high loading test; H<sub>2</sub>/Air, 50 °C, 15–40 A transitions

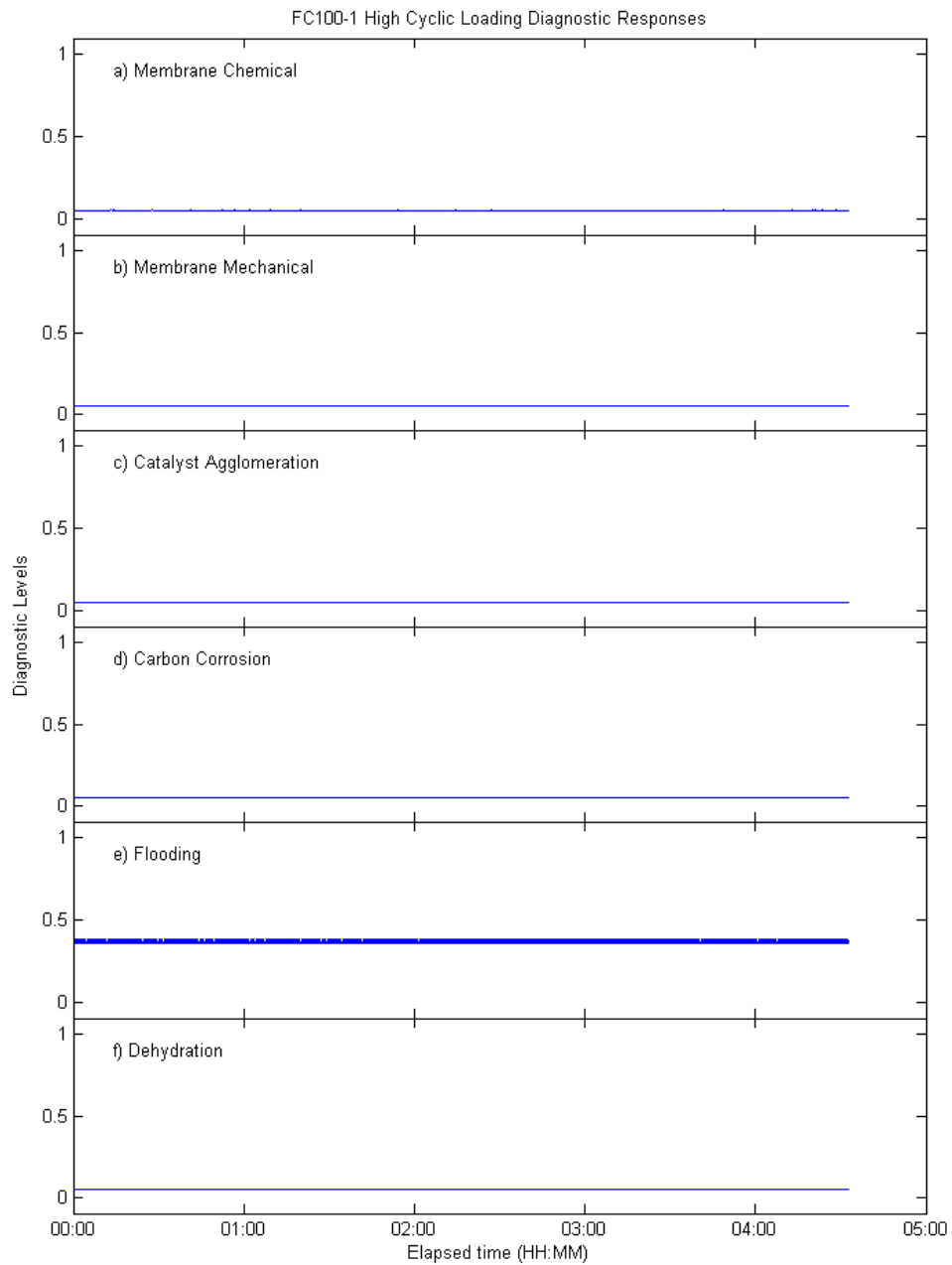


Figure 6.21: Diagnostic output during FC100-1 cyclic high loading test; H<sub>2</sub>/Air, 50 °C, 15–40 A transitions

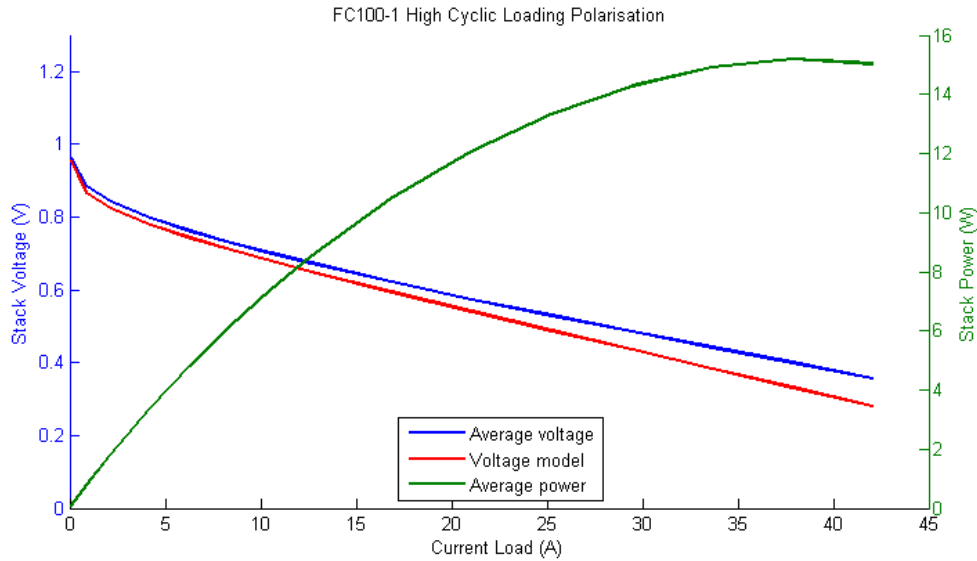


Figure 6.22: Polarisation characterisation after FC100-1 cyclic high loading test, H<sub>2</sub>/Air, 50 °C

measurement at 42 A and 0.35 V is significantly greater than the modelled 0.3 V. Maximum power now reaches 15.8 W at 40 A loading. Comparing the polarisation measurement and prediction suggests that the FC100-1 is exhibiting lower ohmic losses than in the model. This is evident in the gradient change in the measurement plot (refer to figure 3.4 in chapter 3). Based on performance knowledge, it is possible the membrane has increased water content during this cyclic test, which would reduce ohmic resistance [192].

## 6.6 FC100-1 Low Current Cyclic Loading

The cyclic loading approach for the low current load exhibits degradation at both voltage levels in figure 6.23. In contrast to the previous cyclic loading observations, this test does experience voltage loss at the normal loading condition, falling from 0.62 to 0.55 V by the end of the test. The low loading output shows a smaller degradation, from 0.84 to 0.81 V.

Figure 6.24 shows the range of voltage residual values assessed in this test. The voltage loss is smaller at the low current range in this cyclic test than in the steady-state test (figure 6.11). Previously 0.066 was observed, however here only 0.02 is experienced. Whilst this is an indication that stack degradation is occurring during the low loading periods, it is partially mitigated by the normal loading periods. The voltage loss during the normal loading periods is however significantly worse than observed in any previous test,  $\Delta V$  raising to almost 13% loss by the end of the test. This value exceeds the permissible lifetime loss of 10% – this threshold is passed after approximately 1 hour 45 minutes. Operating the fuel cell in this manner is severely degrading

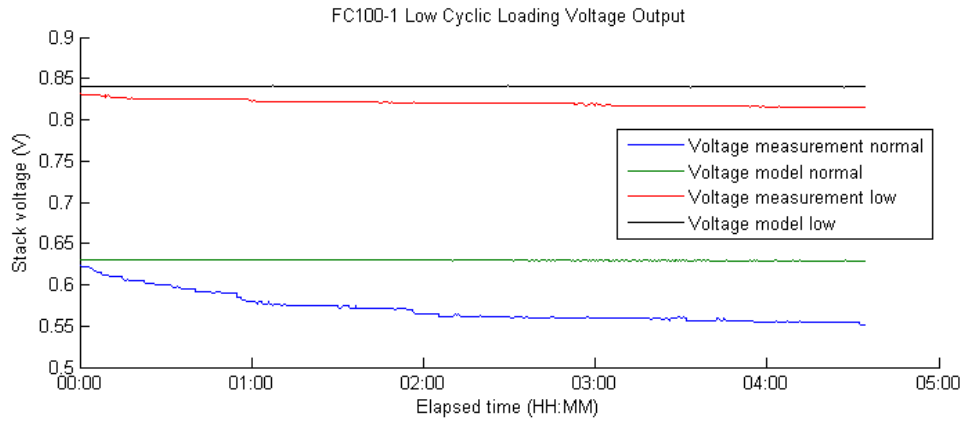


Figure 6.23: Voltage output during FC100-1 cyclic low loading test; H<sub>2</sub>/Air, 50 °C, 2–15 A transitions

for performance, and the operator should receive an alert to avoid such conditions.

The diagnostic for this test shows a new feature because of the switching current load, and associated voltage level. Membrane chemical degradation output in figure 6.25.a cycles with the same period as the loading cycle. The normal voltage level equates to the “none” diagnostic level, and low voltage to the “evidenced” level. This is consistent with the individual steady-state results, and represents alternating between the outputs of rules B and C from table 4.10. Because the diagnostic rules are built largely on knowledge of steady-state durability, or component testing with slow dynamics, the output response varies as rapidly as the loading cycle. It may become difficult for the operator to manage based on this direct output, and so it would be recommended that the control systems can handle dynamic operation.

The flooding diagnostic continues to be evidenced as a result of stack temperature as in figure 6.21.e. All other diagnostic measures are “none” indicating that membrane chemical breakdown is expected to be the dominant cause of voltage loss.

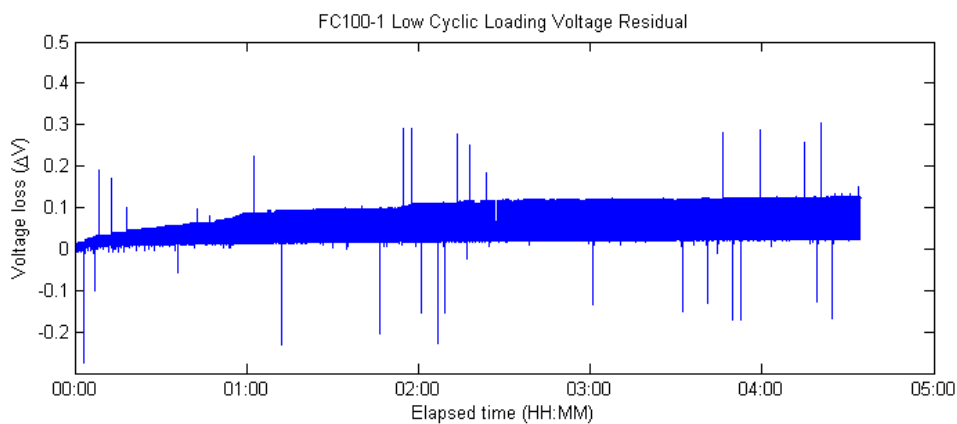


Figure 6.24: Condition assessment output during FC100-1 cyclic low loading test; H<sub>2</sub>/Air, 50 °C, 2–15 A transitions

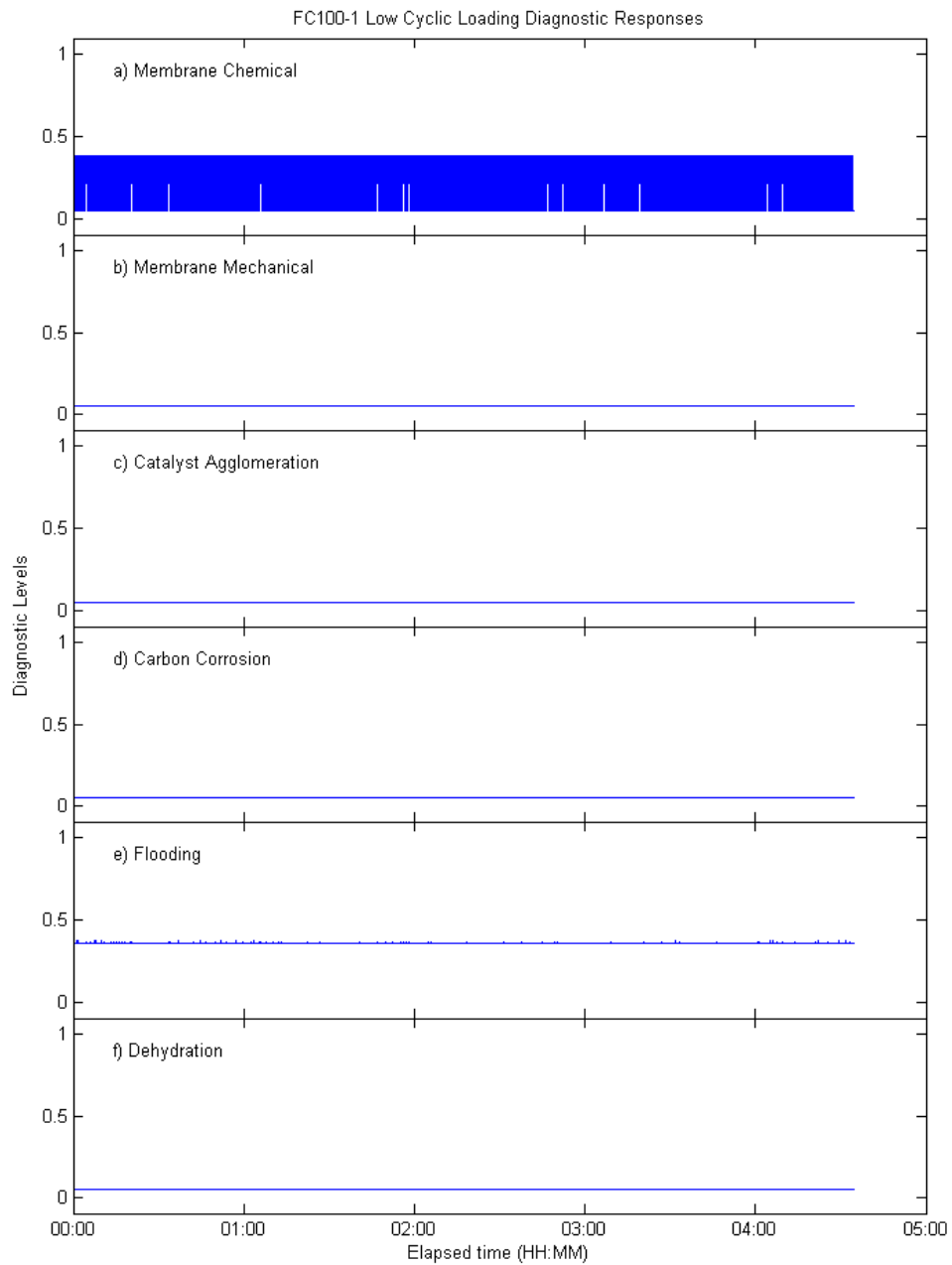


Figure 6.25: Diagnostic output during FC100-1 cyclic low loading test; H<sub>2</sub>/Air, 50 °C, 2–15 A transitions

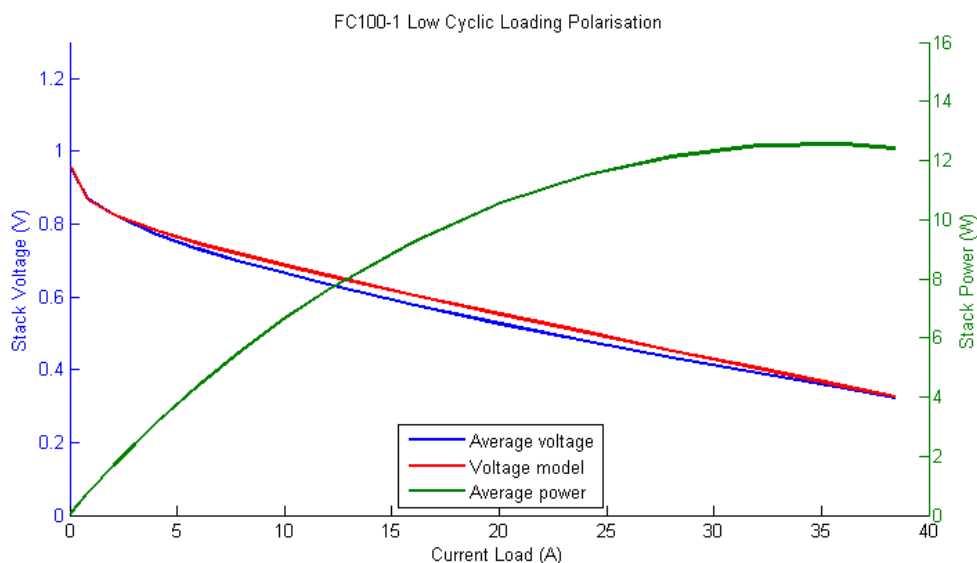


Figure 6.26: Polarisation characterisation after FC100-1 cyclic low loading test, H<sub>2</sub>/Air, 50 °C

With this test the polarisation characterisation in figure 6.26 returns to be closer to the modelled current-voltage relationship. The performance improvement which was seen in figure 6.22 after the high current cyclic loading was either degraded by the low load cycle, or a temporary effect of the former loading condition. Further characterisation testing could be employed to distinguish the detail of these changes; electrochemical impedance spectroscopy is suggested to detect the details of the resistivity contributions [53]. Otherwise, performance at the end of this test remains slightly lower than the modelled prediction.

## 6.7 FC100-1 Open Circuit Cyclic Loading

Rapidly cycling from normal loading to unloaded conditions is predicted by the degradation knowledge to be particularly bad for the platinum catalyst degradation, because of sweeping through the oxidation voltage range multiple times [77]. This test is performed to highlight any potential differences with the steady-state OCV test, as well as the previous cyclic test for low loading.

Figure 6.27 shows the voltage trends at the two limits of the loading cycle. In contrast to the steady-state test, the voltage output at the 0 A load remains very constant at close to the modelled value. It is the output at the normal loading level that reveals the voltage loss. Similar to the previous low load cycle test, the short periods at OCV here have affected the normal voltage region greatly. The voltage at the normal load steps falls from 0.6 to 0.57 V through the test duration. However, this loss impacts quickly, reaching the lower level after just 20 minutes

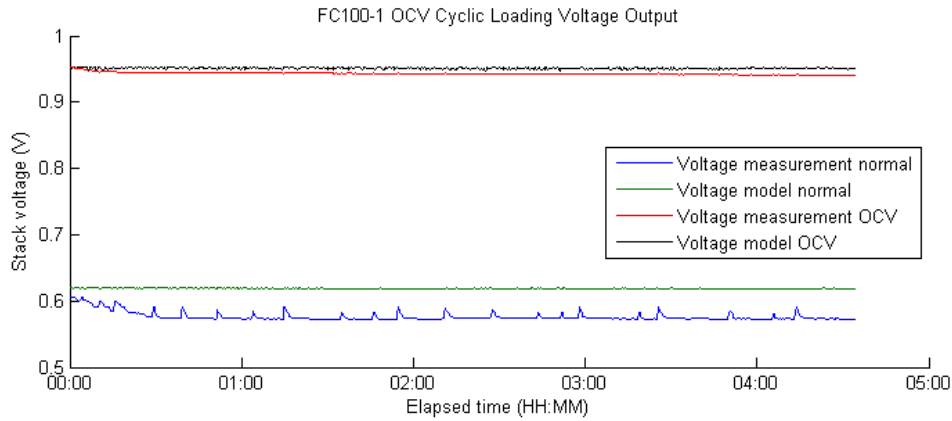


Figure 6.27: Voltage output during FC100-1 cyclic OCV loading test; H<sub>2</sub>/Air, 45 °C, 0–15 A transitions

of cycling.

The residual  $\Delta V$  result for this OCV cyclic test appears to be less severe than the previous low load cycle. In figure 6.28, the voltage loss at the normal range rises to 0.096, whilst the OCV range is at 0.009. This test does show much greater error and noise in the result however; because the real FC100-1 is slower to relax its voltage generation when the load is switched than the model calculation, most cycle steps have an erroneous value for a single time-step. This is the greatest illustration of the inaccuracy of the detection model being based on steady-state performance; whilst more complex dynamic models, such as those by Candusso et al. [116] or Vasilyev et al. [120], would potentially function slower, they would be more accurate in this regard. The voltage loss severity is relatively consistent through the test period, after the initial 20 minutes of cycling.

The diagnostic result for this test shows several features in figure 6.29. As previously, the chance for membrane chemical breakdown cycles to match the loading levels; “none” at the

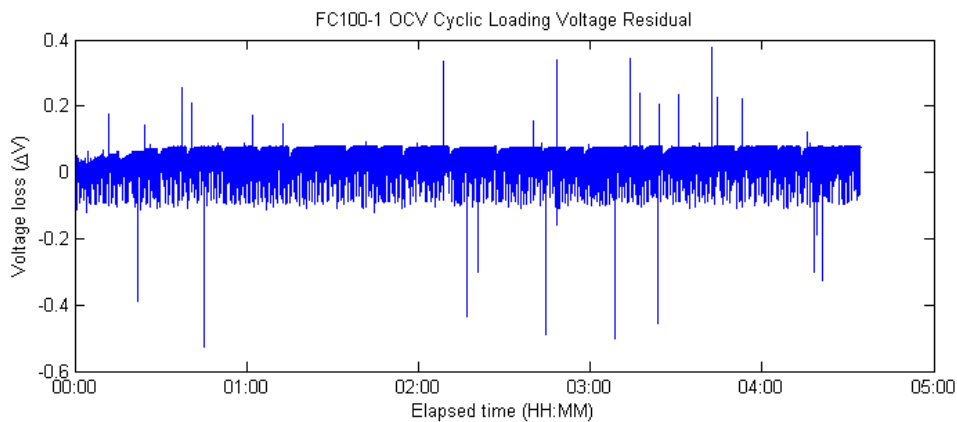


Figure 6.28: Condition assessment output during FC100-1 cyclic OCV loading test; H<sub>2</sub>/Air, 45 °C, 0–15 A transitions

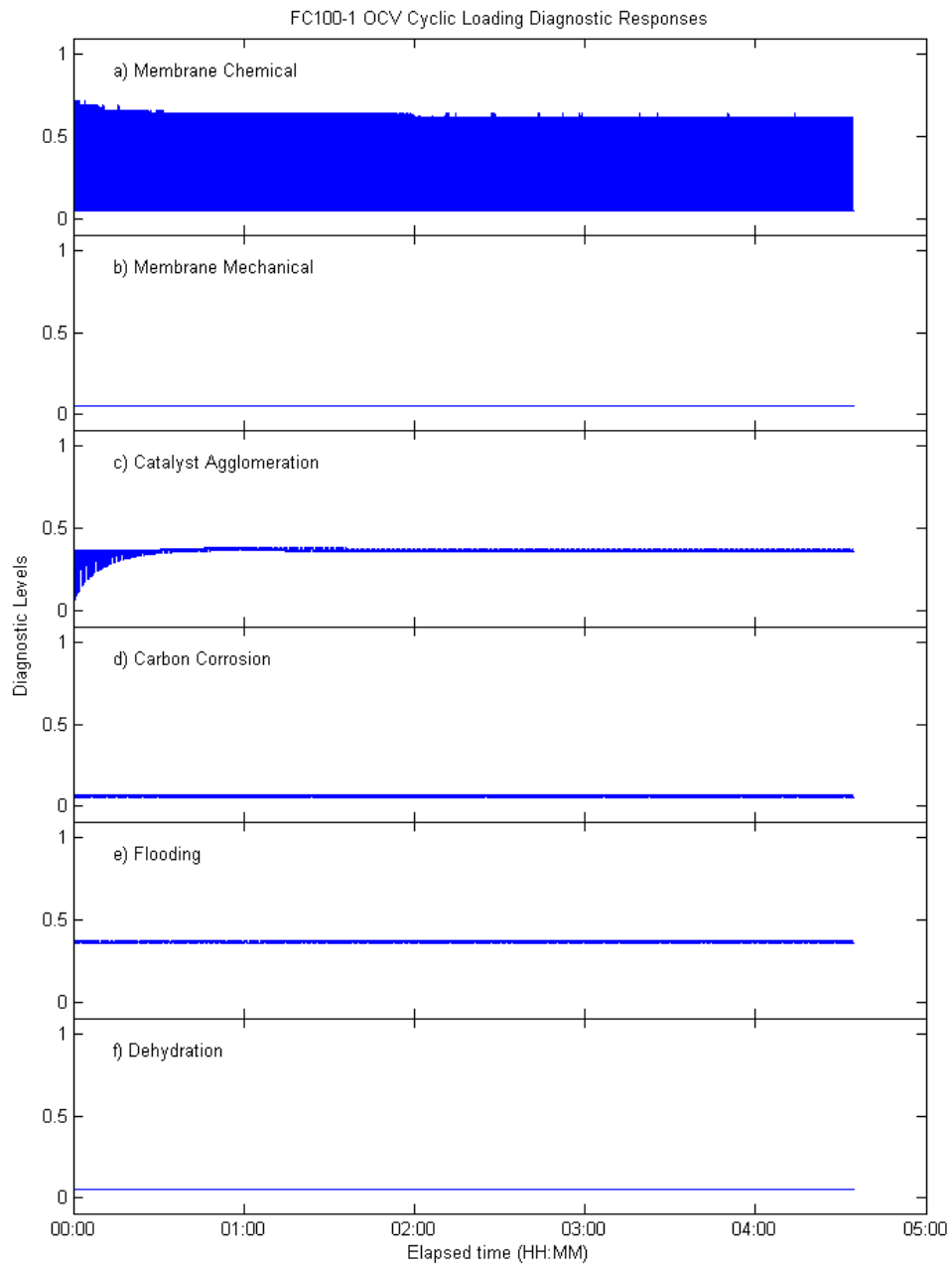


Figure 6.29: Diagnostic output during FC100-1 cyclic OCV loading test; H<sub>2</sub>/Air, 45 °C, 0–15 A transitions

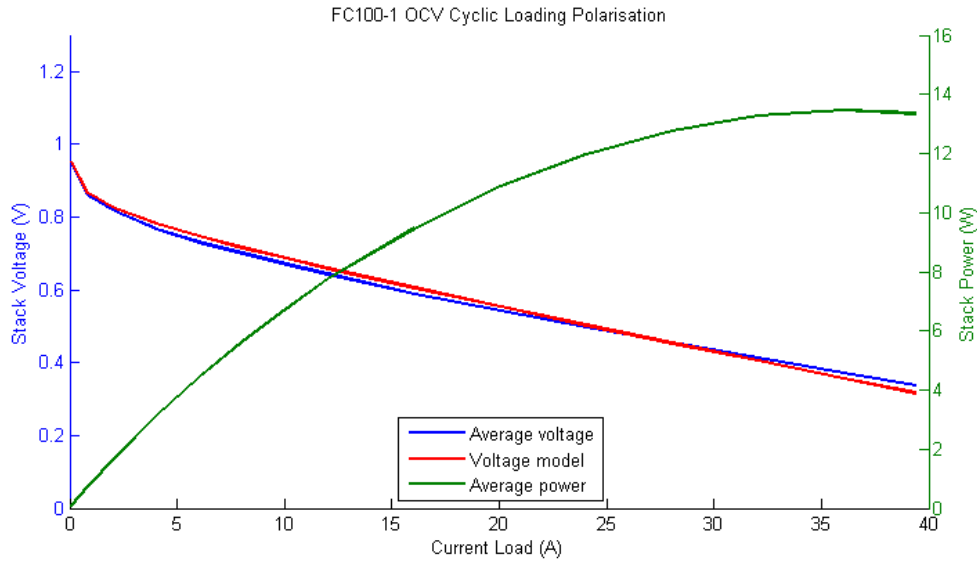


Figure 6.30: Polarisation characterisation after FC100-1 OCV loading test, H<sub>2</sub>/Air, 45 °C

“normal” loading level (despite the voltage loss) and “certain” at the OCV periods in fig. 6.29.a. This shows the same trend in the certainty rating as in the earlier steady-state OCV test, because of the strong link between current loading and chemical breakdown.

Catalyst degradation reveals the effect of the cyclic loading pattern in figure 6.29.c. At the start of the test, the diagnostic fluctuates widely to follow the voltage change, in the same way as the membrane chemical diagnosis. However, the trend is for convergence toward the 0.47 “evidenced” level because of counting the number of cycles with rule E in table 4.10. Cycle number was observed in the knowledge acquisition to have the greatest influence on the loss of catalyst active area. Should this loading pattern continue, the diagnostic will rise again with very high cycle numbers (approaching and above 2000 as defined in rule D).

The degradation of the FC100-1 is still not wholly apparent in figure 6.30. There is some decrease in the voltage measurement in the lower range of the polarisation curve, between 0 and 10 A current load. This is an indication of the catalyst degradation predicted for the OCV cyclic loading and indicated by the diagnostic in figure 6.29.c. However, the majority of the performance loss observed in the voltage measurement figure 6.27 has been recovered. This would imply that a reversible fault is responsible; water flooding and hydration balance.

## 6.8 FC100-1 Drive Cycle Loading

Figure 6.31 shows the voltage output through the 13 NEDC drive cycle repetitions in the 5 hour test duration. The drive cycle loading test applies the greatest variance in current loading on

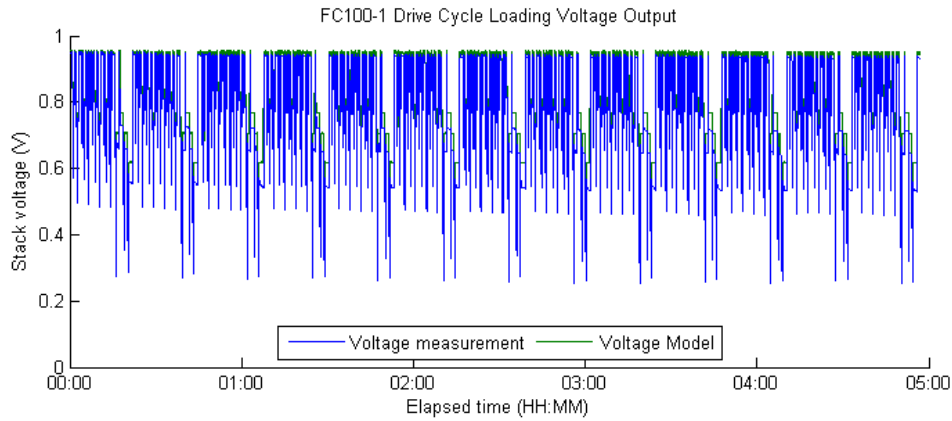


Figure 6.31: Voltage output during FC100-1 drive cycle loading test; H<sub>2</sub>/Air, 50 °C

the fuel cell, including periods of steady load and OCV, ramped sweeps between loading level, as well as instantaneous switching. The voltage observation exhibits voltage loss of the output across all current levels, with trends for degradation in all peaks of equal loading. As observed in previous tests, this will be a combination of the PEFC degradation and the rate of voltage stabilisation when quickly changing loads.

The measured voltage is consistently lower than the modelled behaviour. The voltage residual in figure 6.32 provides values which range between 0.01 for OCV conditions to 0.335 at the greatest load peak – this is 34% performance difference between what is measured and predicted by the condition assessment model. Absolute differential at this point is only 0.13 V (0.38 V predicted compared to 0.25 V measured) however the “low” voltage condition makes this more severe. Inferring from the previous cyclic loading tests, the low current and OCV periods would be most detrimental to the overall performance. The NEDC drive cycle applied includes several periods where the vehicle is either stationary or braking – 0 A current demand – which would

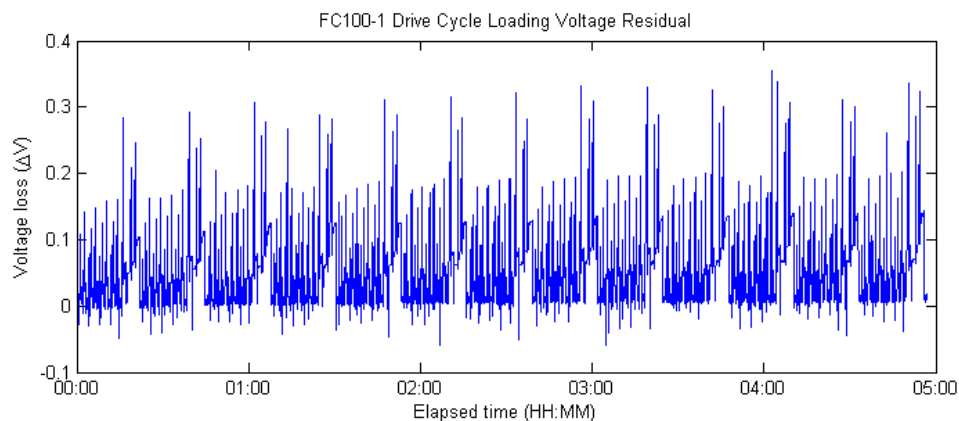


Figure 6.32: Condition assessment output during FC100-1 drive cycle loading test; H<sub>2</sub>/Air, 50 °C

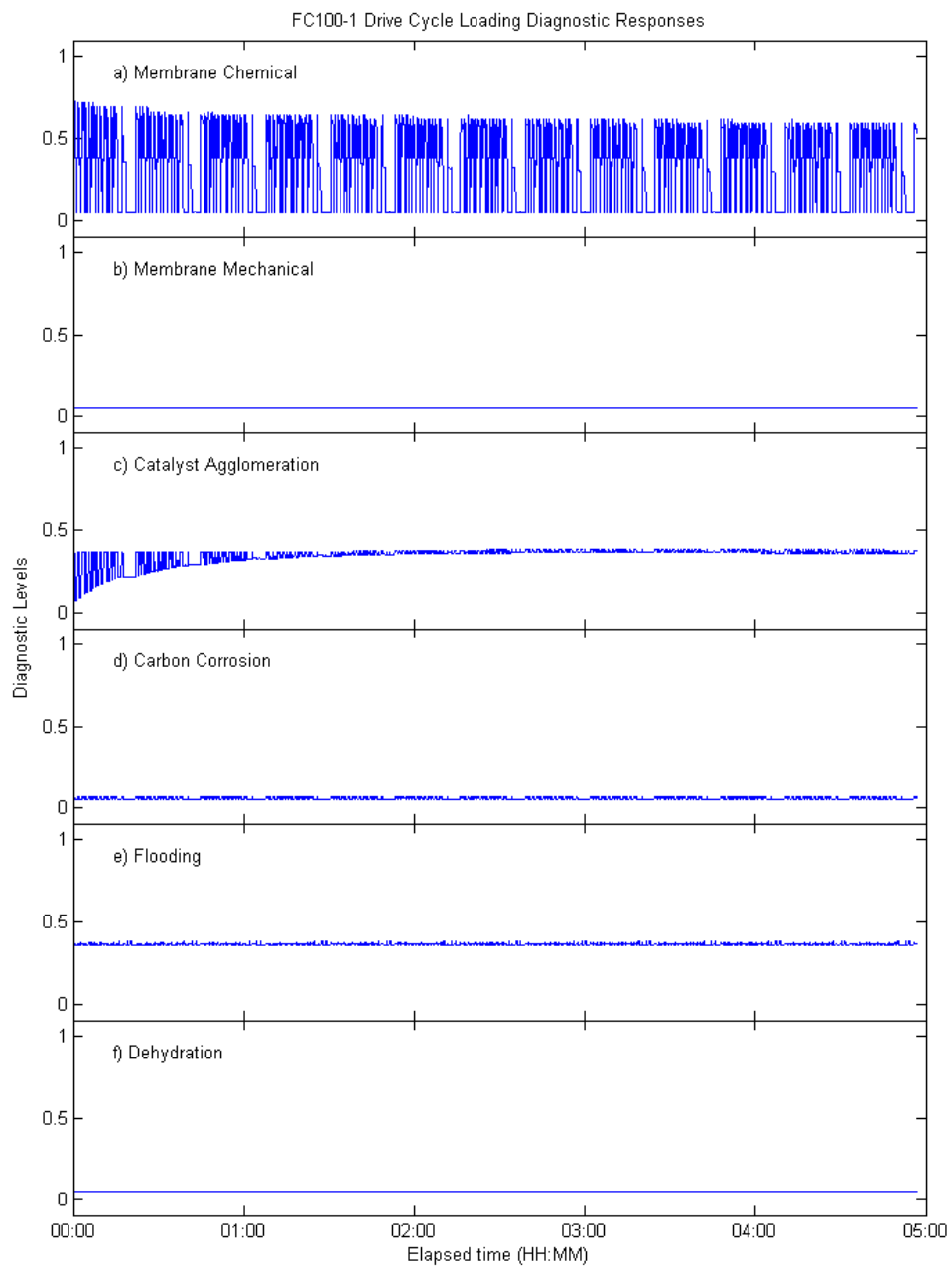


Figure 6.33: Diagnostic output during FC100-1 drive cycle loading test;  $H_2$ /Air, 50 °C

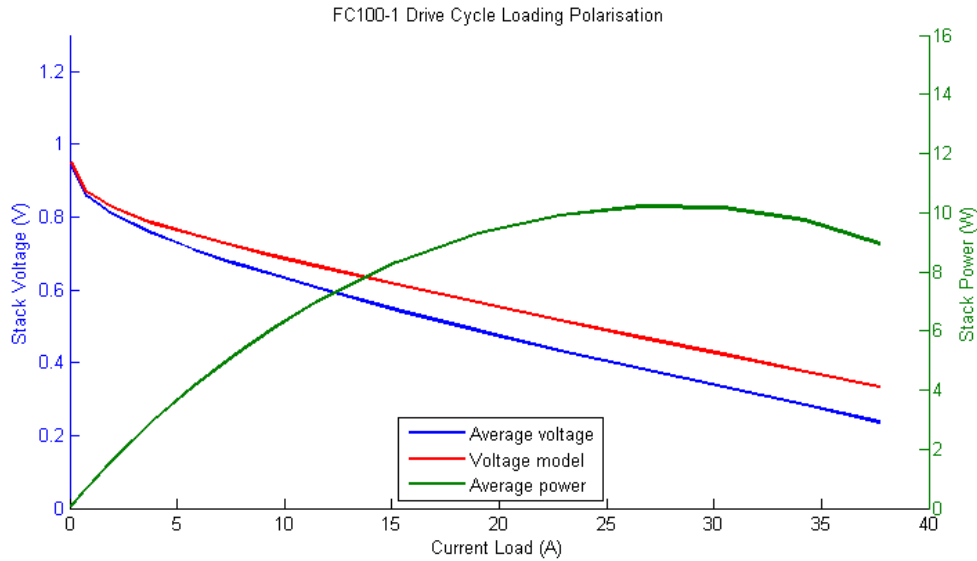


Figure 6.34: Polarisation characterisation after FC100-1 drive cycle loading test, H<sub>2</sub>/Air, 50 °C

draw no load from the PEFC; it is because of these usage conditions that the catalyst is becoming degraded.

The diagnostic response for this testing profile in figure 6.33 shows several features present in the preceding tests. The membrane chemical degradation diagnostic in fig. 6.33.a increases for each low or OCV phase in the cycle; when OCV voltage degrades, the peak diagnosis declines from “certain” to “evidenced” by the final drive cycle. Catalyst degradation in fig. 6.33.c initially follows the voltage profile also, converging to “evidenced” as the number of cycles accumulates. The flooding diagnosis in fig. 6.33.e remains at the “evidenced” level throughout, with some perturbations which reflect the reaction heat output for the very high current phases of the cycle.

Dehydration and membrane mechanical degradation remain at the “none” level, as no significant temperature or humidity changes are made. Carbon corrosion also remains within the “none” diagnosis level, however there is some small value change for periods of very high current loading which approach stoichiometric limits.

This final polarisation characterisation in figure 6.34 shows the most degraded performance, compared to the expectation from the model. At 0 A, OCV voltage is the only value which is similar to the model, at 0.95 V. The activation portion of the polarisation performance, below 5 A, shows a greater degree of curvature, which confers a loss in catalyst active area. Similarly, the ohmic portion of the current-voltage relationship also exhibits a steeper gradient, and therefore increased internal cell resistance from either catalyst degradation or membrane chemical breakdown. The difference between the voltage model and polarisation measurement

is 10% at the highest current load, and the maximal power output has reduced to 10 W at 30 A, 30% lower than the first test in figure 6.5.

## 6.9 Summary

The validation testing has been completed to demonstrate the operability of the health management processes for application towards isolating faulty operational states in the PEFC stack. Testing has also investigated potential degradation phenomena that may be experienced due to different current loading conditions. The goal herein was to demonstrate an ability to diagnose different degradation phenomena within the PEFC in a novel approach of using expert knowledge and forgoing characterisation tests and equipment which are commonly used in published results.

The steady-state “normal” loading test gave the initial fitting and validation to the semi-empirical voltage model. This model was fit to the initial, “healthy” polarisation characterisation with good accuracy, and provided a representation of the performance expected for the FC100-1 when healthy. This initial test did reveal the first diagnostic output in the form of flooding; a result of the FC100-1 test bench being unable to achieve the desired 60 °C operating temperature. Future improvements to the experimental test bench could include more powerful temperature control. The other degradation outputs confirmed that no false-positive would be output by the diagnostic when operating at on-design conditions.

The steady-state high current load, or “low” voltage condition, was the first off-design procedure. For the duration of this test the voltage measurement exceeded the prediction from the model; whilst not a problem in as much as the fuel cell is over performing, it resulted in negative values for the voltage residual. In the health management approach, this may be permissible as no voltage loss is caused. The diagnostic result for flooding with this test should be considered together with the voltage condition assessment; no fault is detected which reduces any urgency to act upon the diagnosis. Indeed, the author poses that the increased water production did improve performance through membrane hydration and reduced ohmic losses.

The steady-state low current loading condition – close to the OCV level, but with a small current demand – is a novel test condition that is not seen in the literature. This was completed to validate the membership sets for stack voltage, and determine if operating in this range is more related to normally loaded performance or to OCV behaviour. The results showing voltage degradation over the duration of the test in figure 6.10 is more similar to the OCV result in figure 6.14, which validates that the fuzzy set and diagnostic rules definitions for this voltage

level are correct. The OCV degradation result is slightly more severe, which is accounted for in the diagnostic as two modes are occurring; catalyst dissolution as well as membrane chemical breakdown.

The dynamic testing was performed to simulate conditions viewed as more similar to the application systems – variable loading, cyclic in nature, and at different current-voltage levels. The first such test, cycling between normal and high current load showed no noticeable voltage degradation through the test duration. Performance at the higher load was again higher than the modelled prediction, as with the steady-state test, and the  $\Delta V$  value improved for the normal loading condition, compared with that steady-state test. This adds further evidence to the conclusion that ohmic losses are improved by the water production and membrane hydration at higher current demands.

The normal to low current cycle showed severe voltage degradation at both ranges; here the off-design loading condition did influence the normal performance negatively. The diagnostic system performed rapidly to follow the cyclic loading pattern, though this led to a highly variable result as in figure 6.25.a. Whilst this is an accurate portrayal of the different degrading states the fuel cell was experiencing, it is perhaps too transient for the operator to manage, but the control systems could consider a cumulative degradation.

The OCV cyclic test validated the performance of the voltage cycle feature extraction, as supported by the literature in [176]. The diagnostic result for catalyst degradation in figure 6.29.c showed the cumulative effect of the operating conditions. This test did also reveal a limitation of the fault detection model in representing the transient behaviour of the PEFC. Capacitive effects within the fuel cell mean the voltage takes a short time to relax to the new level; this created an erroneous result where the fault detection model responded quicker. The FC100-1 did recover the voltage quickly, however a larger scale PEFC stack with slower dynamics would give more significant errors.

The NEDC drive cycle testing saw the greatest voltage loss and evidence of degradation effects. With the great variety in the current profile, a maximal voltage loss residual  $\Delta V$  value of 0.335 was measured. This is far beyond the target lifetime durability of less than 10% performance loss, and an indication of the degrading effects of these operating conditions. The operator did receive a condition warning for this loading condition, which would suggest changing or halting the drive cycle should durability be maximised.

Throughout these tests, the condition assessment model showed good representation of the polarisation performance of the PEFC, however some of the transient effects in dynamic operation were lost and this created errors. The steady-state semi-empirical nature of the model

calculations are adequate as a simple and quick representation of the fuel cell with good applicability in steady-state conditions. Adding the capacitive effects seen in cyclic loading would add complexity but improve performance.

These tests were performed to demonstrate the functionality and effectiveness of the diagnostic rules base. The fuzzy logic diagnostic system generally performed well in identifying the potential causes of performance losses, based on correlating the operational conditions with the degradation knowledge. The outputs are seen to be better suited for steady-state or slow dynamic conditions, where the operator would manage the performance and durability based on the diagnosis. For example, where flooding is seen as a degradation state in the initial “normal” steady-state test, the control decisions would be to increase stack temperature, or decrease reactant humidification to allow the PEFC to recover the 8.5% voltage loss. Alternatively, for the latter OCV cyclic test, the first control approach should be to stop the dynamic loading profile, if this is feasible within the usage. Mitigating and repairative actions were not taken during these validation tests, as the durability was under examination.

In order to improve the diagnostic output for the highly transient operating conditions, it is suggested that a cumulative effect is considered in contrast to the instantaneous responses. The relationship between stack cycle number and catalyst degradation seen in figures 6.29.c and 6.33.c is a good model for this change to the diagnostic rules. Alternatively, the higher PHM processes – the Decision Support layer, chapter section 1.3 – could manage the cumulation of degradation.

The primary rules change that needs to be made in the diagnostic is to change the membrane chemical degradation cause to current load instead of voltage level. The literature showed that OCV conditions lead to the chemical degradation, however it is now apparent this is due to the 0 A current condition rather than the very high voltage condition [147]. This would remedy the erroneous result described for figure 6.16.a, where the diagnostic certainty decreased without a change to the loading condition.

# Chapter 7

## Conclusions and Future Work

### 7.1 Conclusions

This thesis presents the developments of fault detection and diagnosis processes for the health management of polymer electrolyte fuel cell systems. In reference to the objectives discussed in chapter 1:

1. An understanding of PEFC durability issues was gained through a literature review, and an in depth study of operational conditions affecting component degradation was collated within the knowledge acquisition for the fuzzy logic rules base. Loss in the PEFC voltage performance was observed as a result of the constituent component degradations; the MEA is a vital element in this regard, with membrane breakdown, catalyst dissolution, GDE corrosion, and water management issues being the featured degradation modes. Whilst on-design operational conditions are designed to maximise durability, it is the off-design conditions and variations in voltage, temperature, flow rates, and humidity which cause the component degradations.
2. The literature review also established the state of the art of fault detection and diagnosis for PEFC systems. Many techniques were found in model and data-driven approaches to both detection and diagnosis, with numerous examples from recent years within these two areas. Only one publication detailing rule based diagnosis was found in the PEFC literature, and this example was limited to only considering water management issues; this offered an opportunity for this thesis to contribute a novel rule based method, and to take a broad diagnostic approach that considered several degradation modes in a single method.
3. Thus the detection and diagnosis processes were developed to contribute to the fields of

PEFC health management;

- (a) Model based approaches showed good applicability in fault detection, and this method was utilised in this work. A simple electrochemical model was developed, based upon validated examples in the literature with additional calculations to take into account the side reaction losses that are not included in the theoretical calculations. The voltage loss residual  $\Delta V$  characterises the state of health of the system relative to designed performance.
  - (b) The novel rule based diagnostic approach was developed to isolate failure modes within the MEA. This method uses expert knowledge that has been gathered from literature sources and practical experience to define the diagnostic rules. Fuzzy logic is utilised to enable the direct use of the linguistic terms which describe the operating conditions and the degradation modes that are influenced.
4. Experimental testing has been undertaken to confirm the functionality of these health management processes in a practical application. Both the detection model and diagnostic reasoning were quick to respond to changes in the operating conditions of the PEFC test bench, and provide the operator with a certainty rating for which degradation modes are likely affecting the fuel cell. The results show that the health management practices are currently better suited to steady-state or slowly-transient loading conditions, where the operator has time to manage performance and durability. The rule based diagnostic is useful in identifying the faulty PEFC condition, though suggestions have been presented to improve the handling of highly transient conditions.

## 7.2 Contributions

This thesis contributes an approach for using fuzzy logic in a rule based expert knowledge diagnostic system. This includes the compilation of the diagnostic knowledge into the rules database, the first example of its kind for PEFC systems. It is a novel approach to use the linguistic descriptions of durability issues directly from literature outcomes as opposed to a modelled or data-driven representation. In this way, the diagnostic has greater transparency for the operator and user to understand the processes.

A semi-empirical model is utilised for fault detection. This builds upon existing model calculations by O'Hayre et al. [12] and Mann et al. [111], by including an additional voltage correction term  $E_{corrected}$  which takes into account side reaction losses seen in practical systems.

As this model may be used for design and simulation, it is seen as a good approach to represent the healthy PEFC performance.

These processes have been integrated with an experimental test bench and the FCCM software which has been developed by the author. The FCCM software provides continuous performance monitoring and control to manage testing procedures, as well as supporting the health management systems.

The results of the experimental testing show good utility of the fault detection diagnostic processes in isolating the faulty operational conditions and the degradation modes. A novel test point for low current loading was investigated, which showed degradation behaviour similar to the OCV condition. The diagnostic output was demonstrated for steady-state and dynamically cycling current loading conditions.

### 7.3 Future Work

This thesis offers the first developments of the expert health management processes for polymer electrolyte fuel cells. However, there have been a number of limitations identified, which could be improved upon in future iterations. The model used in fault detection, whilst seen to be accurate for steady-state conditions, could be improved in the way it simulates dynamic behaviour of the PEFC. Notably, the inclusion of the capacitive effects of voltage switching would improve performance and could eliminate the erroneous residual measurements seen in the testing results. Alternatively, a more complex model could be used for the condition assessment, such as the electrical equivalence model by Hernandez et al. in [64] or the bond graph approach by Vasilyev et al. in [120]. The usage of any more complex models should be balanced for the processing time for application systems.

The diagnostic rules have been seen to be useful for steady-state and slowly transient current conditions. Improvements suggested for the handling of dynamic operation are to consider the cumulative effect of the degradation effects, beyond the instantaneous responses. This could be included within the diagnostic rules themselves, or within the higher health management processing.

The diagnostic rules considering membrane chemical degradation should be changed so that current loading is given influence rather than the voltage conditions. This problem arose from a misinterpretation of the literature knowledge, where the OCV condition was taken as a description of a “very high” voltage output, as opposed to a current loading state. This would add fuzzy sets for stack current conditions, and three or four rules to reflect these new inputs,

though the diagnostic performance would not be measurably slower.

The testing procedures can be extended for further operational conditions and application specificities, such as long-term storage, start-stop cycling, and environmental conditions. These may require further additions to the diagnostic rules base. Indeed, the rules base is considered a living-resource which should be updated with new knowledge and observations for PEFC systems as the field of reliability continues to grow.

Overall, the fault detection and diagnostic processes presented in this thesis can contribute within an overall health management strategy. The diagnostic results can be combined with a prognostic approach – such as the particle-filtering approaches by Jouin et al. in [70] – to provide a full analysis for the state of health and remaining useful life of the PEFC under observation. Some suggestions have been made for the corrective actions which should be taken for each degradation mode. A full control strategy should be the subject of further study, to define techniques which act with the goal of maintaining PEFC lifetime performance.

# Bibliography

- [1] G. Prins, I. Galiana, C. Green, R. Grundman, M. Hulme, A. Korhola, F. Laird, T. Nordhaus, R. Pielke Jnr, S. Rayner, D. Sarewitz, M. Shellenberger, N. Stehr, and H. Tezuka, “The Hartwell Paper: A new direction for climate policy after the crash of 2009,” tech. rep., London School of Economics, 2010.
- [2] International Energy Agency, “Key World Energy Statistics,” tech. rep., 2016.
- [3] US Energy Information Administration, “Monthly Energy Review - December 2016,” tech. rep., 2016.
- [4] S. Lechtenböhmer, L. Nilsson, M. Åhman, and C. Schneider, “Decarbonising the energy intensive basic materials industry through electrification Implications for future EU electricity demand,” *Energy*, vol. 115, pp. 1623–1631, 2016.
- [5] J. Dong, C. Liu, and Z. Lin, “Charging infrastructure planning for promoting battery electric vehicles: An activity-based approach using multiday travel data,” *Transportation Research Part C: Emerging Technologies*, vol. 38, pp. 44–55, 2014.
- [6] M. Warshay, P. Prokopius, M. Le, and G. Voecks, “The NASA fuel cell upgrade program for the Space Shuttle orbiter,” *IECEC-97 Proceedings of the Thirty-Second Intersociety Energy Conversion Engineering Conference (Cat. No.97CH6203)*, pp. 228–231, 1997.
- [7] T. R. Ralph, “Principles of Fuel Cells,” *Platinum Metals Review*, vol. 50, no. 4, pp. 200–201, 2006.
- [8] Arcola Energy, “Research,” *arcolaenergy.com*, 2015.
- [9] Toyota, “Toyota Fuel Cell Vehicle,” *toyota-global.com*, 2014.
- [10] H. F. C. Technologies, “Horizon Fuel Cells,” *horizonfuelcell.com*, 2018.
- [11] Johnson Matthey, “Johnson Matthey Fuel Cells,” *jmfuelcells.com*, 2018.

- [12] R. O’Hayre, S.-W. Cha, W. Colella, and F. B. Prinz, *Fuel Cell Fundamentals*. John Wiley & Sons, 2nd ed., 2009.
- [13] EG&G Technical Services, *Fuel Cell Handbook*. No. November, U.S. Department of Energy, 7th ed., 2004.
- [14] T. E. Springer, T. A. Zawodzinski, and S. Gottesfeld, “Polymer electrolyte fuel cell model,” *Journal of the Electrochemical Society*, vol. 138, pp. 2334–2342, Aug. 1991.
- [15] M. N. Tsampas, A. Pikos, S. Brosda, A. Katsaounis, and C. G. Vayenas, “The effect of membrane thickness on the conductivity of Nafion,” *Electrochimica Acta*, vol. 51, no. 13, pp. 2743–2755, 2006.
- [16] A. Kirubakaran, S. Jain, and R. Nema, “A review on fuel cell technologies and power electronic interface,” *Renewable and Sustainable Energy Reviews*, vol. 13, pp. 2430–2440, Dec. 2009.
- [17] O. Z. Sharaf and M. F. Orhan, “An overview of fuel cell technology: Fundamentals and applications,” *Renewable and Sustainable Energy Reviews*, vol. 32, pp. 810–853, 2014.
- [18] TÜV SÜD, “Hydrogen Filling Stations Worldwide,” *H2Stations.org*, 2018.
- [19] US Office of energy efficiency & renewable energy, “3.4 Fuel Cells,” *Fuel Cell Technologies Office Multi-Year Research, Development, and Demonstration Plan*, vol. 2015, pp. 3.4.1–3.4.58, 2017.
- [20] K. Wipke, S. Sprik, J. Kurtz, T. Ramsden, C. Ainscough, and G. Saur, “National Fuel Cell Electric Vehicle Learning Demonstration Final Report,” tech. rep., 2012.
- [21] A. Van Der Toorn, “The maintenance of civil engineering structures,” tech. rep., University of Twente, 1996.
- [22] M. Jouin, R. Gouriveau, D. Hissel, M.-C. Pera, and N. Zerhouni, “Prognostics and Health Management of PEMFC – State of the art and remaining challenges,” *International Journal of Hydrogen Energy*, vol. 38, pp. 15307–15317, Nov. 2013.
- [23] R. Petrone, Z. Zheng, D. Hissel, M. Péra, C. Pianese, M. Sorrentino, M. Becherif, and N. Yousfi-Steiner, “A review on model-based diagnosis methodologies for PEMFCs,” *International Journal of Hydrogen Energy*, vol. 38, pp. 7077–7091, June 2013.
- [24] Z. Zheng, R. Petrone, M. C. Péra, D. Hissel, M. Becherif, C. Pianese, N. Yousfi Steiner, and M. Sorrentino, “A review on non-model based diagnosis methodologies for PEM fuel cell

- stacks and systems,” *International Journal of Hydrogen Energy*, vol. 38, no. 21, pp. 8914–8926, 2013.
- [25] L. Fan and Y. Liu, “Fuzzy Logic Based Constant Power Control of a Proton Exchange Membrane Fuel Cell,” *Electrical Review*, no. 5, pp. 72–75, 2012.
- [26] P. W. Kalgren, C. S. Byington, M. J. Roemer, and M. J. Watson, “Defining PHM, A Lexical Evolution of Maintenance and Logistics,” in *Autotestcon*, 2006.
- [27] K. Tüber, M. Zobel, H. Schmidt, and C. Hebling, “A polymer electrolyte membrane fuel cell system for powering portable computers,” *Journal of Power Sources*, vol. 122, no. 1, pp. 1–8, 2003.
- [28] C. Harms, F. Köhrmann, and A. Dyck, “Validation of the Influence of Test Parameters in Performance Measurements of a PEMFC Stack,” *ECS Meeting Abstracts*, vol. MA2014-02, no. 21, 2014.
- [29] S. Simon Araya, S. Juhl Andreasen, and S. Knudsen Kær, “Parametric Sensitivity Test-European Polymer Electrolyte Membrane Fuel Cell Stack Test Procedures,” *Journal of Fuel Cell Science and Technology*, vol. 11, no. 6, p. 061007, 2014.
- [30] P. Piela and J. Mitzel, “Polymer electrolyte membrane fuel cell efficiency at the stack level,” *Journal of Power Sources*, vol. 292, pp. 95–103, 2015.
- [31] L. Wang, A. Husar, T. Zhou, and H. Liu, “A parametric study of PEM fuel cell performances,” *International Journal of Hydrogen Energy*, vol. 28, pp. 1263–1272, Nov. 2003.
- [32] N. V. Dale, M. D. Mann, H. Salehfar, a. M. Dhirde, and T. Han, “AC Impedance Study of a Proton Exchange Membrane Fuel Cell Stack Under Various Loading Conditions,” *Journal of Fuel Cell Science and Technology*, vol. 7, no. 3, 2010.
- [33] K. R. Cooper and M. Smith, “Electrical test methods for on-line fuel cell ohmic resistance measurement,” *Journal of Power Sources*, vol. 160, pp. 1088–1095, 2006.
- [34] R. Guzmán-Blas, C. L. Menéndez, C. A. Vélez, E. R. Fachini, A. Johnston-Peck, S. D. Senanayake, D. Stacchiola, K. Sasaki, and C. R. Cabrera, “Vulcan/Pt/Ce Catalysts Prepared by Impregnation Using EDTA for Direct Methanol Fuel Cell, Direct Ethanol Fuel Cell, and Polymer Electrolyte Membrane Fuel Cell,” *Smart Grid and Renewable Energy*, vol. 4, no. October, pp. 1–9, 2013.

- [35] S. Vengatesan, M. W. Fowler, X. Z. Yuan, and H. Wang, "Diagnosis of MEA degradation under accelerated relative humidity cycling," *Journal of Power Sources*, vol. 196, no. 11, pp. 5045–5052, 2011.
- [36] K. R. Cooper, "In Situ PEMFC Fuel Crossover & Electrical Short Circuit Measurement," *Fuel Cell Magazine*, 2008.
- [37] H. Liu, W. K. Epting, and S. Litster, "Gas Transport Resistance in Polymer Electrolyte Thin Films on Oxygen Reduction Reaction Catalysts," *Langmuir*, vol. 31, no. 36, pp. 9853–9858, 2015.
- [38] J. Wu, X. Zi Yuan, H. Wang, M. Blanco, J. J. Martin, and J. Zhang, "Diagnostic tools in PEM fuel cell research: Part II Physical/chemical methods," *International Journal of Hydrogen Energy*, vol. 33, no. 6, pp. 1747–1757, 2008.
- [39] J. Tan, Y. Chao, M. Yang, C. Williams, and J. Van Zee, "Degradation Characteristics of Elastomeric Gasket Materials in a Simulated PEM Fuel Cell Environment," *Journal of Materials Engineering and Performance*, vol. 17, pp. 785–792, Apr. 2008.
- [40] J. Park, X. Li, D. Tran, T. Abdel-Baset, D. S. Hussey, D. L. Jacobson, and M. Arif, "Neutron imaging investigation of liquid water distribution in and the performance of a PEM fuel cell," *International Journal of Hydrogen Energy*, vol. 33, no. 13, pp. 3373–3384, 2008.
- [41] T. A. Zawodzinski, M. Neeman, L. O. Sillerud, and S. Gottesfeld, "Determination of water diffusion coefficients in perfluorosulfonate ionomeric membranes," *The Journal of Physical Chemistry*, vol. 95, no. JULY 1991, pp. 6040–6044, 1991.
- [42] R. L. Borup, J. R. Davey, F. H. Garzon, D. L. Wood, and M. A. Inbody, "PEM fuel cell electrocatalyst durability measurements," *Journal of Power Sources*, vol. 163, no. 1, pp. 76–81, 2006.
- [43] C. Chen and T. F. Fuller, "XPS Analysis of Polymer Membrane Degradation in PEMFCs," *Journal of The Electrochemical Society*, vol. 156, no. 10, p. B1218, 2009.
- [44] L. Martins, J. Gardolinski, J. Vargas, J. Ordonez, S. Amico, and M. Forte, "The experimental validation of a simplified PEMFC simulation model for design and optimization purposes," *Applied Thermal Engineering*, vol. 29, no. 14, pp. 3036–3048, 2009.
- [45] J. Larminie, A. Dicks, and M. McDonald, *Fuel cell systems explained*. John Wiley & Sons, 2 ed., 2003.

- [46] J. Chen and B. Zhou, “Diagnosis of PEM fuel cell stack dynamic behaviors,” *Journal of Power Sources*, vol. 177, pp. 83–95, Feb. 2008.
- [47] N. Y. Steiner, D. Hissel, P. Moçotéguy, and D. Candusso, “Non intrusive diagnosis of polymer electrolyte fuel cells by wavelet packet transform,” *International Journal of Hydrogen Energy*, vol. 36, pp. 740–746, Jan. 2011.
- [48] T. J. Mason, “Advanced diagnostic techniques to study the electrochemical and mechanical properties of polymer electrolyte fuel cells,” *Chemical Engineering*, vol. Ph.D., 2013.
- [49] E. Laffly, M.-C. Pera, and D. Hissel, “Polymer Electrolyte Membrane Fuel Cell Modelling and Parameters Estimation for Ageing Consideration,” in *2007 IEEE International Symposium on Industrial Electronics*, pp. 180–185, June 2007.
- [50] K. Tüber, D. Pócza, and C. Hebling, “Visualization of water buildup in the cathode of a transparent PEM fuel cell,” *Journal of Power Sources*, vol. 124, no. 2, pp. 403–414, 2003.
- [51] X. Liu, H. Guo, F. Ye, and C. F. Ma, “Flow dynamic characteristics in flow field of proton exchange membrane fuel cells,” *International Journal of Hydrogen Energy*, vol. 33, no. 3, pp. 1040–1051, 2008.
- [52] C. G. Chung, L. Kim, Y. W. Sung, J. Lee, and J. S. Chung, “Degradation mechanism of electrocatalyst during long-term operation of PEMFC,” *International Journal of Hydrogen Energy*, vol. 34, no. 21, pp. 8974–8981, 2009.
- [53] R. Onanena, L. Oukhellou, D. Candusso, F. Harel, D. Hissel, and P. Aknin, “Fuel cells static and dynamic characterizations as tools for the estimation of their ageing time,” *International Journal of Hydrogen Energy*, vol. 36, pp. 1730–1739, Jan. 2011.
- [54] N. Fouquet, C. Doulet, C. Nouillant, G. Dauphin-Tanguy, and B. Ould-Bouamama, “Model based PEM fuel cell state-of-health monitoring via ac impedance measurements,” *Journal of Power Sources*, vol. 159, no. 2, pp. 905–913, 2006.
- [55] X. Yuan, H. Wang, J. Colin Sun, and J. Zhang, “AC impedance technique in PEM fuel cell diagnosis – A review,” *International Journal of Hydrogen Energy*, vol. 32, no. 17, pp. 4365–4380, 2007.
- [56] A. Zeller, O. Rallières, J. Régnier, and C. Turpin, “Diagnosis of a hydrogen/air fuel cell by a statistical model-based method,” *2010 IEEE Vehicle Power and Propulsion Conference, VPPC 2010*, 2010.

- [57] J. Hua, J. Li, M. Ouyang, L. Lu, and L. Xu, "Proton exchange membrane fuel cell system diagnosis based on the multivariate statistical method," *International Journal of Hydrogen Energy*, vol. 36, no. 16, pp. 9896–9905, 2011.
- [58] C. Lebreton, M. Benne, C. Damour, N. Yousfi-Steiner, B. Grondin-Perez, D. Hissel, and J. P. Chabriat, "Fault Tolerant Control Strategy applied to PEMFC water management," *International Journal of Hydrogen Energy*, vol. 40, no. 33, pp. 10636–10646, 2015.
- [59] A. Bosco and M. Fronk, "United States Patent 6103409 – Fuel Cell Flooding Detection and Correction," 2000.
- [60] C. Fennie, D. Reisner, J. Barbetta, and P. Singh, "Fuzzy Logic-Based State-of-Health Determination of PEM Fuel Cells," tech. rep., 2001.
- [61] D. Hissel, M. Péra, and J. Kauffmann, "Diagnosis of automotive fuel cell power generators," *Journal of Power Sources*, vol. 128, pp. 239–246, Apr. 2004.
- [62] V. Anghel, "Prediction Failure for PEM Fuel Cells," *International Journal of Advances in Engineering & Technology*, vol. 4, no. 2, pp. 1–14, 2012.
- [63] T. Escobet, D. Feroldi, S. de Lira, V. Puig, J. Quevedo, J. Riera, and M. Serra, "Model-based fault diagnosis in PEM fuel cell systems," *Journal of Power Sources*, vol. 192, pp. 216–223, July 2009.
- [64] A. Hernandez, D. Hissel, and R. Outbib, "Modeling and fault diagnosis of a polymer electrolyte fuel cell using electrical equivalent analysis," *IEEE Transactions on Energy Conversion*, vol. 25, no. 1, pp. 148–160, 2010.
- [65] J. Kim, I. Lee, Y. Tak, and B. H. Cho, "State-of-health diagnosis based on hamming neural network using output voltage pattern recognition for a PEM fuel cell," *International Journal of Hydrogen Energy*, vol. 37, no. 5, pp. 4280–4289, 2012.
- [66] L. A. M. Riascos, M. G. Simoes, and P. E. Miyagi, "A Bayesian network fault diagnostic system for proton exchange membrane fuel cells," *Journal of Power Sources*, vol. 165, no. 1, pp. 267–278, 2007.
- [67] Y. Vural, D. B. Ingham, and M. Pourkashanian, "Performance prediction of a proton exchange membrane fuel cell using the ANFIS model," *International Journal of Hydrogen Energy*, vol. 34, pp. 9181–9187, Nov. 2009.

- [68] S. Becker and V. Karri, “Predictive models for PEM-electrolyzer performance using adaptive neuro-fuzzy inference systems,” *International Journal of Hydrogen Energy*, vol. 35, no. 18, pp. 9963–9972, 2010.
- [69] R. Silva, R. Gouriveau, S. Jemeï, D. Hissel, L. Boulon, K. Agbossou, and N. Yousfi Steiner, “Proton exchange membrane fuel cell degradation prediction based on Adaptive Neuro-Fuzzy Inference Systems,” *International Journal of Hydrogen Energy*, vol. 39, pp. 11128–11144, July 2014.
- [70] M. Jouin, R. Gouriveau, D. Hissel, M. C. Péra, and N. Zerhouni, “Prognostics of PEM fuel cell in a particle filtering framework,” *International Journal of Hydrogen Energy*, vol. 39, no. 1, pp. 481–494, 2014.
- [71] J. Hua, X. Lin, L. Xu, J. Li, and M. Ouyang, “Bluetooth wireless monitoring, diagnosis and calibration interface for control system of fuel cell bus in Olympic demonstration,” *Journal of Power Sources*, vol. 186, no. 2, pp. 478–484, 2009.
- [72] C. Ziogou, S. Papadopoulou, M. C. Georgiadis, and S. Voutetakis, “On-line nonlinear model predictive control of a PEM fuel cell system,” *Journal of Process Control*, vol. 23, pp. 483–492, Apr. 2013.
- [73] V. Venkatasubramanian, R. Rengaswamy, K. Yin, and S. N. Kavuri, “A review of process fault detection and diagnosis Part I: Quantitative model-based methods,” *Computers & Chemical Engineering*, vol. 27, no. 3, pp. 293–311, 2003.
- [74] V. Venkatasubramanian, R. Rengaswamy, and S. N. Kavuri, “A review of process fault detection and diagnosis: Part II: Qualitative models and search strategies,” *Computers & Chemical Engineering*, vol. 27, no. 3, pp. 313–326, 2003.
- [75] V. Venkatasubramanian, R. Rengaswamy, S. N. Kavuri, and K. Yin, “A review of process fault detection and diagnosis Part III: Process history based methods,” *Computers & Chemical Engineering*, vol. 27, no. 3, pp. 293–311, 2003.
- [76] F. A. de Bruijn, V. A. T. Dam, and G. J. M. Janssen, “Review: Durability and Degradation Issues of PEM Fuel Cell Components,” *Fuel Cells*, vol. 8, pp. 3–22, Feb. 2008.
- [77] R. Borup, J. Meyers, B. Pivovar, Y. S. Kim, R. Mukundan, N. Garland, D. Myers, M. Wilson, F. Garzon, D. Wood, P. Zelenay, K. More, K. Stroh, T. Zawodzinski, J. Boncella, J. E. McGrath, M. Inaba, K. Miyatake, M. Hori, K. Ota, Z. Ogumi, S. Miyata, A. Nishikata, Z. Siroma, Y. Uchimoto, K. Yasuda, K.-I. Kimijima, and N. Iwashita, “Scientific aspects

- of polymer electrolyte fuel cell durability and degradation.,” *Chemical reviews*, vol. 107, pp. 3904–51, Oct. 2007.
- [78] Q. Yan, H. Toghiani, and J. Wu, “Investigation of water transport through membrane in a PEM fuel cell by water balance experiments,” *Journal of Power Sources*, vol. 158, pp. 316–325, July 2006.
- [79] H. Wang, H. Li, and X.-Z. Yuan, eds., *PEM Fuel Cell Failure Mode Analysis*. CRC Press, 2012.
- [80] V. A. Sethuraman, J. W. Weidner, A. T. Haug, S. Motupally, and L. V. Protsailo, “Hydrogen Peroxide Formation Rates in a PEMFC Anode and Cathode,” *Journal of The Electrochemical Society*, vol. 155, no. 1, p. B50, 2008.
- [81] D. E. Curtin, R. D. Lousenberg, T. J. Henry, P. C. Tangeman, and M. E. Tisack, “Advanced materials for improved PEMFC performance and life,” *Journal of Power Sources*, vol. 131, pp. 41–48, May 2004.
- [82] C. Zhou, T. A. Zawodzinski, and D. A. Schiraldi, “Chemical degradation of Nafion membranes,” *Fourth International Symposium on Proton Conducting Membrane Fuel Cells*, vol. 206, p. 1968, 2004.
- [83] W. Liu, K. Ruth, and G. Rusch, “Membrane Durability in PEM Fuel Cells,” *Journal of New Materials for Electrochemical Systems*, vol. 4, pp. 227–231, 2001.
- [84] P. Rama, R. Chen, and J. Andrews, “A review of performance degradation and failure modes for hydrogen-fuelled polymer electrolyte fuel cells,” *Proceedings of the Institution of Mechanical Engineers, Part A: Journal of Power and Energy*, vol. 222, pp. 421–441, Aug. 2008.
- [85] N. Yousfi-Steiner, P. Moçotéguy, D. Candusso, and D. Hissel, “A review on polymer electrolyte membrane fuel cell catalyst degradation and starvation issues: Causes, consequences and diagnostic for mitigation,” *Journal of Power Sources*, vol. 194, pp. 130–145, Oct. 2009.
- [86] T. W. Patterson and R. M. Darling, “Damage to the Cathode Catalyst of a PEM Fuel Cell Caused by Localized Fuel Starvation,” *Electrochemical and Solid-State Letters*, vol. 9, p. A183, Apr. 2006.
- [87] L. Placca and R. Kouta, “Fault tree analysis for PEM fuel cell degradation process modelling,” *International Journal of Hydrogen Energy*, vol. 36, no. 19, pp. 12393–12405, 2011.

- [88] Z. Noda, K. Hirata, a. Hayashi, S. Taniguchi, N. Nakazato, a. Seo, I. Yasuda, S. Ariura, H. Shinkai, and K. Sasaki, “PEFC-type impurity sensors for hydrogen fuels,” *International Journal of Hydrogen Energy*, vol. 37, pp. 16256–16263, Nov. 2012.
- [89] T. Akita, A. Taniguchi, J. Maekawa, Z. Siroma, K. Tanaka, M. Kohyama, and K. Yasuda, “Analytical TEM study of Pt particle deposition in the proton-exchange membrane of a membrane-electrode-assembly,” *Journal of Power Sources*, vol. 159, pp. 461–467, Sept. 2006.
- [90] S. Ohyagi, T. Matsuda, Y. Iseki, T. Sasaki, and C. Kaito, “Effects of operating conditions on durability of polymer electrolyte membrane fuel cell Pt cathode catalyst layer,” *Journal of Power Sources*, vol. 196, no. 8, pp. 3743–3749, 2011.
- [91] W. Schmittinger and A. Vahidi, “A review of the main parameters influencing long-term performance and durability of PEM fuel cells,” *Journal of Power Sources*, vol. 180, pp. 1–14, May 2008.
- [92] T. F. Fuller, “Diagnostics for PEMFC Performance and Durability,” *ECS Transactions*, vol. 41, no. 1, pp. 621–628, 2011.
- [93] S. D. Knights, K. M. Colbow, J. St-Pierre, and D. P. Wilkinson, “Aging mechanisms and lifetime of PEFC and DMFC,” *Journal of Power Sources*, vol. 127, pp. 127–134, Mar. 2004.
- [94] J. F. Joseph Fairweather, Bo Li, Rangachary Mukundan, “In situ and ex situ characterization of carbon corrosion in PEMFCs,” in *218th Electrochemical Society Meeting*, Jan. 2010.
- [95] N. Dandekar and A. Mendonca, *Electrochemical Characterization and Aging in PEM Fuel Cells*. Degree of bachelor of science, Worcester Polytechnic Institute, 2012.
- [96] A. Pozio, R. Silva, M. De Francesco, and L. Giorgi, “Nafion degradation in PEMFCs from end plate iron contamination,” *Electrochimica Acta*, vol. 48, pp. 1543–1549, May 2003.
- [97] W. Yoon, X. Huang, P. Fazzino, K. L. Reifsnider, and M. A. Akkaoui, “Evaluation of coated metallic bipolar plates for polymer electrolyte membrane fuel cells,” *Journal of Power Sources*, vol. 179, pp. 265–273, Apr. 2008.
- [98] J. St-Pierre, D. P. Wilkinsoin, S. Knights, and M. Bos, “Relationships between water management, contamination and lifetime degradation in PEFC,” *Journal of New Materials for Electrochemical Systems*, vol. 3, pp. 99–106, 2000.

- [99] J. Imamura and Y. Tarutani, “Stainless Steel Foil for Bipolar Plates of PEFCs,” Tech. Rep. 106, 2014.
- [100] J. Wu, X. Z. Yuan, H. Wang, M. Blanco, J. J. Martin, and J. Zhang, “Diagnostic tools in PEM fuel cell research: Part I Electrochemical techniques,” *International Journal of Hydrogen Energy*, vol. 33, no. 6, pp. 1735–1746, 2008.
- [101] D. H. Ye and Z. G. Zhan, “A review on the sealing structures of membrane electrode assembly of proton exchange membrane fuel cells,” *Journal of Power Sources*, vol. 231, pp. 285–292, 2013.
- [102] M. Schulze, T. Knöri, A. Schneider, and E. Gülzow, “Degradation of sealings for PEFC test cells during fuel cell operation,” *Journal of Power Sources*, vol. 127, no. 1-2, pp. 222–229, 2004.
- [103] J. Scholta, N. Berg, P. Wilde, L. Jörissen, and J. Garche, “Development and performance of a 10 kW PEMFC stack,” *Journal of Power Sources*, vol. 127, no. 1-2, pp. 206–212, 2004.
- [104] L. a.M. Riascos, “Relative humidity control in polymer electrolyte membrane fuel cells without extra humidification,” *Journal of Power Sources*, vol. 184, pp. 204–211, Sept. 2008.
- [105] A. Aitouche, S. C. Olteanu, B. O. Bouamama, and B. Ould Bouamama, “A Survey of Diagnostic of Fuel Cell Stack Systems,” in *IFAC Safeprocess*, vol. 8, (Mexico), pp. 84–89, 2012.
- [106] W. He, G. Lin, and T. Van Nguyen, “Diagnostic Tool to Detect Electrode Flooding in Proton-Exchange Membrane Fuel Cells,” *American Institute of Chemical Engineers Journal*, vol. 49, pp. 3221–3228, Dec. 2003.
- [107] H. Ma, H. Zhang, J. Hu, Y. Cai, and B. Yi, “Diagnostic tool to detect liquid water removal in the cathode channels of proton exchange membrane fuel cells.” 2006.
- [108] A. Ingimundarson, “Model-based detection of hydrogen leaks in a fuel cell stack,” *IEEE Transactions on Control Systems Technology*, vol. 16, no. 5, pp. 1004–1012, 2008.
- [109] D. Hissel, D. Candusso, and F. Harel, “Fuzzy-Clustering Durability Diagnosis of Polymer Electrolyte Fuel Cells Dedicated to Transportation Applications,” *IEEE Transactions on Vehicular Technology*, vol. 56, pp. 2414–2420, Sept. 2007.
- [110] M. Mench, Q. Dong, and C. Wang, “In situ water distribution measurements in a polymer electrolyte fuel cell,” *Journal of Power Sources*, vol. 124, no. 1, pp. 90–98, 2003.

- [111] R. F. Mann, J. C. Amphlett, M. A. Hooper, H. M. Jensen, B. A. Peppley, and P. R. Roberge, "Development and application of a generalised steady-state electrochemical model for a PEM fuel cell," *Journal of Power Sources*, vol. 86, pp. 173–180, Mar. 2000.
- [112] A. Shokuhi-Rad, N. Nariman-Zadeh, and M. Naghash-Zadegan, "Model Development and Optimisation Base on Generalised Steady-State Electrochemical Equations for a PEM Fuel Cell," in *Proceedings 23rd European Conference on Modelling and Simulation*, 2009.
- [113] C. Francia, V. S. Ijeri, S. Specchia, and P. Spinelli, "Estimation of hydrogen crossover through Nafion® membranes in PEMFCs," *Journal of Power Sources*, vol. 196, pp. 1833–1839, Feb. 2011.
- [114] W. He, J. S. Yi, and T. Van Nguyen, "Two-phase flow model of the cathode of PEM fuel cells using interdigitated flow fields," *American Institute of Chemical Engineers Journal*, vol. 46, pp. 2053–2064, Oct. 2000.
- [115] M. J. Khan and M. T. Iqbal, "Modelling and Analysis of Electro-chemical, Thermal, and Reactant Flow Dynamics for a PEM Fuel Cell System," *Fuel Cells*, vol. 5, pp. 463–475, Dec. 2005.
- [116] D. Candusso, F. Harel, a. Debernardinis, X. Francois, M. Pera, D. Hissel, P. Schott, G. Coquery, and J. Kauffmann, "Characterisation and modelling of a 5kW PEMFC for transportation applications," *International Journal of Hydrogen Energy*, vol. 31, pp. 1019–1030, July 2006.
- [117] S. Asghari, A. Mokmeli, and M. Samavati, "Study of PEM fuel cell performance by electrochemical impedance spectroscopy," *International Journal of Hydrogen Energy*, vol. 35, pp. 9283–9290, Sept. 2010.
- [118] A. Narjiss, D. Depernet, D. Candusso, F. Gustin, and D. Hissel, "Online diagnosis of PEM Fuel Cell," in *2008 13th International Power Electronics and Motion Control Conference*, pp. 734–739, IEEE, Sept. 2008.
- [119] B. Legros, P. X. Thivel, F. Druart, Y. Bultel, and R. Nogueira, "Diagnosis and Modelling of Proton-Exchange-Membrane Fuel Cell via and Acoustic-Emission Measurements," *Cell*, no. July, pp. 1–3, 2009.
- [120] A. Vasilyev, S. Dunnett, and L. Jackson, "Model-Based Fault Detection and Isolation of PEM fuel cells using Bond Graphs," *Safety and Reliability of Complex Engineered Systems - Proceedings of the 25th European Safety and Reliability Conference, ESREL 2015*, 2015.

- [121] A. Aitouche, Q. Yang, and B. Ould Bouamama, “Fault detection and isolation of PEM fuel cell system based on nonlinear analytical redundancy,” *The European Physical Journal Applied Physics*, vol. 54, p. 23408, May 2011.
- [122] M. Shao, X. J. Zhu, H. F. Cao, and H. F. Shen, “An artificial neural network ensemble method for fault diagnosis of proton exchange membrane fuel cell system,” *Energy*, vol. 67, pp. 268–275, 2014.
- [123] Z. Zheng, R. Petrone, and M. Pera, “Diagnosis of a commercial PEM fuel cell stack via incomplete spectra and fuzzy clustering,” in *IECON 2013 - 39th Annual Conference of the IEEE Industrial Electronics Society*, pp. 1595–1600, 2013.
- [124] S. Wasterlain, D. Candusso, F. Harel, X. Francois, and D. Hissel, “Diagnosis of a fuel cell stack using electrochemical impedance spectroscopy and Bayesian Networks,” *2010 IEEE Vehicle Power and Propulsion Conference*, pp. 1–6, 2010.
- [125] I. Gadaras and L. Mikhailov, “An interpretable fuzzy rule-based classification methodology for medical diagnosis,” *Artificial Intelligence in Medicine*, vol. 47, no. 1, pp. 25–41, 2009.
- [126] L. I. Kuncheva and F. Steimann, “Fuzzy diagnosis,” *Artificial Intelligence in Medicine*, vol. 16, no. 2, pp. 121–128, 1999.
- [127] V. C. Georgopoulos, G. a. Malandraki, and C. D. Stylios, “A fuzzy cognitive map approach to differential diagnosis of specific language impairment,” *Artificial Intelligence in Medicine*, vol. 29, no. 3, pp. 261–278, 2003.
- [128] S. Suryanarayanan, N. P. Reddy, and E. P. Canilang, “A fuzzy logic diagnosis system for classification of pharyngeal dysphagia,” *International Journal of Bio-Medical Computing*, vol. 38, no. 3, pp. 207–215, 1995.
- [129] R. Isermann, “Model-based fault-detection and diagnosis - Status and applications,” 2005.
- [130] R. Stetter and M. Witczak, “Degradation Modelling for Health Monitoring Systems,” in *Journal of Physics: Conference Series*, vol. 570, 2014.
- [131] Yann-Chang Huang, Hong-Tzer Yang, Ching-Lien Huang, Y.-C. Huang, and H.-T. Yang, “Developing a New Transformer Fault Diagnosis System through Evolutionary Fuzzy Logic,” *IEEE Transactions on Power Delivery*, vol. 12, pp. 761–767, Apr. 1997.
- [132] Z. Zheng, M.-C. C. Péra, D. Hissel, M. Becherif, K.-S. S. Agbli, and Y. Li, “A double-fuzzy diagnostic methodology dedicated to online fault diagnosis of proton exchange membrane fuel cell stacks,” *Journal of Power Sources*, vol. 271, pp. 570–581, Dec. 2014.

- [133] J. C. Amphlett, R. F. Mann, B. A. Peppley, P. R. Roberge, A. Rodrigues, and J. P. Salvador, "Simulation of a 250 kW diesel fuel processor/PEM fuel cell system," *Journal of Power Sources*, vol. 71, no. 1-2, pp. 179–184, 1998.
- [134] R. Borup, "V.B.1 Fuel Cell-Performance and Durability (FC-PAD) Consortium Overview," vol. 2, pp. 1–8, 2016.
- [135] J. Zhang, Y. Tang, C. Song, J. Zhang, and H. Wang, "PEM fuel cell open circuit voltage (OCV) in the temperature range of 23 C to 120 C," *Journal of Power Sources*, vol. 163, no. 1, pp. 532–537, 2006.
- [136] M. Jouin, R. Gouriveau, D. Hissel, C. Marie, and A. Savary, "Prognostics of PEM fuel cells under a combined heat and power profile," *IFAC-PapersOnLine*, vol. 48, no. 3, pp. 26–31, 2015.
- [137] J. B. Benziger, M. B. Satterfield, W. H. J. Hogarth, J. P. Nehlsen, and I. G. Kevrekidis, "The power performance curve for engineering analysis of fuel cells," *Journal of Power Sources*, vol. 155, pp. 272–285, 2006.
- [138] L. Zadeh, "Fuzzy sets," *Information and Control*, vol. 8, no. 3, pp. 338–353, 1965.
- [139] J. Abonyi, *Fuzzy Model Identification for Control*. Boston, USA: Birkhauser, 1 ed., 2002.
- [140] B. Kosko, "Fuzziness vs. Probability," *International Journal of General Systems*, vol. 17, no. 2-3, pp. 211–240, 1990.
- [141] J. Harris, *An Introduction to Fuzzy Logic Applications*. Netherlands: Kluwer Academic Publishers, 2000.
- [142] S. Zhang, X. Yuan, H. Wang, W. Merida, H. Zhu, J. Shen, S. Wu, and J. Zhang, "A review of accelerated stress tests of MEA durability in PEM fuel cells," *International Journal of Hydrogen Energy*, vol. 34, no. 1, pp. 388–404, 2009.
- [143] J. S. Cooper, "Design analysis of PEMFC bipolar plates considering stack manufacturing and environment impact," *Journal of Power Sources*, vol. 129, no. 2, pp. 152–169, 2004.
- [144] M. B. Satterfield, P. W. Majsztrik, H. Ota, J. B. Benziger, and A. B. Bocarsly, "Mechanical properties of Nafion and titania/Nafion composite membranes for polymer electrolyte membrane fuel cells," *Journal of Polymer Science, Part B: Polymer Physics*, vol. 44, no. 16, pp. 2327–2345, 2006.

- [145] P. Adcock, A. Kells, and C. Jackson, "PEM Fuel Cells for Road Vehicles," in *EET-2008 European Ele-Drive Conference*, 2008.
- [146] V. Murthi, R. Urian, and S. Mukerjee, "Oxygen reduction kinetics in low and medium temperature acid environment: correlation of water activation and surface properties in supported Pt and Pt alloy," *The Journal of Physical Chemistry B*, vol. 108, pp. 11011–11023, 2004.
- [147] B. Sompalli, B. a. Litteer, W. Gu, and H. a. Gasteiger, "Membrane Degradation at Catalyst Layer Edges in PEMFC MEAs," *Journal of The Electrochemical Society*, vol. 154, no. 12, p. B1349, 2007.
- [148] N. Ramaswamy, N. Hakim, and S. Mukerjee, "Degradation mechanism study of perfluorinated proton exchange membrane under fuel cell operating conditions," *Electrochimica Acta*, vol. 53, pp. 3279–3295, Mar. 2008.
- [149] M. Inaba, T. Kinumoto, M. Kiriake, R. Umebayashi, A. Tasaka, and Z. Ogumi, "Gas crossover and membrane degradation in polymer electrolyte fuel cells," *Electrochimica Acta*, vol. 51, pp. 5746–5753, Aug. 2006.
- [150] H. Liu, J. Zhang, F. Coms, and W. Gu, "Impact of gas partial pressure on PEMFC chemical degradation," *ECS Transactions*, vol. 3, no. 1, pp. 493–505, 2006.
- [151] W. Liu and D. Zuckerbrod, "In Situ Detection of Hydrogen Peroxide in PEM Fuel Cells," *Journal of The Electrochemical Society*, vol. 152, no. 6, p. A1165, 2005.
- [152] V. O. Mittal, H. R. Kunz, and J. M. Fenton, "Membrane Degradation Mechanisms in PEMFCs," *Journal of The Electrochemical Society*, vol. 154, no. 7, p. B652, 2007.
- [153] X. Huang, R. Solasi, Y. Zou, M. Feshler, K. Reifsnider, D. Condit, S. Burlatsky, and T. Madden, "Mechanical endurance of polymer electrolyte membrane and PEM fuel cell durability," *Journal of Polymer Science, Part B: Polymer Physics*, vol. 44, no. 16, pp. 2346–2357, 2006.
- [154] F. Bauer, S. Denneler, and M. Willert-Porada, "Influence of temperature and humidity on the mechanical properties of Nafion 117 polymer electrolyte membrane," *Journal of Polymer Science, Part B: Polymer Physics*, vol. 43, no. 7, pp. 786–795, 2005.
- [155] H. Li, Y. Tang, Z. Wang, Z. Shi, S. Wu, D. Song, J. Zhang, K. Fatih, J. Zhang, H. Wang, Z. Liu, R. Abouatallah, and A. Mazza, "A review of water flooding issues in the proton

- exchange membrane fuel cell,” *Journal of Power Sources*, vol. 178, no. 1, pp. 103–117, 2008.
- [156] Y.-H. Lai, C. S. Gittleman, C. K. Mittelsteadt, and D. a. Dillard, “Viscoelastic stress model and mechanical characterizat on of perfluorosulfonic acid (PFSA) polymer electrolyte membranes,” *Proceedings of the 3rd International Conference on Fuel Cell Science, Engineering, and Technology, 2005*, pp. 161–167, 2005.
- [157] M. F. Mathias, R. Makharia, H. a. Gasteiger, J. J. Conley, T. J. Fuller, C. J. Gittleman, S. S. Kocha, D. P. Miller, C. K. Mittelsteadt, T. Xie, S. G. Yan, and P. T. Yu, “Two fuel cell cars in every garage?,” *The Electrochemical Society Interface*, vol. 14, pp. 24–35, 2005.
- [158] H. Y. Jung and J. W. Kim, “Role of the glass transition temperature of Nafion 117 membrane in the preparation of the membrane electrode assembly in a direct methanol fuel cell (DMFC),” *International Journal of Hydrogen Energy*, vol. 37, no. 17, pp. 12580–12585, 2012.
- [159] N. Yoshida, T. Ishisaki, a. Watakabe, and M. Yoshitake, “Characterization of Flemion® membranes for PEFC,” *Electrochimica Acta*, vol. 43, no. 24, pp. 3749–3754, 1998.
- [160] Y. Shao, G. Yin, and Y. Gao, “Understanding and approaches for the durability issues of Pt-based catalysts for PEM fuel cell,” *Journal of Power Sources*, vol. 171, no. 2, pp. 558–566, 2007.
- [161] P. J. Ferreira, G. J. la O’, Y. Shao-Horn, D. Morgan, R. Makharia, S. Kocha, and H. A. Gasteiger, “Instability of Pt/C Electrocatalysts in Proton Exchange Membrane Fuel Cells,” *Journal of The Electrochemical Society*, vol. 152, no. 11, p. A2256, 2005.
- [162] R. Borup, J. Davey, F. Garzon, D. Wood, P. Welch, and K. More, “PEM Fuel Cell Durability With Transportation Transient Operation,” *ECS Transactions*, vol. 3, no. 1, pp. 879–886, 2006.
- [163] R. K. Ahluwalia, S. Arisetty, J.-K. Peng, R. Subbaraman, X. Wang, N. Kariuki, D. J. Myers, R. Mukundan, R. Borup, and O. Plevaya, “Dynamics of Particle Growth and Electrochemical Surface Area Loss due to Platinum Dissolution,” *Journal of the Electrochemical Society*, vol. 161, pp. F291–F304, Jan. 2014.
- [164] J. Wang, G. Yin, Y. Shao, S. Zhang, Z. Wang, and Y. Gao, “Effect of carbon black support corrosion on the durability of Pt/C catalyst,” *Journal of Power Sources*, vol. 171, no. 2, pp. 331–339, 2007.

- [165] Q. Li, R. He, J. Jensen, and N. Bjerrum, "Approaches and recent development of polymer electrolyte membranes for fuel cells operating above 100 C," *Chemistry of materials*, vol. 15, pp. 4896–4915, 2003.
- [166] T. R. Ralph, S. Hudson, and D. P. Wilkinson, "Electrocatalyst Stability in PEMFCs and the Role of Fuel Starvation and Cell Reversal Tolerant Anodes," *ECS Transactions*, vol. 1, no. 8, pp. 67–84, 2006.
- [167] L. M. Roen, C. H. Paik, and T. D. Jarvi, "Electrocatalytic Corrosion of Carbon Support in PEMFC Cathodes," *Electrochemical and Solid-State Letters*, vol. 7, no. 1, p. A19, 2004.
- [168] A. Taniguchi, T. Akita, K. Yasuda, and Y. Miyazaki, "Analysis of degradation in PEMFC caused by cell reversal during air starvation," *International Journal of Hydrogen Energy*, vol. 33, pp. 2323–2329, May 2008.
- [169] A. Taniguchi, T. Akita, K. Yasuda, and Y. Miyazaki, "Analysis of electrocatalyst degradation in PEMFC caused by cell reversal during fuel starvation," *Journal of Power Sources*, vol. 130, pp. 42–49, May 2004.
- [170] Y. Yu, H. Li, H. Wang, X.-Z. Yuan, G. Wang, and M. Pan, "A review on performance degradation of proton exchange membrane fuel cells during startup and shutdown processes: Causes, consequences, and mitigation strategies," *Journal of Power Sources*, vol. 205, pp. 10–23, 2012.
- [171] H. Tang, Z. Qi, M. Ramani, and J. F. Elter, "PEM fuel cell cathode carbon corrosion due to the formation of air/fuel boundary at the anode," *Journal of Power Sources*, vol. 158, no. 2, pp. 1306–1312, 2006.
- [172] P. Pei, Q. Chang, and T. Tang, "A quick evaluating method for automotive fuel cell lifetime," *International Journal of Hydrogen Energy*, vol. 33, pp. 3829–3836, July 2008.
- [173] Y. Wang and C.-Y. Wang, "Dynamics of polymer electrolyte fuel cells undergoing load changes," *Electrochimica Acta*, vol. 51, pp. 3924–3933, May 2006.
- [174] C. Cadet, S. Jemeï, F. Druart, and D. Hissel, "Diagnostic tools for PEMFCs: From conception to implementation," *International Journal of Hydrogen Energy*, vol. 39, no. 20, pp. 10613–10626, 2014.
- [175] C. A. Ramos-Paja, A. Romero, R. Giral, E. Vidal-Idiarte, and L. Martinez-Salamero, "Fuzzy-based modelling technique for PEMFC electrical power generation systems emulation," *Power Electronics, IET*, vol. 2, no. 3, pp. 241–255, 2009.

- [176] R. Borup, J. Meyers, B. Pivovar, Y. S. Kim, R. Mukundan, N. Garland, D. Myers, M. Wilson, F. Garzon, D. Wood, P. Zelenay, K. More, K. Stroh, T. Zawodzinski, J. Boncella, J. E. McGrath, M. Inaba, K. Miyatake, M. Hori, K. Ota, Z. Ogumi, S. Miyata, A. Nishikata, Z. Siroma, Y. Uchimoto, K. Yasuda, K.-I. Kimijima, and N. Iwashita, “Scientific aspects of polymer electrolyte fuel cell durability and degradation.,” *Chemical reviews*, vol. 107, pp. 3904–51, Oct. 2007.
- [177] A. Kulikovskiy, “The effect of stoichiometric ratio on the performance of a polymer electrolyte fuel cell,” *Electrochimica Acta*, vol. 49, no. 4, pp. 617–625, 2004.
- [178] E. Endoh, S. Terazono, H. Widjaja, and Y. Takimoto, “Degradation Study of MEA for PEMFCs under Low Humidity Conditions,” *Electrochemical and Solid-State Letters*, vol. 7, p. A209, July 2004.
- [179] A. Debenjak, M. Gašperin, B. Pregelj, M. Atanasijevic-Kunc, J. Petrovic, and V. Jovan, “Detection of Flooding and Drying inside a PEM Fuel Cell Stack,” *Journal of Mechanical Engineering*, vol. 59, no. 1, pp. 56–64, 2013.
- [180] C. Chen and T. F. Fuller, “The effect of humidity on the degradation of Nafion® membrane,” *Polymer Degradation and Stability*, vol. 94, pp. 1436–1447, Sept. 2009.
- [181] K. Panha, M. Fowler, X. Z. Yuan, and H. Wang, “Accelerated durability testing via reactants relative humidity cycling on PEM fuel cells,” *Applied Energy*, vol. 93, pp. 90–97, 2012.
- [182] P. Hu, G. Y. Cao, X. J. Zhu, and M. Hu, “Coolant circuit modeling and temperature fuzzy control of proton exchange membrane fuel cells,” *International Journal of Hydrogen Energy*, vol. 35, pp. 9110–9123, Sept. 2010.
- [183] D. Liu and S. Case, “Durability study of proton exchange membrane fuel cells under dynamic testing conditions with cyclic current profile,” *Journal of Power Sources*, vol. 162, no. 1, pp. 521–531, 2006.
- [184] Y. Fujii, S. Tsushima, K. Teranishi, K. Kawata, T. Nanjo, and S. Hirai, “Degradation Investigation of PEMFC by Scanning Electron Microscopy and Direct Gas Mass Spectroscopy,” in *ECS Transactions*, vol. 3, pp. 735–741, ECS, Oct. 2006.
- [185] T. Tian, J. Tang, Y. Chen, J. Tan, S. Li, and M. Pan, “Study on accelerated stress test for fuel cell lifetime,” *International Journal of Electrochemical Science*, vol. 13, no. 2, pp. 2022–2032, 2018.

- [186] S. Samuel, L. Austin, and D. Morrey, “Automotive test drive cycles for emission measurement and real-world emission levels - A review,” *Proceedings of the Institution of Mechanical Engineers, Part D: Journal of Automobile Engineering*, vol. 216, no. 7, pp. 555–564, 2002.
- [187] C. N. Maxoulis, D. N. Tsinoglou, and G. C. Koltsakis, “Modeling of automotive fuel cell operation in driving cycles,” *Energy Conversion and Management*, vol. 45, no. 4, pp. 559–573, 2004.
- [188] K. Chen, A. Bouscayrol, A. Berthon, P. Delarue, D. Hissel, and R. Trigui, “Global modeling of different vehicles using Energetic Macroscopic Representation,” *2008 IEEE Vehicle Power and Propulsion Conference*, pp. 1–7, Sept. 2008.
- [189] F. Roy, S. Garnit, and J. Crouvezier, “Fisypac project: The first vehicle integration of genepac fuel cell stack,” *World Electric Vehicle Journal*, vol. 3, pp. 1–7, 2009.
- [190] T. Yoshida and K. Kojima, “Toyota MIRAI Fuel Cell Vehicle and Progress Toward a Future Hydrogen Society,” *Interface magazine*, vol. 24, pp. 45–49, Jan. 2015.
- [191] X. Z. Yuan, S. Zhang, J. C. Sun, and H. Wang, “A review of accelerated conditioning for a polymer electrolyte membrane fuel cell,” *Journal of Power Sources*, vol. 196, no. 22, pp. 9097–9106, 2011.
- [192] N. Yousfi-Steiner, P. Moçotéguy, D. Candusso, D. Hissel, A. Hernandez, and A. Aslanides, “A review on PEM voltage degradation associated with water management: Impacts, influent factors and characterization,” *Journal of Power Sources*, vol. 183, pp. 260–274, Aug. 2008.
- [193] J. Baschuk and X. Li, “Modelling of polymer electrolyte membrane fuel cells with variable degrees of water flooding,” *Journal of Power Sources*, vol. 86, pp. 181–196, Mar. 2000.
- [194] J. Hou, “A study on polarization hysteresis in PEM fuel cells by galvanostatic step sweep,” *International Journal of Hydrogen Energy*, vol. 36, no. 12, pp. 7199–7206, 2011.
- [195] T. Aarhaug and A. Svensson, “Degradation rates of PEM fuel cells running at open circuit voltage,” *ECS Transactions*, vol. 3, no. 1, pp. 775–780, 2006.
- [196] M. Zaton, J. Rozière, and D. Jones, “Current Understanding of Chemical Degradation Mechanisms of Perfluorosulfonic Acid Membranes and their Mitigation Strategies: A Review,” *Sustainable Energy Fuels*, pp. 409–438, 2017.

- [197] N. Garland, T. Benjamin, and J. Kopasz, "DOE Fuel Cell Program: Durability Technical Targets and Testing Protocols," in *ECS Transactions*, vol. 11, pp. 923–931, 2007.



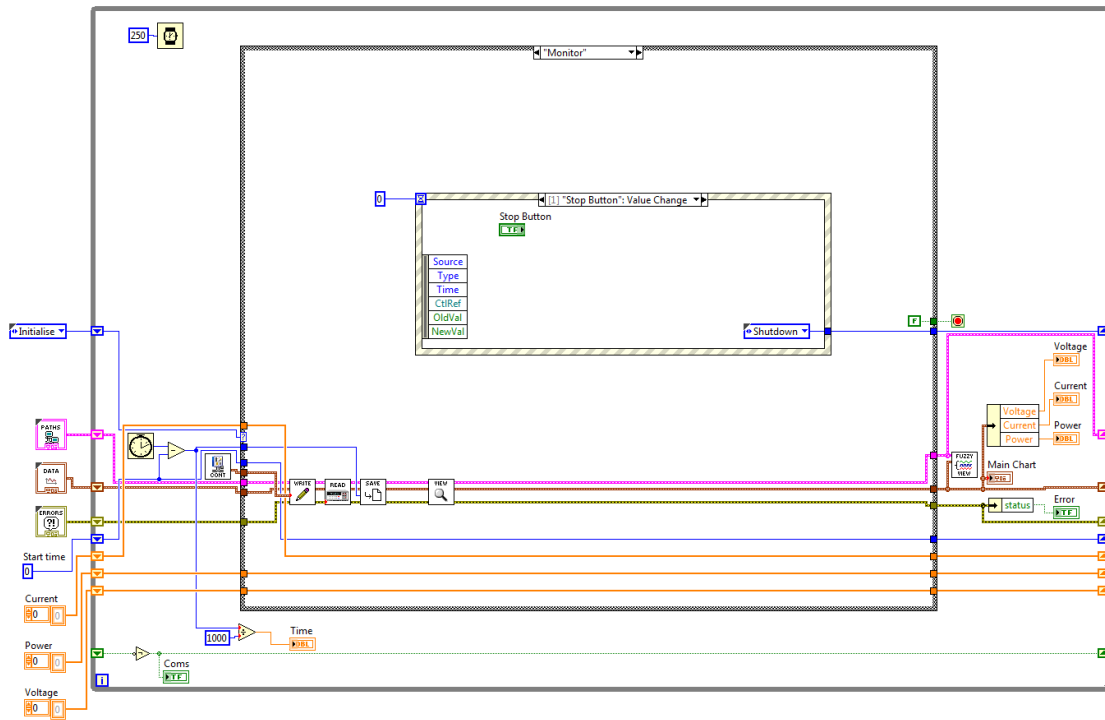


Figure A.2: FCCM main interface code structure during monitoring

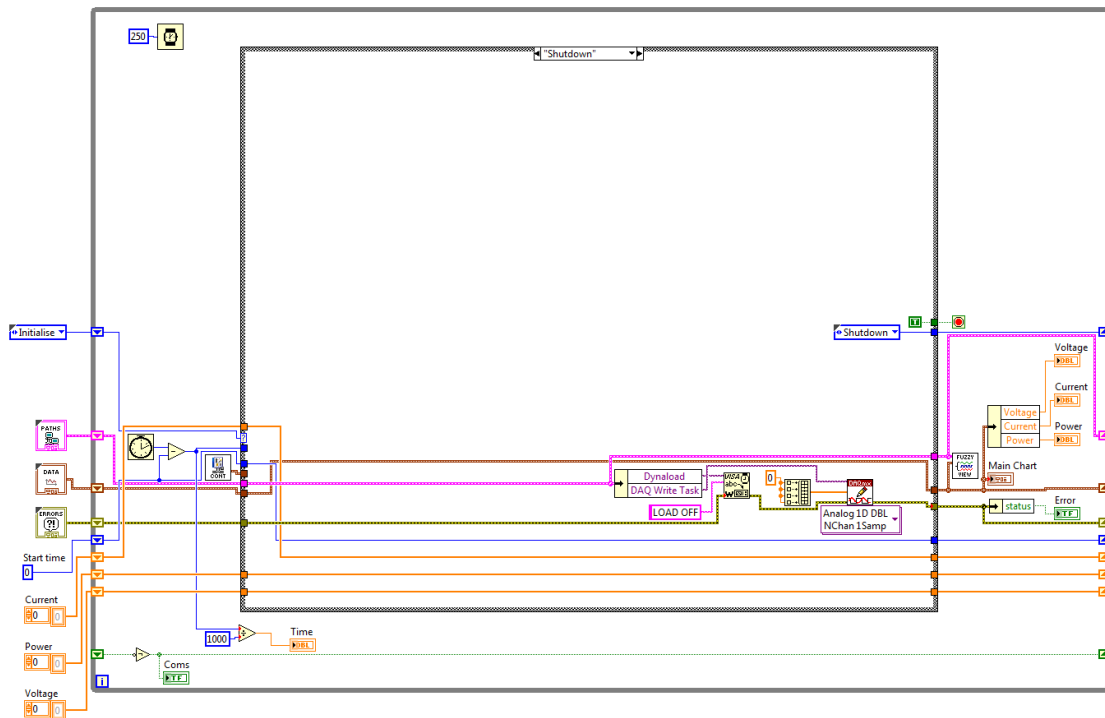


Figure A.3: FCCM main interface code structure during shut down



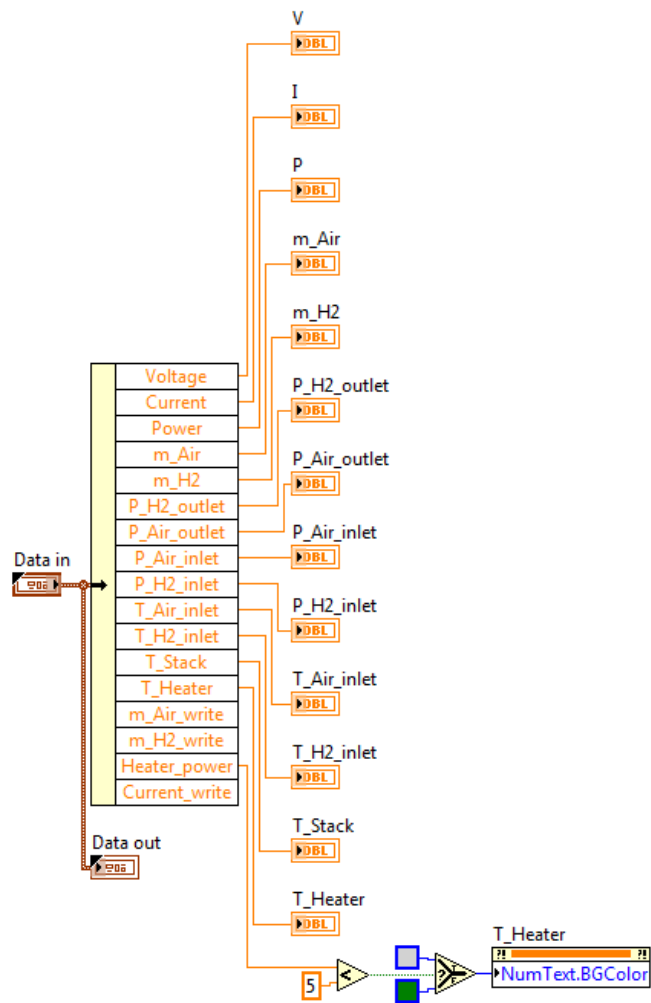


Figure A.6: FCCM view panel code structure

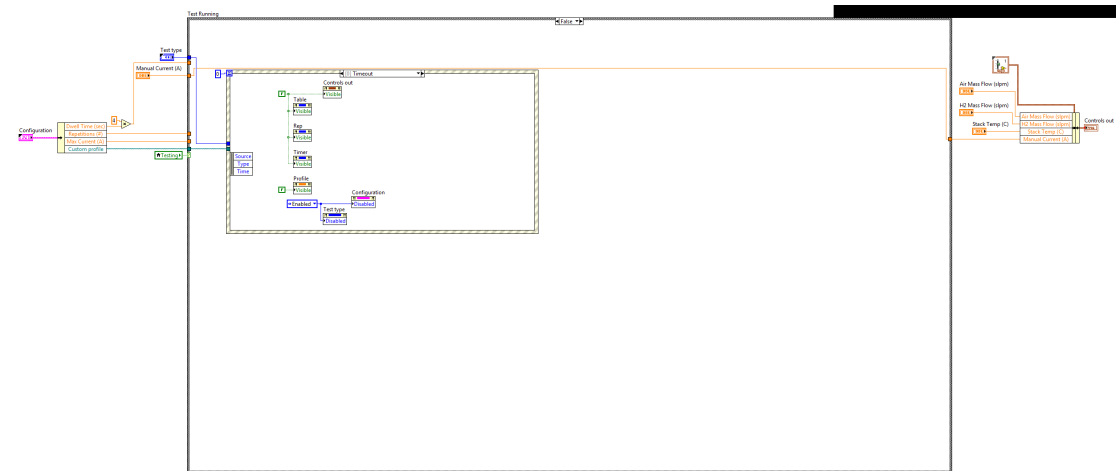


Figure A.7: FCCM control interface code structure during monitoring



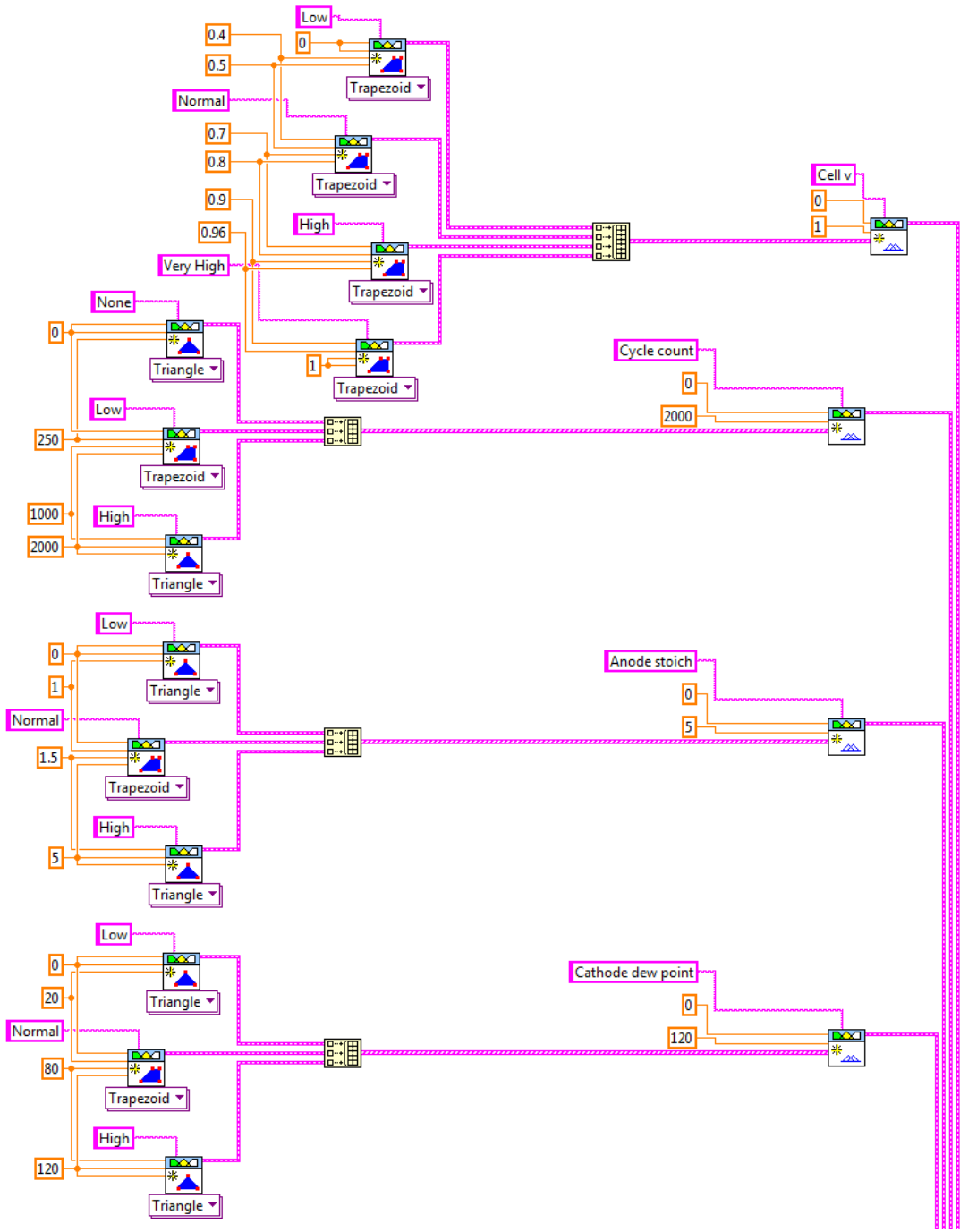


Figure A.10: Fuzzy logic diagnostic code structure for inputs

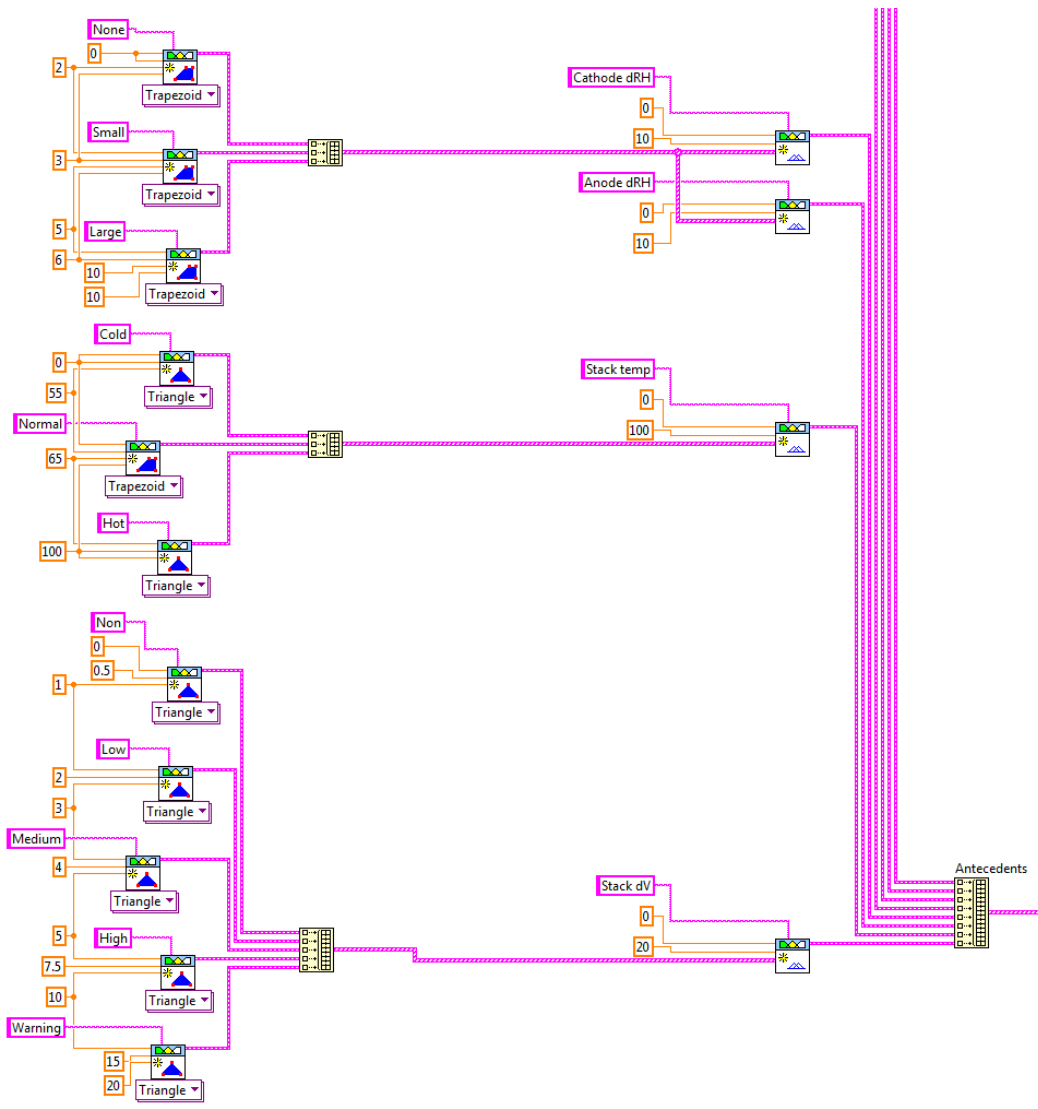


Figure A.11: Fuzzy logic diagnostic code structure for inputs (cont.)

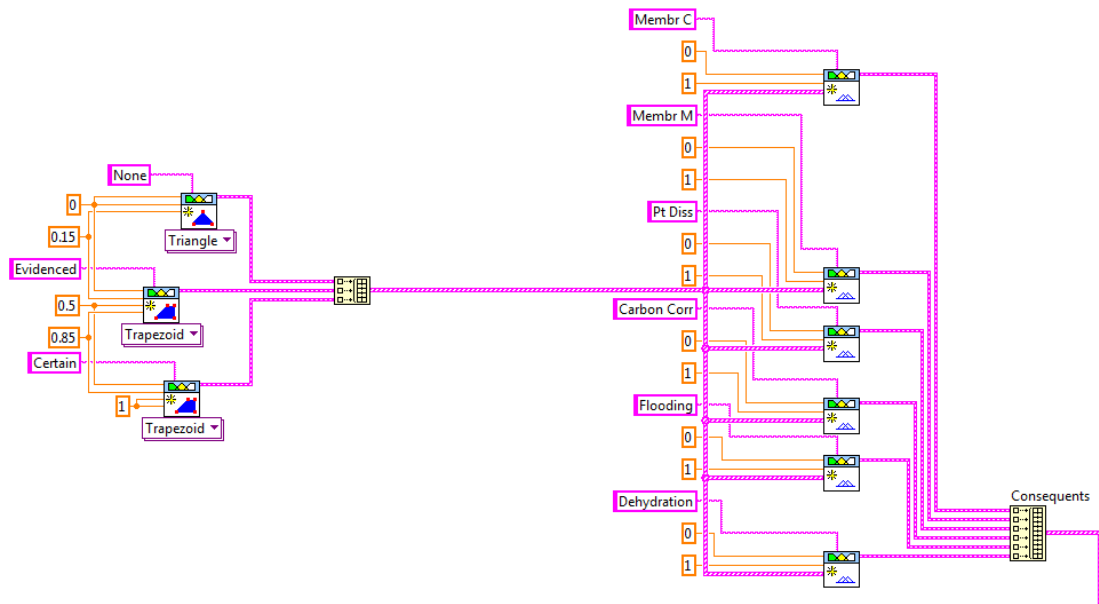


Figure A.12: Fuzzy logic diagnostic code structure for outputs

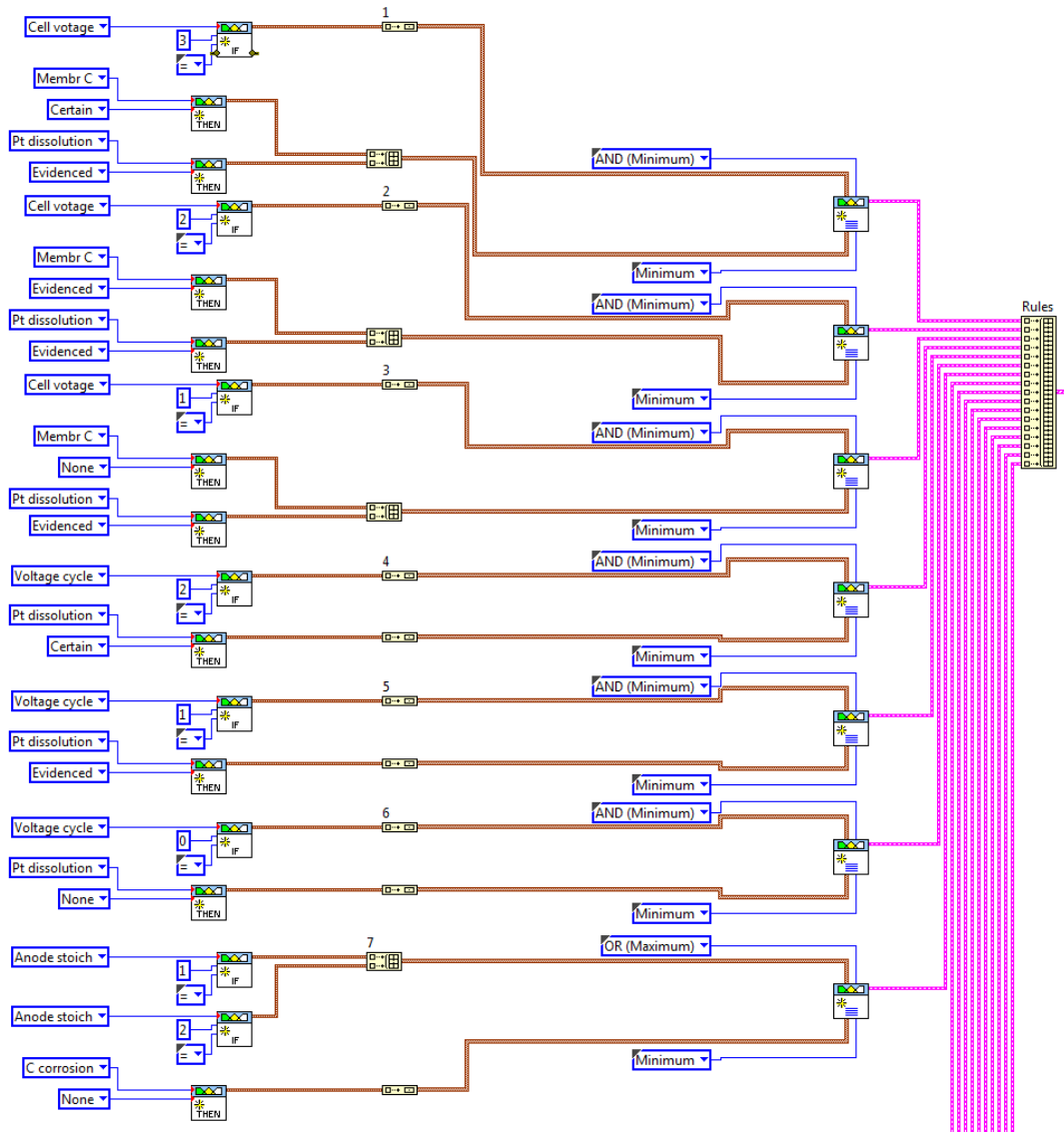


Figure A.13: Fuzzy logic diagnostic code structure for rules

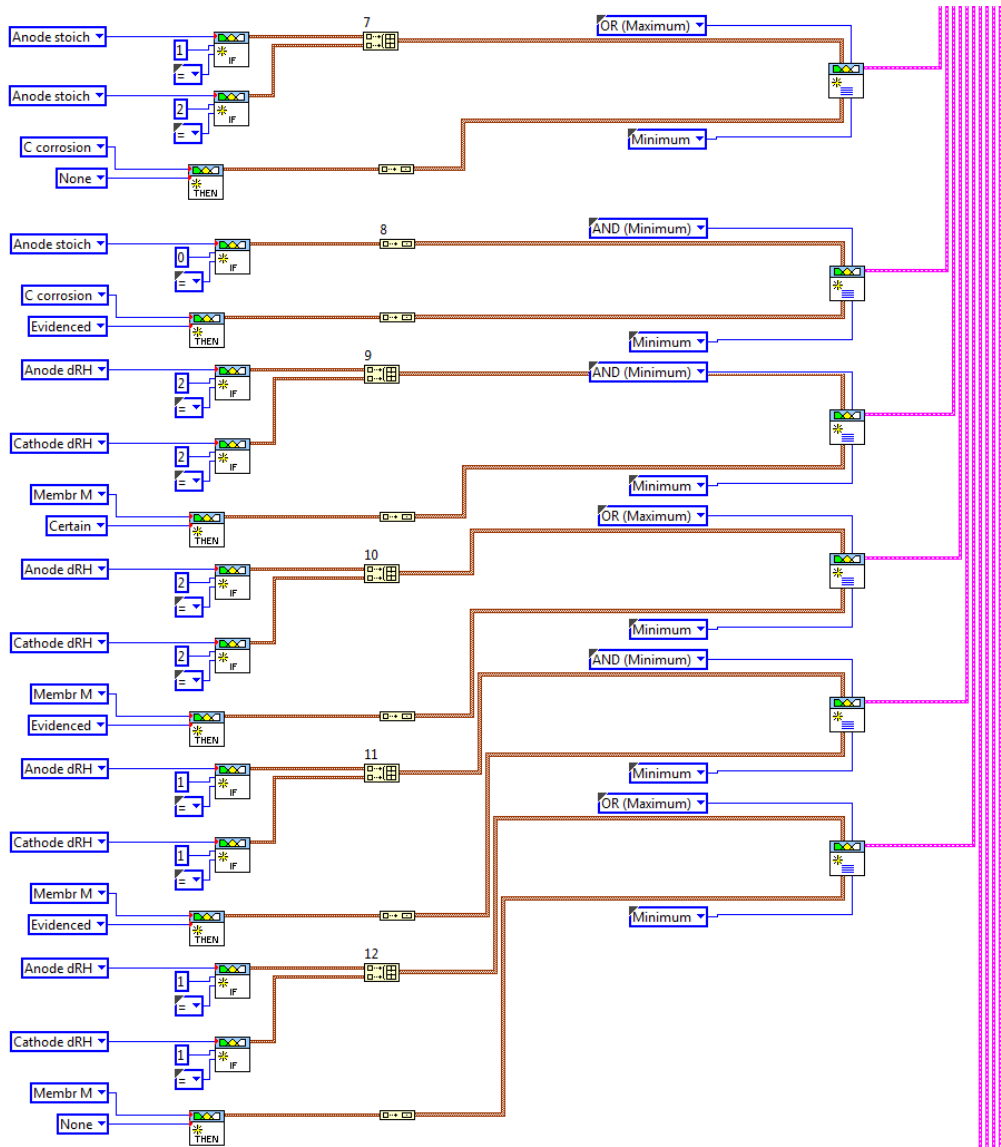


Figure A.14: Fuzzy logic diagnostic code structure for rules (cont.)

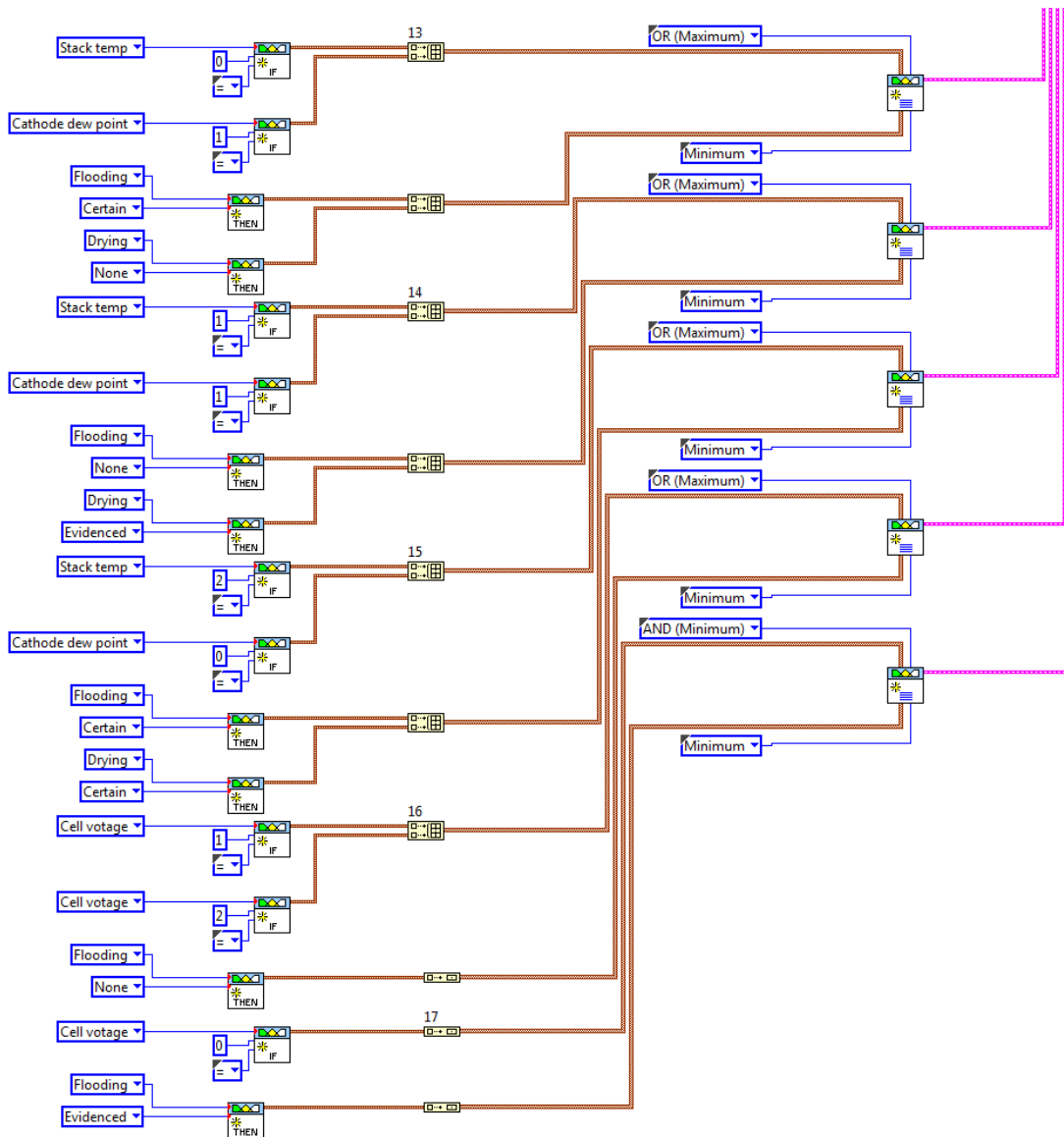


Figure A.15: Fuzzy logic diagnostic code structure for rules (cont.)

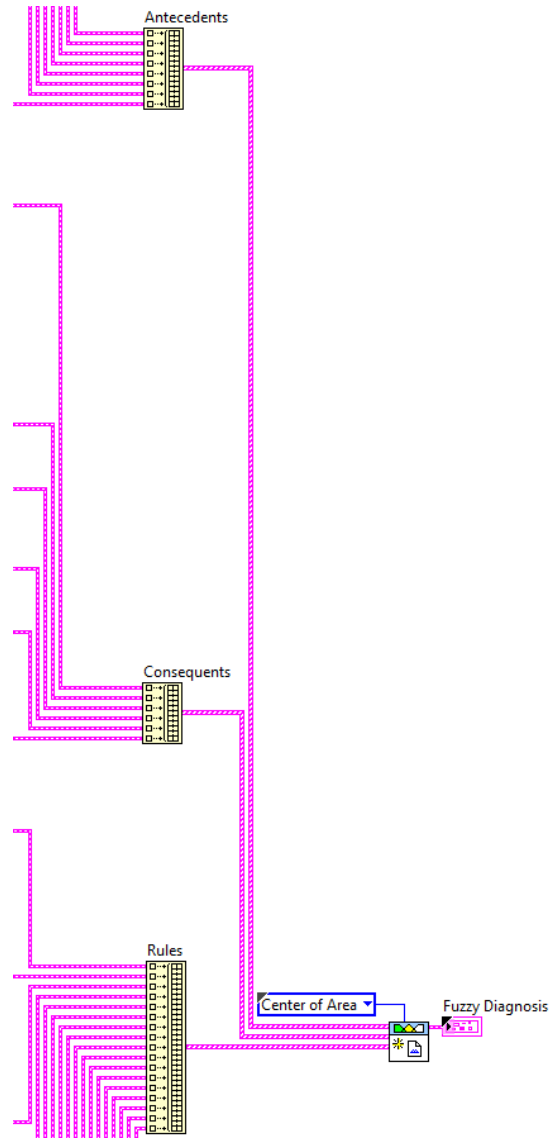


Figure A.16: Fuzzy logic diagnostic code structure